NURail Project
NURail2012-UIC-RO2-combined

The final report for NURail project: **NURail2012-UIC-R02** consists of six distinct documents.

- Section 1, 28 pages, titled “Flexural Behavior of High Density Polyethylene Railroad Crossties”, written byMohsen A. Issa, Ibrahim Lotfy, Maen Farhat and Mustafa Al-Obaidi.
- Section 2, 25 pages, titled “Temperature Effect on the Performance of Glass Fiber Reinforced High DensityPolyethylene Composite Railroad Crossties”, written by Mohsen A. Issa, Ibrahim Lotfy and Maen Farhat.
- Section 3, 32 pages, titled “Effect of Pre-drilling, Loading Rate and Temperature Variation on the Behavior of Railroad Spikes used for High Density Polyethylene Crossties”, written by Mohsen A. Issa, Ibrahim Lotfy and Maen Farhat.
- Section 4, 36 pages, titled “Evaluation of the longitudinal restraint, uplift resistance, and long-term performance of High Density Polyethylene crosstie rail support system using static and cyclic testing”, written by Mohsen A. Issa, Ibrahim Lotfy and Maen Farhat.
- Section 5, 57 pages, titled “Accelerated Bridge Construction for Railroad Elevated Structures”, written byMohsen A. Issa, Ibrahim Lotfy and Maen Farhat.
- Section 6, 18 pages in length, titled “Structural Adhesive Behavior – Experimental and Computational Study”, written by Mohsen A. Issa and Aiman Shibli.

These were completed under grant number: DTRT12-G-UTC18.

NURail Project ID: NURail2012-UIC-R02-A

Flexural Behavior of High Density Polyethylene Railroad Crossties

By

Mohsen A. Issa
Professor of Civil and Material Engineering
University of Illinois at Chicago
missa@uic.edu

Ibrahim Lotfy
PhD Student of Civil and Material Engineering
University of Illinois at Chicago
ilotfy2@uic.edu

Maen Farhat
PhD Student of Civil and Material Engineering
University of Illinois at Chicago
mfarha3@uic.edu

and

Mustafa Al-Obaidi
Staff Structural Engineer
HBM Engineering Group, LLC
obaidi.eng@gmail.com

DISCLAIMER

Funding for this research was provided by the NURail Center, University of Illinois at Urbana - Champaign under Grant No. DTRT12-G-UTC18 of the U.S. Department of Transportation, Office of the Assistant Secretary for Research & Technology (OST-R), University Transportation Centers Program. The contents of this report reflect the views of the authors, who are responsible for the facts and the accuracy of the information presented herein. This document is disseminated under the sponsorship of the U.S. Department of Transportation's University Transportation Centers Program, in the interest of information exchange. The U.S. Government assumes no liability for the contents or use thereof. The content of this document were accepted for publication as "Lotfy I, Farhat M, Issa M, and Al-Obaidi M. Flexural behavior of high-density polyethylene railroad crossties. Journal of Rail and Rapid Transit; In press, accepted for publication on 17 November 2014. DOI: 10.1177/0954409714565655."

TECHNICAL SUMMARY

Title
Flexural Behavior of High Density Polyethylene Railroad Crossties

Introduction

This report presents the findings of an experimental research program addressing the flexural behavior of HDPE railroad crossties and their mechanical properties. An analytical finite element model constructed using calibrated material model to accurately portray the crossties behavior is also presented. This model was constructed using the existing and obtained testing results. Several tools were employed in order to properly conduct this study including analytical and finite element modeling, HDPE material and coupons testing and consultation of the existing HDPE testing database in UIC. The objective of this report is as follows:

- Understand and assess the flexural behavior of HDPE crossties.
- Evaluate the performance of the crossties with the AREMA manual, past applications, and the available literature.
- Construct a calibrated material model for use in finite element analysis.
- Develop an accurate finite element modeling technique, which accurately portray the behavior of the crossties using the calibrated material model.

Approach and Methodology

In order to investigate the flexural behavior of HDPE composite crossties, two tests from the AREMA manual were conducted; the center bending test (AREMA Part 2- Section 2.2.3 – Test 1C) and rail seat bending (AREMA Part 2- Section 2.2.1 – Test 1A). Since the cross section of the crossties is uniform rendering the positive and negative flexural capacities identical, both of the above tests were enough to characterize both the positive and negative flexural behavior eliminating the need for the rail seat negative bending test (AREMA Part 2- Section 2.2.2 – Test 1B).
Finite element analysis was also performed to simulate the performed experimental tests. The objective of this analysis was to construct a material properties model capable of representing the HDPE crossties. The validity of the model was assessed by matching its results with the experimental data.

Findings

All the specimens satisfied and surpassed the AREMA recommendations for MOR and MOE which were 170,000(1170) psi(MPa) and 2000(14) psi(MPa) respectively.
All the tested specimens exhibited a similar and consistent trend; the deflection increased monotonically with the increase in load. No cracks were observed at any stage of the test until the fracture stage where a single crack was observed at the mid-span accompanied with a pronounced acoustic emission, i.e. loud fracture sound.

The results of the detailed finite element analysis for the average, and hollow sections agreed well with the experimental data. Slight discrepancy was noticed in the rail seat model due to the steel loading plate, which was not considered in the model, but had an effect on the experimental results due to the small span. Finally, seeing as the experimental results exhibited some variations, all the modeling approaches, excluding the uniform section with the upper bound direct tensile properties, are deemed capable of portraying the crossties flexural behavior with acceptable accuracy.

Conclusion

1. The extrusion process employed to manufacture HDPE crossties results in an efficient cross-sectional composition with a strong exterior region (with high concentration fiber reinforcement and low void content); and a core region with no fiber reinforcement.
2. All the tested specimens fulfilled and surpassed their corresponding AREMA recommendations, which is indicative of their expected performance.
3. The installation of the rail and fastening system enhanced the performance of the crossties. This was attributed to the load distribution quality of the steel bearing plate and the partial composite action between the crosstie and the steel bearing plate.
4. A detailed, nonlinear, finite element modeling approach accounting for the crossties section composition was achieved and accurately portrayed the flexural behavior and failure of the crossties. A uniform section with equivalent properties was achieved without sacrificing much accuracy and will be used in computational intensive models.

Publications

- Lotfy I, Farhat M, Issa M A, and Al-Obaidi M, "**Flexural Behavior of High Density Polyethylene Railroad Crossties**" Journal of Rail and Rapid Transit; In press, accepted for publication on 17 November 2014.

Contacts

Principal Investigator
Mohsen A. Issa
Professor of Civil and Material Engineering
University of Illinois at Chicago
312-996-2426
missa@uic.edu

NURail Center
217-244-4444
nurail@illinois.edu
http://www.nurailcenter.org/

TABLE OF CONTENTS

LIST OF FIGURES

SECTION 1 INTRODUCTION

Railroad crossties are the transverse beams positioned directly under the track. They are the rail's first support (1). Their main purpose is to provide lateral support for the rails, retaining the track gauge constant, while anchoring them to the base in order to withstand the dynamic train loads. Moreover, they have to withstand or minimize any indentation of rail bearing plates or loss of section due to friction and abrasion with the different rail and fastening system components as well as the underlying ballast (2). The US railroad industry often opts to fix the crossties and the rail with cut or screw spikes resulting in a small crosstie spacing as oppose to the larger spacing and steel chairs used in European countries; therefore, a mile of track in the US would include over 3,000 crossties (3).

Hardwood timber has been the predominant material of choice for crossties since the establishment of the railroad industry in the US. Recently however, several issues, including higher speeds, heavier loads, timber survivability and environmental effects, have invoked the industry's interest in alternative materials for crossties. Concerns have arose regarding the timber's ability to keep pace with the increasing track capacities and speeds for both freight and passenger rail. Moreover, in addition to sparsity and deforestation issues, timber crossties are susceptible to rot and organic decay due to attacks from biological organisms, which further decrease their service life, especially in a humid environment with moist soil. Wood preservatives, primarily creosote, are employed to limit these attacks. However, creosote is a health hazard. Its exposure can cause skin rashes, lung cancer, and other health problems. When handled without appropriate caution, it penetrates into the soil contaminating the groundwater and affecting nearby plant life. Creosote fumes emanating from treatment plants affect the surrounding areas and cause illness and diseases (4). Moreover, in Europe, timber crossties containing amounts of creosote exceeding the limit specified by the European Union are treated as hazardous waste (5). Morris (6) also expressed the need of standards and regulations to control the storage and disposal of old, creosote treated, timber crossties. Several countries, including the US, have tighten their regulations of creosote use due to its destructive effect on the environment (7 and 8). The environmental protection regulations are becoming increasingly stringent and the use of creosote is not guaranteed to continue without additional restrictions and precautions. Therefore, alternative crossties materials, not requiring preservatives, are beneficial to the railroad industry.

Replacement operations of crossties represent one of the main maintenance expenditures for the railroad industry (9). In order to ease these expenses, one to one replacement strategies have been implemented (2, 10 and 11). This strategy replaces only the deteriorated segments of the track or even individual degraded crossties on a one to one basis with new crossties to boost the

structural integrity of the entire track. This technique however has its limitation: the new crosstie has to have a simple installation procedure; also, it has to be compatible with the installed crossties in terms of size and mechanical properties in order to avoid any deferential settlement or stress concentration on individual crossties.

Currently, a significant number prestressed concrete crosstie application were successfully implemented and accepted by the railroad industry. Prestressed concrete has become wide spread and its longer life span and low maintenance are the catalysts that grant it an economic and structural competitiveness. Prestressed concrete crossties have a larger cross section than that of timber crossties (12) and its heavier weight (about 2.5 times heavier than timber) enables it to assume its correct position and maintain the stability of the track. Numerous studies and research has gone through the development of the prestressed concrete crossties (13 and 14).

Limitations of the prestressed concrete crossties are presented in its higher initial cost, which can reach double that of the hardwood timber. Another concern is the increased weight of the crossties which render handling and installation procedures difficult requiring specialized equipment; e.g. track renewal train (TRT). Its larger size heavier weight and higher stiffness eliminate the possibility of one to one replacement of old deteriorated timber crossties. Concrete crossties are also vulnerable to mechanical damage, wear, abrasion, and pumping track due to poor subgrade conditions. Durability is also an issue if the concrete manufacturing and installation are not properly controlled. In the absence of rail pads, rail seat corrosion and abrasion often occurs (15).

Composite plastic crosstie, specifically High Density Polyethylene (HDPE), is ideal for new and replacement operations of railroad track. It has high strength and durability while offering similar weight and lateral stability as its timber counterpart. It can be engineered and customized to provide the desired mechanical properties with the same size and depth as wooden crossties enabling one to one replacement strategies (16). It has a prolonged service life due to its enhanced durability and requires less maintenance. Its light weight combined with its similar installation procedures with timber crossties render it a very competitive solution.

Recycling plastic waste to manufacture crossties is a green process. This makes it even a much more appealing solution in today's society, where the emphasis is directed towards environmental issues, reduction of CO2 emissions and limiting climate changes. When compared to creosote treated wooden crossties, recycled plastic composite crossties have numerous and apparent environmental advantages. The implementation of plastic composite crossties can reduce greenhouse gas emissions significantly (3) and the ability of recycling and reusing old plastic crossties further increase its sustainability and life cycle economy (17).

Even though timber crossties are initially cheaper than plastic crossties, the latter proved to be a cost efficient and competitive solution after considering replacement operations and life cycle costs (18). Knowing the advantages of plastic composite crossties, Schut (16), urged the railroad industry to increase its implementation for freight lines especially in hot and humid regions.

The implementation of HDPE in crossties application offers adequate performance with an enhanced service life and environmental advantages, as it is inherently resistant to rot, insects and harmful preservatives (19 and 20). Currently several manufacturers offer alternative solutions using different recycled plastic composite materials. Thousands of plastic crossties are currently in service in a wide variety of railroad applications in the US and other countries (21).

SECTION 2 PAST RESEARCH

Several researchers have performed studies to identify the best alternative to timber including plantation timber, steel, prestressed concrete, polymer concrete, reinforced plastics, rubber, and composite materials (14, 22, 23, 24, 25, 26, 27 and 28). More to the point, the following studies addressed mainly plastic composite crossties experimental laboratory testing.

Jimenez (29) presented an experimental study addressing the vertical track modulus in both plastic and wooden crossties. The effect of temperature on the dynamic modulus (stiffness) was investigated. Two different types of the fastener systems were employed. He concluded that the plastic crosstie showed acceptable results and comparable track modulus to that of their wooden counterpart. Lampo (30) investigated and discussed the performance of the composite crossties through several laboratories and field-testing. The study confirmed the acceptable performance of the composite crossties. Roybal (31) conducted another study addressing the cyclic loading response of composite crosstie. The test was performed on a half section of crosstie with ambient temperature of 70° F and cut spikes were employed to fasten the rail and the steel tie plate to the crosstie. Water and sand were added over the rail seat area to simulate an abrasive environment. The performance of the crossties was deemed adequate in terms of maximum lateral railhead displacements, lateral tie plate movement, and performance of the cut spikes. The crosstie showed normal wear and abrasion in the tie plate area and no cracks or anomalies developed. More recently, Reiff and Trevizo (32) studied the effect of several factors on the performance of the plastic composite crossties such as temperature variation, type of spikes used, and effect of impact forces. A series of experimental tests were performed on three types of plastic composite crossties and their behavior was deemed adequate. They also observed that HDPE reinforced with glass fiber exhibited better performance than the other types tested in terms of flexural stiffness and impact resistance. Additionally, they also noticed that the installation of the rail and fastening system to the crossties enhanced their resistance to impact loading. Finally, they expressed some concerns regarding spike pre-drilling and overdriving, however, it did not have a significant effect.

As evident from the past studies, the behavior of HDPE crossties when subjected to rail loading is not fully understood yet. Uncertainties in mechanical properties, failure modes, and fracture render their performance and safety questionable. More research is required to properly characterize, describe and model the behavior of these materials as well as assess the feasibility of implementing these materials in railroad applications.

SECTION 3 OBJECTIVES

The University of Illinois at Chicago (UIC) conducted a study to assess the feasibility of implementing HDPE crossties in both conventional and high speed rail (HSR) applications. This report presents the findings of an experimental research program addressing the flexural behavior of HDPE railroad crossties and their mechanical properties. An analytical finite element model constructed using calibrated material model to accurately portray the crossties behavior is also presented. This model was constructed using the existing and obtained testing results. Several tools were employed in order to properly conduct this study including analytical and finite element modeling, HDPE material and coupons testing and consultation of the existing HDPE testing database in UIC. The objective of this report is as follows:

- Understand and assess the flexural behavior of HDPE crossties.
- Evaluate the performance of the crossties with the AREMA manual, past applications, and the available literature.
- Construct a calibrated material model for use in finite element analysis.
- Develop an accurate finite element modeling technique, which accurately portray the behavior of the crossties using the calibrated material model.

SECTION 4 EXPERIMENTAL PROGRAM

4.1 HDPE Crossties

A major advantage of HDPE composite plastic is presented in its versatility as it can be designed to meet the requirements and needs of the project. The plastic composite crossties tested in this study were manufactured from recycled plastic waste; milk and detergent bottles; which 7.2 billion pounds of these bottles are land filled each year in the US (3). They are manufactured through an extrusion process where the reinforcing glass fibers is added to the hot HDPE polymer mixture and then guided through a die to take the shape of the final crosstie product; 9(22.86) × 7(17.78) in.(cm); resulting in HDPE composite crossties reinforced with discrete, discontinuous, randomly distributed glass fibers. During the process, foaming agents are added to the mixture to control the final product weight and cost. These agents create some voids and air bubbles in the core region of the crossties where the applied stresses during the service life are expected to be minimal compared to the exterior region. The reinforcing fibers are pushed by the foaming agents to the exterior region of the cross section where the maximum stresses are expected. This process creates a significant difference in the mechanical properties between the core and exterior regions of the cross section, which was taken into consideration when creating the finite element model. UV inhibitors and anti-oxidants are also added to a thin skin layer, which protects the crossties from weathering conditions and sunlight exposure. The weight of the tested specimens was recorded and the density of the crossties was determined to be 56.8(910) pcf(kg/m3) which is comparable to timber crossties. Figure 1 shows the HDPE composite crosstie specimens before testing at the UIC structural laboratories.

Figure 1. HDPE composite crosstie specimens.

4.2 Testing procedures and results

In order to investigate the flexural behavior of HDPE composite crossties, two tests from the AREMA manual (33) were conducted; the center bending test (AREMA Part 2- Section 2.2.3 – Test 1C) and rail seat bending (AREMA Part 2- Section 2.2.1 – Test 1A). Since the cross section of the crossties is uniform rendering the positive and negative flexural capacities identical, both of the above tests were enough to characterize both the positive and negative flexural behavior eliminating the need for the rail seat negative bending test (AREMA Part 2- Section 2.2.2 – Test 1B). The rail seat bending test was performed once using the crossties without the rail and fastening system as recommended by the AREMA manual and another time with the rail and fastening system installed. These configurations granted a wider view of the behavior of the crossties and allowed the determination of the effect of the predrilling and installation of the rail and fastening system on the flexural behavior of the crossties. Concerns regarding the structural integrity of the rail seat region were expressed in the literature; as the stress concentrations arising from the installation of screw spikes along with the cross-sectional area reduction due to predrilling in the rail seat region might affect its bending strength (32).

A three-point test configuration was implemented. The span length was used as 60(152.4) and 30(76.2) in.(cm) for the center and rail seat bending tests respectively. Figure 2 and 3. illustrate the test configurations. The loading was applied as a concentrated load at the specimen's mid-span using a perpendicular hydraulic loading system. An adjustable rigid reaction steel testing frame was built specifically for this study to properly support the specimens. Two 2×9×1(5.1×22.9×2.5) in.(cm) elastomeric bearing pads were used at the support locations and another one 5.5×9×1(14×22.9×2.5) in.(cm) was provided at the loading location.

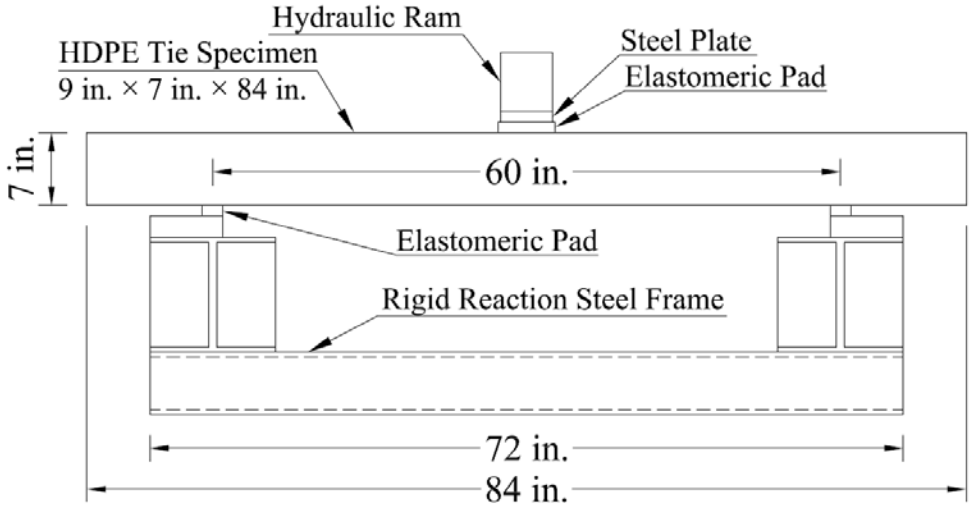

Figure 2. Center bending test setup (1 in. = 2.54 cm).

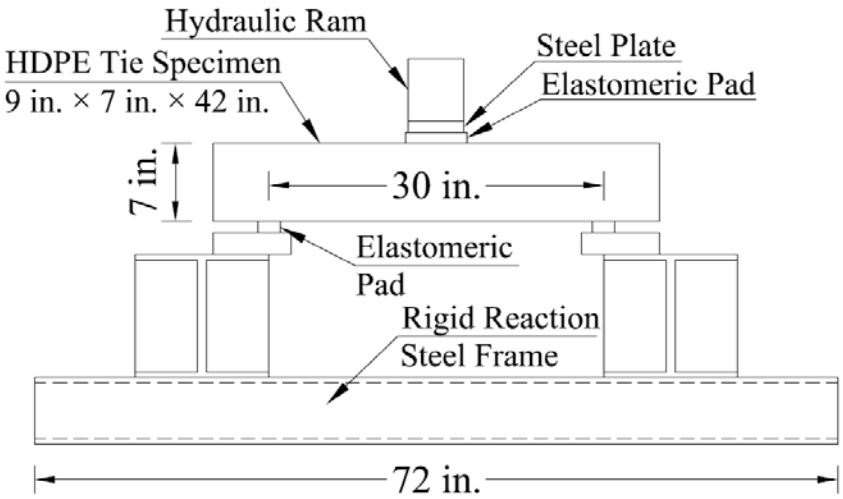

Figure 3. Rail seat bending test setup (1 in. = 2.54 cm).

The specimens were loaded until failure with a, stroke controlled rate of 1.0(2.54) in./min(cm/min) and a load controlled rate of 10,000(44.5) lb/min(kN/min) for the center and rail seat bending respectively. Five specimens were tested for the center bending test and six for the rail seat bending test; three specimens with, and another three without the rail and fastening system installed Figure 4. depicts the center bending test and the rail seat bending for a specimen with the rail and fastening system installed.

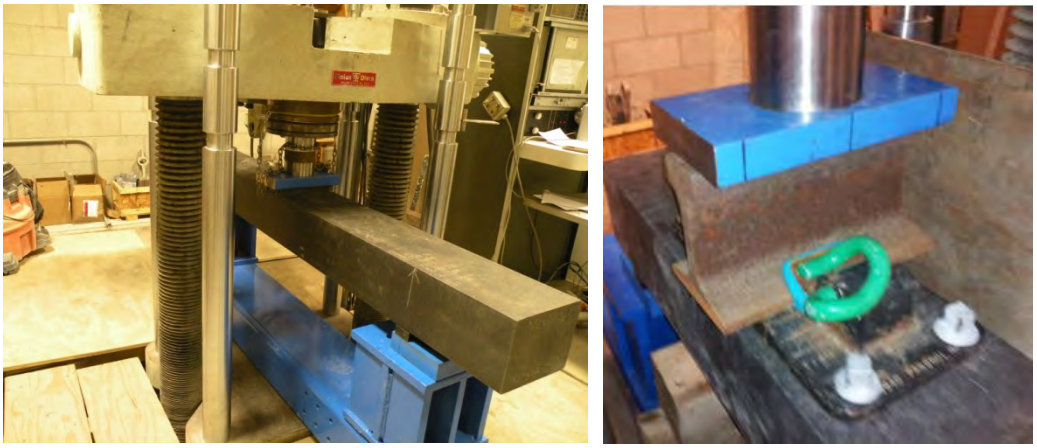

Figure 4. Center bending test (left) and rail seat bending with the rail system (right).

The load and mid-span deflection measurements were recorded for each specimen. The stress-strain curves were plotted and the flexural strength, modulus of rupture (MOR) and elasticity (MOE) and secant modulus were determined. The stress-strain and modulus of elasticity were computed as per AREMA manual (33) and the ASTM standards D790 (34). Both publications outline similar and comprehensive procedures for computing stresses and strains based on a three point bending configuration; based on beam theory assumptions.

All the specimens satisfied and surpassed the AREMA recommendations for MOR and MOE which were 170,000(1170) psi(MPa) and 2000(14) psi(MPa) respectively. Table 1 summarizes the results of the center bending test while Figure 5 presents the stress-strain relationship of all the crosstie specimens. Figure 6 present the load-curves for the specimens with and without the rail and fastening system installed.

Table 1. Summary of the test results for the new crossties.

Specimen No.	1	2	3	4	5	Average
MOR, psi	3,122	3,024	3,089	3,125	3,566	3,185
Ultimate Strain, με	32,643	31,080	33,903	28,548	35,111	32,257
Initial Tangent, psi	188,442	182,569	190,056	193,340	196,347	190,151
MOE at 600psi, psi	185,107	180,356	178,323	180,026	192,330	183,228
Modulus at 1% strain, psi	163,137	163,500	161,659	166,238	176,492	166,205

1 psi = 6.9 kPa

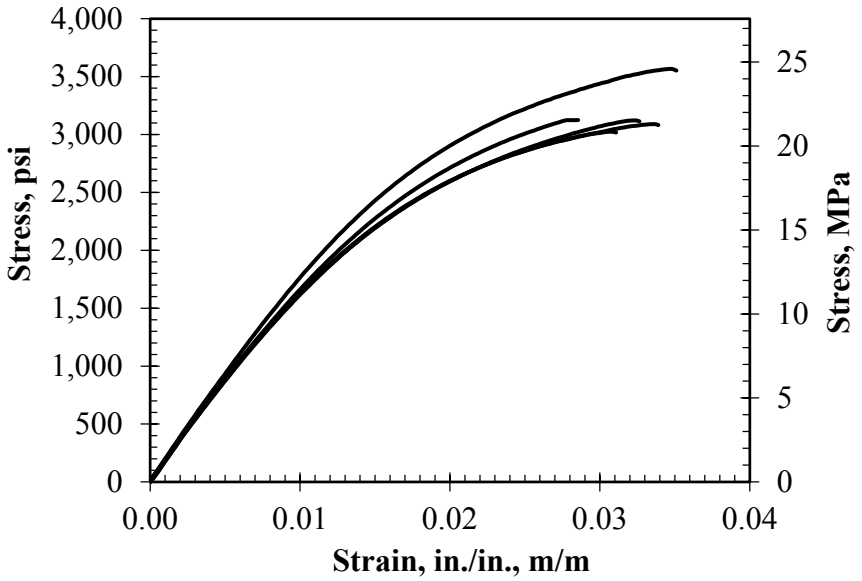

Figure 5. Stress-strain relationship for the five new specimens.

4.3 Discussion and test observations

All the tested specimens exhibited a similar and consistent trend; the deflection increased monotonically with the increase in load. After a certain point, a small increase in load was accompanied with significant increase in deflection until brittle fracture occurred (less apparent in rail seat bending due to smaller span). All the specimens experienced the same mode of failure, which was a brittle fracture due to mid-span tensile bending stress, see Figure 7. No cracks were observed at any stage of the test until the fracture stage where a single crack was

observed at the mid-span accompanied with a pronounced acoustic emission, i.e. loud fracture sound.

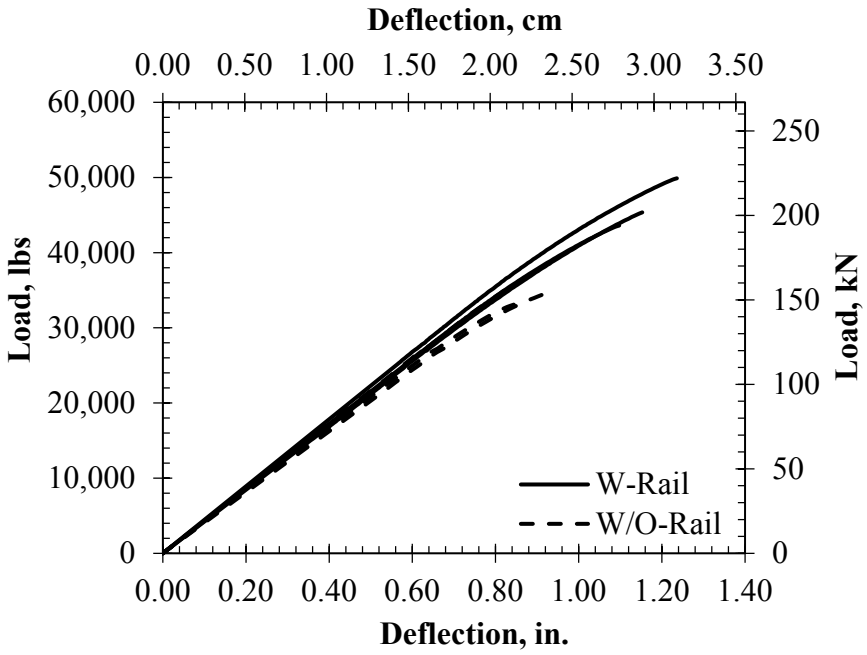

Figure 6. Load-deflection relationship for the specimens with and without rail system.

Figure 7. Failure of the center bending test (left) and rail seat bending with the rail (right).

The fractured surface of the specimens provided an indication on the quality of the plastic crossties. As illustrated in Figure 8, the crossties tested had an excellent quality cross sections featuring very little voids, properly recycled plastic material with few impurities, if any, and a great distribution of discontinuous glass fibers in the exterior region of the cross section to resist the bending stresses. After research, a past application of plastic crossties in the Chicago area was discovered, however, the crossties performance was not as good as expected. Some of these old decommissioned crossties were tested within the scope of this experimental program and the reason for their questionable performance was uncovered. The lack of reinforcement along with

the presence of impurities like rubber, rope pieces and the high void percentage diminished the quality of these old crossties, refer to Figure 8. This significant difference in the HDPE crossties composition and design is reflected in the performance of the crossties as presented in Figure 9. Moreover, it illustrates the extent to which the industry has evolved in the past couple of year.

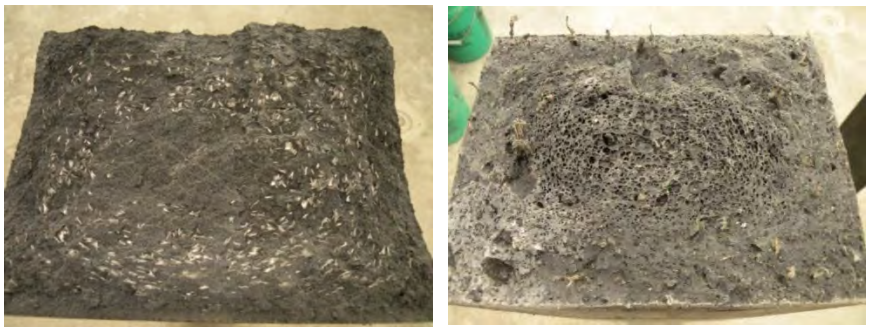

Figure 8. Fracture surface of the proposed (left) and the old decommissioned (right) specimens.

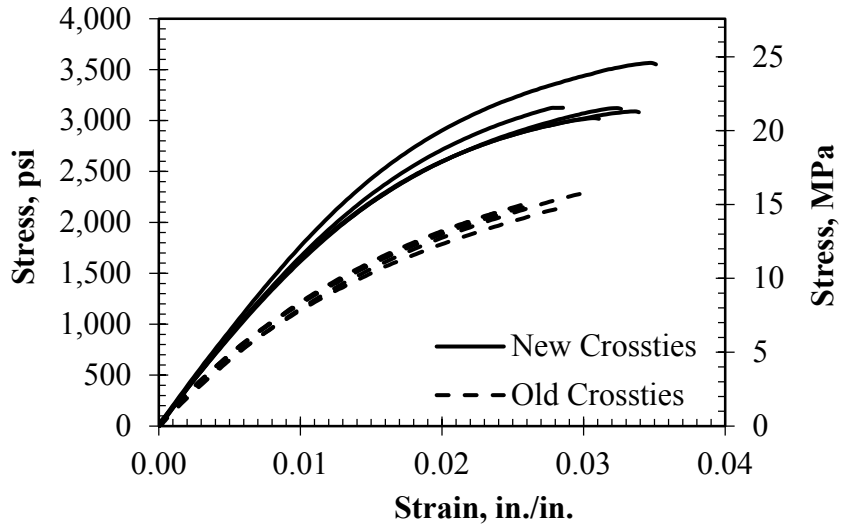

Figure 9. Behavior of the New and Old crossties.

As expected, the rail seat bending specimens showed higher flexural capacities and lower ductility than their center bending counterpart due to their smaller span. Otherwise, their behavior and failure modes are similar. An increase in the ultimate flexural strength was observed in the specimens with the rail system installed as indicated by Figure 6. This additional capacity is mainly attributed to two factors. The high stiffness of the steel tie plate granted it the ability to distribute the concentrated load over its area. Secondly, no movement or pullout was noticed in the screw spikes, which indicate that the tie plate was always firmly connected to the crosstie even after failure as depicted in Figure 7, however a small rotation occurred. As

illustrated in Figure 10, a partial composite action was detected between the steel tie plate and the crosstie. This composite action was evident by the fact that, in order for the crosstie to continue deflecting until it reaches its ultimate strain, the steel plate had to partially deflect as well since the screw spikes were firmly connected. A small gap between the crosstie and the tie plate appeared due to the difference in rotations at the spikes location between the crosstie and the tie plate. This gap, however small, confirmed that the composite action occurring was not full but rather partial. It also altered the loading scheme from a distributed load over the tie plate area to concentrated loads at the edges of the tie plate reminiscent of a four-point bending test configuration. Moreover, upon removal of the rail and fastening system, inception of the crossties did not reveal any cracks in the vicinity of the screw spikes. These observations confirms that proper predrilling and installation of the screw spikes does not result in local cracking emanating from the pilot holes as a results to driving the screw spikes. Even when overdriving the spikes in smaller pilot holes, no cracking was observed rather small local yielding around the vicinity of the spike. Additionally, the installation of the rail and fastening system has a positive effect on the behavior of HDPE crossties as it enhances its flexural capacity and increases its ductility, which agrees with Reiff and Trevizo's findings (32).

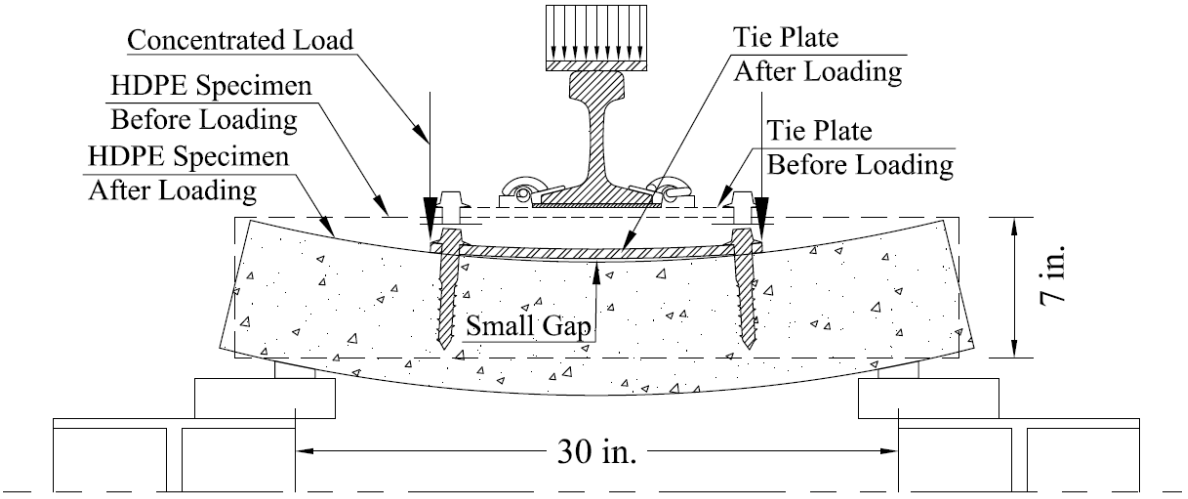

Figure 10. Exaggerated deflected shape illustrating crosstie/tie plate interactions.

SECTION 5 FINITE ELEMENT ANALYSIS

The objective of this analysis was to construct a material properties model capable of representing the HDPE crossties. The validity of the model was assessed by matching its results with the experimental data. First, in order to describe the material model, the basic material properties are required, thus direct tension test was performed as per the ASTM D638 (36) using coupon (dogbone) specimens. Figure 11 present the results of the direct tension tests.

As explained earlier, the manufacturing process of these crossties creates a significant difference in the properties between the core and exterior regions of the cross section as illustrated in Figure 12. The large variation between the upper and lower bounds (Figure 11) is indicative of the difference between coupon specimens extracted from the exterior and core regions. However, the dimensions of both regions are not specified and exhibit some variations. Therefore, the dimensions of the regions were measured for all the tested specimens and compared with a study conducted by Martinez-Guerrero (37) where he addressed a similar issue. Core region dimensions of 4(10.2) × 6(15.2) in.(cm) are proposed for this application and employed in further modeling.

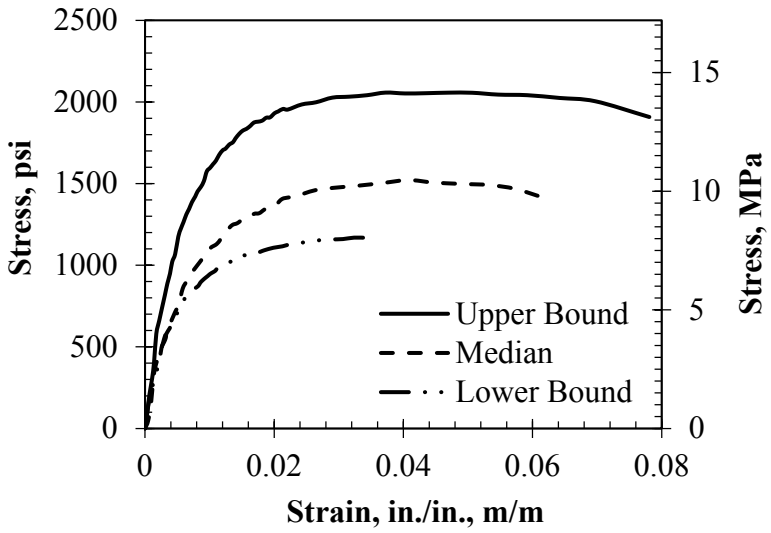

Figure 11. Direct tension test results.

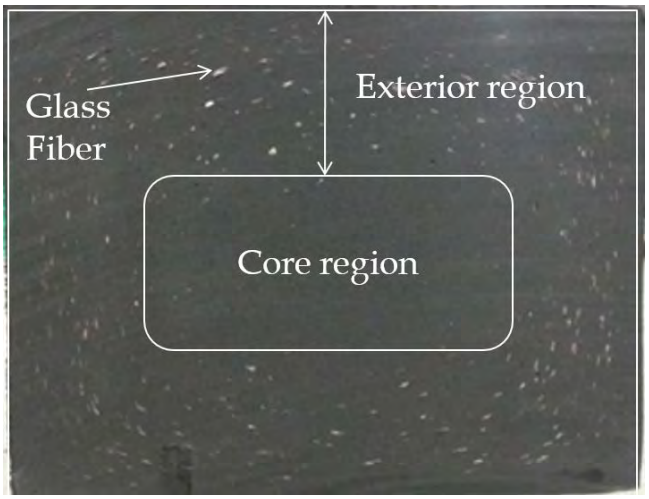

Figure 12. Crosstie's exterior and core regions.

A detailed model was constructed accounting for the external and core regions and it provided a very good presentation of the behavior of the crossties. However, in bigger scale applications, where hundreds of crossties are present in the model, this method becomes very taxing and computationally inefficient. Therefore, two simplified approaches were considered and assessed terms of accuracy and consistency. The first is simply considering the crosstie as one region with uniform material properties and the second is simulating the crossties as a hollow section by converting the core region area to an equivalent exterior region area using the ratio of the elasticity secant moduli.

Striving to simulate the flexural behavior of the crossties, the elastomeric bearing pads have to be considered in the model. These pads were recommended by the AREMA manual and were adopted in the testing program. Thus, without their inclusion in the model, any validation against the test results could be questioned. Therefore, another experimental test was performed to assess the bearing behavior of the bearing pads. The observed stress-strain relationship was hyper-elastic, however, since the main interest in the crosstie, this behavior was simplified as linear with an elastic modulus of 2,100(14.5) psi(MPa).

Both the crosstie and the bearing were represented using solid elements. The specimen dimensions and configuration was modeled as described in Figure 2 and 3. After several trials, the exterior and core regions were found to provide accurate results using the upper and median direct tensile material properties respectively (refer to Figure 11). The model was assumed to be symmetric about the mid-span and the boundary conditions were achieved by restraining the vertical movement of the nodes located at the bottom face of the bearing support pads. The loading was applied on the nodes located at the top face of the loading pad. The failure criteria implemented was a manual, post-process, procedure using maximum principal tensile stresses

and strains described as 2050(14.1) psi(MPa) and 5.0% respectively (average of the experimental results for the exterior region). Figure 13 and 14 present the center bending specimen finite element model and stresses obtained at failure respectively.

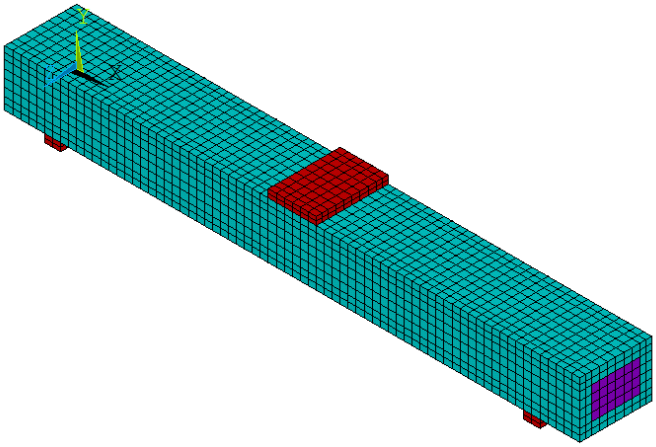

Figure 13. Finite element model of the center bending test.

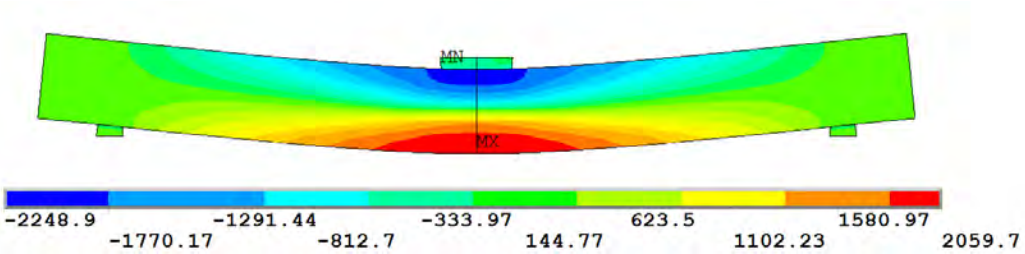

Figure 14. Stress distribution of the center bending specimens at failure in psi (1 psi = 6.9 kPa).

The load-defection relationships was plotted for the center and rail seat bending models and compared with their corresponding test results as shown in Figure 15. As noticed, the detailed section approach results agreed well with the experimental data. Slight discrepancy was noticed in the rail seat model due to the steel loading plate, which was not considered in the model, but had an effect on the experimental results due to the small span.

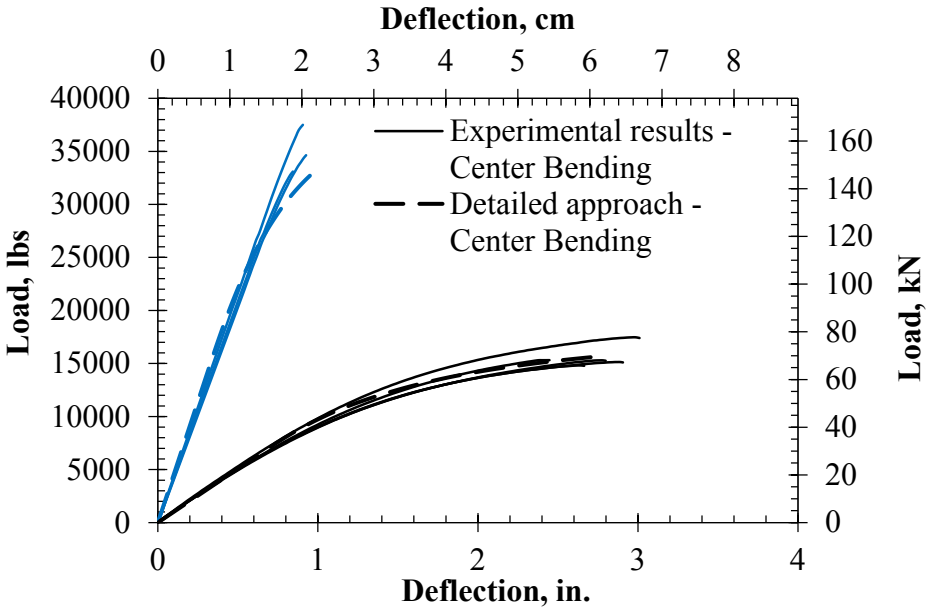

Figure 15. Validation of the center bending model against the test results.

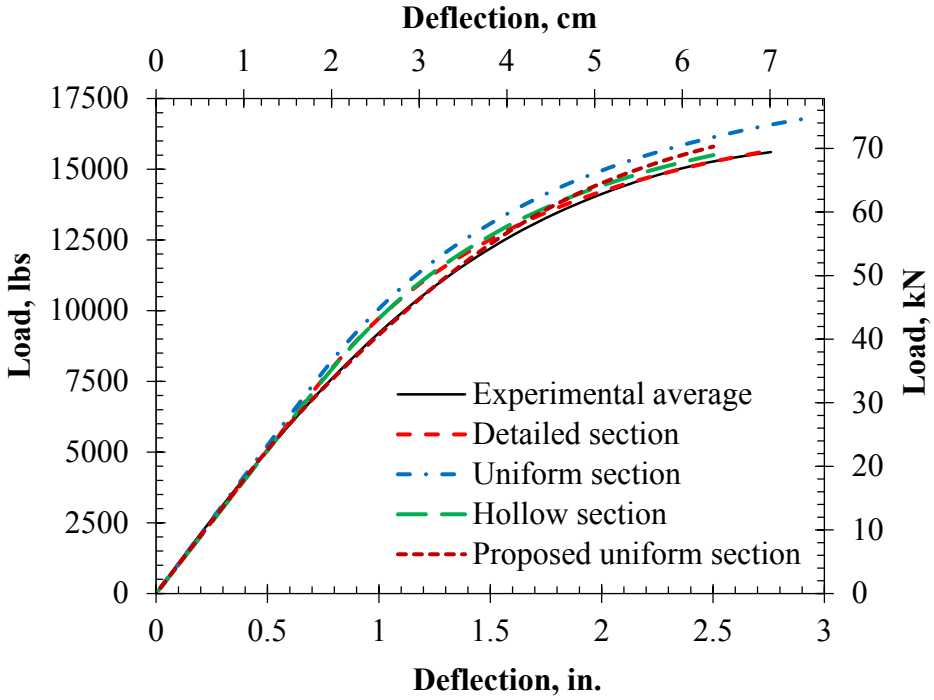

Figure 16. Comparison of the modeling approaches and the experimental data.

The same procedures were employed to develop the average and hollow sections modeling approaches. The upper bound direct tensile material properties yielded the most accurate representation of the crossties flexural behavior. Additionally, a uniform section approach using

slightly lower tensile properties was also considered. Figure 16 presents a comparison between the results of the different modeling approaches and the experimental data.

Inspection of Figure 16 reveals that the detailed approach yielded the closest results to the average of the experimental tests. Moreover, it predicted the failure of the crossties very accurately. On the other hand, the simplified approaches showed slight discrepancy with the experimental average which was expected. Out of the three models, the uniform section with the upper bound direct tensile properties exhibited the most error because it completely neglects the core region. The hollow section approach accounts for the core region and showed better accuracy. The best accuracy out of the simplified models was exhibited by the uniform section with lower tensile properties to account for the core region. Moreover, this approach is the simplest and quickest in terms of model construction and computation time. Finally, seeing as the experimental results exhibited some variations (refer to Figure 5 and 6), all the modeling approaches, excluding the uniform section with the upper bound direct tensile properties, are deemed capable of portraying the crossties flexural behavior with acceptable accuracy.

SECTION 6 SUMMARY AND CONCLUSION

1. The extrusion process employed to manufacture HDPE crossties results in an efficient cross-sectional composition with a strong exterior region (with high concentration fiber reinforcement and low void content); and a core region with no fiber reinforcement. UV inhibitor and anti-oxidants are added to a thin skin layer, which protects the surface of the crosstie. This efficient section yields high bending stiffness and durability while maintaining a low weight of the crosstie. By adjusting the percentage of fiber reinforcement added to the mixture, the stiffness, ductility, and cost can be controlled.
2. All the tested specimens fulfilled and surpassed their corresponding AREMA recommendations, which is indicative of their expected performance.
3. The installation of the rail and fastening system enhanced the performance of the crossties. This was attributed to the load distribution quality of the steel bearing plate and the partial composite action between the crosstie and the steel bearing plate. This observation negates concerns regarding cracks in the vicinity of the pilot holes and agrees with Reiff and Trevizo's findings (32).
4. A detailed, nonlinear, finite element modeling approach accounting for the crossties section composition was achieved and accurately portrayed the flexural behavior and failure of the crossties. This model will be employed in our future, full-scale, investigations. Moreover, a uniform section with equivalent properties was achieved without sacrificing much accuracy and will be used in computational intensive models.

SECTION 7 REFERENCES

1. Ellis DC. Track terminology. In: *British railway track*. England: The Permanent Way Institution; 2001.
2. Zhao J, Chan AHC, Burrow MPN. Reliability analysis and maintenance decision for railway sleepers using track condition information. *Journal of Operational Research Society*. 2007; 58: p. 1047-1055.
3. Goldgaber A. Plastic Railroad Ties: Growing Market for Alternative Materials. *SmallcapInsights.com*. 2009 December 21.
4. Zagier AS. Creosote: 'Witch's Brew. *Naples Daily News*. 2004 May 24.
5. Thierfelder T, Sandstrom E. The creosote content of used railway crossties as compared with European stipulations for hazardous waste. *Science of the Total Environment*. 2008; 402: p. 106-112.
6. Morris T. Poisonous railway sleepers pose health risk. *The Greens Tasmania*. 2008 October.
7. Pruszinski A. Review of the landfill disposal risks and the potential for recovery and recycling of preservative treated timber. South Australia: Sinclair Knight Merz, Environmental Protection Agency Report; 1999.
8. Coffin B. Coalition sues EPA to ban toxic wood preservatives. (Risk Reporter). *Risk Management*. 2003 Februay 1.
9. Hagaman BR, McAlphine RJ. ROA timber sleeper development project. In: *the eight international rail track conference*, Rail Track Association of Australia; 1991. p. 233-237.
10. Zhang YJ, Murray MH, Ferreira L. Modelling of rail track performance: an integrated approach. *Transport Journal*. 2000;: p. 187-194.
11. Yun WY, Ferreira L. Prediction of the demand of the railway sleepers: a simulation model for the replacement strategies. *International Journal of Production Economics*. 2003 January ; 81-82: p. 589–595.
12. Kohoutek R. Dynamic and static performance of interspersed railway track. In: *Railway engineering conference*; 1991; Adelaide, Australia.
13. Smith RL, Shiau RJ. An industry evaluation of the reuse, recycling and reduction of spent CCA wood products. *Forest Products Journal*. 1998 February; 48(2): p. 44.
14. Miura S, Takai H, Uchida M, Fukuda Y. The mechanism of railway tracks. *Japan Rail & Transit Review*. 1998 March; 15: p. 38-45.
15. Cope DL, Ellis JB. Plain line maintenance. In: *British Railway Track*. England: The Permanent Way Institution; 2001.
16. Schut JH. They've Been Working on the Railroad. *Plastics Technology*. 2004 April.
17. Weart W. With a weak economy at the forefront and railroad spending cuts on the horizon, crosstie demand will be restrained for the rest of '09, then drop in '10. *Progressive Railroad*. 2009 October.
18. Jackson LM, Nosker TJ. Technology, Applicability, and the Future of Thermoplastic Lumber. In: *the DoD Corrosion Conference*; 2009.

19. Nosker T, Lutz M, Gillespie B, Van Ness K, Lampoo R. A Performance-Based Approach to the Development of a Recycled Plastic/Composite Crosstie. Report. 1994.
20. Lampoo R, Nosker T, Gillespie B, Schriks R. Performance and Safety Issues Regarding the use of Plastic Composite Crossties. Report. 1997.
21. Manalo A, Aravinthan T, Karunasena W, Ticoal A. A review of alternative materials for replacing existing timber sleepers. *Composite Structures*. 2010; 92: p. 603-611.
22. Adams JCB. Cost effective strategy for track stability and extended asset life through planned sleeper retention. In: *Demand Management of Assets National Conference Publication*; 1991; Australia: Institution of Engineers. p. 145-152.
23. Qiao P, Davalos JF, Zipfel MG. Modelling and optimal design of composite reinforced wood railroad crosstie. *Composite Structures*. 1998 January; 41(1): p. 87–96.
24. Hoger DI. *Fibre composite railway sleepers*. University of Southern Queensland, Toowoomba, Queensland, Australia; 2000.
25. Lampoo R. Recycled-Plastic Composite Railroad Crossties. In: *Construction Innovation Forum*; 2002; Bloomfield Hills, MI.
26. Humphreys MF, Francey KL. An investigation into the rehabilitation of timber structures with fibre composite materials. In: *Developments in Mechanics of Structures and Materials*; 2005; Perth, Western Australia. p. 1317-1322.
27. Shokrieh MM, Rahmat M. On the reinforcement of concrete sleepers by composite. *Composite Structures*. 2006 December; 76(4): p. 326–337.
28. Ticoalu ANE. *Investigation on fibre composite turnout sleepers*. Master of engineering dissertation. University of Southern Queensland, Toowoomba,; 2008.
29. Jimenez R. Vertical Track Modulus in Plastic Composite Ties Test Zones at FAST. Technical Report. Pueblo, CO: Transportation Technology Center, Inc. , U.S. Department of Transportation, Federal Railroad Administration; 2003.
30. Lampo RG, Nosker TJ, Sullivan HW. Development, testing, and applications of recycled-plastic composite cross ties. In: *World Congress on Railway Research*; 2003; Edinburgh, UK.
31. Roybal S. Composite Crosstie Test Cyclic Load. Letter Report No. P-09-003. Pueblo, Colorado: Transportation Technology Center, Inc., Prepared for IntegriCo Composites, LLC; 2009.
32. Reiff , Trevizo C. Cracking and Impact Performance Characteristics of Plastic Composite Ties. Technical Report. Pueblo, CO: Transportation Technology Center, Inc., U.S. Department of Transportation, Federal Railroad Administration; 2012.
33. America Railway Engineering and Maintenance-of-Way Association, Chapter 30, Part 2, Evaluative Tests for Tie Systems. In AREMA Specifications.; 2011.
34. ASTM D790-10: Flexural Properties of Unreinforced and Reinforced Plastics and Electrical Insulating Materials. ASTM International. West Conshohocken, PA. DOI:10.1520/D0790-10; 2010.
35. ASTM D6109-10: Flexural Properties of Unreinforced and Reinforced Plastic Lumber and Related Products. ASTM International. West Conshohocken, PA. DOI:10.1520/D6109-10; 2010.
36. ASTM D638-10: Tensile Properties of Plastics. ASTM International. West Conshohocken,

PA. DOI:10.1520/D0638-10.; 2010.
37. Martinez-Guerrero JN. *Flexural Creep Analysis of Recycled Polymeric*. PhD dissertation. Louisiana State University; 1999 December.

Contacts

Principal Investigator
Mohsen A. Issa
Professor of Civil and Material Engineering
University of Illinois at Chicago
312-996-2426
missa@uic.edu

NURail Center
217-244-4444
nurail@illinois.edu
http://www.nurailcenter.org/

National University Rail Center - NURail
US DOT OST-R Tier 1 University Transportation Center

NURail Project ID: NURail2012-UIC-R02-B

Temperature Effect on the performance of Glass Fiber Reinforced High Density Polyethylene Composite Railroad Crossties

By

Mohsen A. Issa
Professor of Civil and Material Engineering
University of Illinois at Chicago
missa@uic.edu

Ibrahim Lotfy
PhD Student of Civil and Material Engineering
University of Illinois at Chicago
ilotfy2@uic.edu

and

Maen Farhat
PhD Student of Civil and Material Engineering
University of Illinois at Chicago
mfarha3@uic.edu

DISCLAIMER

Funding for this research was provided by the NURail Center, University of Illinois at Urbana - Champaign under Grant No. DTRT12-G-UTC18 of the U.S. Department of Transportation, Office of the Assistant Secretary for Research & Technology (OST-R), University Transportation Centers Program. The contents of this report reflect the views of the authors, who are responsible for the facts and the accuracy of the information presented herein. This document is disseminated under the sponsorship of the U.S. Department of Transportation's University Transportation Centers Program, in the interest of information exchange. The U.S. Government assumes no liability for the contents or use thereof. The content of this document were accepted for publication as "Lotfy I, Farhat M, and Issa M. Temperature Effect on the performance of Glass Fiber Reinforced High Density Polyethylene Composite Railroad Crossties. Journal of Rail and Rapid Transit; In press, accepted for publication on 17 March 2015. DOI: 10.1177/0954409715583384"

TECHNICAL SUMMARY

Title

Temperature Effect on the performance of Glass Fiber Reinforced High Density Polyethylene Composite Railroad Crossties

Introduction

The authors investigated the flexural performance of HDPE composite railroad crossties reinforced with discontinuous randomly distributed glass fibers (7). In this report, the effect of temperature on this performance is presented. Each vital property of the crossties was evaluated and temperature-scaling models were established for exposure conditions within the studied temperature range. The temperatures investigated ranged from 10°F (-12.22°C) to 125°F (51.67°C) which represent typical operating service temperature range. The objective of this report is as follows:

- Understand the temperature effect on the vital properties of HDPE crossties.
- Establish temperature-scaling relationships for use in further investigations and applications.
- Identify potentially susceptible performance criteria under certain exposure conditions.
- Recommend potential solutions based on the findings.
- Identify potential criteria requiring further evaluation and testing.

Approach and Methodology

In order to assess the behavior of the crossties within the temperature range proposed; experimental flexural testing was carried out at different selected temperatures within the range under investigation. Afterwards, temperature-scaling models were established to predict/extrapolate the behavior of the HDPE crossties throughout the entire temperature range. A total of 21 experimental tests were conducted over the investigated temperature range as presented in Table 1. Two additional specimens were tested at 110 and 120°F (43.33 and 48.89°C) after the scaling curves were established to validate their accuracy.

Findings

The crosstie specimens exhibited a similar and consistent trend throughout the program. The same mode of failure, which was a brittle fracture due to mid-span tensile bending stress, was

observed for all the tested crossties. No cracks were observed at any stage of the test until the fracture stage where a single crack was observed at the mid-span accompanied with a pronounced acoustic emission, i.e. loud fracture sound. The fracture was significantly more brittle at lower temperatures as indicated by higher fracture sound and a rougher fracture surfaces compared to higher temperatures. The specimens experienced lower stiffness and higher ductility at high temperature exposure and higher stiffness and lower ductility at low temperature exposure.

Conclusion

- The stiffness and MOR of the crossties increased at low temperature (22% on average) and decreases in elevated temperature (50% on average). Moreover, the ductility of the crossties decreases in low temperature (51% on average) and increases in elevated temperature (52% on average). While this trend was expected, it was interesting to observe that the increase in stiffness at lower temperatures was less pronounced than its decay at higher temperatures.
- A 10 to 12 hour period was required for the core to attain the temperature of the environmental chamber. Therefore the core temperature of the crossties will not vary significantly with normal sun exposure or day and night cycles but rather prolonged seasonal changes. However, this period is not reliable as the, critically stressed, exterior region of the crossties (with the glass fiber reinforcement) will heat up faster than the core.
- The increased ductility at higher temperatures allowed the glass fiber reinforcement to be activated earlier and get stretched and oriented towards the maximum stresses. Thus increasing the percentage of fiber reinforcement is expected to enhance the crosstie's properties at higher temperatures with more efficiency and consistency than at lower temperatures. Moreover, decreasing the content of fiber reinforcement at lower temperature would increase its ductility thus increasing the efficiency of the remaining fiber reinforcement. This notion can be employed to optimize the crossties based on their expected exposure condition.

Publications

- Lotfy I, Farhat M, and Issa M A, "**Temperature Effect on the performance of Glass Fiber Reinforced High Density Polyethylene Composite Railroad Crossties**" Journal of Rail and Rapid Transit; In press, accepted for publication on 17 March 2015.

Contacts

Principal Investigator
Mohsen A. Issa
Professor of Civil and Material Engineering
University of Illinois at Chicago
312-996-2426
missa@uic.edu

NURail Center
217-244-4444
nurail@illinois.edu
http://www.nurailcenter.org/

TABLE OF CONTENTS

LIST OF FIGURES

SECTION 1 INTRODUCTION

The effect of temperature on structural materials has always been a concern in engineering applications. Thermoplastic composites, in general, are highly sensitive to temperature changes and recycled high density polyethylene (HDPE) is no different. Even the best designed HDPE compositions will experience variations in mechanical properties as a result of temperature variation. Thermoplastic materials usually experience lower modulus of elasticity and higher ductility at high temperature condition and higher modulus of elasticity and lower ductility at low temperature condition. Therefore, it is of vital importance to study and fully understand the nature and extent of this effect. This knowledge will enable the safe implementation of these materials in structural applications where low or elevated temperature exposure is expected.

Several researchers have investigated the effect of temperature on the properties of polymers and plastic composite materials and membranes (1, 2 and 3). Alkan, et al., investigated the effect of temperature on the mechanical and electrical properties of HDPE manufactured using hot pressing technique (3). They evaluated the tensile strength, elongation percent, modulus of elasticity and electrical properties of unreinforced HDPE and HDPE with glass fiber reinforcement; moreover, they demonstrated that the 0.5% glass fiber reinforcement significantly enhanced the mechanical properties of HDPE composite when compared to unreinforced HDPE (3).

Additionally, the size and shape of the HDPE member affects the extent of the temperature influence on its properties. Therefore, it is important to investigate the effect of temperature specifically on HDPE composite railroad crossties. The following studies strived to assess this effect on the performance of plastic composite crossties. Jimenez conducted two experimental tests to evaluate the effect of both plastic and wooden crossties on the vertical track modulus in curved tracks (4). The effect of temperature on the dynamic modulus was also evaluated. He concluded that the plastic crosstie showed acceptable results and relatively higher track modulus than that of their wooden counterpart (4). Lampo, et al., investigated the performance of the composite crossties through several laboratories and field testing (5). No experimental evaluation of the temperature effect on HDPE was conducted. However, they expressed concerns regarding the temperature variation effect on the spike holding power; i.e. fatigue stresses generated due to the difference in the thermal expansions between the plastic crossties and steel spikes could result in spike workout and loosening over time (5).

Reiff and Trevizo studied the effect of several factors on the performance of three types of plastic composite crossties including temperature variation (6). They evaluated the flexural

behavior of the crossties at different temperatures: -25°F (-31.67°C), 80°F (26.67°C), and 120°F (48.89°C). They observed higher flexural stiffness at -25°F (-31.67°C). They also demonstrated that HDPE crossties reinforced with glass fibers showed better performance than the other two plastic composite types evaluated. Moreover, they conducted impact testing, at -25°F (-31.67°C) temperature, where only the HDPE crossties reinforced with glass fibers survived 10 impacts without the rail and fastening system installed. Overall, they observed acceptable performance for the plastic composite crossties when compared to wooden (oak) crossties (6).

As evident from the past studies, the temperature effect on the properties and performance of the HDPE composite crossties is not fully developed yet. HDPE reinforced with glass fibers demonstrated the best crosstie performance so far when subjected to temperature variations. Additional research is needed to properly characterize, describe, and optimize the behavior of these materials. This knowledge can be used to assess the safety of implementing these materials in railroad applications where low or elevated temperature exposure is expected.

SECTION 2 RESEARCH OBJECTIVES

The University of Illinois at Chicago conducted a series of studies to assess the feasibility of implementing HDPE crossties in both conventional and high speed rail (HSR) applications. The authors investigated the flexural performance of HDPE composite railroad crossties reinforced with discontinuous randomly distributed glass fibers (7). In this report, the effect of temperature on this performance is presented. Each vital property of the crossties was evaluated and temperature-scaling models were established for exposure conditions within the studied temperature range. The temperatures investigated ranged from 10°F (-12.22°C) to 125°F (51.67°C) which represent typical operating service temperature range. The objective of this report is as follows:

- Understand the temperature effect on the vital properties of HDPE crossties.
- Establish temperature-scaling relationships for use in further investigations and applications.
- Identify potentially susceptible performance criteria under certain exposure conditions.
- Recommend potential solutions based on the findings.
- Identify potential criteria requiring further evaluation and testing.

SECTION 3 HDPE CROSSTIES' COMPOSITION

The temperature effect on the mechanical properties of HDPE is highly influenced by its composition; e.g. type of polymer, presence of voids or reinforcing elements, the manufacturing process, component size, etc. In this study, the HDPE composite crossties evaluated were fabricated from recycled plastic waste; milk and detergent bottles; which 7.2 billion pounds (3.27 billion kilograms) of these bottles are land filled each year in the US (8). The crossties were produced using an extrusion process where reinforcing glass fibers were mixed with the hot polymer mixture and extruded through a forming die. Foam inducing agents were introduced in the mixture to create air bubbles in the center of the cross section and push the reinforcing glass fibers to the exterior region of the cross section. Finally, UV inhibitors and anti-oxidants were also added to a thin skin surface layer to protect the surface of the crossties. The resulting crossties are HDPE composites reinforced with discrete, discontinuous, randomly distributed glass fibers in the exterior region and have sectional dimensions of 9 × 7 in. (22.86 × 17.78 cm) and total lengths of 8 to 9 ft (2.44 to 2.74 m). This process allows for the fabrication of an efficient cross section with optimum distribution of the reinforcing fibers and minimal weight. The average density of the tested crossties was recorded as 56.8 pcf (910 kg/m3). However, this process also creates a difference in the mechanical and thermal properties between the core and exterior regions of the cross section. Figure 1 shows the HDPE composite crosstie specimens before testing at the UIC structural laboratories and illustrates their cross-sectional composition.

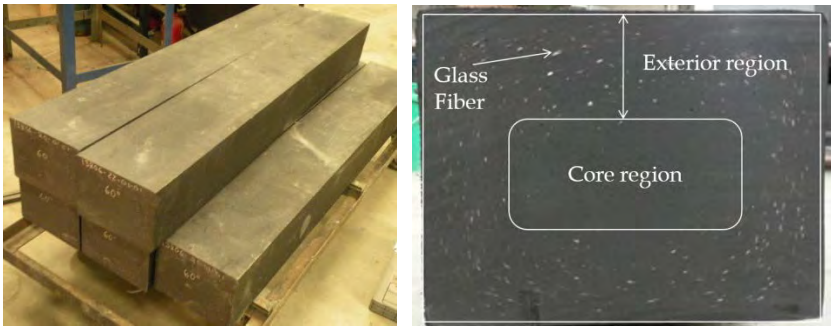

Figure 1. Fiber reinforced HDPE composite crosstie specimens.

SECTION 4 EXPERIMENTAL PROGRAM

In order to assess the behavior of the crossties within the temperature range proposed; experimental flexural testing was carried out at different selected temperatures within the range under investigation. Afterwards, temperature-scaling models were established to predict/extrapolate the behavior of the HDPE crossties throughout the entire temperature range. A total of 21 experimental tests were conducted over the investigated temperature range as presented in Table 1. Two additional specimens were tested at 110 and 120°F (43.33 and 48.89°C) after the scaling curves were established to validate their accuracy.

Table 1. Testing schedule.

Temperature		Number of tests
°F	°C	
10	-12.22	4
40	4.44	3
70	21.11	5
100	37.78	3
125	51.67	4
110*	43.33*	1*
120*	48.89*	1*

* Two additional tests were conducted at 110 and 120°F (43.33 and 48.89°C) after the scaling curves were established to validate their accuracy.

4.1 Temperature Control

To achieve these exposure conditions, the crosstie specimens were placed in a sophisticated "Hotpack" controlled environmental chamber, at the University of Illinois at Chicago structural laboratories, to simulate the desired temperature prior to the testing. The temperature of the chamber was also rechecked using a digital "Weiss" thermometer for redundancy. The temperature of the crosstie specimens was monitored using another infrared "Omega" thermometer. In order to determine the temperature inside the core of the crosstie specimens, temperature-sensing probes (type-K thermocouples) were installed inside all the crosstie specimens as illustrated in Figure 2. The test was conducted when the four temperature monitoring thermometers displayed the desired testing temperature. Seeing as the plastic HDPE material is an insulating material, the specimens needed to be kept overnight in the environmental chamber to ensure that the temperature inside the core of the crosstie reached the desired testing temperature. A 10 to 12 hour period was required for the core temperature to reach the temperature of the environmental chamber. This observation is significant as it implies

that, in actual railroad applications, the temperature inside the core of the crossties will not vary significantly with normal sun exposure or day and night cycles but rather seasonal changes and prolonged periods of temperature exposure. However, the 10 to 12 hours period is not reliable as the, critically stressed, exterior region of the crossties (with the glass fiber reinforcement) will heat up faster than the core. After the test was conducted, the core temperature of the specimens was recorded again at the broken plain of the crosstie, using the infrared "Omega" thermometer, to ensure that the temperature of the core did not vary significantly as illustrated in Figure 5. In all cases, the core temperature after failure was within ±3°F (±1.67°C) of the desired testing temperature.

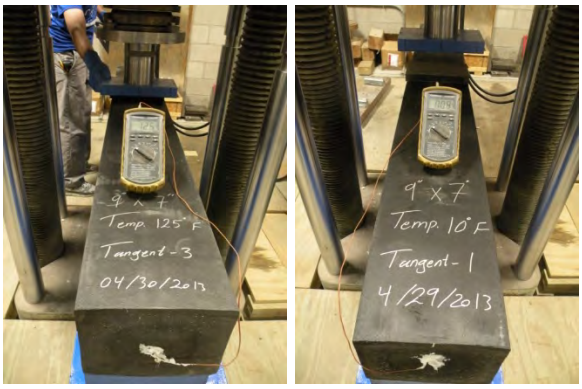

Figure 2. Measuring the core temperature using sensing probes (type-K thermocouples).

In this program, a three-point bending test configuration was adopted following the AREMA recommendations, Part 2- Section 2.2.3 – Test 1C (9). A concentrated load in the middle of the 60 in. (152.4 cm) span was applied using an automated hydraulic system. A rigid reaction steel testing frame was used to support the specimens. An elastomeric bearing pad of 5.5 × 9 × 1 in. (14 × 22.9 × 2.5 cm) was used under the loading plate and two other bearing pads of 2 × 9 × 1 in. (5.1 × 22.9 × 2.5 cm) were used at the support locations. All the specimens were loaded until failure with a stroke controlled rate of 1.0 in./min (2.54 cm/min). Figure 3 shows the testing setup and bending of the specimen under the applied load while Figure 4 presents the mode of failure and cracking pattern observed for all crosstie specimens. As mentioned earlier, after the test was conducted, the core temperature of the specimens was recorded again at the broken plain of the crosstie to ensure that the core temperature did not vary significantly as illustrated in Figure 5.

Figure 3. Testing of the HDPE crossties under different temperatures.

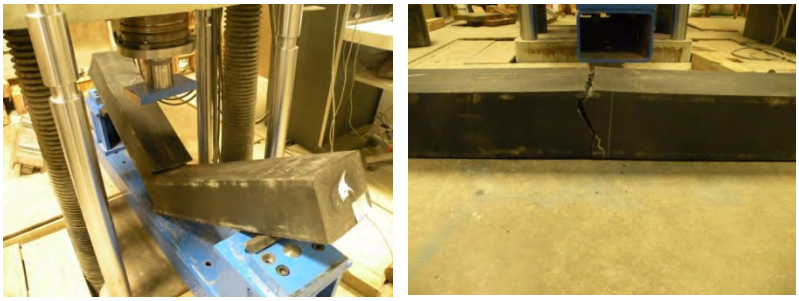

Figure 4. Mode of failure of the HDPE crosstie specimen.

Figure 5. Measuring the core temperature after failure.

4.2 Testing procedures and Results

The load and mid-span deflection measurements were recorded for each specimen. The stress-strain curves were plotted to determine the flexural strength, modulus of rupture (MOR), elasticity and secant modulus as per AREMA recommendations (9) as well as the ASTM standards D790 (10). Whenever necessary, toe compensation was performed in accordance with Annex A1 of the ASTM standards D790 to overcome the artificial effects caused by a take-up of slack and alignment or seating of the specimens. The Initial/Tangent Modulus is described as the initial slope to the steepest initial straight-line portion of the load-deflection. The AREMA manual recommends the MOE using the slope of the stress-strain curve at a point where the applied stress is 600 psi (4.14 MPa). The ASTM D6109 recommends the Secant Modulus using the slope of the stress-strain curve at a point where the applied strain is 1% (11). All the

specimens exhibited the same trend; they underwent an almost linear initial stage followed by a non-linear stress-strain relationship. Tables 2 to 6 summarize the results of all the tested specimens for all the temperatures in the range investigated.

Table 2. Summary of the crossties' test results at 10°F (-12.22°C).

Specimen No.	1	2	3	4	Average	St. Dev.	Percent of 70°F
MOR, psi	3,400	2,932	3,764	3,650	3,185	369	108%
Ultimate Strain, με	14,457	13,130	17,443	17,733	32,257	2,260	49%
Initial Tangent, psi	237,756	225,054	223,788	217,584	190,151	8,462	119%
Modulus at 600 psi (4.14 MPa), psi	237,080	224,583	222,727	216,869	183,228	8,505	123%
Modulus at 1% strain, psi	236,064	224,407	222,502	216,833	166,205	8,076	135%

1 psi = 6.9 kPa

Table 3. Summary of the crossties' test results at 40°F (4.44°C).

Specimen No.	1	2	3	Average	St. Dev.	Percent of 70°F
MOR, psi	3,603	3,851	2,781	3,412	560	107%
Ultimate Strain, με	21,063	21,346	15,898	19,436	3,067	60%
Initial Tangent, psi	189,937	196,467	179,967	188,790	8,309	99%
Modulus at 600 psi (4.14 MPa), psi	189,173	195,194	179,574	187,981	7,878	103%
Modulus at 1% strain, psi	189,001	194,528	179,407	187,646	7,651	113%

1 psi = 6.9 kPa

Table 4. Summary of the crossties' test results at 70°F (21.11°C) [reference point].

Specimen No.	1	2	3	4	5	Average	St. Dev.
MOR, psi	3,122	3,024	3,089	3,125	3,566	3,185	217
Ultimate Strain, με	32,643	31,080	33,903	28,548	35,111	32,257	2,557
Initial Tangent, psi	188,442	182,569	190,056	193,340	196,347	190,151	5,220
Modulus at 600 psi (4.14 MPa), psi	185,107	180,356	178,323	180,026	192,330	183,228	5,678
Modulus at 1% strain, psi	163,137	163,500	161,659	166,238	176,492	166,205	5,984

1 psi = 6.9 kPa

Table 5. Summary of the crossties' test results at 100°F (37.78°C).

Specimen No.	1	2	3	4	Average	St. Dev.	Percent of 70°F
MOR, psi	2,386	2,491	2,317	2,681	2,469	158	78%

Ultimate Strain, με	50,683	41,175	47,424	73,486	46,427	4,832	144%
Initial Tangent, psi	114,181	136,662	129,079	132,488	128,102	9,786	67%
Modulus at 600 psi (4.14 MPa), psi	113,750	131,340	124,671	128,611	124,593	7,729	68%
Modulus at 1% strain, psi	109,629	119,528	111,671	114,589	113,854	4,295	69%

1 psi = 6.9 kPa

Table 6. Summary of the crossties' test results at 125°F (51.67°C).

Specimen No.	1	2	3	4	Average	St. Dev.	Percent of 70°F
MOR, psi	1,772	1,804	1,806	1,888	1,818	49	57%
Ultimate Strain, με	50,015	48,271	49,039	49,132	49,114	714	152%
Initial Tangent, psi	83,262	85,384	85,935	88,966	85,887	2,354	45%
Modulus at 600 psi (4.14 MPa), psi	82,953	84,866	85,662	88,690	85,543	2,386	47%
Modulus at 1% strain, psi	81,296	82,522	83,584	86,161	83,391	2,070	50%

1 psi = 6.9 kPa

It should be noted that specimen 4 tested at 100°F (37.78°C) exhibited extraordinary ductility and failed after 6.3 in. (16.1 cm) of deflection (refer to Table 5); consequently it was considered as an outlier and eliminated from subsequent calculations.

4.3 Discussion and test observations

The crosstie specimens exhibited a similar and consistent trend throughout the program. The deflection increased monotonically with the increase in load. After a certain point, a small increase in load resulted in a significant increase in deflection. The same mode of failure, which was a brittle fracture due to mid-span tensile bending stress, was observed for all the tested crossties, refer to Figure 4. No cracks were observed at any stage of the test until the fracture stage where a single crack was observed at the mid-span accompanied with a pronounced acoustic emission, i.e. loud fracture sound. The fracture was significantly more brittle at lower temperatures as indicated by higher fracture sound and a rougher fracture surfaces compared to higher temperatures.

Inspection of Tables 2 to 6 confirms the expected temperature effect on the properties of HDPE crossties. The specimens experienced lower stiffness and higher ductility at high temperature exposure and higher stiffness and lower ductility at low temperature exposure. Considering the room temperature; i.e. 70°F (21.11°C), as a reference temperature, at 125°F (51.67°C)

temperature, the specimens experienced an increase of about 52% in ductility and a reduction of about 50% in the stiffness. However, at 10°F (-12.22°C), they experienced a reduction of about 51% in ductility and an increase of 22% in the stiffness. To better illustrate the temperature effect on the performance of the crossties, all the tested specimens were plotted on the same graph, as presented in Figure 6.

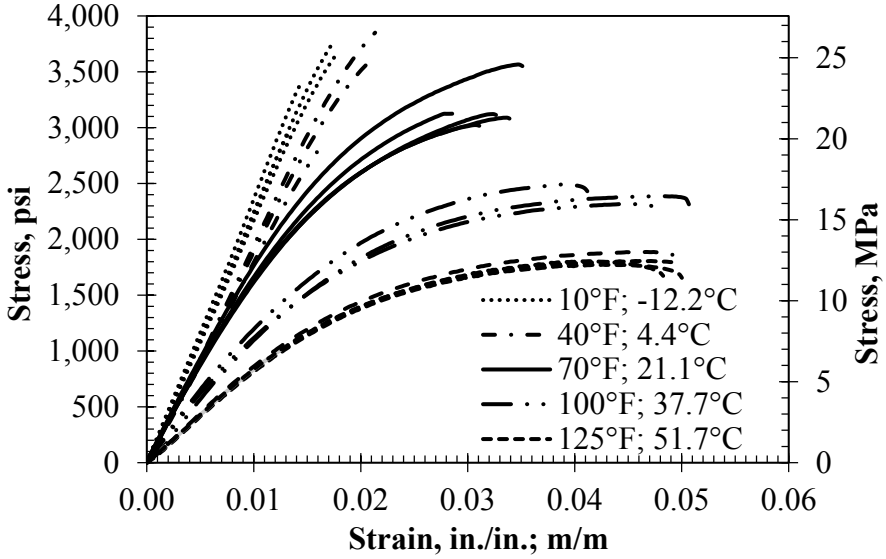

Figure 6. Temperature effect on the HDPE material compliance.

Inspection of Figure 6 clearly confirms the change in the material compliance due to temperature variations. At low temperature, the stress-strain relationship is almost linear exhibiting high stiffness and lower ductility and vice versa for higher temperatures. Figure 6 also illustrates the relative gain and loss of stiffness and ductility considering room temperature as a reference point; the increase in stiffness (slope of the straight-line portion of the stress strain curve) at lower temperature is significantly less than the reduction in stiffness at higher temperature. As noticed the stiffness reduction is relatively small from 10°F (-12.22°C) to 70°F (21.11°C). However, the stiffness reduction is more pronounced from 70°F (21.11°C) to 125 F (51.67 C). It is apparent that the optimum stiffness and ductility performance occur at 70°F (21.11°C) for this particular HDPE mixture composition. Figure 7 present the average ultimate strains reached for each temperature.

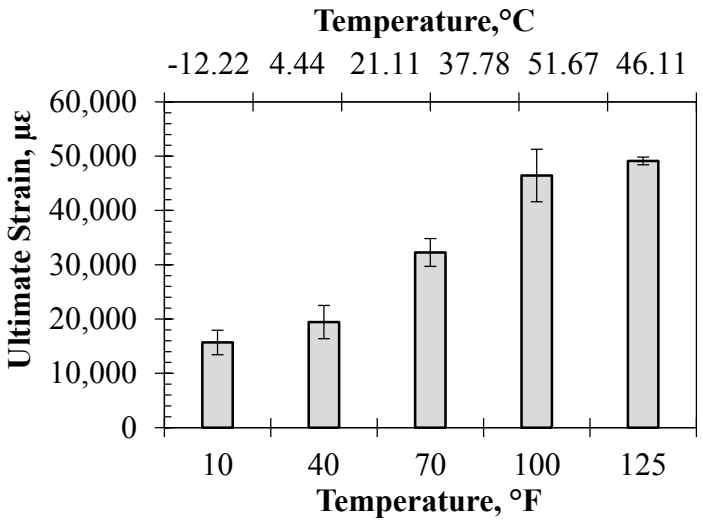

Figure 7. Ultimate strain for the different temperatures.

The ultimate strain at failure provides an indication of the ductility of the specimens. As noticed from Figure 7, the ultimate strain increases with the temperature increase. The obtained results were consistent (as indicated by the error bars) for all temperature except at 100°F (37.78°C) where the variations in the ultimate strains were higher even after excluding the outlier; specimen 4. Figure 8 presents the average modulus of rupture attained for each testing temperature.

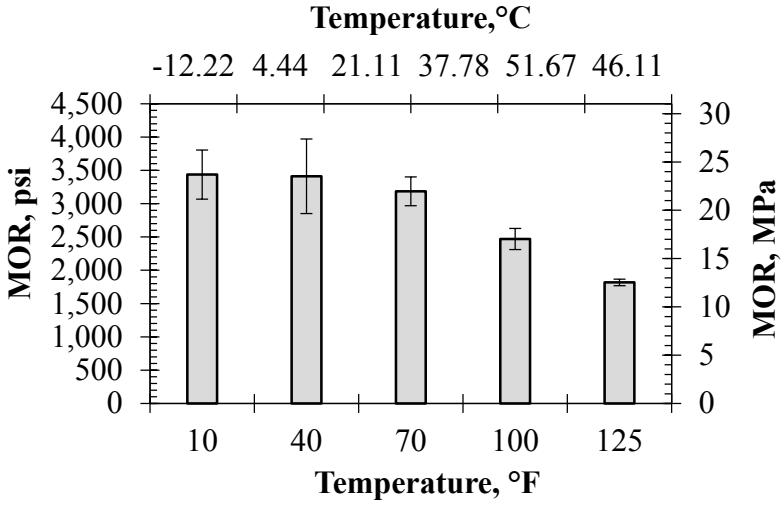

Figure 8. MOR for the different temperatures.

Figure 8 indicates that the MOR; ultimate stress withstood before failure, decreases with the temperature increase. As noticed earlier, when considering the relative gain and loss of MOR relative to room temperature; the increase in MOR at lower temperatures is significantly less than the reduction at higher temperatures. In other words, the MOR reduction is small from 10°F

(-12.22°C) to 70°F (21.11°C), however, it is more pronounced from 70°F (21.11°C) to 125°F (51.67°C). Another observation to note is the variation in the results obtained. The variations are high at lower temperatures, which were observed earlier. However, it decreases significantly with the increase in temperature. At 125°F (51.67°C) there is almost no variation in the ultimate stress attained before failure. This observation is significant and it was noticed in several criteria other than the MOR. This observation is believed by the author to be attributed to the increased ductility of the crossties specimens. Initially the glass fiber reinforcements are randomly scattered in the specimens with random orientations. At lower temperatures, the MOR is determined by the strength of the randomly orientated glass fiber reinforcement thus increasing the variations in the results. However, at higher temperatures, the increased ductility of the specimens allows the glass fiber reinforcement to be activated earlier and be stretched and oriented towards the maximum stresses. At failure, a larger portion of the glass fiber reinforcement will be oriented in the maximum stresses direction, which, in turn, increases the consistency of the results. This was a reproducible observation that was noticed throughout the testing program. The significance of this observation is that at higher temperatures, the stiffness of the HDPE crossties is decreased; however, it is using the glass fiber reinforcement more efficiently than at lower temperatures. Therefore, increasing the percentage of fiber reinforcement is expected to enhance the crosstie properties at higher temperatures with more efficiency and consistency than at lower temperatures. Moreover, decreasing the percentage of fiber reinforcement at lower temperature would decrease the stiffness of the crosstie and increase its ductility (as the HDPE material is more ductile that the glass fibers) and thus increasing the efficiency the remaining fiber reinforcement. As noticed from Figure 6, this composition is optimized for operation at 70°F (21.11°C), at low temperature it is too brittle and at high temperature it is too ductile. It is believed that optimizing the fiber reinforcement content can enhance the performance of the crossties at low and elevated temperatures; however, more testing is needed to confirm this notion. Figure 9 presents the average initial tangent, elastic (AREMA recommendations) and secant (ASTM specifications) moduli recorded for each testing temperature.

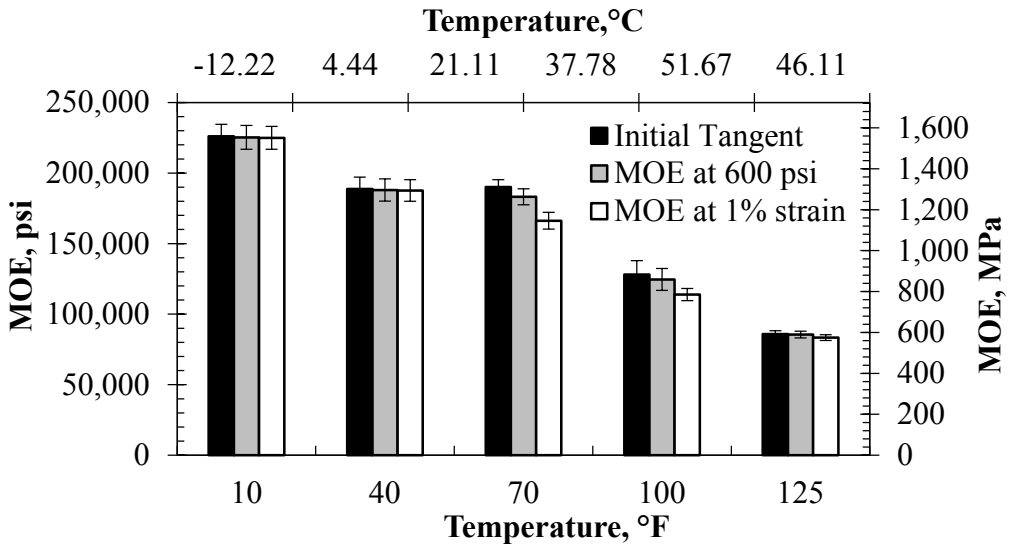

Figure 9. Tangent, secant and elasticity moduli for the different temperatures.

Inspection of Figure 9 reveals that the elasticity moduli decrease with the temperature increase. Moreover, the initial tangent, MOE at 600 psi (4.14 MPa) and secant modulus at 1% strain are almost identical at low and elevated temperatures. This observation occurred because at low temperatures the compliance is almost a straight line resulting in equal moduli. However, at high temperatures, the identical moduli along with the very low variations in the results support the aforementioned notion and the consistency in the stiffness and resistance of the HDPE crossties obtained at high ductility.

Using the acquired experimental data, a linear regression scheme was employed to establish the temperature scaling curves. Each curve is accompanied with its formula. The goodness of fit of each curve was determined using the coefficient of determination "R2" with a perfect fit is equivalent to R2=1.0.

To further validate the scaling curves, two additional tests were performed at 110°F (43.33°C) and 120°F (48.89°C) and checked against the aforementioned curves. Table 7 summarizes the results of the two additional crosstie specimens.

Table 7. Summary of the crossties' test results at 110°F (43.33°C) and 120°F (48.89°C).

Temperature, °F(°C)	110°F (43.33°C)	Percent of 70°F (21.11°C)	120°F (48.89°C)	Percent of 70°F (21.11°C)
MOR, psi	2,364	74%	1,987	62%
Ultimate Strain, με	54,256	168%	48,423	150%
Initial Tangent, psi	146,761	77%	103,280	54%
MOE at 600 psi (4.14 MPa), psi	137,286	75%	101,776	56%

Modulus at 1% strain, psi	118,055	71%	95,298	57%

1 psi = 6.9 kPa

The results obtained in Table 7 were within the expected range, apart from the ultimate strain at 110°F (43.33°C) which was larger than expected. Unfortunately, no additional specimens were available for further testing at these two temperatures. Figures 10 through 14 present the temperature scaling curves for each of the parameters under investigation and the two additional testing results obtained with the established temperature scaling curves for each of the investigated criteria.

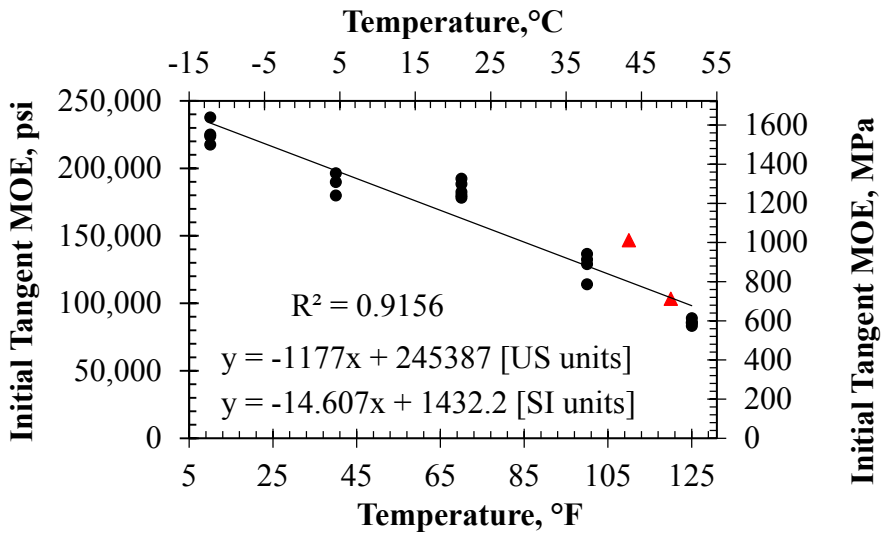

Figure 10. Temperature scaling curve for the initial tangent modulus.

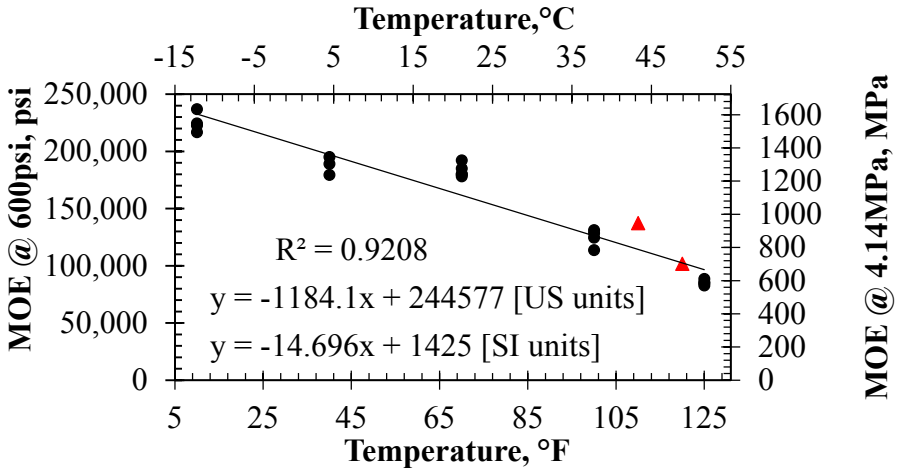

Figure 11. Temperature scaling curve for the modulus of elasticity at 600 psi (4.14 MPa).

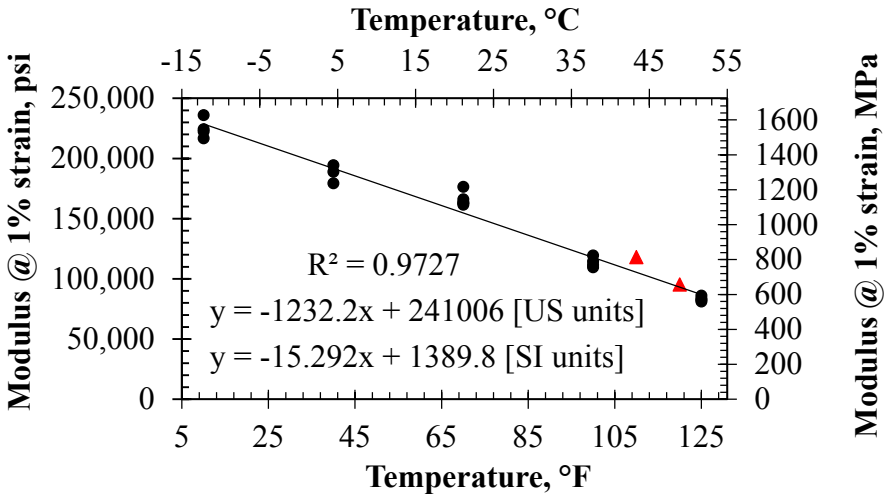

Figure 12. Temperature scaling curve for the secant modulus at 1% strain.

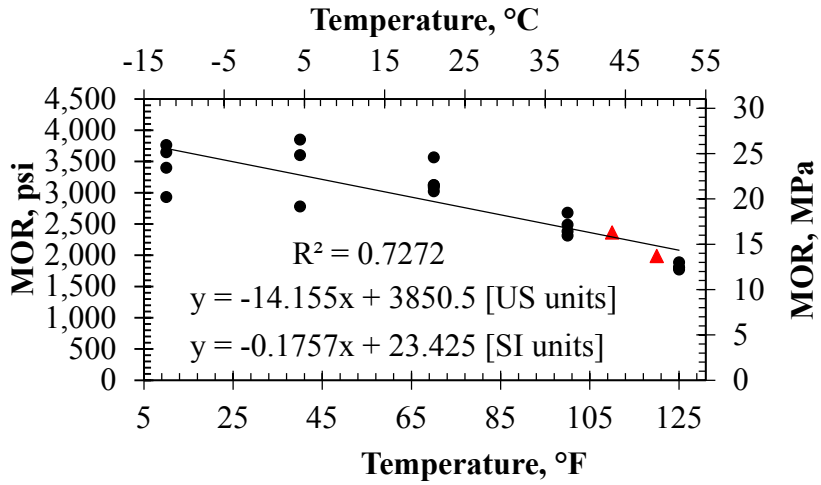

Figure 13. Temperature scaling curve for the MOR.

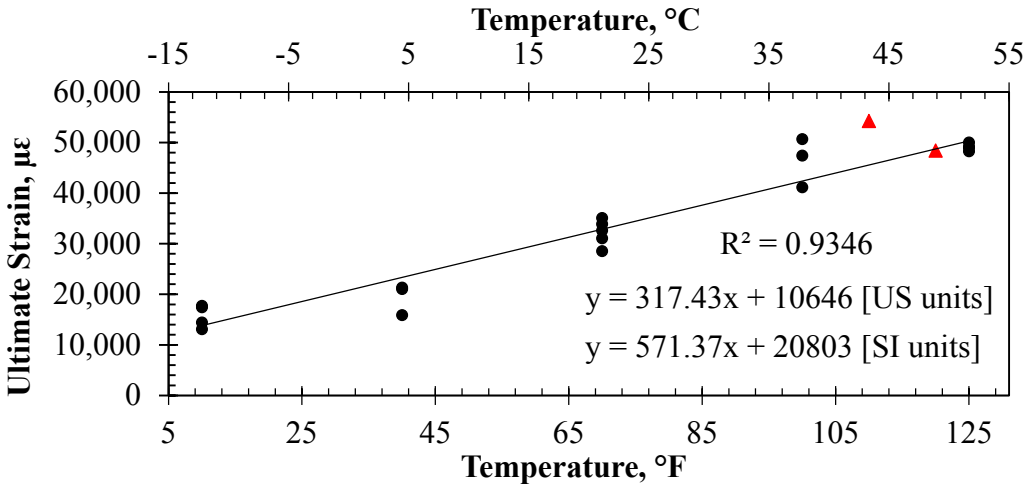

Figure 14. Temperature scaling model for the ultimate strain.

Inspection of Figures 10 to 14 reveals that all the scaling curves established exhibited satisfactory goodness of fit providing a great level of confidence (above 90%) for all the criteria under investigation except for the MOR criterion (73%). Fracture of materials typically is a, difficult to predict, stochastic phenomenon which is the reason behind the high variation in the failure stress results and the poor MOR scaling curve. The secant modulus at 1% strain provided the most consistent and accurate results, and thus have the best fitting scaling curve with above 97% confidence level. These curves can be used to predict the behavior of the crossties when subjected to any arbitrary temperature within the investigated range. Additional testing would strengthen the validity of these curves further especially for poor fitting criteria. The curves were assumed to scale linearly with the temperature, which is an acceptable assumption considering the goodness of fits obtained however, more testing and research is needed to confirm this assumption.

As noticed, the two additional experimental results showed good agreement with the established temperature scaling curves. Unfortunately, no additional specimens were available for further testing at other temperatures. The only major discrepancy was observed for the ultimate strain and initial tangent at 110°F (43.33°C). As noticed from Figure 12, the secant modulus at 1% strain provided the most consistent and accurate results. The results obtained strengthen the notion expressed earlier as the results of the testing at high temperature showed great agreement with and almost perfect fit with the curve in all criteria.

SECTION 5 CONCLUSION AND RECOMMENDATIONS

- The stiffness and MOR of the crossties increased at low temperature (22% on average) and decreases in elevated temperature (50% on average). Moreover, the ductility of the crossties decreases in low temperature (51% on average) and increases in elevated temperature (52% on average). While this trend was expected, it was interesting to observe that the increase in stiffness at lower temperatures was less pronounced than its decay at higher temperatures.
- The fracture energy was significantly larger at lower temperatures as indicated by louder fracture sound and a rougher fracture surfaces compared to higher temperatures.
- A 10 to 12 hour period was required for the core to attain the temperature of the environmental chamber. Therefore the core temperature of the crossties will not vary significantly with normal sun exposure or day and night cycles but rather prolonged seasonal changes. However, this period is not reliable as the, critically stressed, exterior region of the crossties (with the glass fiber reinforcement) will heat up faster than the core.
- Additional information/testing is required in order to assess the performance of the HDPE crossties when subjected to prolonged exposure to UV light waves from the sun or thermal fatigue from repeated day and night cycles. However this effect is secondary as observed during the testing performed by Lampo, et al., (5); a degradation rate of 0.003 in (0.0076 cm) per year was observed and no significant degradation after 15 years of exposure. Additionally, the crosstie's surface exposure to UV radiation is minimal and the inclusion of UV inhibitors to the skin layer would limit its degradation.
- The increased ductility at higher temperatures allowed the glass fiber reinforcement to be activated earlier and get stretched and oriented towards the maximum stresses. Thus increasing the percentage of fiber reinforcement is expected to enhance the crosstie's properties at higher temperatures with more efficiency and consistency than at lower temperatures. Moreover, decreasing the content of fiber reinforcement at lower temperature would increase its ductility thus increasing the efficiency of the remaining fiber reinforcement. This notion can be employed to optimize the crossties based on their expected exposure condition.
- The temperature scaling relationships were able to predict the performance of the crossties with reasonable accuracy at arbitrary exposure temperatures within the investigated range.
- The secant modulus at 1% strain criterion provided the most consistent and accurate results, and thus have the best fitting scaling curve with above 97% confidence level. This could be the reason driving the plastic manufacturers to employ it as a characteristic defining criterion.

- The test results were accurate and consistent for all temperatures with the exception of a few oddities. Additional testing and wider temperature range investigation would strengthen the results obtained in this program and refine the temperature scaling relationships.

SECTION 6 REFERENCES

1. Boydag FS, Özcanlı L, Alekberov VA, Hikmet I. Temperature and time dependence of electrical and mechanical durability of LDPE/diamond composites. Journal of Composites, Part B: Engineering. 2006; 37: p. 249–254.
2. Rowe RK, Abdelaal FB, Islam MZ, Hsuan YG. The strange effect of increasing temperature in accelerated ageing of HDPE geomembranes immersed in liquids. In; 2010; Brazil: 9th International Conference on Geosynthetics.
3. Alkan U, Özcanlı Y, Alekberov V. Effect of Temperature and Time on Mechanical and Electrical Properties of HDPE/Glass Fiber Composites. Journal of Fibers and Polymers. 2013; 14: p. 115-120.
4. Jimenez R. Vertical Track Modulus in Plastic Composite Ties Test Zones at FAST. Technical Report. Report no. DOT/FRA/ORD-03/13. Pueblo, CO: Transportation Technology Center, Inc., U.S. Department of Transportation, Federal Railroad Administration; 2003.
5. Lampo RG, Nosker TJ, Sullivan HW. Development, testing, and applications of recycled-plastic composite cross ties. In World Congress on Railway Research; Scotland, Edinburgh, UK, 28 September to 1 October 2003.
6. Reiff R and Trevizo C. Cracking and Impact Performance Characteristics of Plastic Composite Ties. Technical Report. Report no. DOT/FRA/ORD-12/03. Pueblo, CO: Transportation Technology Center, Inc., U.S. Department of Transportation, Federal Railroad Administration; 2012.
7. Lotfy I, Farhat M, Issa M, and Al-Obaidi M. Flexural behavior of high-density polyethylene railroad crossties. Journal of Rail and Rapid Transit; accepted for publication on 17 November 2014. DOI: 10.1177/0954409714565655.
8. Goldgaber A. Plastic Railroad Ties: Growing Market for Alternative Materials. SmallcapInsights.com. 2009, accessed 5 May 2014.
9. America Railway Engineering and Maintenance-of-Way Association (AREMA) manual for railway engineering, Chapter 30, Part 2, Evaluative Tests for Tie System, 2006, pp.30-I to 30-A-14. Lanham, MD, USA
10. American Society for Testing and Materials (ASTM) D790-10: Flexural Properties of Unreinforced and Reinforced Plastics and Electrical Insulating Materials. ASTM International. West Conshohocken, PA. DOI:10.1520/D0790-10; 2010.
11. American Society for Testing and Materials (ASTM) D6109-10: Flexural Properties of Unreinforced and Reinforced Plastic Lumber and Related Products. ASTM International. West Conshohocken, PA. DOI:10.1520/D6109-10; 2010.

National University Rail Center - NURail
US DOT OST-R Tier 1 University Transportation Center

NURail Project ID: NURail2012-UIC-R02-C

Effect of Pre-drilling, Loading Rate and Temperature Variation on the Behavior of Railroad Spikes used for High Density Polyethylene Crossties

By

Mohsen A. Issa
Professor of Civil and Material Engineering
University of Illinois at Chicago
missa@uic.edu

Ibrahim Lotfy
PhD Student of Civil and Material Engineering
University of Illinois at Chicago
ilotfy2@uic.edu

and

Maen Farhat
PhD Student of Civil and Material Engineering
University of Illinois at Chicago
mfarha3@uic.edu

DISCLAIMER

Funding for this research was provided by the NURail Center, University of Illinois at Urbana - Champaign under Grant No. DTRT12-G-UTC18 of the U.S. Department of Transportation, Office of the Assistant Secretary for Research & Technology (OST-R), University Transportation Centers Program. The contents of this report reflect the views of the authors, who are responsible for the facts and the accuracy of the information presented herein. This document is disseminated under the sponsorship of the U.S. Department of Transportation's University Transportation Centers Program, in the interest of information exchange. The U.S. Government assumes no liability for the contents or use thereof. The content of this document are currently under review for publication as "Lotfy I, Farhat M, and Issa M. Effect of Pre-drilling, Loading Rate and Temperature Variation on the Behavior of Railroad Spikes used for High Density Polyethylene Crossties. Journal of Rail and Rapid Transit; In review"

National University Rail Center - NURail
US DOT OST-R Tier 1 University Transportation Center

TECHNICAL SUMMARY

Title

Effect of Pre-drilling, Loading Rate and Temperature Variation on the Behavior of Railroad Spikes used for High Density Polyethylene Crossties

Introduction

The study encompassed comprehensive experimental investigations and analytical finite element modeling. The testing program evaluated the railroad spikes using static testing methods recommended by the AREMA manual. These tests addressed the railroad spike pullout and lateral restraint for both screw and cut spikes. Then, an analytical finite element model was constructed using the existing and obtained testing results to accurately portray the railroad spike behavior and interactions with the HDPE crosstie. This model will be used for future, full-scale, investigations beyond the scale of laboratory experiments. The objective of this report is as follows:

- Understand the behavior of rail spikes under pure pullout forces and their interactions with the HDPE crosstie.
- Assess the effect of temperature, rate of loading and type of spike on the spike pullout behavior.
- Investigate the behavior of rail spikes when subjected to lateral forces.
- Develop an accurate finite element modeling techniques, which accurately portray the behavior of the fastening system using the experimental data.

Approach and Methodology

- The spike pullout test was performed as per the AREMA manual recommendations; AREMA Part 2- Section 2.4.1 – Test 3A. It was used to measure the ability of an embedded railroad spike to resist withdrawal from the plastic composite crosstie. The total rail and fastening system resistance to pullout is a combination of both the spikes

and fastening clips pullout resistances; this test investigated the spikes pullout resistance while the fastening clips will be investigated in future research.

- Four different pre-drilled pilot hole configurations; A through D, were investigated. Five specimens were tested for each pre-drilling configuration. Screw spikes were used in this investigation as the pre-drilled hole profiles affect screw spikes more noticeably compared to cut spikes.
- The two most commonly used rail spikes were investigated; cut and screw spikes. Five specimens were tested using each spike type. A loading rate of 0.5 in./min (1.27 cm/min) was used and the tests were conducted at room temperature of 70°F (21.11°C)
- Three different, stroke controlled, loading rates within the AREMA recommended range were investigated; 0.5, 1 and 2 in./min (1.27, 2.54 and 5.08 cm/min). Five specimens were tested using each loading rate. Screw spikes were used in this investigation and the tests were conducted at room temperature of 70°F (21.11°C).
- The railroad spike lateral restraint test was performed to identify the ability of an embedded screw spike to withstand lateral forces, thus, in turn, giving an indication of the total system resistance to lateral movement. The test was performed as per AREMA recommendation; AREMA Part 2- Section 2.4.2 – Test 3B.
- The finite element analyses were performed using a general-purpose finite element software ANSYS Version 14.

Findings

- A total of 55 pullout test were performed to investigate several parameters affecting the interactions between the spike and the HDPE composite crosstie including: pre-drilled pilot holes size and shape, type of spikes used, rate of loading and temperature variation. It is worth noting that all the tested specimens surpassed the minimum AREMA recommendations by a significant margin in all the tested conditions. The minimum AREMA recommendations are 5000 lbs (22.2 kN) for screw spike pullout and 1900 lbs (8.5 kN) for cut spike pullout.
- The maximum lateral displacement recommended by the AREMA manual is 0.2 in. (0.51 cm) to limit gauge widening. In all the tested specimens, the yielding point (proportionality limit) occurred before 0.2 in. (0.51 cm) which is ideal, as, when properly designed, the system should not reach yielding under normal conditions.
- The finite element analysis reveals a good correlation between the finite element models and the experimental data obtained from the testing program for the spike pullout testing and lateral restraint. The results were used for further detailed investigation.

Conclusions

- All the tested specimens surpassed the AREMA recommendations for screw and cut spike in polymer composite crossties. Moreover, screw spikes exhibited greater than expected performance surpassing the minimum recommendations by a significant margins (up to more than 200%) and thusly are highly recommended for future implementation.
- An optimal pre-drilling configuration was proposed for screw spikes; setup "D". This configuration exhibited the best holding power without introducing stress concentrations nor causing material build-up and bulging in the vicinity of the spikes. Pre-drilling did not affect the pullout capacity of cut spikes and is only recommended to achieve proper installation.
- The slowest loading rate produced the most conservative spike pullout resistances. Therefore it is recommended for evaluation or characterization of spike pullout resistance in future applications.
- At low temperatures, the pullout capacity significantly increased due to material hardening. Most intriguing, the pullout capacity of the specimens was not negatively affected, in a significant way, by elevated temperatures as material softening was compensated by confinement due to thermal expansion/squeezing.
- Both the crosstie and the spike acted together as a composite section when resisting lateral forces. Moreover the observed failure was ductile as evident by the absence of cracks and the prolonged phase of yielding/strain hardening that the specimens experiment. Additionally, there is a significant reserve capacity in the system after yielding.
- The finite element model constructed showed good accuracy and correlation with the experimental results. The model was greatly optimized and refined to have optimal computational time and cost while maintaining accuracy. This model will be implemented in future studies in this research program.

Publications

- Lotfy I, Farhat M, and Issa M A, "**Structural Behavior of Rail Fastening System used for Recycled Plastic Composite Crossties**" In the proceedings of the 2015 Joint Rail and Rapid Transit, San Jose, CA, 23-25 March 2015.

Contacts

Principal Investigator
Mohsen A. Issa
Professor of Civil and Material Engineering
University of Illinois at Chicago
312-996-2426
missa@uic.edu

NURail Center
217-244-4444
nurail@illinois.edu
http://www.nurailcenter.org/

TABLE OF CONTENTS

LIST OF FIGURES

SECTION 1 INTRODUCTION

Railroad crossties are traditionally manufactured using hardwood timber in the US. However, concerns regarding the sustainability and efficiency of wooden crossties have recently threatened the status quo. The main issues facing timber crossties are their susceptibility to rot and organic decay which render the use of toxic wood treating chemicals a necessity; in addition to sparsity and deforestation (1 to 5). Currently, alternative solutions to the traditional hardwood timber crossties are increasing being adopted by the railroad industry.

Engineered composite plastic are among these alternatives materials for railroad crossties applications. Recycled composite plastic is well suited for both new and replacement operations of railroad crossties. It can be designed and engineered to meet the required performance criteria. It is manufactured with the same geometry and weight as its timber counterparts, thus allowing one to one replacement strategies (6). It can offer high strength and durability when properly designed and manufactured. In addition, its inherent damping capability can result in a prolonged service life with enhanced rideability and passenger comfort. Moreover, recycling plastic waste to manufacture crossties is a green process, which makes it very appealing in today's society, where the emphasis is directed towards environmental issues, greenhouse gas emissions reduction, and limiting climate changes.

Recycled plastic composite crossties have numerous and apparent environmental and structural advantages ranging from pollution and waste reduction to life cycle cost efficiency (6 to 9). As a result, several manufacturers are currently commercially offering alternative solutions using different recycled plastic composite crossties. Moreover, thousands of plastic crossties are currently in service in a wide variety of railroad applications in the US and other countries (10).

SECTION 2 PAST RESEARCH

Several researchers have performed studies addressing plastic composite crossties and its fastening system assemblies using experimental laboratory or field-testing. Jimenez (11) conducted an experimental study addressing the vertical track modulus for both plastic and wooden crossties using two different types of the fastening systems. Lampo (12) investigated the performance of the composite crossties through several laboratory and field-testing. Roybal (13) conducted another study addressing the cyclic loading response of composite crossties. The test was performed using cut spikes to fasten the rail and the steel bearing plate to the crosstie. Reiff and Trevizo (14) studied the effect of several factors on the performance of the plastic composite crossties including the type of spikes used.

As evident from the past studies, little literature is available on composite plastic crossties and its fastening spikes. The behavior of the railroad spike and their interactions with the composite plastic crossties when subjected to rail loading is not fully understood yet. Moreover, the prevalent US rail design manual; the American Railway Engineering and Maintenance-of-Way Association (AREMA) manual, does not have fully developed criteria for composite crossties and their fastening system (15). Therefore, additional research is necessary to properly characterize, describe and model the behavior of railroad spikes when used with composite plastic crossties as well as assess the feasibility of implementing them in railroad applications.

SECTION 3 RESEARCH OBJECTIVE

The University of Illinois at Chicago conducted a series of studies to assess the feasibility of implementing High Density Polyethylene (HDPE) crossties in both conventional and high speed rail applications. Previous reports have explored the flexural performance of HDPE composite railroad crossties, reinforced with discontinuous randomly distributed glass fibers, as well as its sensitivity to temperature variations. In this report, an investigation aiming to understand and assess the performance of typical railroad spikes used with recycled HDPE crossties is presented. The study encompassed comprehensive experimental investigations and analytical finite element modeling. The testing program evaluated the railroad spikes using static testing methods recommended by the AREMA manual. These tests addressed the railroad spike pullout and lateral restraint for both screw and cut spikes. Then, an analytical finite element model was constructed using the existing and obtained testing results to accurately portray the railroad spike behavior and interactions with the HDPE crosstie. This model will be used for future, full-scale, investigations beyond the scale of laboratory experiments. The objective of this report is as follows:

- Understand the behavior of rail spikes under pure pullout forces and their interactions with the HDPE crosstie.
- Assess the effect of temperature, rate of loading and type of spike on the spike pullout behavior.
- Investigate the behavior of rail spikes when subjected to lateral forces.
- Develop an accurate finite element modeling techniques, which accurately portray the behavior of the fastening system using the experimental data.

SECTION 4 EXPERIMENTAL PROGRAM

4.1 Description of the crosstie and fastening components

The HDPE crossties used in this study were manufactured using an extrusion process from recycled plastic milk and detergent bottles; of which 7.2 billion pounds (3.27 billion kilograms) are land filled each year in the US (7). The crossties are reinforced with randomly distributed discontinuous glass fibers to achieve the desired stiffness. Foam inducing agents were used to control the density and cost of the final product. Finally, UV inhibitors and anti-oxidants were also added to a thin skin surface layer to protect the surface of the crossties. This process creates an efficient cross section with optimum distribution of the reinforcing fibers and minimal weight. It also produces a difference in the properties between the core and exterior regions of the cross section (16). The final products have sectional dimensions of 9 x 7 in. (22.86 x 17.78 cm), length of 8 to 9 ft (2.44 to 2.74 m) and an average density of 56.8 pcf (910 kg/m3).

The railroad spikes used in this study were provided by the Chicago Transit Authority (CTA). They correspond to the same spikes used for actual plastic composite crossties applications within the state of Illinois. Figure 1 shows the HDPE composite crosstie and the railroad spikes used in this study. Railroad cut spikes/screw spikes are used to fix the steel bearing plate to the HDPE crosstie. They are manufactured from A36 steel with yield stress of 36,000 psi (248 MPa), yield strain of 0.00124 in./in. (0.00124 cm/cm) modulus of elasticity of 29,000,000 psi (20,000 MPa).

Figure 1. HDPE composite crosstie specimens and typical railroad spikes.

4.2 Spike Pullout

The spike pullout test was performed as per the AREMA manual recommendations; AREMA Part 2- Section 2.4.1 – Test 3A (15). It was used to measure the ability of an embedded railroad spike to resist withdrawal from the plastic composite crosstie. The total rail and fastening system resistance to pullout is a combination of both the spikes and fastening clips pullout resistances; this test investigated the spikes pullout resistance while the fastening clips will be investigated in future research. For this test, the crosstie specimens were cut into 12 in. (30.5 cm) long segments. A spike pilot hole was pre-drilled in the center of each specimen to enable spike installation. In order to fix the specimens to the testing bed, four through holes were drilled near each corner of the specimens and two; 1 in. (2.54 cm) thick, steel plates were used to restraint the specimen from each side. A spike pullout device was specially designed with the same thickness as the rail bearing plate and was used to apply the pullout force. All the spikes were installed manually using an adjustable wrench for the screw spikes and a sledgehammer for the cut spikes. A total of 55 pullout test were performed to investigate several parameters affecting the interactions between the spike and the HDPE composite crosstie including: pre-drilled pilot holes size and shape, type of spikes used, rate of loading and temperature variation. It is worth noting that all the tested specimens surpassed the minimum AREMA recommendations by a significant margin in all the tested conditions. The minimum AREMA recommendations are 5000 lbs (22.2 kN) for screw spike pullout and 1900 lbs (8.5 kN) for cut spike pullout (15). Figure 2 illustrates the test configuration, the mode of failure/spike pullout, and the specially designed steel pullout device.

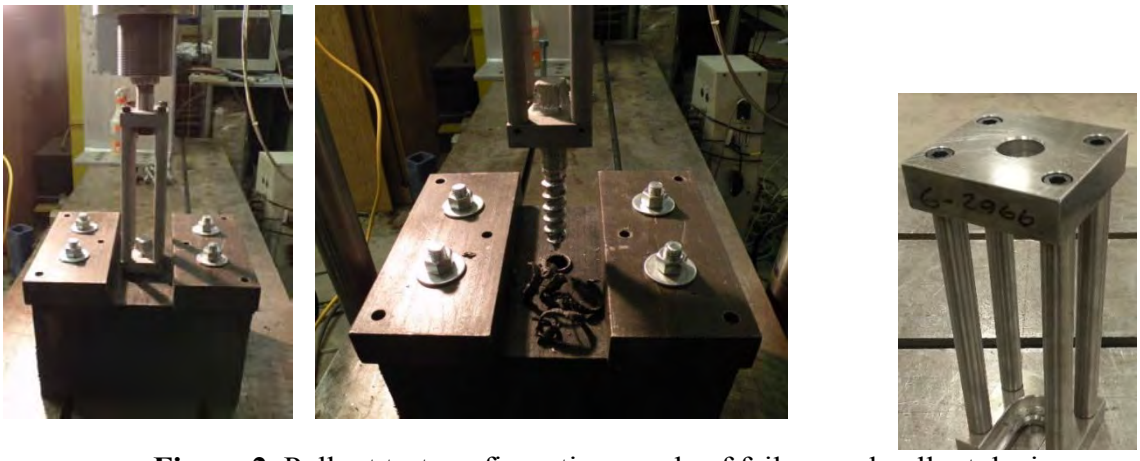

Figure 2. Pullout test configuration, mode of failure and pullout device.

4.2.1 Pre-drilled pilot holes size and shape.

Four different pre-drilled pilot hole configurations; A through D, were investigated. Five specimens were tested for each pre-drilling configuration. Screw spikes were used in this investigation as the pre-drilled hole profiles affect screw spikes more noticeably compared to cut

spikes. A, stroke controlled, rate of loading of 0.5 in./min (1.27 cm/min) was used. The rate of loading was kept constant to properly determine the effect of the different predrilling configurations. All the tests were conducted at room temperature of 70°F (21.11°C). The best performing configuration was determined in terms of allowing the screw spikes to be installed in the specimens without creating excessive stress and material deformation around the spike while providing enough bond and friction to resist pullout. Figure 3 presents the different pre-drilled pilot hole configurations investigated as well as the screw spike dimensions. Figure 4 present a sample of the results obtained; i.e. the five specimens tested using setup B. Figure 5 presents a summary of all the tests comparing the different pre-drilling configurations.

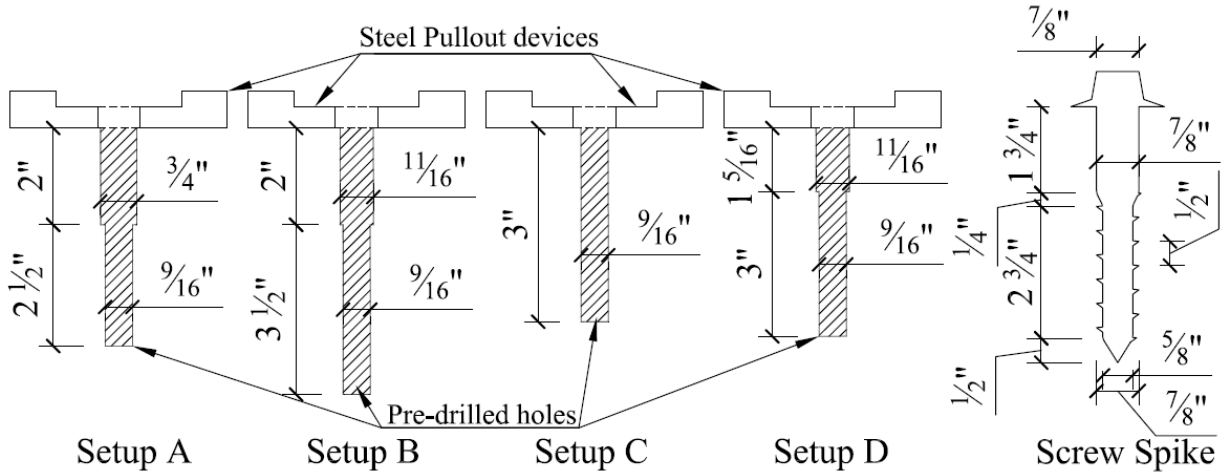

Figure 3. Pre-drilled pilot holes configurations and screw spike dimensions (1”= 2.54cm).

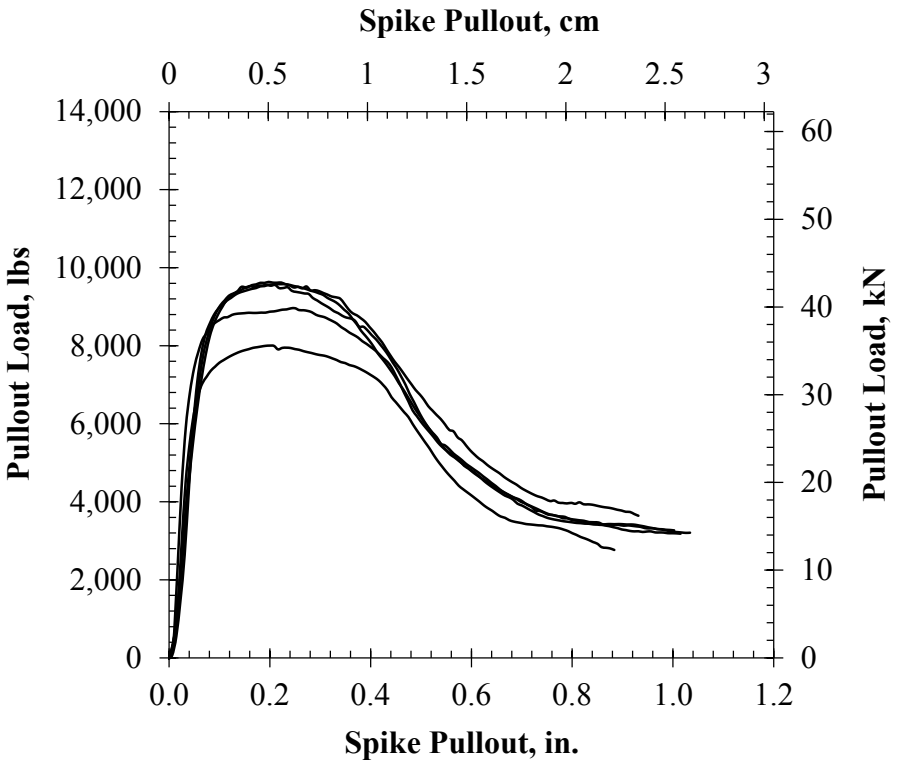

Figure 4. Sample result; load-pullout curve for the five specimen using setup B.

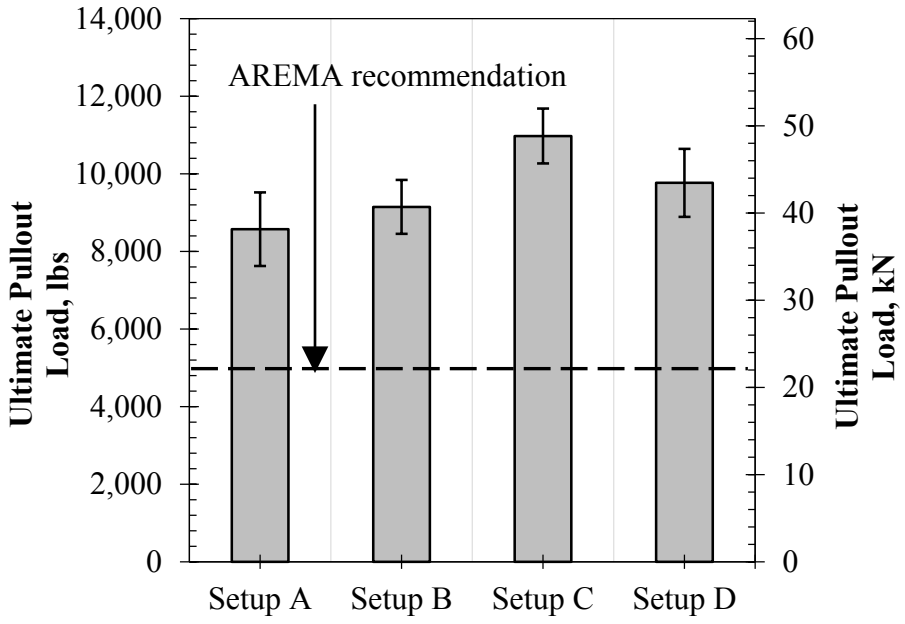

Figure 5. Ultimate pullout load comparison between the four pre-drilling configurations.

The same trend was observed in all the tested specimens as illustrated in Figure 4. Three phases were observed; the first begins with the application of the load where the load increases substantially with little deflection until the specimen reaches its ultimate pullout load. The second phase begins after bond failure where the load remains almost constant with an increase in deflection; in this phase, the resistance to pullout is provided by HDPE material yielding and friction with the spike. In the third and final phase the load decreases significantly with an increase in deflection; this represents failure state; i.e. withdrawal of the spike from the HDPE specimen.

The pullout resistance of the screw spike is largely dependent on the size, shape, and depth of the pre-drilled hole. The pullout resistance is provided by the bearing of the spike threads on the HDPE material between the spike threads. A direct indication of the volume and density of the material between the spike threads can be acquired by the material between the threads, extracted after spike pullout as shown in Figure 6.

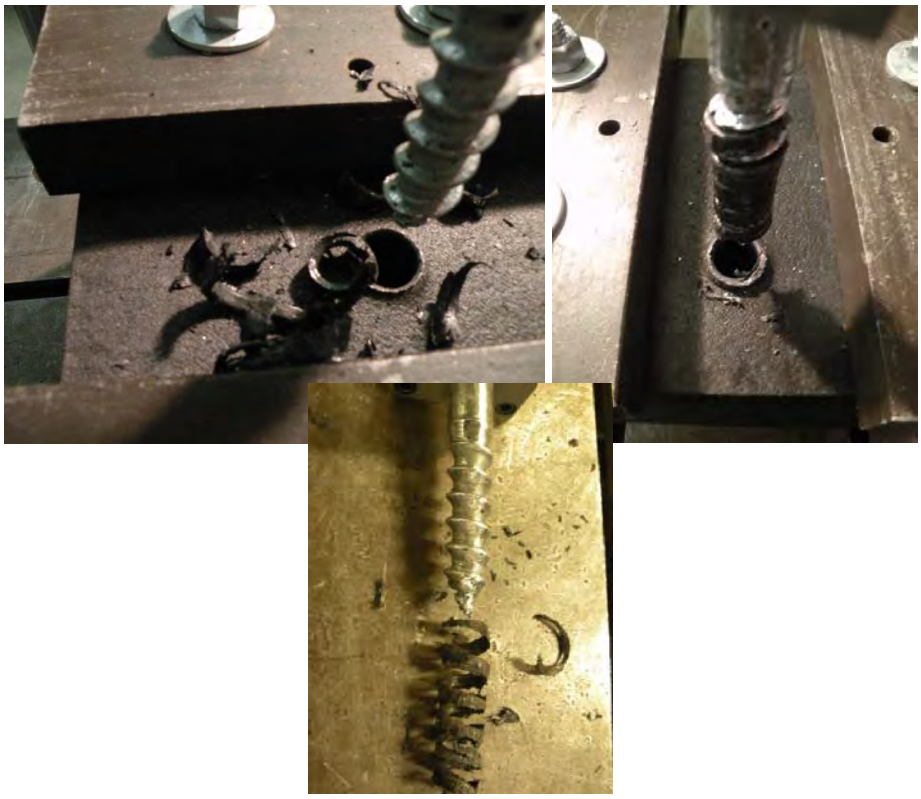

Figure 6. Material between the threads extracted after pullout [setup A and B- loose material (left); setup C – very tight material (center); setup D – tight material (right)].

Setup A and B both had relatively large pre-drilled holes and did not provide enough material for the spike threads to bear on, as shown by the loose material extracted after pullout in Figure 6, which is reflected in their relatively low pullout resistance. Setup C produced the most (tightly compacted) extracted material between the spike threads (see Figure 6) and the highest pullout

resistance out of all the setups as demonstrated by Figure 5. However, overdriving screw spikes in undersized holes introduced local stress concentrations around the spike. Moreover, the installation of the spikes using this configuration required a lot of effort and often caused material bulging/build-up under the steel plate/pullout device. This build-up often introduced a small gap between the steel plate/pullout device and the HDPE crosstie, which could cause problems in actual application. Therefore, setup C is not recommended. Setup D is the recommended configuration by the authors because it provides a good bond without causing material bulging/build-up in the vicinity of the spike. Setup D tailors the actual profile of the screw spike while being slightly undersized, refer to Figure 3. Even though setup C exhibited better pullout resistance, excessive material bulging occurred due to its significantly undersized pilot hole which prevented proper contact between the crosstie and the bearing plate and thus was not recommended.

4.2.2 Type of rail spike.

The two most commonly used rail spikes were investigated; cut and screw spikes. Five specimens were tested using each spike type. A loading rate of 0.5 in./min (1.27 cm/min) was used and the tests were conducted at room temperature of 70°F (21.11°C). As previously recommended, all the specimens were pre-drilled using setup D pilot hole profiles for the screw spikes. When testing the cut spikes, all the pre-drilling configurations were evaluated; A though D, as well as no pre-drilling at all. The pullout resistance of the cut spikes did not vary significantly due to pre-drilling configuration, or lack thereof. However, material build-up/bulging occurred when driving spikes in undersized holes as well as the case with no pre-drilling at all. In addition driving cut spikes in undersized holes was very challenging. Therefore, the authors recommended using pre-drilling pilot holes to enable proper installation/contact of the rail bearing plate and the HDPE crossties and not to optimize the pullout resistance of cut spikes. Figure 7 presents the applied load – spike pullout relationship for all the tested cut spikes. Figure 8 presents a summary of all the tests comparing both the screw spikes and the cut spikes pullout resistances.

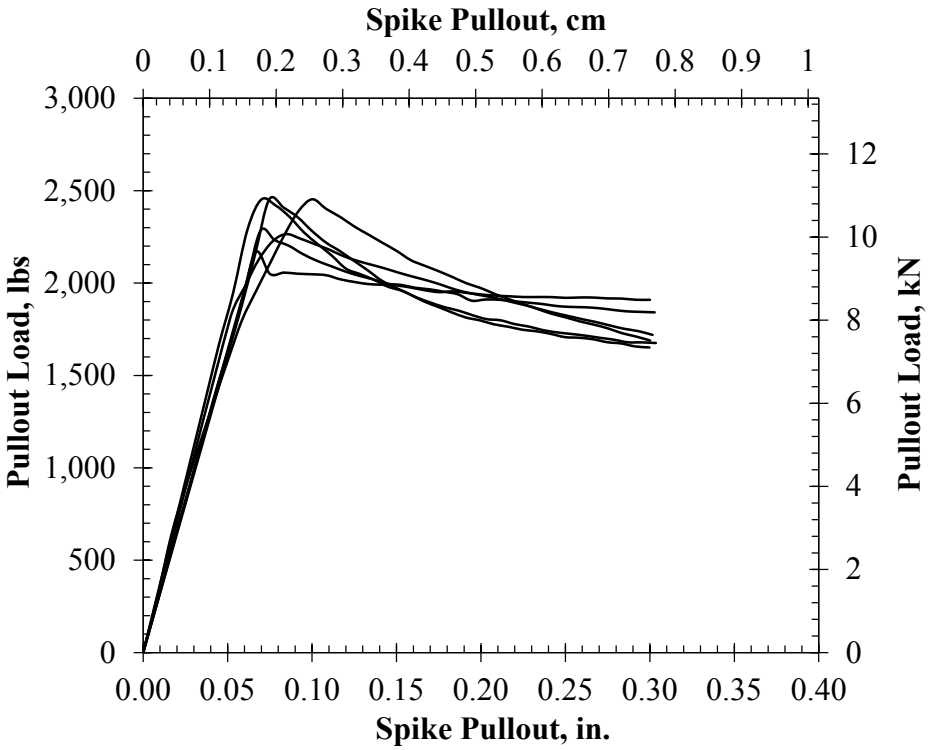

Figure 7. Load-pullout curve for the five specimen using cut spikes.

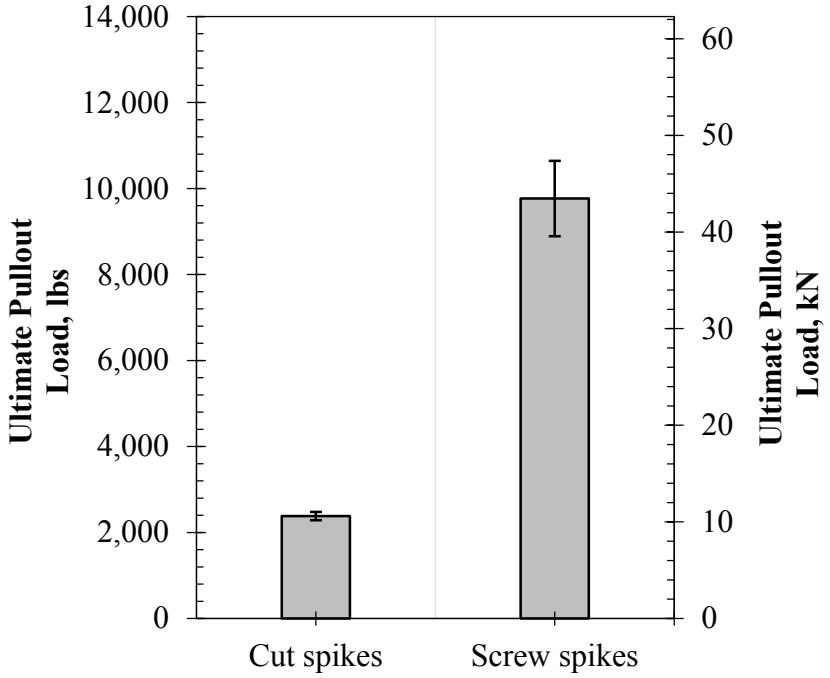

Figure 8. Ultimate pullout load comparison between the three loading rates.

The cut spikes investigated exhibited significantly less holding power than screw spikes as expected, however, they still surpassed the AREMA minimum recommendations for cut spike which was 1900 lbs (8.5 kN) (15). Inspection of Figure 7 reveals that, unlike the three stages observed in screw spikes, the behavior observed for cut spikes is similar to pure friction behavior with only two stages. The first begins with the application of the load where the load increases substantially with little deflection until the specimen reaches its ultimate pullout load. The second phase begins immediately after the ultimate pullout force was surpassed; a slightly reduced, steady, approximately constant, relationship was observed until spike complete withdrawal from the HDPE specimen. The behavior of cut spikes is mainly controlled by friction, as the spikes are smooth. After the initial bond was overcome, the friction force remained almost constant until failure; i.e. complete withdrawal from the HDPE specimen. Since the behavior is governed mainly by friction forces, the results obtained for cut spikes are very consistent when compared with the results of the screw spikes, as shown in Figure 8. Even though cut spikes fulfilled the AREMA minimum recommendations, it is clear that screw spikes performed significantly better when combined with HDPE composite plastic crossties as they surpassed the minimum AREMA recommendations with a significant margin.

4.2.3 Loading rate.

Three different, stroke controlled, loading rates within the AREMA recommended range were investigated; 0.5, 1 and 2 in./min (1.27, 2.54 and 5.08 cm/min). Five specimens were tested using each loading rate. Screw spikes were used in this investigation and the tests were conducted at room temperature of 70°F (21.11°C). All the specimens were pre-drilled using setup D pilot hole profiles as previously recommended. Figure 9 presents a summary of all the tests comparing the three different loading rates investigated.

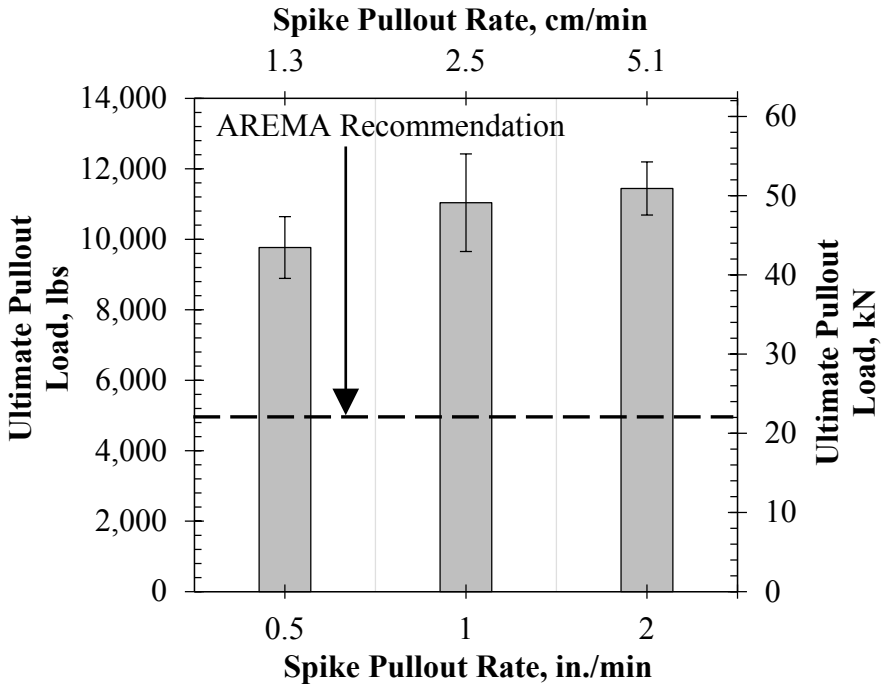

Figure 9. Ultimate pullout load comparison between the three loading rates.

Inspection of Figure 9 reveals that the ultimate pullout resistance displayed at faster loading rates was higher than slower loading rates. This result was excepted as the HDPE crossties have high inherent damping and energy absorption, which provide great performance when subjected to dynamic forces. When the loading rate increase from 0.5 to 2 in./min (1.27 to 5.08 cm/min), the speed of the load application is multiplied by four, effectively reaching the ultimate pullout load within a few seconds which is closer to a dynamic load, thus increasing the pullout resistance of the specimens. Therefore, it is recommended to use the slowest and most conservative loading rate for evaluation or characterization of pullout resistance in future applications. It is worth noting that actual train wheel loading is significantly faster than the loading rates investigated which will further increase the spikes efficiency when resisting withdrawal from the HDPE crossties.

4.2.4 Temperature variation.

The pullout resistance of the railroad spikes was investigated at different temperatures; 10, 40, 70, 100 and 125 °F (-12.22, 4.44, 21.11, 37.78 and 51.67 °C). Five specimens were tested at each investigated temperature. A loading rate of 0.5 in./min (1.27 cm/min) was used and the tests were conducted using screw spikes and pre-drilling setup D. To achieve the desired temperature, the HDPE crosstie specimens were placed in a sophisticated "Hotpack" controlled environmental chamber. The temperature of the chamber was rechecked using a digital "Weiss" thermometer for additional redundancy. The temperature of the specimens was also monitored using another

infrared “Omega” thermometer. The test was conducted when the three temperature monitoring thermometers displayed the desired testing temperature. After the test was concluded, the temperature of the specimens was recorded again to ensure that it did not vary significantly. In all cases, the temperature of the specimens after failure was within ±5°F (±2.78°C) of the desired testing temperature. Figure 10 presents the test results for the five different temperatures investigated.

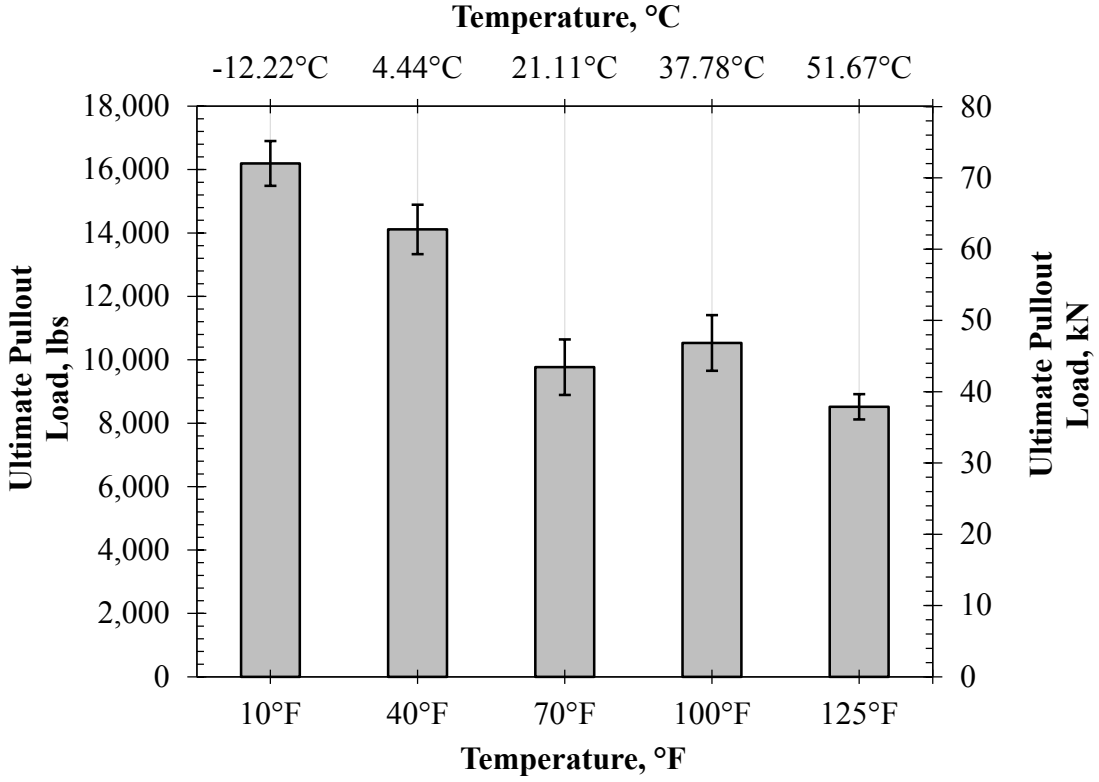

Figure 10. Ultimate spike pullout resistance at different temperatures.

The expected outcome of this test was that, at lower temperatures, the pullout resistance would increase due to the hardening of the HDPE material, and vice versa at higher temperatures. Inspection of Figure 10 reveals that at lower temperatures the pullout resistance increased which was expected, however, at higher temperature, the pullout resistance remained almost constant, which was very interesting. More to the point, the ultimate pullout capacity increased from 70 to 100 °F (21.11 to 37.78 °C) which was not expected as the material softens at higher temperatures. The authors believe that this was a result of the additional stresses/confinement introduced as a result of thermal expansion/squeezing, of the HDPE specimen and the steel spike. These additional stresses enhanced the bond and friction between the HDPE specimen and the steel spike and were able to overcome the softening of the HDPE material. However, these additional thermal stresses were not sufficient to overcome the softening of the HDPE material at 125 °F (51.67 °C) temperature as the pullout capacity slightly decreased. Considering the authors

previous experience when investigating the temperature effect on the behavior of HDPE crossties (17), it is apparent that without these additional thermal stresses/confinement, the softening of the HDPE would have been significantly more pronounced, reducing the pullout capacity. Thus, as evident form the test results; the pullout capacity of the specimens was not affected negatively, in a significant way, by the variation in temperature, which is a notable, previously unexpected, outcome.

4.3 Spike Lateral Restraint

The railroad spike lateral restraint test was performed to identify the ability of an embedded screw spike to withstand lateral forces, thus, in turn, giving an indication of the total system resistance to lateral movement. The test was performed as per AREMA recommendation; AREMA Part 2- Section 2.4.2 – Test 3B (15). The crosstie specimens were cut into 10 in. (25.4 cm) long segments for this test. A spike pilot hole was pre-drilled in the center of each segment using the setup D profile. Four holes were drilled through the side of the specimens, near the corners, to properly fix the specimens to the testing bed during load application. Another specially made steel device with a thickness of 0.5 in. (1.27 cm) was employed to properly apply the lateral load. Figure 11 illustrates the test configuration and the lateral loading device.

As per AREMA recommendations, a stroke controlled loading rate of 0.2 in./min (0.51 cm/min) was used and the load producing 0.2 in (0.51 cm) lateral deflection was recorded as well as the ultimate load. A total of five specimens were investigated.

Figure 11. Spike lateral restraint test setup and loading device.

As presented in Figure 12, the trend observed in the tested specimens displayed two distinct phases. The first begins with the application of the load where the load increases substantially with little deflection. During the phase the load deflection relationship is linear and the spike and

the HDPE specimen are working together to resist lateral movement. The second phase begins with a change in the slope of the load deflection curve; i.e. after the end of the proportionality limit. The specimen continues to resist lateral forces with significant lateral deformation and yielding. The lateral load deflection relationship continues almost linearly until failure. During this phase the spike starts to bend bearing on the HDPE material underneath and both the steel spike and the HDPE material experience significant yielding and permanent deformations. After the ultimate lateral resistance is reached, the specimen is badly damaged and cannot resist more load. The mode of failure observed was bending/yielding of the steel spike and deformation /yielding of the HDPE material under the spike as illustrated in Figure 13. It is important to note that no cracking was observed in any stage of the test for all the tested specimens.

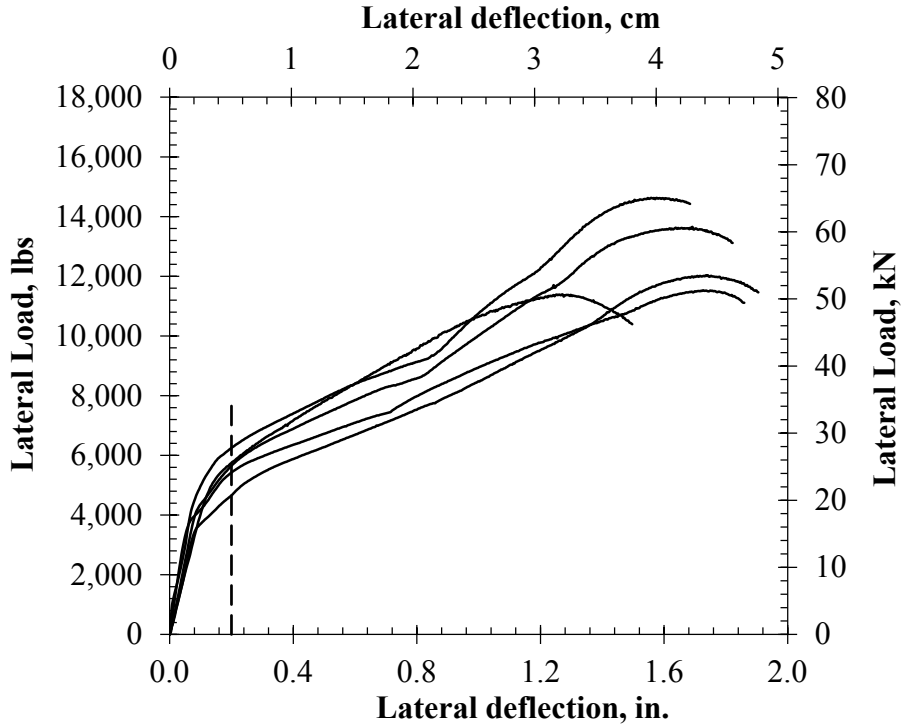

Figure 12. Lateral load and deflection for the spike lateral restraint specimens.

Figure 13. Spike lateral restraint mode of failure.

As noticed from Figure 13, the HDPE specimen and the spike experienced composite action; i.e. they were working together to resist the lateral force in all stages of the test. It should be noted that the spike was bend at the section where the threads started, as shown in Figure 13, which is the weakest section of the spike under the applied bending stresses. It should also be noted that the lower portion of the spike, i.e. the threaded part, did not experience any bending, rather it was straight and upright when it was extracted from the specimen. Moreover, it was very challenging to extract the bent spike from the specimen as the plastic material has to be deformed more to release the spike. Therefore, the spike was completely fixed in the specimen, further validating the composite behavior between the spike and the crosstie. It can be inferred that the first linear phase is elastic and can be fully recoverable while the second phase causes yielding and permanent deformation. Figure 14 shows a summary of all the tested specimens.

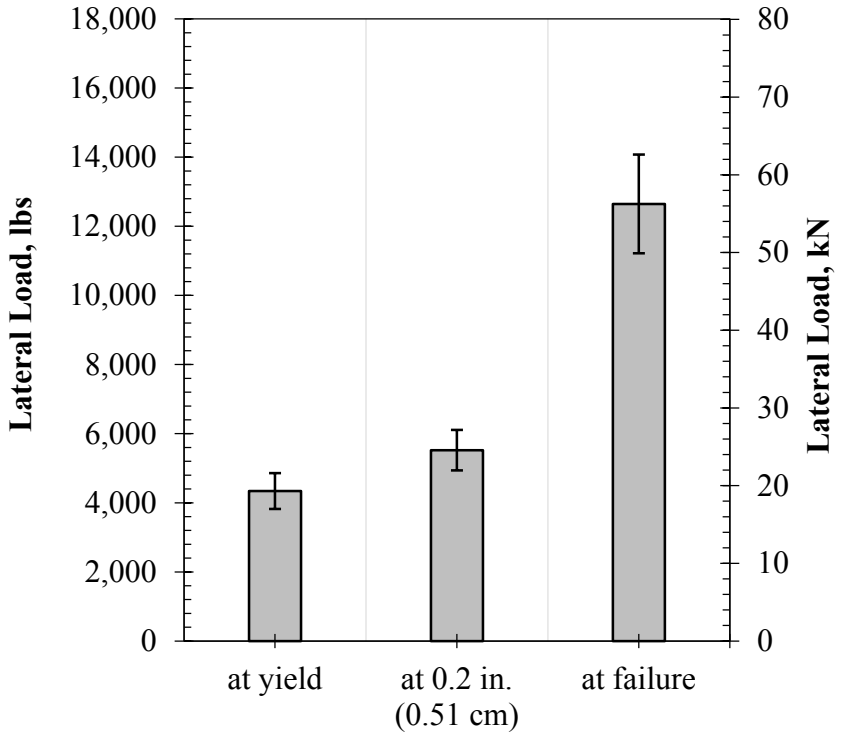

Figure 14. Lateral capacity at yield, 0.2 in. (0.51 cm) and at failure.

The maximum lateral displacement recommended by the AREMA manual is 0.2 in. (0.51 cm) to limit gauge widening. In all the tested specimens, the yielding point (proportionality limit) occurred before 0.2 in. (0.51 cm) which is ideal, as, when properly designed, the system should not reach yielding under normal conditions. However, it is good to note that the specimens have a lot of reserve capacity/ductility and did not crack at any time during testing which eliminates the possibility of sudden brittle failure.

4.4 Finite element analysis

Several previous studies, in medical fields such as surgery and dentistry, have used finite element analyses to model threaded bolts. It was used to simulate the behavior of screw bolts in certain applications where experimental evaluation was infeasible as it may involve human organs or tissues. Zhang et al. (18) investigated the pullout strength of a fixation screw in human spine using finite element analysis where the threads were modeled in details based on given geometry and dimensions. Similarly, Chi-Hsu (19) used finite element analysis to assess the stripping torque and pullout strength of three types of pedicle screws embedded in polyurethane foam. The model showed promising indications as the results mimicked the experimental data.

In engineering and railroad applications, the use of finite element analysis to study the performance of different system components is increasingly growing. It provides means to

examine the structural behavior of a given system and extrapolate/predict the behavior of full-scale applications beyond the scale of laboratories. In this study, it was used to simulate the pullout and lateral resistance of the screw spikes embedded in HDPE crossties. After its construction, the finite element model was calibrated/validated using the experimental data presented earlier.

The finite element analyses were performed using a general-purpose finite element software ANSYS Version 14 (20). For the 3-D modeling, the geometry of the system was separately created using the ANSYS Workbench Design Modeler software and then imported to ANSYS APDL.

Two models were created to study the pullout and lateral restraint behavior of a fixation screw in HDPE crosstie. The models were built with maximum detail possible, to simulate the actual behavior of the spikes, and were optimized to maintain computational and time efficiency. The spike pullout model consists of a screw spike, with the exact dimensions (refer to Figure 3), HDPE crosstie specimen, bottom steel plate for support, and upper steel plate for fixation. The model was assumed quarter symmetry to minimize the computational cost. Similarly, the lateral restraint model consists of the same screw spike, HDPE crosstie specimen, bottom steel plate for support, and though steel rods with upper knots for fixation. The difference between the pullout and lateral restraint models is in the boundary/symmetry conditions. In the pullout model, the fixation plate is placed in the same plane with the screw spike. The load is applied as vertical displacement parallel to the screw spike vertical axis. In the lateral restraint model, the fixation knots are placed a perpendicular plane to the screw spike and the load is applied as vertical displacement perpendicular to the screw spike vertical axis. The geometry of the finite element model for spike pullout and lateral restraint are shown in Figure 15.

As mentioned earlier, the manufacturing procedure of the HDPE crossties, investigated in this study, creates a difference in the properties between the core and exterior regions of the cross section. The properties and dimensions of both regions were investigated in details in previous work; Lotfy et.al. (16) and the findings were implemented in this study; i.e. core region dimensions of 4×6 in. (10.2×15.2 cm) with the material properties presented in Figure 16 were used.

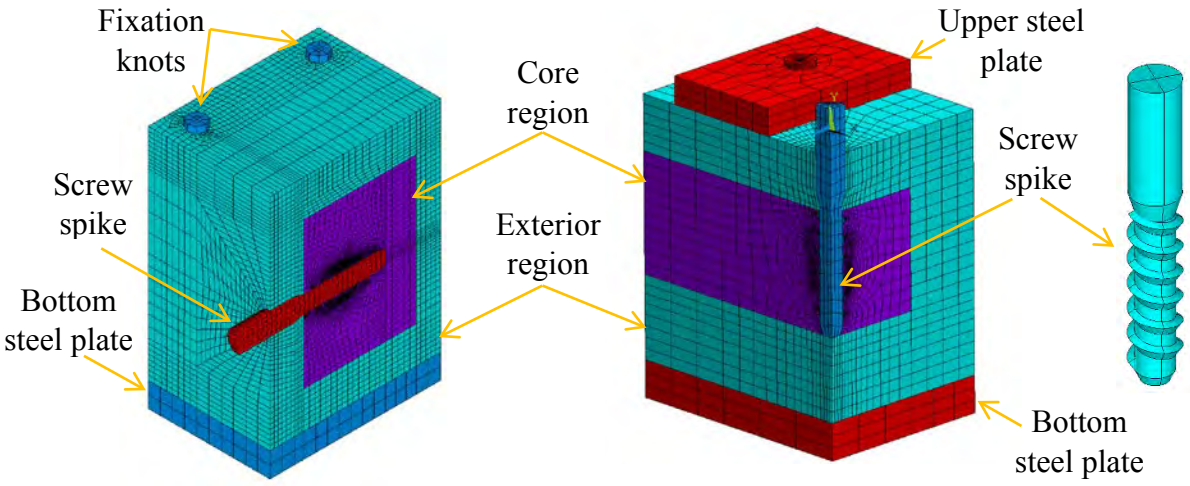

Figure 15. Description of the two finite element models; spike lateral restraint (left-half symmetry), and spike pullout (right-quarter symmetry).

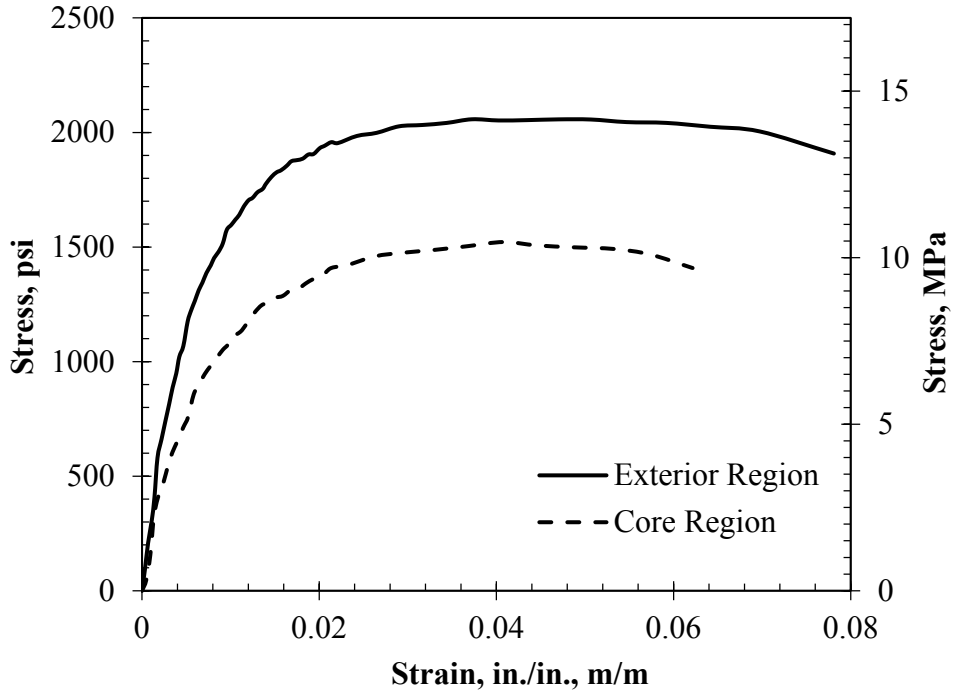

Figure 16. Stress-strain curves for both exterior and core regions of the HDPE crossties.

In the finite element models, eight-node Isoparametric brick solid 185 elements were used to model all the solid geometry. It is defined by three translational degrees of freedom at each node. The element has the capability for undergoing plasticity, stress stiffening and large deformations (21). To optimize calculation time, a fine mesh was used in regions of high stress gradient and a coarser mesh was used in other areas. Additional mesh refinement was applied to the areas close to the vicinity of the screw spike threads, based on the findings of Grewal and Sabbaghian (22),

in order to accurately represent the stress distribution around the thread. Moreover, the screw spike thread tips were slightly modified with small fillets to produce a circular contact at the tip of the threads. This technique was used to eliminate stress concentrations due to sharp contact edges between the threads and the HDPE crosstie as shown in Figure 17.

To simulate contact between the steel spike, the HDPE crosstie, and the steel plates; surface-to-surface, flexible-to-flexible contact elements were employed in the model. The surface of the screw spike/steel plates were meshed with the elements of TARGE 170, and the surfaces of HDPE crosstie was meshed with CONTA 174 elements. The boundary conditions and loading were identical to those applied in the experimental testing. The bottom steel plate was fixed at the bottom surface. For the spike pullout model, the loading condition was a vertical displacement of 0.2 in. (0.51 cm) applied to the top of the spike. Symmetric boundary conditions were applied to two inner planes to account for quarter symmetry. The total number of elements in the models was around 32,200 elements. For the lateral restraint model, the loading condition was a vertical displacement of 0.3 in. (0.76 cm). It was applied at the top surface of spike over an area of 0.2 in. (0.51 cm) to account for the contact area of the loading device as shown in Figure 17. Similarly, symmetric boundary condition was applied to the inner plane to account for half symmetry. The total number of elements in the models is 64,493 elements.

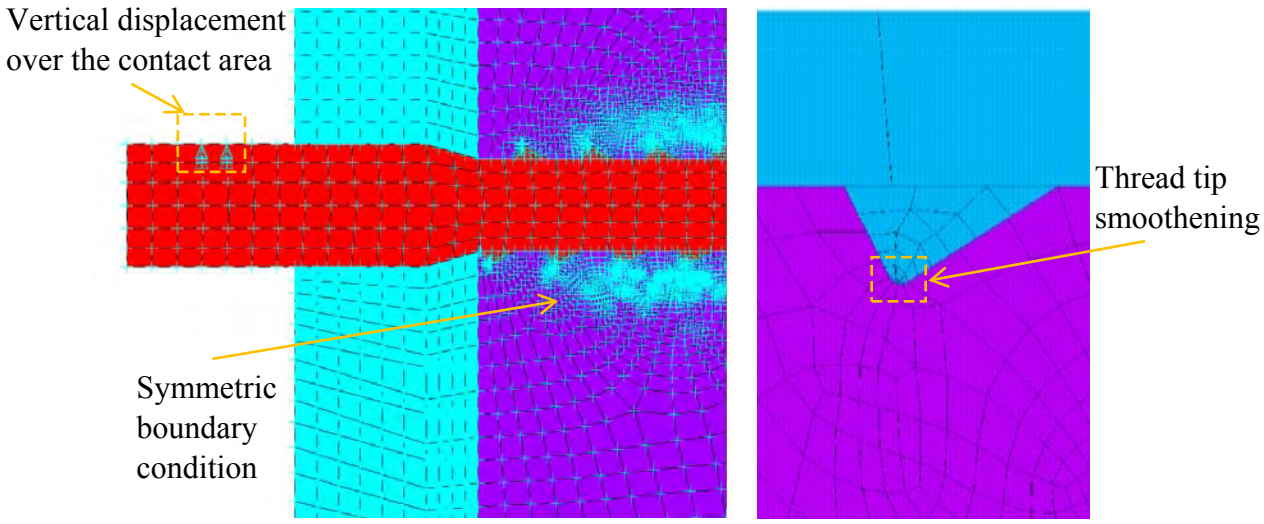

Figure 17. Load application for lateral restraint model (left); thread circular contact (right).

4.4.1 Finite Element Results

Figure 18 presents a sample of the models result; stress distribution at failure for the spike pullout model and deformation for the lateral restraint model at 0.25 in. (0.64 cm) deflection at the point of load application. For the spike screw pullout, it is apparent that the HDPE plastic in

the vicinity of the threads experienced yielding due to the threads bearing on the plastic material. Failure occurred in the HDPE material at the top thread where the stresses exceeded the material resistance; which was 2050 psi (14.1 MPa). Only the elements close to the threads reached the ultimate capacity followed by large plastic strain before failure; i.e. pullout from the plastic. At failure, the shear stresses in the HDPE material near the threads reaching 1170 psi (8.06 MPa) which is also significant. The stress value of the outer circumference surface of the spike can be much smaller than those at the inner diameter. In this condition, it can be deduced that the pull-out failure occurred along a surface around the inner diameter of the spike, where the screw threads cut a cylinder formed by those failed areas.

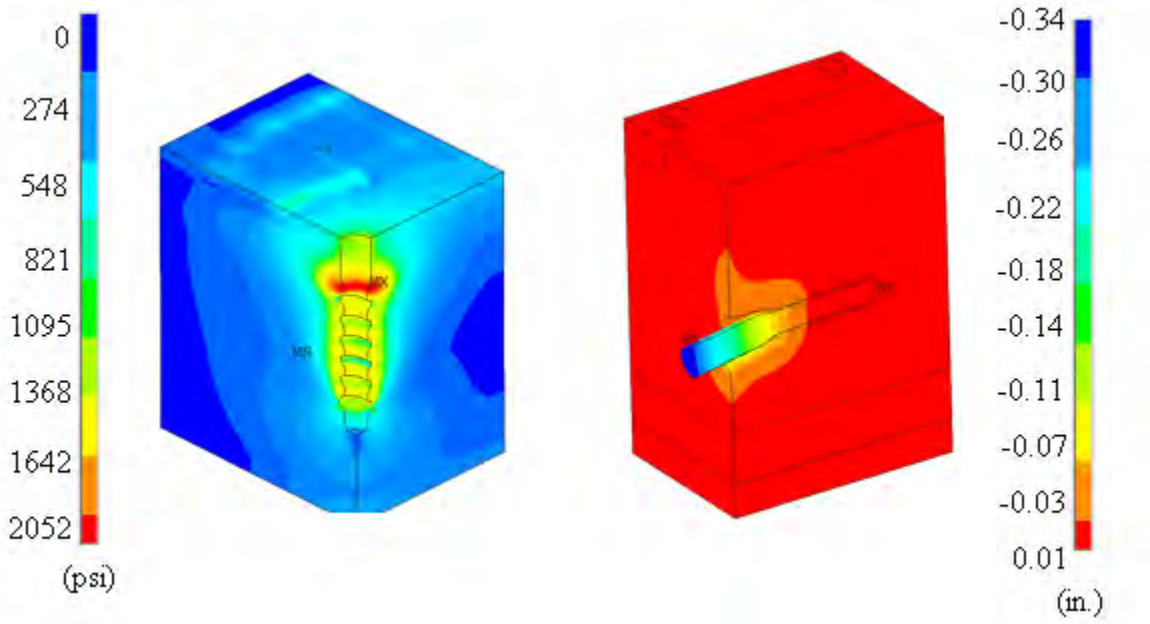

Figure 18. Stress distribution for the spike pullout model (left) and deformation for the lateral restraint model (right) (1 in.= 2.54 cm & 1 psi = 6.9 kPa).

For the lateral restraint model, the bearing of the spike on the HDPE material led to a complicated combined stress state of tension, compression and bending stresses. The bearing area below the spike was subjected to direct compression stresses while the HDPE around the sides was subjected to tensile stresses. The spike exhibited a bending behavior occurring at the section with the smallest cross-sectional area; i.e. the start of the threads. The stress analysis shows yielding in the steel accompanied with significant deformation in the HDPE material around the spike as shown in Figure 18. As observed in the experimental tests, the threaded section of the spike (the lower section) was straight all throughout the test phases and experienced negligible deformations. Figure 19 presents a comparison between the finite element models and the experimental testing which was used to validate the finite element models (FEMs).

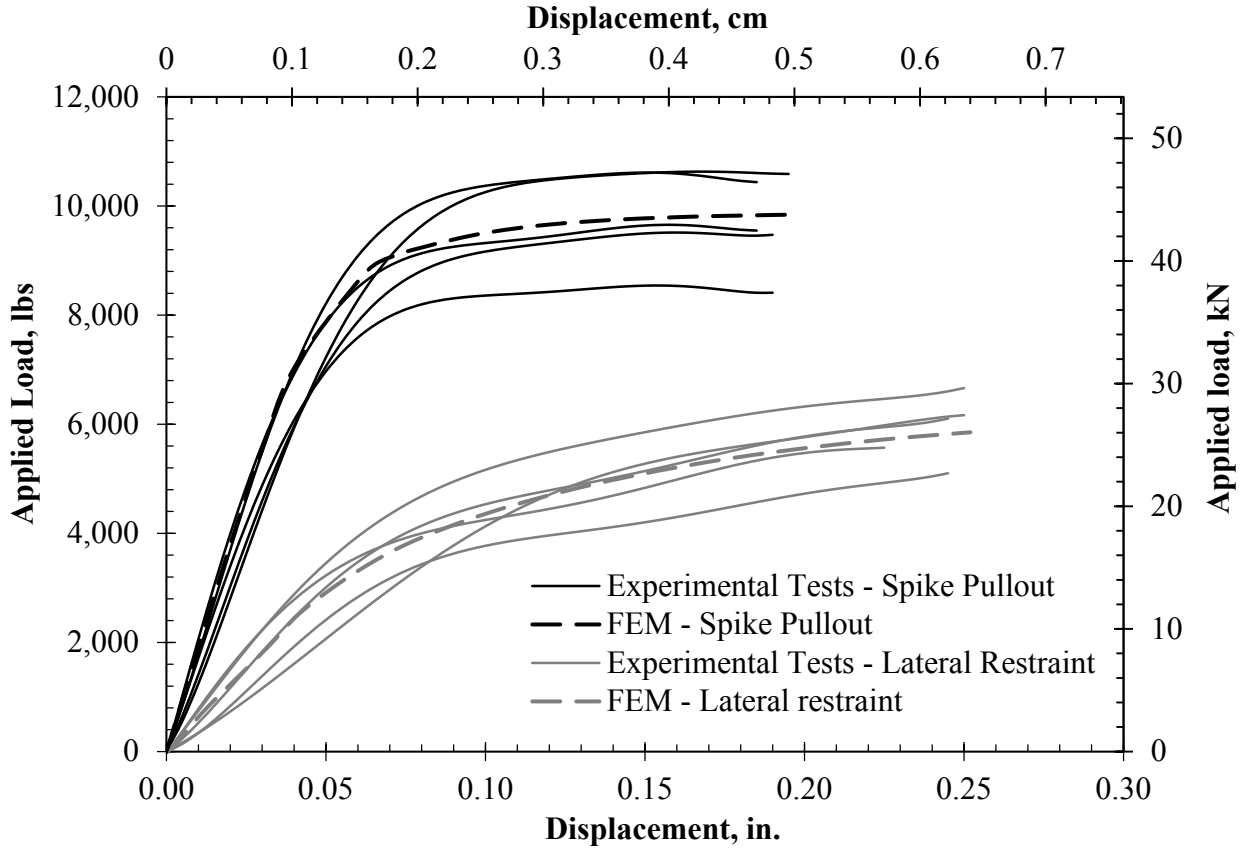

Figure 19. Finite element model validation.

Inspection of Figure 19 reveals a good correlation between the finite element models and the experimental data obtained from the testing program. The pullout model shows a shooting escalation of the curve at the initial stages of loading. When the system reaches ultimate load, the curve exhibits a plateau. From the lateral restrain model, the model shows a consistent behavior with that of the average of the experimental test data. The load versus deflection curve shows a linear increase followed by a hardening behavior. The hardening behavior is due to the yielding of the screw spike and the HDPE material, which had a slightly increasing hardening behavior rather than a steady plateau. It was also found that the spike experienced zero displacement at the bottom and acted as a cantilever restrained at the bottom and bearing on the side of the plastic.

SECTION 5 CONCLUSION AND RECOMMENDATIONS

- All the tested specimens surpassed the AREMA recommendations for screw and cut spike in polymer composite crossties. Moreover, screw spikes exhibited greater than expected performance surpassing the minimum recommendations by a significant margins (up to more than 200%) and thusly are highly recommended for future implementation.
- An optimal pre-drilling configuration was proposed for screw spikes; setup "D" (refer to **Figure 3**). This configuration exhibited the best holding power without introducing stress concentrations nor causing material build-up and bulging in the vicinity of the spikes. Pre-drilling did not affect the pullout capacity of cut spikes and is only recommended to achieve proper installation.
- The slowest loading rate produced the most conservative spike pullout resistances. Therefore it is recommended for evaluation or characterization of spike pullout resistance in future applications.
- At low temperatures, the pullout capacity significantly increased due to material hardening. Most intriguing, the pullout capacity of the specimens was not negatively affected, in a significant way, by elevated temperatures as material softening was compensated by confinement due to thermal expansion/squeezing.
- Both the crosstie and the spike acted together as a composite section when resisting lateral forces. Moreover the observed failure was ductile as evident by the absence of cracks and the prolonged phase of yielding/strain hardening that the specimens experiment. Additionally, there is a significant reserve capacity in the system after yielding.
- The finite element model constructed showed good accuracy and correlation with the experimental results. The model was greatly optimized and refined to have optimal computational time and cost while maintaining accuracy. This model will be implemented in future studies in this research program.

SECTION 6 REFERENCES

1. Thierfelder T and Sandstrom E. The creosote content of used railway crossties as compared with European stipulations for hazardous waste. Sci Total Environ 2008; 402:106–112.
2. Zagier AS. Creosote: 'Witch's Brew'. http://www.mindfully.org/Pesticide/2004/Creosote-Illness-Death24may04.htm (accessed 24 May 2014).
3. Morris T. Poisonous railway sleepers pose health risk. October 2008. http://lists.greens.org.au/mailman/public/media/2008-October/010679.html (accessed 28 May2014).
4. Pruszinski A. Review of the landfill disposal risks and the potential for recovery and recycling of preservative treated timber. Environmental Protection Agency Report, 1999. South Australia: Sinclair Knight Merz.
5. Coffin B. Coalition sues EPA to ban toxic wood preservatives. Risk Mngmnt 2003; 50: 2.
6. Schunt JH. They've been working on the railroad. April 2004. Plastic Technology [Online magazine], www.ptonline.com (accessed 26 May 2014).
7. Goldgaber A. Plastic railroad ties: growing market for alternative materials, www.SmallcapInsights.com (2009, accessed 5 May 2014).
8. Weart W. With a weak economy at the forefront and railroad spending cuts on the horizon, crosstie demand will be restrained for the rest of '09, then drop in '10. Progressive Railroading [Online magazine], http://www.progressiverailroading.com/ (accessed 10 June 2014).
9. Jackson LM and Nosker TJ. Technology, applicability, and the future of thermoplastic lumber. In: The DoD corrosion conference, 2009.
10. Manalo A, Aravinthan T, Karunasena Wand Ticoal A. A review of alternative materials for replacing existing timber sleepers. Compos Struct 2010; 92: 603–611.
11. Jimenez R. Vertical track modulus in plastic composite ties test zones at FAST. Report no. DOT/FRA/ORD-03/13, 2003. Pueblo, CO: Transportation Technology Center, Inc.
12. Lampo RG, Nosker TJ and Sullivan HW. Development, testing, and applications of recycled plastic composite cross ties. In: World Congress on Railway Research, Edinburgh, Scotland, UK, 28 September – 1 October 2003.
13. Roybal S. Composite crosstie test cyclic load. Report no. P-09-003, 2009. Pueblo, CO: Transportation Technology Center, Inc.
14. Reiff R, Trevizo C. Cracking and impact performance characteristics of plastic composite ties. Report no. DOT/FRA/ORD-12/03, 2012. Pueblo, CO: Transportation Technology Center, Inc.
15. America Railway Engineering and Maintenance of-Way Association. Evaluative tests for tie systems. In: AREMA specifications, 2011.

16. Lotfy I, Farhat M, Issa M, and Al-Obaidi M. Flexural behavior of high-density polyethylene railroad crossties. Journal of Rail and Rapid Transit; accepted for publication on 17 November 2014. DOI: 10.1177/0954409714565655.
17. Lotfy I, Farhat M, and Issa M. Temperature Effect on the performance of Glass Fiber Reinforced High Density Polyethylene Composite Railroad Crossties. Journal of Rail and Rapid Transit; In review.
18. Zhang Q.H., Tan S.H., Chou S.M. 2004. Investigation of fixation screw pull-out strength on human spine. El-Sevier, Journal of Biomechanics 37, 479–485, 91–95.
19. Hsu C.C., Chao C.K., Wang J.L, Hou S.M, Tsai Y.T, Lin J. 2005. Increase of pullout strength of spinal pedicle screws with conical core: biomechanical tests and finite element analyses. El-Sevier, Journal of Orthopaedic Research 23, 788-794
20. ANSYS® Multiphysics, Ansys Mechanical APDL and workbench Release 14.0, ANSYS, Inc.
21. ANSYS® Academic Research, Release 14.0, Help System, Mechanical APDL element reference, ANSYS, Inc.
22. Grewal, A.S., Sabbaghian, M., 1997. Load distribution between threads in threads connections, Journal of Pressure Vessel Technology, Transactions of the ASME 119, 91–95.

Contacts

Principal Investigator
Mohsen A. Issa
Professor of Civil and Material Engineering
University of Illinois at Chicago
312-996-2426
missa@uic.edu

NURail Center
217-244-4444
nurail@illinois.edu
http://www.nurailcenter.org/

NURail Project ID: NURail2012-UIC-R02-D

Evaluation of the longitudinal restraint, uplift resistance, and long-term performance of High Density Polyethylene crosstie rail support system using static and cyclic testing

By

Mohsen A. Issa
Professor of Civil and Material Engineering
University of Illinois at Chicago
missa@uic.edu

Ibrahim Lotfy
PhD Student of Civil and Material Engineering
University of Illinois at Chicago
ilotfy2@uic.edu

and

Maen Farhat
PhD Student of Civil and Material Engineering
University of Illinois at Chicago
mfarha3@uic.edu

DISCLAIMER

Funding for this research was provided by the NURail Center, University of Illinois at Urbana - Champaign under Grant No. DTRT12-G-UTC18 of the U.S. Department of Transportation, Office of the Assistant Secretary for Research & Technology (OST-R), University Transportation Centers Program. The contents of this report reflect the views of the authors, who are responsible for the facts and the accuracy of the information presented herein. This document is disseminated under the sponsorship of the U.S. Department of Transportation's University Transportation Centers Program, in the interest of information exchange. The U.S. Government assumes no liability for the contents or use thereof. The content of this document are currently under review for publication as "Lotfy I and Issa M. Evaluation of the longitudinal restraint, uplift resistance, and long-term performance of High Density Polyethylene crosstie rail support system using static and cyclic loading. Journal of Rail and Rapid Transit; In review"

TECHNICAL SUMMARY

Title

Evaluation of the longitudinal restraint, uplift resistance, and long-term performance of High Density Polyethylene crosstie rail support system using static and cyclic testing

Introduction

The study encompassed a comprehensive experimental investigation using static and cyclic test methods recommended by the AREMA manual. The static test addressed the performance of the rail support system when subjected to vertical uplift forces as well as longitudinal loading in the direction parallel to the rail track; e.g. breaking and traction forces. The dynamic test evaluated the long-term performance of the rail support system while being subjected to repeated loading for three million fatigue cycles. This performance provides an indication of the expected service life of the crossties. The objective of this report is as follows:

- Understand the behavior of the full system and the interactions between the rail, the different fastening components, and the HDPE crosstie.
- Evaluate the performance of the rail support system when subjected to longitudinal loading.
- Investigate the uplift behavior of the system and the contributions of each component of the fastening assembly to the uplift resistance.
- Assess the long-term performance of the rail support system.
- Identify any weak points in the system and recommend possible improvements/modifications.

Approach and Methodology

- The longitudinal restraint experimental test was performed as per the AREMA manual recommendations; AREMA Part 2- Section 2.6.2 – Test 5B (15). It was conducted to measure the ability of the rail support system to resist longitudinal rail movement.
- The fastener uplift test was performed following the AREMA recommendations; AREMA Part 2- Section 2.6.1 – Test 5A (15). It is used to measure the ability of the rail and fastener system to resist vertical uplift forces. The systems uplift resistance is provided by both the fastening clips and the spikes pullout resistances.
- The fastener repeated load test was performed by subjecting the complete system to fatigue loading cycles. It was conducted to measure the ability of the complete system to

resist cycles of vertical and horizontal loading. The durability of the crossties and the fastening system assembly can be assessed by quantifying the damage occurring after 3 million cycles of fatigue loading. The magnitude and frequency of the fatigue loading cycles are selected to simulate the expected loading on the system during its service life, i.e. the load and frequency of train wheel passes.

Findings

- For the Longitudinal Restraint of Rail Support System, The tested specimens showed a behavior similar to friction behavior with two distinct phases. The first phase is the static friction phase where the specimens experienced no motion. After the maximum static friction; i.e. impeding motion friction, was reached, the second phase starts, which corresponds to kinetic friction where the specimens experience friction with motion. The AREMA manual recommends that the maximum longitudinal displacement at 2400 lbs (10.67 kN) applied load is 0.2 in. (0.51 cm). This threshold was established to limit alteration in the track geometry and ensure constant gauge length.
- The fastener uplift test reveals that the rail fastening clips were the most significant contributor to the uplift resistance of the entire system. The contribution of the spikes was relatively insignificant compared to that of the fastening clips; i.e. about 7.0% on average at failure. Naturally, these contributions would change if cut spikes were used instead of the screw spikes.
- After 3 million cycles of fatigue loading, the HDPE crosstie experienced superficial surface abrasion under the steel bearing plate towards the field side. Similarly, the rail pads showed almost no damage towards the gauge side while the filed side showed deterioration and minor disintegration of the rubber material. Minor bite marks occurred on the filed side spikes. The fastening clips and the steel bearing plate showed no signs of deterioration or damage. However, the HDPE crosstie experienced material yielding, which was not initially detected by visual inspection.

Conclusions

- The longitudinal resistance of the full system is provided mainly by friction between the rail and the lower bearing plate and the upper insulators. The specimens' longitudinal resistance surpassed the AREMA recommendations by a significant margin. Moreover, the maximum static friction should not be reached under normal operating conditions, if properly designed.
- The rail fastening e-clips were the most significant contributor to the uplift resistance of this system. The contribution of the screw spikes was relatively insignificant: 7.0% at failure.
- The response of the fastening clips was similar to steel compliance with elastic and plastic phases. After unloading, the deflection was recovered with a steeper slope than that of the proportionality limit which is likely to be a result of the fastening clip's complex geometry.
- Throughout all the fatigue tests, no failure occurred in any of the fastening system components or the HDPE crossties.

- The deformations and strains experienced in the system during the fatigue testing were very low with the maximum occurring at the railhead horizontal movement and the minimum in the HDPE crosstie.
- The railhead experienced the most significant permanent horizontal deformation. Minor indentation and material yielding was experienced by the HDPE crossties.
- The system survived the fatigue test with normal wear and without any critical or major issues.
- After being subjected to 3 million cycles of fatigue loading, the HDPE crossties experienced a reduction in the stiffness and strength. Even though this reduction was small, it was significant enough to be taken into consideration when predicting service lives.
- The results of this experimental study illustrate that HDPE crossties have great performance and durability to be considered as a viable solution in real application after further field-testing.

Publications

- Lotfy I, and Issa M A, "**Evaluation of the longitudinal restraint, uplift resistance, and long-term performance of High Density Polyethylene crosstie rail support system using static and cyclic loading**" Journal of Rail and Rapid Transit; In review.
- Lotfy I, Farhat M, and Issa M A, "**Effect of Pre-drilling, Loading Rate and Temperature Variation on the Behavior of Railroad Spikes used for High Density Polyethylene Crossties**" Journal of Rail and Rapid Transit; In review.

Contacts

Principal Investigator
Mohsen A. Issa
Professor of Civil and Material Engineering
University of Illinois at Chicago
312-996-2426
missa@uic.edu

NURail Center
217-244-4444
nurail@illinois.edu
http://www.nurailcenter.org/

TABLE OF CONTENTS

LIST OF FIGURES

SECTION 1 INTRODUCTION

Rail track longevity is a primary concern for the railroad industry in the US. Thus, in an effort to enhance the durability and life-cycle cost efficiency of crossties, the railroad industry is increasingly leaning towards implementing alternative solutions to the traditional hardwood timber. Aside from deforestation concerns, hardwood timber crossties are vulnerable to rot and organic decay, drastically limiting their service life, which forces the manufacturers to use wood preservatives; e.g. creosote, which are toxics and hazardous to public health (1 to 5).

One of the available alternative materials for railroad crossties is recycled engineered composite plastic. Recycled composite plastic crossties can be engineered to meet the required performance criteria while maintaining the same geometry and weight as its timber counterparts, thus enabling one to one replacement strategies (6). Moreover, its inherent damping and durability can result in a prolonged service life with enhanced rideability and passenger comfort. These benefits render recycled plastic crossties a competitive solution fitting for both new and replacement operations of railroad crossties. Moreover, recycling plastic waste is a green process, which is very appealing in today's modern society that has a greater awareness of environmental issues.

Recycled plastic composite crossties have numerous and apparent environmental and structural advantages ranging from pollution and waste reduction to life cycle cost efficiency (6 to 9). Subsequently, several US manufacturers are currently offering commercial crosstie solutions using different recycled plastic composite materials and thousands of plastic crossties are currently in service in a wide variety of railroad tracks (10).

SECTION 2 PAST RESEARCH

Recycled composite plastic crossties have been studied by researchers in the past using experimental laboratory and field-testing. Jimenez (11) conducted an experimental investigation to evaluate the vertical track modulus of curved tracks using plastic and wooden. Lampo (12) investigated the performance of the composite crossties through several laboratory and field tests. The fatigue performance of composite crossties was investigated in a study conducted by Roybal (13). He performed a cyclic test on a half section of crosstie using cut spikes to fasten the rail and the steel bearing plate to the crosstie. The composite plastic crossties demonstrated adequate performance with normal wear and abrasion in the tie plate area and without any cracks or anomalies. Reiff and Trevizo (14) performed a series of experimental tests on three types of plastic composite crossties to investigate the effect of several factors on the performance of the crossties such as temperature variation, type of spikes used, and effect of impact forces. They concluded that the plastic composite crossties showed adequate performance, with HDPE reinforced with glass fiber showing the best performance out of the three types tested in terms of flexural stiffness and impact resistance.

As evident from the past studies, limited research data is available on composite plastic crossties and more specifically its long-term performance. Moreover, the prevalent US rail manual; the American Railway Engineering and Maintenance-of-Way Association (AREMA) manual, does not yet have fully developed criteria for composite crossties testing (15). Therefore, additional research is necessary to properly characterize and describe the behavior the rail support system and understand the interactions between the rail, the different fastening components, and the crosstie as well as assess its long-term performance.

SECTION 3 RESEARCH OBJECTIVE

The University of Illinois at Chicago conducted a series of studies to assess the feasibility of implementing High Density Polyethylene (HDPE) crossties in both conventional and high-speed rail applications. Previous reports have explored the flexural performance of HDPE composite railroad crossties, reinforced with discontinuous randomly distributed glass fibers, as well as its sensitivity to temperature variations (16, 17). Additionally, a parametric experimental investigation was also conducted to assess the effect of pre-drilling, loading rate, temperature, and type of spike on the behavior of rail fastening spikes (18). In this report, the behavior of the entire system is being investigated using recommendations from the previous work. This report presents an experimental investigation aiming to understand and assess the performance of the full rail support system; i.e. HDPE crosstie with the rail section and the fastening system installed. This includes understanding the interactions between the rail, the different fastening components, and the crosstie then evaluating its performance. The study encompassed a comprehensive experimental investigation using static and cyclic test methods recommended by the AREMA manual. The static test addressed the performance of the rail support system when subjected to vertical uplift forces as well as longitudinal loading in the direction parallel to the rail track; e.g. breaking and traction forces. The dynamic test evaluated the long-term performance of the rail support system while being subjected to repeated loading for three million fatigue cycles. This performance provides an indication of the expected service life of the crossties. The objective of this report is as follows:

- Understand the behavior of the full system and the interactions between the rail, the different fastening components, and the HDPE crosstie.
- Evaluate the performance of the rail support system when subjected to longitudinal loading.
- Investigate the uplift behavior of the system and the contributions of each component of the fastening assembly to the uplift resistance.
- Assess the long-term performance of the rail support system.
- Identify any weak points in the system and recommend possible improvements/modifications.

SECTION 4 EXPERIMENTAL PROGRAM

4.1 Description of the crosstie and fastening assembly

The composite plastic crossties investigated in this study were made from HDPE and were reinforced with randomly distributed discontinuous glass fibers. They were manufactured through an extrusion process from recycled plastic milk and detergent bottles; of which 7.2 billion pounds (3.27 billion kilograms) are land filled each year in the US (7). Foam inducing agents were used to control the density and cost of the final product and UV inhibitors and anti-oxidants were added to a thin skin surface layer to protect the surface of the crossties. These manufacturing procedures produced an efficient cross section with optimum distribution of the reinforcing fibers and minimal weight; however, it also creates a difference in the properties between the core and exterior regions of the cross section (16). The final HDPE crosstie has sectional dimensions of 9×7 in. (22.86×17.78 cm), length of 8 to 9 ft (2.44 to 2.74 m) and an average density of 56.8 pcf (910 kg/m3).

The fastening system components used in this study were provided by the Chicago Transit Authority (CTA). They corresponded to the same fastening components used for actual plastic composite crossties applications within the city of Chicago. Figure 1 shows the HDPE composite crosstie and the fastening system components used in this study. For each tested specimen, four rail screw spikes were used to fasten the steel bearing plate to the crosstie. The rail-bearing pad was placed in between the rail section and the steel bearing plate to provide friction and elasticity while insulating electricity. Two fastening e-clips were used to clamp the rail to the steel bearing plate from each side while two plastic insulators were placed in between the clip toes and the rail to provide electric insulation. This configuration represents the typical fastening system used with engineered plastic composite crossties in the city of Chicago.

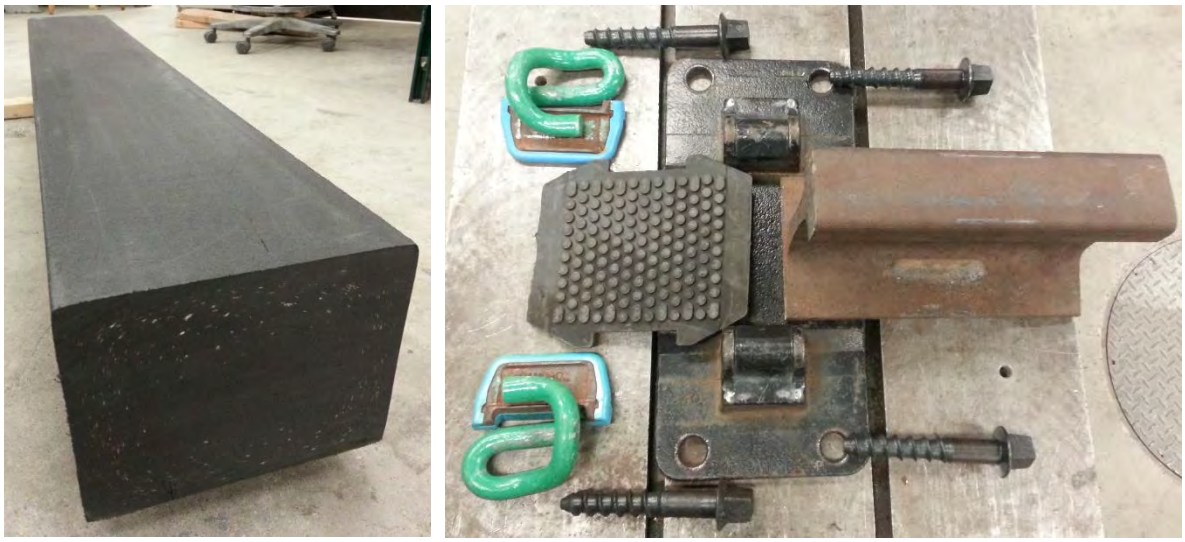

Figure 1. Rail, HDPE composite crosstie, rail section and fasting system assembly.

4.2 Testing Equipment

A sophisticated universal testing machine; "Instron 8500 Series Servo-hydraulic Testing System", was used in this study for all the experimental evaluations. This system has an actuator with a capacity of ±50,000 lbs (±222.4 kN) and the capability of applying both static and dynamic loading. The system has a 26 in. (66 cm) wide rigid steel testing bed with a total length of 144 in. (365.7 cm). The system is highly controlled using four distinct controlling schemes; load, deflection, strain and crack opening allowing for open and closed loop testing configurations.

4.3 Longitudinal Restraint of Rail Support System

The longitudinal restraint experimental test was performed as per the AREMA manual recommendations; AREMA Part 2- Section 2.6.2 – Test 5B (15). It was conducted to measure the ability of the rail support system to resist longitudinal rail movement. This movement can occur as a result of longitudinal forces in the direction of the rail track; e.g. breaking and traction forces. The support system rigidity is very important to retain the track geometry and ensure constant gauge length to avoid derailment. Moreover, train acceleration, deceleration, and breaking require a rigid support to ensure proper traction with the wheels. The longitudinal track rigidity is provided by contributions from consecutive crossties and fastening systems. This test assesses only one of the rail supports in details; i.e. the interactions between the rail, fastening assembly and HDPE crosstie. The support system resistance to longitudinal forces is expected to be a combination of the frictions between the rail and the underlying rail pad and steel bearing plate as well as the two insulator pads which are clamped to the rail by the, pre-strained,

fastening e-clips. For this test, the crosstie specimens were cut into 24 in. (60.9 cm) long segments and the rail was cut into a 14 in. (35.56 cm) long segment. The full rail and fastening system assembly were installed to the crosstie specimen. The spikes were installed manually using an adjustable wrench with the pre-drilling configuration proposed by the authors in the previous study; "setup D" profile (18). Seeing as the testing machine can only apply vertical loading, the specimens were rotated 90° and were fixed on their side in order to achieve the desired testing configuration. A wide flange steel I-beam was cut into a 24 in. (60.9 cm) long segment and was modified and stiffened with two steel pipe sections. This specially made I-beam was used to properly support the specimen while elevating it from the testing machine bed, which enabled free movement of the rail. Then six holes were drilled through the side of the specimens to properly fix them to the steel I-beam. The specimens were then fixed to the I-beam using six, 0.5 in. (1.27 cm), threaded rods and three, 1 in. (2.54 cm) thick, aluminum plates on the top. The loading was applied at the bottom edge of the rail cross-section as per AREMA recommendations and five specimens were tested to increase the reliability of the results. Figure 2 and 3 illustrate the longitudinal restraint test schematics and configuration.

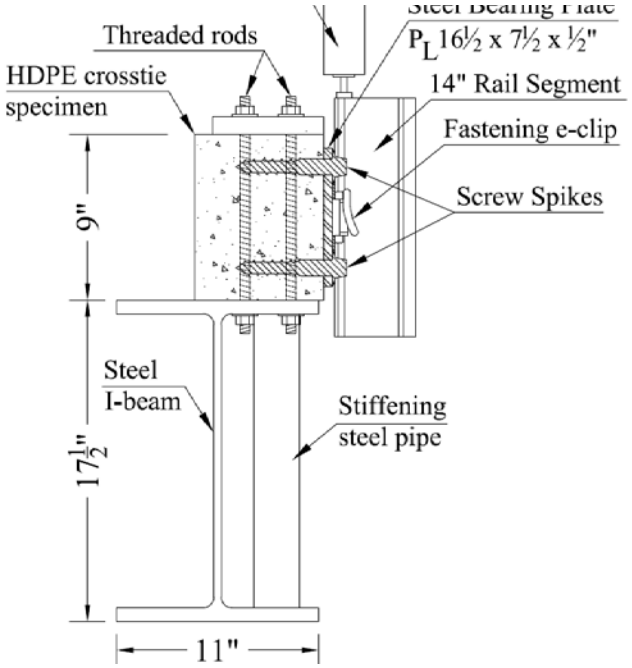

Figure 2. Longitudinal restraint test schematics. (All units are in inches; 1"= 2.54cm).

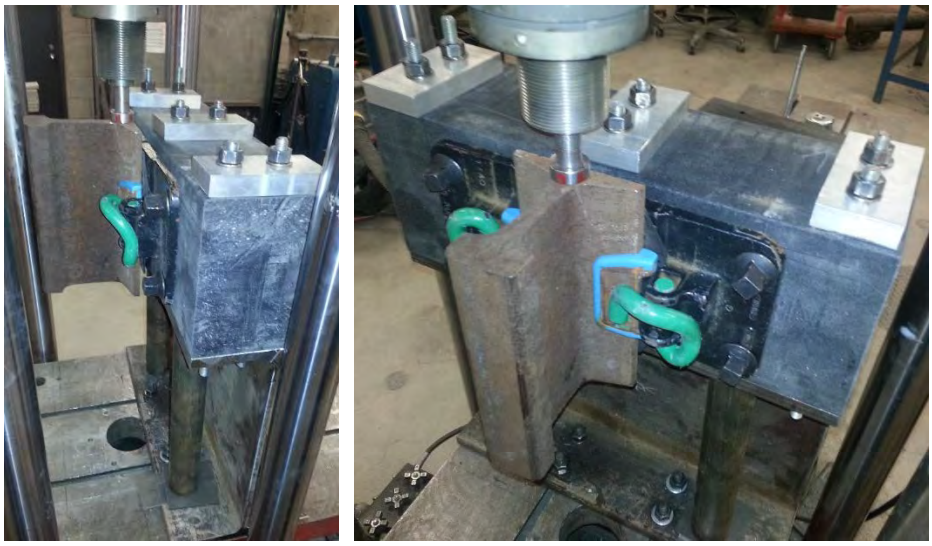

Figure 3. Longitudinal restraint test setup.

The loading was applied as a downward displacement, perpendicular to the specimen, with a, stroke controlled, loading rate of 0.05 in./min (0.13 cm/min) and the rail displacement was recorded with an accuracy of 1×10-5 in. (2.54×10-5 cm). The loading was applied until the rail section slipped by at least 0.2 in (0.51 cm) from the fastening system. Figure 4 and 5 present the test results for the five tested specimens.

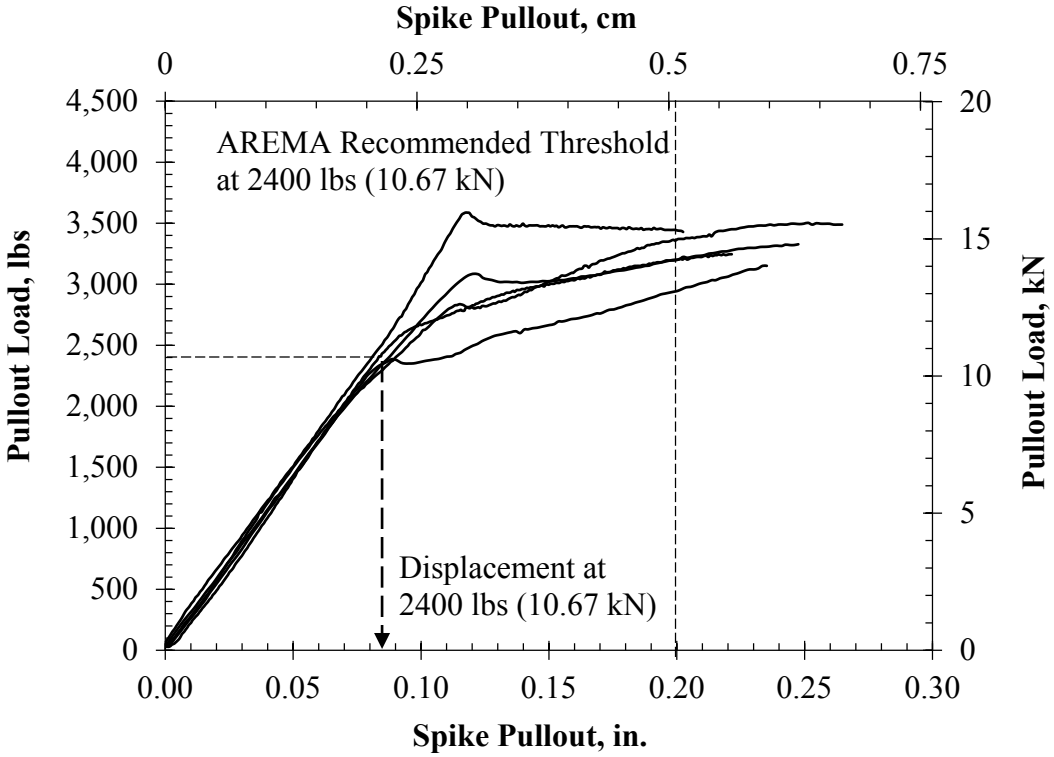

Figure 4. Fastener uplift sample test result.

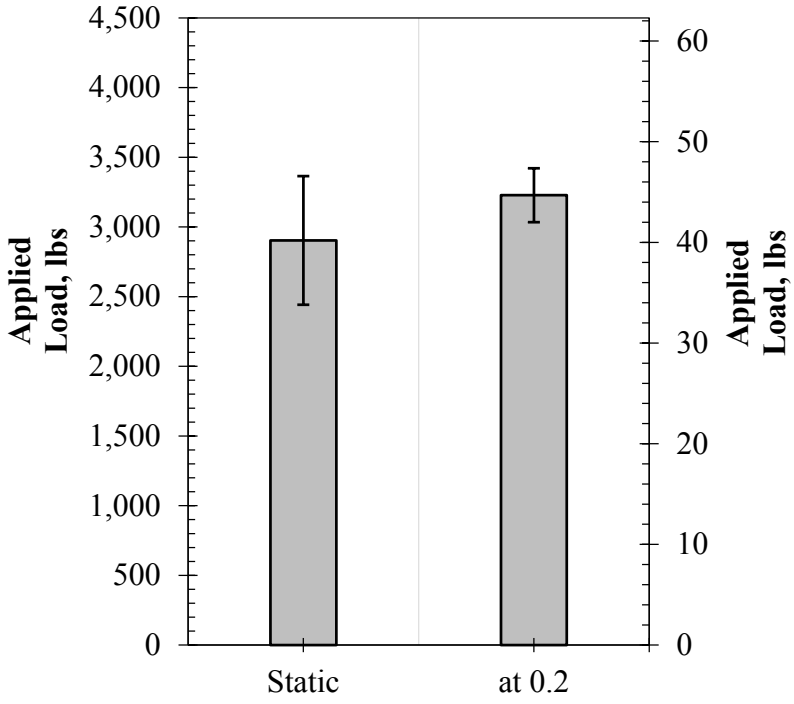

Figure 5. Fastener uplift test result summary for all the tested specimens.

The tested specimens showed a behavior similar to friction behavior with two distinct phases. The first phase is the static friction phase where the specimens experienced no motion. After the maximum static friction; i.e. impeding motion friction, was reached, the second phase starts, which corresponds to kinetic friction where the specimens experience friction with motion. As mentioned earlier, this behavior is reasonable as the resistance to longitudinal straining actions is provided by friction between the rail and the underlying rail pad and steel bearing plate and the two insulator pads. Inspection of Figure 4 and 5 reveals that the maximum static friction was relatively inconsistent and varied slightly between the different tested specimens, which could be attributed to the different rail pads, and insulators used for each specimen, as well as the installation procedures. It is also noticed that, regardless of the maximum static friction, all the specimens were converging on a constant friction value as afterwards; i.e. the kinetic friction. In addition, it is expected that the specimens' resistance will continue to level until they reach a constant friction force of about 3300 lbs (14.68 kN). The AREMA manual recommends that the maximum longitudinal displacement at 2400 lbs (10.67 kN) applied load is 0.2 in. (0.51 cm) (15). This threshold was established to limit alteration in the track geometry and ensure constant gauge length. As noticed from Figure 4, all the specimens experienced longitudinal displacements of about 0.09 in. (0.23 cm) at 2400 lbs (10.67 kN) applied load, which surpassed the recommendations by a significant margin. It is also important to note that the maximum static friction for all the tested specimens was reached before 0.2 in. (0.51 cm) displacement, which is significant as the maximum static friction should not be reached under normal operating conditions in a properly designed system.

4.4 Fastener Uplift

The fastener uplift test was performed following the AREMA recommendations; AREMA Part 2- Section 2.6.1 – Test 5A (15). It is used to measure the ability of the rail and fastener system to resist vertical uplift forces. The systems uplift resistance is provided by both the fastening clips and the spikes pullout resistances. Since the spikes pullout resistance was already investigated in previous tests (18), this test will enable the assessment of the fastening clips pullout resistance as well as the identification of the contributions of the spikes and the fastening clips to the pullout resistance of the entire system. For this test, the crosstie specimens were cut into 3 ft (0.91 m) long segments and the rail was cut into a 20 in. (50.8 cm) long segment. The complete rail and fastening system assembly was installed using, the recommended, setup D pre-drilled pilot holes as mentioned earlier (18). Two steel channels section were used in order to fix the specimens to the testing bed when applying the vertical uplift loading. A 20 in. (50.8 cm) rail segment was cut and machined specifically for this test setup. The rail segment was drilled and taped from the top, then a threaded rod was installed to enable the application of tensile uplift forces. Two linear

variable displacement transducers (LVDTs) were installed to monitor both the railhead and the steel bearing plate vertical displacements. The railhead displacement indicates the total uplift of the system while the steel bearing plate displacement provides an indication of the spikes pullout only without the fastening clip contribution. This scheme enables the identification of the contribution of both components to the overall system uplift resistance. Five specimens were tested at room temperature. Figure 6 and 7 illustrate the test configuration.

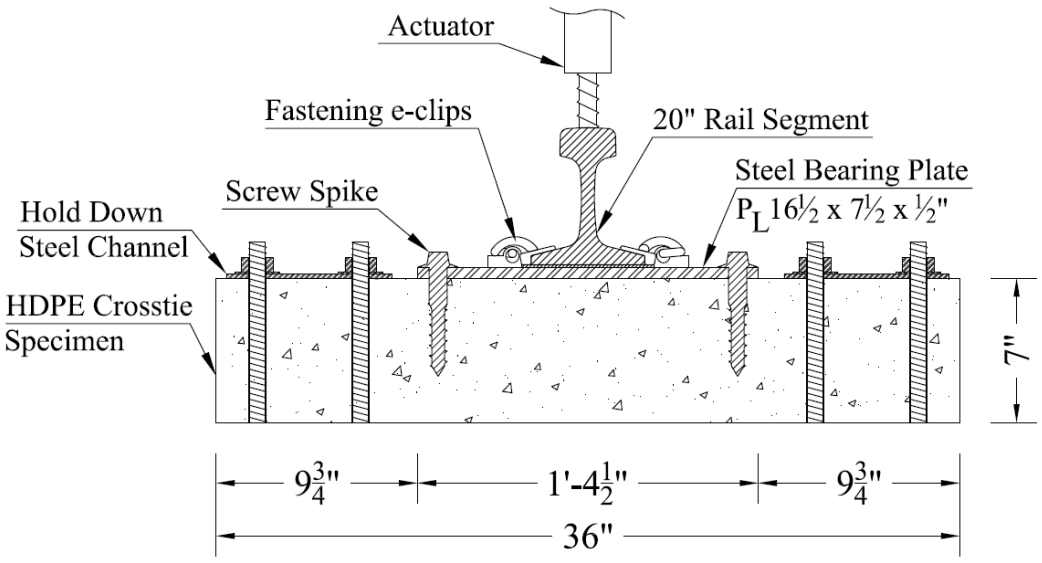

Figure 6. Fastener uplift test schematics. (All units are in inches; 1”= 2.54cm).

Figure 7. Fastener uplift test setup.

The vertical uplift load was applied until separation occurred between the rail and the assembly. The separation load was recorded then two cycles of reloading/unloading were applied until the load reached one and a half times the separation loading. Additionally, the first specimen only

was then loaded until failure. The failure was sudden and occurred in the fastening clips, and the failed clip fragment was then propelled with a great force across the laboratory, which was a safety risk, see Figure 8. Therefore, the remaining specimens were not loaded to failure and were stopped after the second reloading as per AREMA recommendations. Figure 9 presents a sample of the results while Figure 10 summarizes the test results for all the tested specimens.

Figure 8. Failure of the fastening clip.

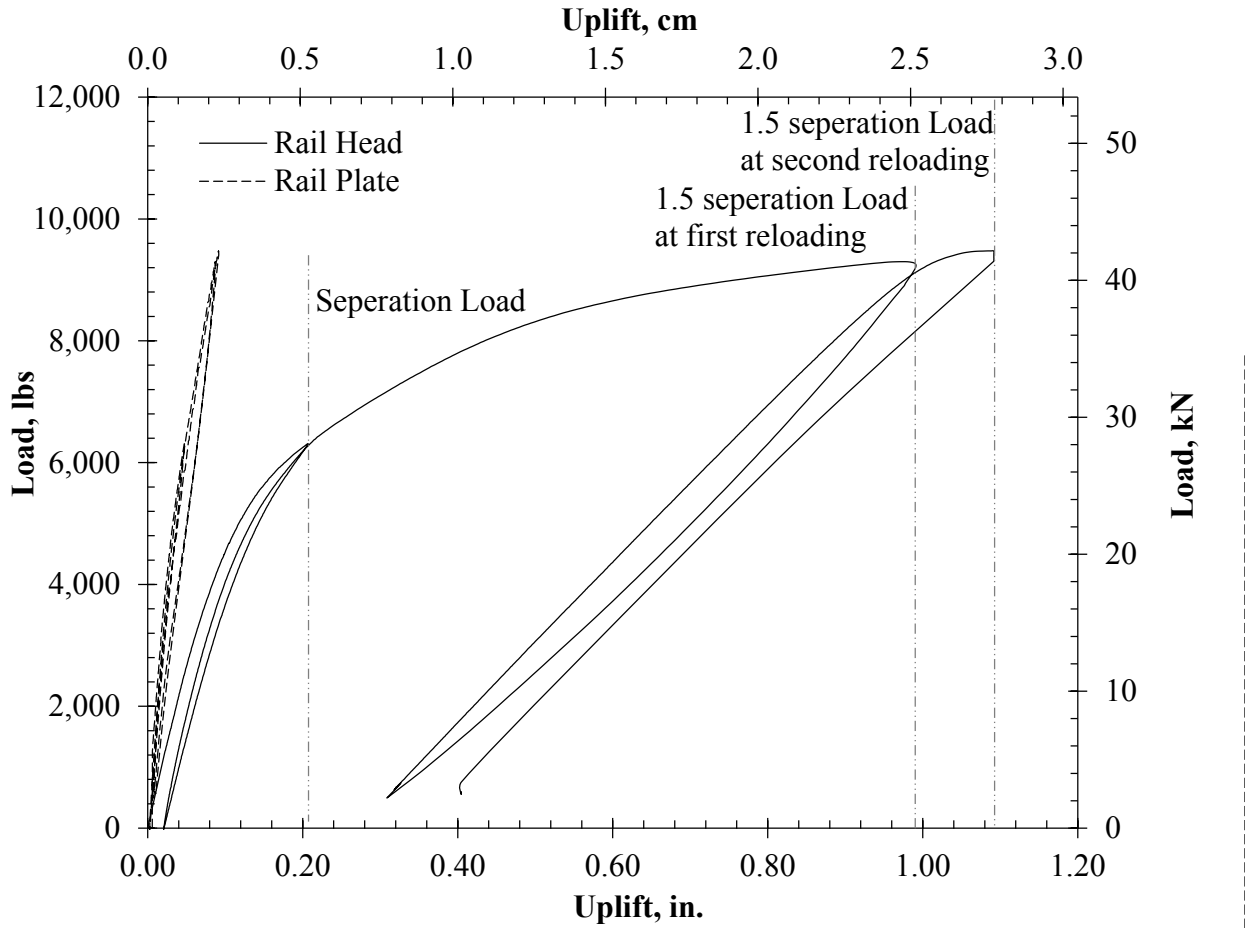

Figure 9. Fastener uplift sample test result.

In Figure 9, the measurement designated as "Rail Head" indicates the total uplift of the system while the measurement designated as "Rail Plate" provides an indication of the spikes pullout only without the fastening clip contribution. Thus, the contribution of the fastening clips is the difference between the two measurements. Inspection of Figure 9 reveals that the rail fastening clips were the most significant contributor to the uplift resistance of the entire system. The contribution of the spikes was relatively insignificant compared to that of the fastening clips; i.e. about 7.0% on average at failure. Naturally, these contributions would change if cut spikes were used instead of the screw spikes. However, in this configuration, the fastening clips were the main contributors to the system uplift resistance as evident by the fracture of the clips shown in Figure 8. The response of the fastening clips was similar to the normal compliance of steel with two distinct phases: elastic and plastic. The first separation load occurred at or shortly after yielding of the clips. After unloading, most of the deflection was recovered, with a small permanent deformation. However, after reloading to 1.5 separation load, the permanent deformation significantly increased which indicates that the clips transitioned into the plastic

region. It is curious to note that, after unloading, the deflection was recovered with a steeper slope than that of the proportionality limit which was not expected. This is likely to be a result of the fastening clip's complex geometry as it is not subjected to pure tension/compression. Figure 10 presents a summary of all the tested specimens.

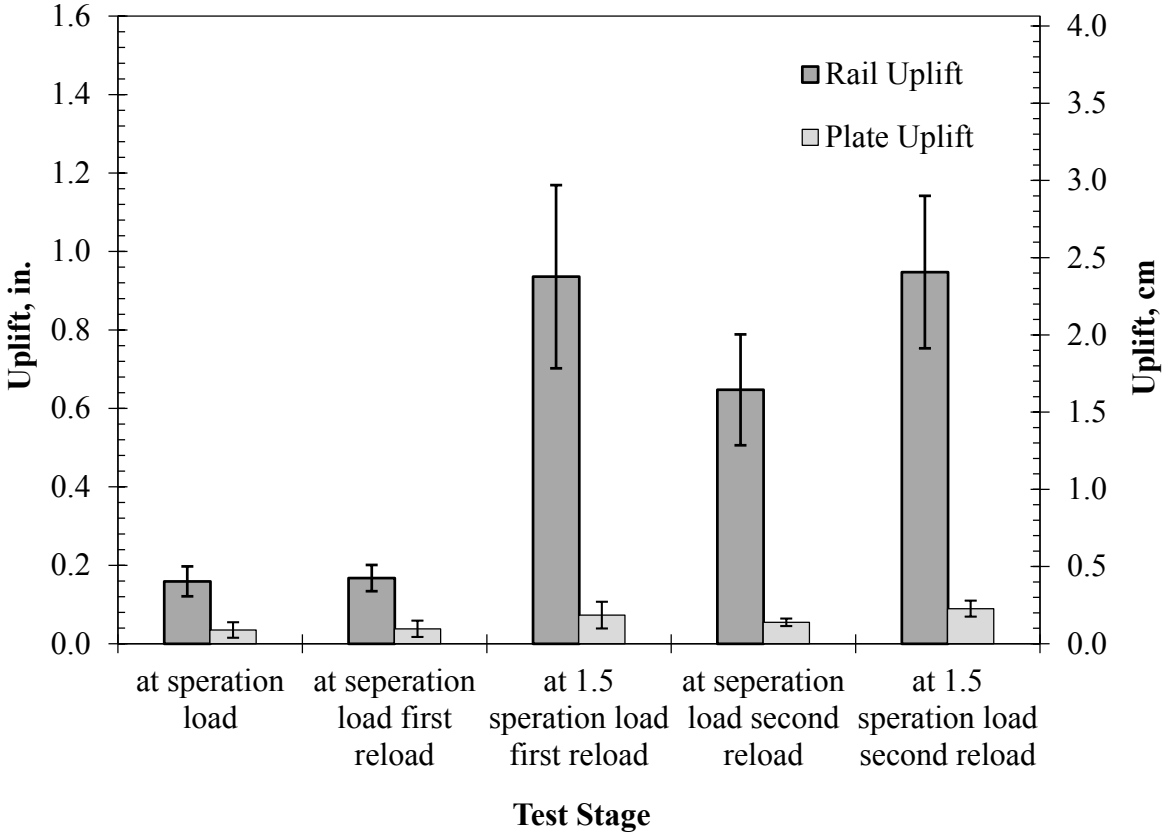

Figure 10. Fastener uplift test result summary for all the tested specimens.

Inspection of Figure 10 reveals further validates the minor contribution of the rail spikes. Moreover, it also validates that, at the separation load, the specimens were at or shortly after yielding, as after the first reloading the deformation at the separation load was almost identical. However, at the second reloading, the deformation was much larger; there was obvious permanent deformation in addition to the elastic deformations. Another important indication was the consistency of the results, which is indicated by the error bars. While the clips were still in the elastic range, the consistency was high, represented by the small error bars. On the other hand, the larger error bars indicate that clips have transitioned into plastic range.

4.5 Fastener Repeated Load

The fastener repeated load test was performed by subjecting the complete system to fatigue loading cycles. It was conducted to measure the ability of the complete system to resist cycles of vertical and horizontal loading. The durability of the crossties and the fastening system assembly can be assessed by quantifying the damage occurring after 3 million cycles of fatigue loading. The magnitude and frequency of the fatigue loading cycles are selected to simulate the expected loading on the system during its service life, i.e. the load and frequency of train wheel passes. As such, trains would have separate loading configurations resulting in different expected lives. Additionally, the effect of the accelerated, continuous loading in a laboratory setting is magnified compared to real applications where the system experience rest periods between consecutive trains. Therefore, experience plays a major role in determining the loading parameters that achieve a simulation appropriate for the desired application. In past research studies, Roybal (13) elected to simulate 9000 passes of a 110-car train for 2 million cycles, however, each cycle consisted of two 21,000 lbs (93.4 kN) loads (two actuators) with different angles of attack that accounted for vertical and horizontal loads with a loading frequency of 220 cycles per minute. The AREMA manual; AREMA Part 2- Section 2.6.3 – Test 5C (15), recommends using one actuator with a 20° inclination (to account for vertical and horizontal components of the wheel load) with a load magnitude of 30,000 lbs (133.45 kN) and a frequency of 300 cycles per minute for a total 3 million cycles. This configuration does not correspond to a specific train, but rather recommended as a general qualification criterion for crosstie systems. In this study, the AREMA recommendations were adopted with two minor modifications. Figure 11 illustrates the test schematics and the different designations used for each measurement recording instruments.

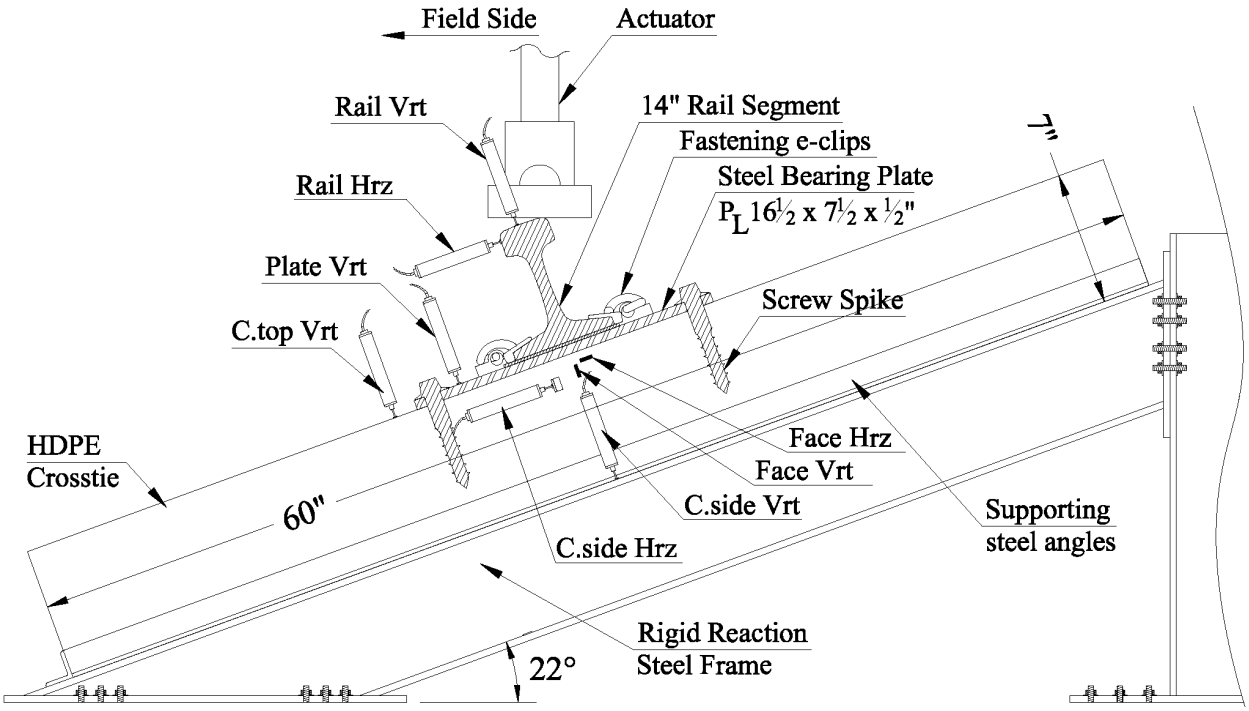

Figure 11. Test schematics and measurement designations for LVDTs and strain gauges.

For this test, the crosstie specimens were cut into 60 in. (152.4 cm) long segments and the rail was cut into a 14 in. (35.56 cm) long segment. The complete rail and fastening system assembly was installed using setup D predrilled pilot holes, as mentioned earlier (18). The specimens were then mounted on an inclined rigid reaction steel frame with supporting angles encasing them for the sides and the bottom. The steel frame was manufactured with an inclination angle of 22° to simulate, using only one actuator, the vertical and horizontal components of the rail wheel loading, yielding lateral to vertical load ratio of 0.4 (L/V = 0.4). This is the first of the two minor modifications applied to the AREMA recommendations; i.e. using 22° inclination angle instead of 20° which provides L/V = 0.4 instead of 0.36. The authors believe that L/V = 0.4 is a more conservative representation of the wheel load components especially in the case of curved tracks. The lateral component of the wheel load is more critical than the vertical component, as it produces lateral deformations leading to gauge widening and derailment. The second modification to the AREMA recommendations was required due to a laboratory limitation rather than a test optimization. The AREMA manual recommends the fatigue loading range to be from 0.6P upwards to 30,000 lbs (133.45 kN) downwards with a frequency of 300 cycles per minute [where P is the separation load acquired from the fastener uplift test; thus 0.6P = 3500 lbs (15.57 kN)]. However, as illustrated in Figure 11, the loading was applied, as a point load, using a single actuator. Due to the geometry of the railhead, it is very difficult to fix the actuator to the railhead in order to provide upward and downward loading while keeping them aligned with no

eccentricities or tolerance to avoid movement/impact in the system. Unfortunately, there were no available resources to manufacture a complicated loading device and fix the specimens to the testing bed to apply this loading nor to use two perpendicular actuators. Therefore, to account for this limitation, the loading was shifted to retain the fatigue stress range constant. The loading range used in this study was from 1500 lbs (6.67 kN) downwards to 35,000 lbs (155.69 kN) downwards. This modification maintained the same fatigue stress range; however, it shifted it from tension-compression to compression-compression. This alteration is less critical when studying the fastening system components contributing to its uplift resistance; i.e. rail spikes and fastening clips. However, it is significantly more critical for the HDPE crossties, rail pads and bearing plate, which was acceptable considering the scope of this research program. Due to the higher magnitude of the applied load, the loading frequency was kept at 3Hz; i.e. 180 cycles per minute, for added safety, which extended the testing time of one specimen to approximately 12 days in order to reach 3 million cycles.

To record the different deformations and strains, six LVDTs and four strain gauges were installed, as illustrated in Figure 11 and depicted in Figure 12 and 13. The LVDTs were used to monitor the deformations in the specimens: railhead vertical (designated as “Rail vrt”) and horizontal deformations (designated as “Rail Hrz”), steel bearing plate vertical deformation (designated as “Plate Vrt”), crosstie’s top surface vertical deformation (designated as “C.top Vrt”) and crosstie’s side vertical and horizontal deformations (designated as “C.side Vrt” and “C.side Hrz” respectively). The LVDTs were equipped with, specially made, color-coded, bolts at their tips to enable their retraction, without affecting accuracy, while the loading cycles were applied to avoid damage. The LVDTs were released only when recording the deformations; before fatigue loading (initial), then after 10,000 cycles; 50,000 cycles; 100,000 cycles; 250,000 cycles then every 250,000-cycle intervals until 3,000,000 cycles were reached. The strain gauges were mounted on the crosstie to measure the strains in the specimen throughout the whole duration of the test. The four strain gauges were installed as two T-rosettes (vertical and horizontal strains) on both sides of the crossties (designated as “Face Vrt”, “Face Hrz”, Back Vrt”, and “Back Hrz”).

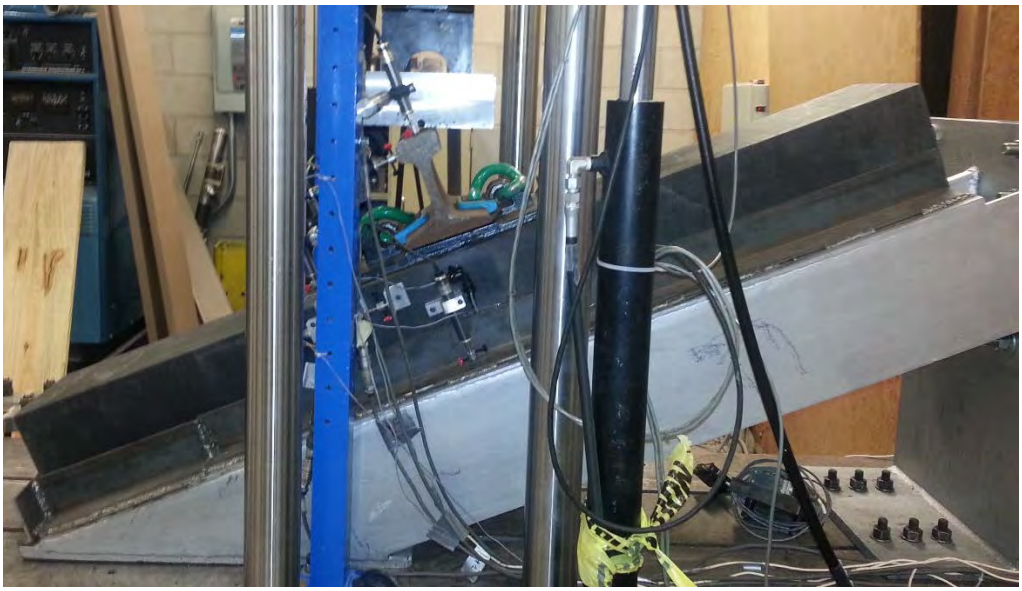

Figure 12. Test setup.

Figure 13. Test instrumentation and strain gauge installation.

Five specimens were tested and the data was recorded. The test was stopped after 3 million cycles and flexural tests were conducted on the specimens after fatigue to quantify the damage in the HDPE crosstie compared to new ones. No failure occurred in any of the fastening system components or the HDPE crossties throughout all the tests. Figure 14 presents the HDPE crosstie, rail pad, and the spike after the 3 million cycles showing the extent of the damage occurring in each component.

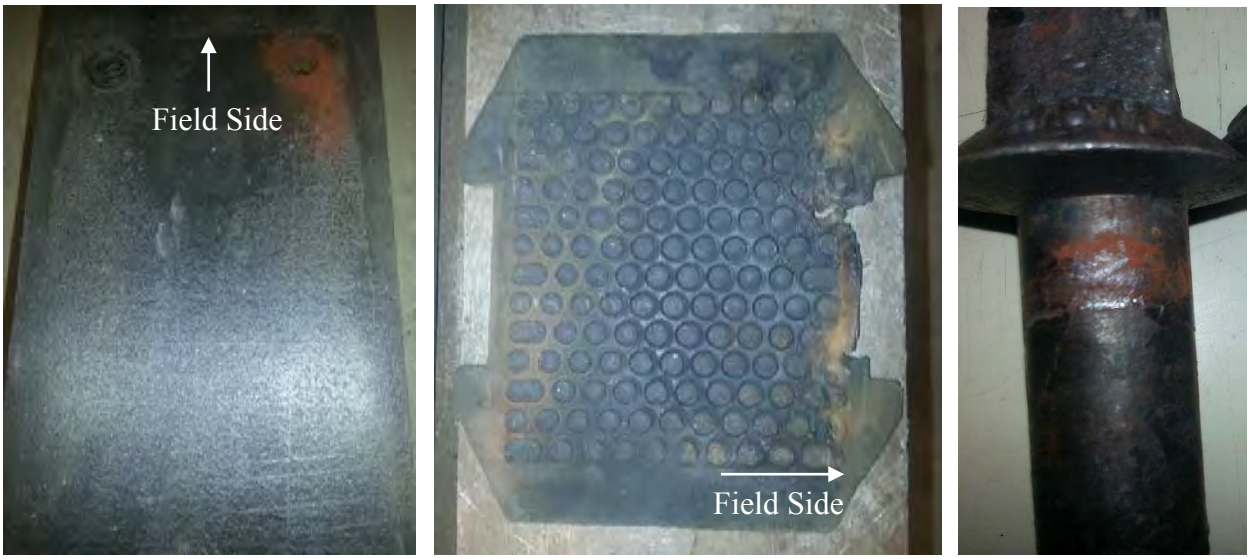

Figure 14. HDPE crosstie abrasion, pad damage, and spikes bite marks after 3 million cycles.

As depicted in Figure 14, the HDPE crosstie showed minor, superficial surface abrasion under the steel bearing plate. The abrasion occurred towards the field side while the gauge side showed little damage. Similarly, the rail pads showed almost no damage towards the gauge side while the filed side showed deterioration and minor disintegration of the rubber material, as shown in Figure 14. Minor bite marks occurred on the filed side spikes as well. The fastening clips and the steel bearing plate showed no signs of deterioration or damage. The deformation reading was collected and the peak deformation was identified for each recorded cycle. Figure 15 presents, on a log-log scale, the peak deformations of the system at all the recorded cycles for a sample specimen, and Figure 16 presents the peak strains recordings for the same specimen.

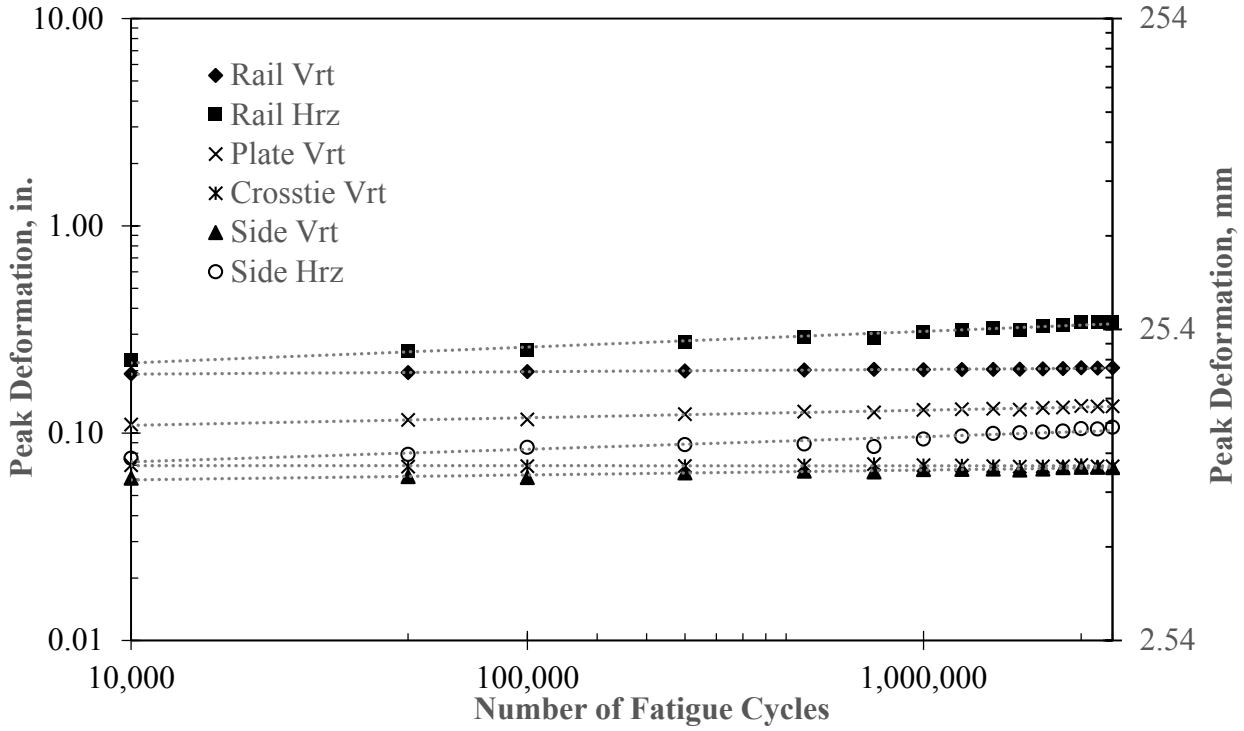

Figure 15. Peak deformations vs number of cycles for a sample specimen.

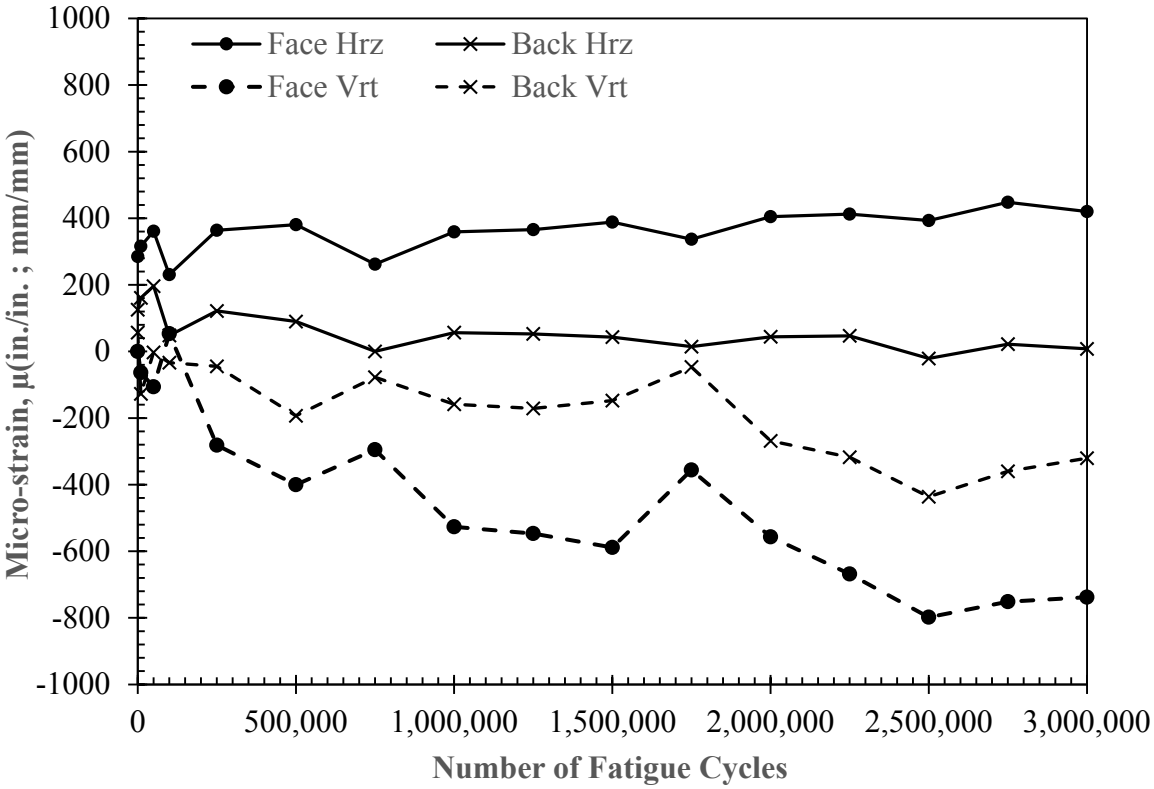

Figure 16. Peak stains readings vs number of cycles for a sample specimen

Inspection of Figure 15 reveals that the deformations experienced in the system were small; ranging from 0.05 to 0.35 in. (0.13 to 0.89 cm) with the maximum occurring at the railhead horizontal movement as expected. The minimum deformations occurred in the HDPE crosstie. The strain gauges reading further confirmed the LVDT results; the strains experienced by the HDPE crosstie were low, with the maximum strain reaching 798×10-6 (in./in.; cm/cm), refer to Figure 16. Moreover, the peak deformations of the system did not change significantly throughout the test duration. As noticed from Figure 15, most of the recordings were almost constant (parallel to the x-axis) throughout the test which indicates that the peak deformations at the beginning and end of the fatigue cycles did not increase by much, thus no significant damage occurred. To better illustrate and quantify this damage, the gain in peak deformations was calculated by subtracting the initial deformation, i.e. initial peak deformation was shifted to zero, and the resulting gain in peak deformations (indication of the permanent deformation) were plotted in Figure 17.

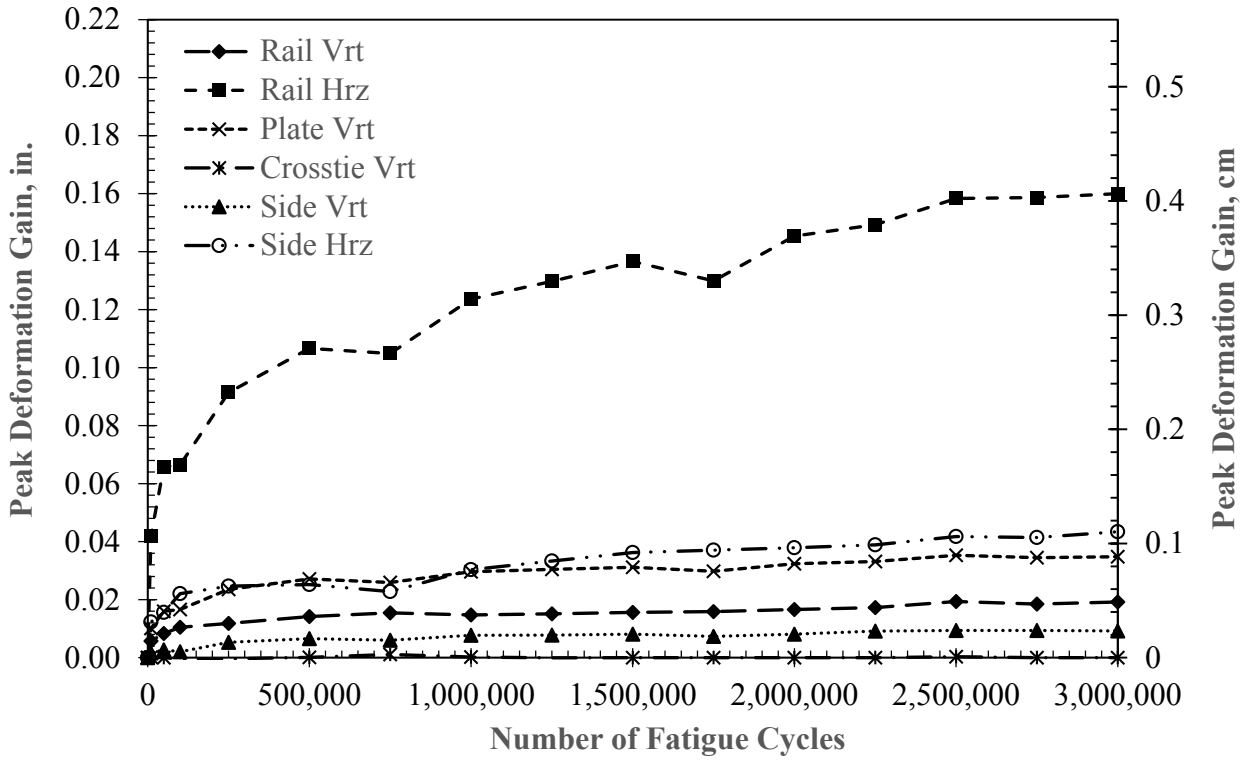

Figure 17. Peak deformation gain vs number of cycles.

Inspection of Figure 17 reveals clearly that the railhead horizontal movement is the most affected part of the system by the accumulated fatigue deterioration. The railhead horizontal movement directly affects the gauge length thus has to be monitored closely. Apart for the horizontal railhead movement, all the accumulated permanent deformations due to fatigue were minor. Figure 18 summarizes the results of all the five tested specimens using the maximum gained peak deformation after 3 million cycles, which provides an indication of the permanent deformations in the system. The AREMA manual recommends a maximum permanent deformation of 0.2 in. (0.51 cm) for the railhead lateral deflection.

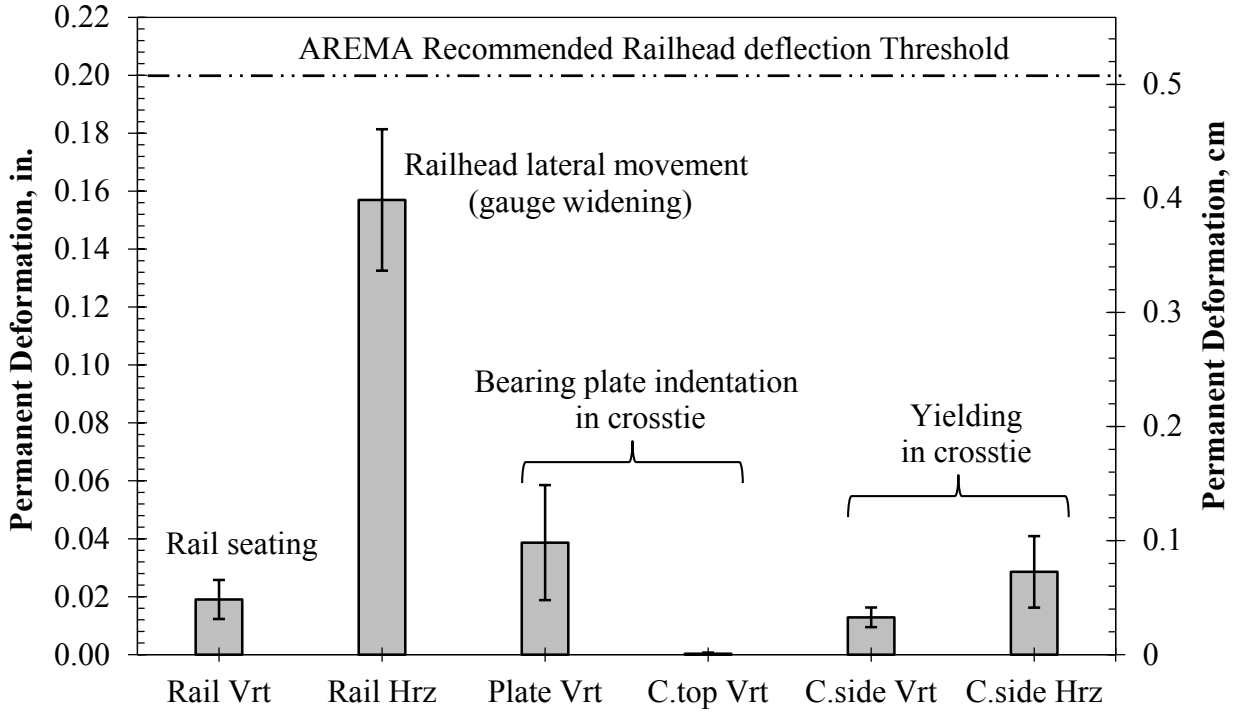

Figure 18. Maximum gained peak deformation after 3MM cycles for all the tested specimens.

As shown in Figure 18, the maximum gained peak vertical deformation of the railhead, (average of 0.019in. (0.048 cm)), is an indication of the rail seating, which occurred due to installation tolerances and imperfections. The railhead lateral movement is of great interest as it indicates the gauge widening. The difference between the bearing plate and the crosstie's surface vertical deflections quantifies the bearing plate indentation in the HDPE material, which averaged 0.039in. (0.099 cm). It is important to note that the crosstie's top surface vertical deflection was almost zero which means that, outside the vicinity of the bearing plate (refer to Figure 11 for the LVDTs' locations), the crosstie was experienced no damage or permanent deformation as a result of fatigue loading. Another important observation to note is that bearing plate vertical deflection gained was greater than that of the railhead vertical deflection, which, at first could appear illogical. However, after considering the location of both LVDTs, it becomes apparent that the bearing plate vertical deflection would be experience more damaged because it is located on the field side as oppose to the railhead vertical deflection, which is in the center of the system, refer to Figure 11. The applied vertical and horizontal loads creates a bending actions that affected the field side more significantly than the other areas, which was evident by the visual investigation of the component's damage shown in Figure 14. Finally, both the crosstie side defamations indicate permanent damage, in the form of yielding, in the HDPE material. As

observed before, apart for the horizontal railhead movement, all the accumulated permanent deformations due to fatigue were minor.

After the fatigue tests were concluded, the damaged specimen were then tested using a three point bending configuration are per the AREMA recommendations; AREMA Part 2- Section 2.2.3 – Test 1C (15). The results of the flexural test were compared with the new crossties, previously tested by the authors as part of this research effort (16). All the tested specimens failed at the mid-span of the crosstie and not at the predrilled holes' locations nor at the filed side, as shown in Figure 19. The behavior of the crosstie was similar to the new crossties tested before. Figure 20 presents the stress-strain relationship for the new and fatigued crossties. Table 1 summarizes the flexural parameters of the new and fatigued crossties and compares between them.

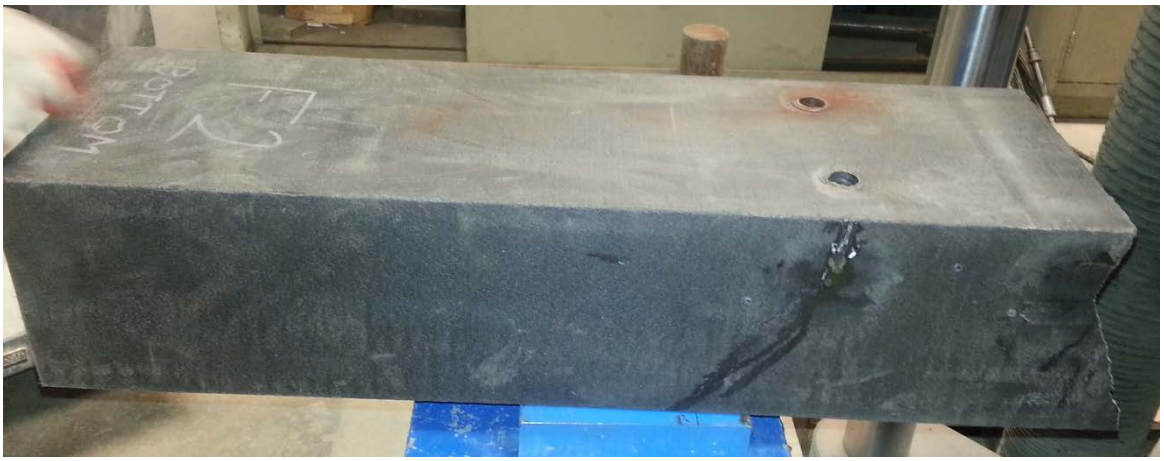

Figure 19. Failure of the specimens in flexure after 3 million fatigue cycles.

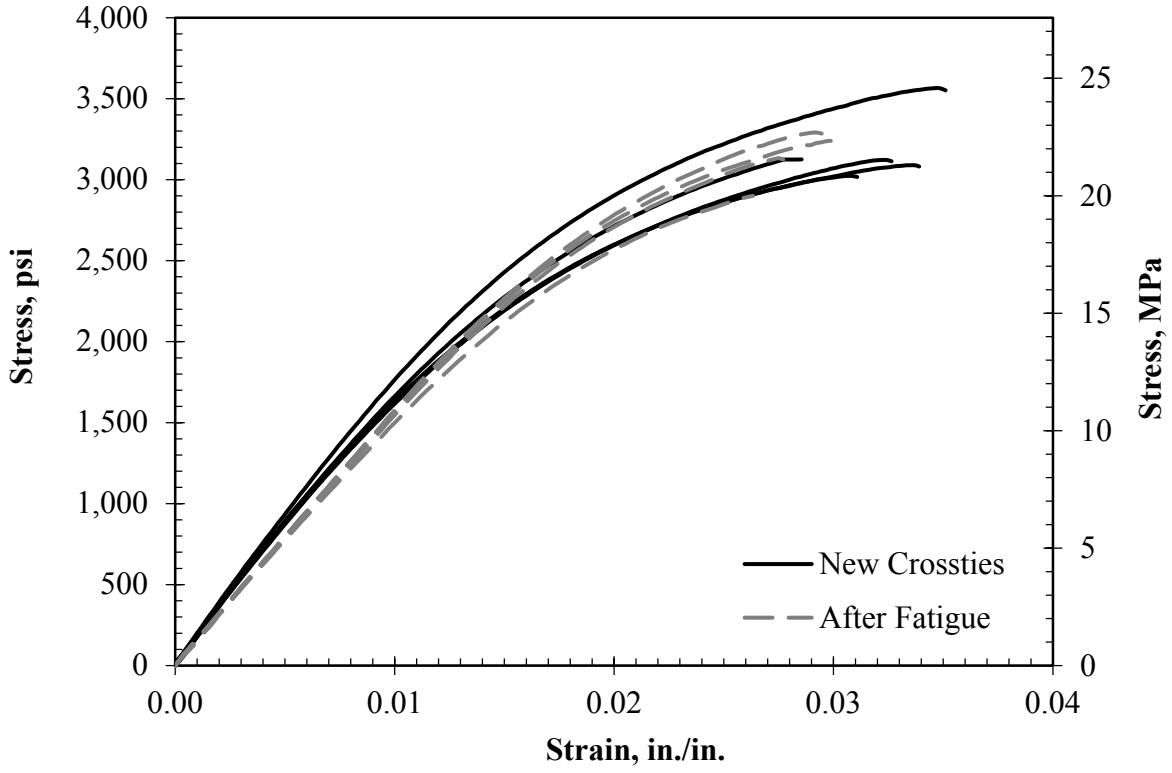

Figure 20. Stress-strain relationship for the new and fatigued crossties.

Table 1. Summary of the flexural parameters for both the new and fatigued crossties.

Crosstie Condition	New*		After fatigue		After fatigue/New
	psi	MPa	psi	MPa	
Modulus of Rupture	3,185	21.96	3,131	21.59	98%
Ultimate Strain, με	32,257		28,630		89%
Initial Tangent	190,151	1311.05	159,975	1102.99	84%
Modulus at 600 psi (4.14 MPa)	183,228	1263.31	158,275	1091.27	86%
Modulus at 1% strain	166,205	1145.93	154,110	1062.55	93%

*Flexural test data for the New crossties were tested previously by the authors (15).

At first glance of Figure 20, the difference between the new specimens and the specimens after fatigue is not very clear. However, after careful investigation, it becomes clear that there is a noticeable difference in the initial modulus between the two; i.e. the initial slope of the stress-strain curve was reduced after fatigue. This observation was confirmed by Table 1; the initial tangent modulus dropped 16% due to the fatigue damage. From the data presented in Figure 20 and Table 1, the following can be concluded. In the initial stage of the test, the specimens' resistance is mainly dependent on the HDPE material, as the fiber reinforcements were not yet activated. The HDPE material experienced yielding due to the fatigue test, which reduced the initial modulus as evident by the 16% reduction. As the test progresses, the fiber reinforcements get gradually activated reducing the effect of the HDPE material yielding, as evident by the diminishing reduction in the flexural moduli as the test progresses; e.g. 14% reduction at 600 psi (4.14 MPa), then 7% reduction at 1% strain. The modulus of rupture remained almost constant, dropping only 2%, as it is mainly dependent on the ultimate strength of the fiber reinforcement which were unaffected by the fatigue cycles. The ultimate strain however is dependent on the ductility of the HDPE material, thus experienced a reduction of 11%.

SECTION 5 SUMMARY AND CONCLUSION

- The longitudinal resistance of the full system is provided mainly by friction between the rail and the lower bearing plate and the upper insulators. The specimens' longitudinal resistance surpassed the AREMA recommendations by a significant margin. Moreover, the maximum static friction should not be reached under normal operating conditions, if properly designed.
- The rail fastening e-clips were the most significant contributor to the uplift resistance of this system. The contribution of the screw spikes was relatively insignificant: 7.0% at failure.
- The response of the fastening clips was similar to steel compliance with elastic and plastic phases. After unloading, the deflection was recovered with a steeper slope than that of the proportionality limit which is likely to be a result of the fastening clip's complex geometry.
- Throughout all the fatigue tests, no failure occurred in any of the fastening system components or the HDPE crossties.
- After 3 million cycles of fatigue loading, the HDPE crosstie experienced superficial surface abrasion under the steel bearing plate towards the field side. Similarly, the rail pads showed almost no damage towards the gauge side while the filed side showed deterioration and minor disintegration of the rubber material. Minor bite marks occurred on the filed side spikes. The fastening clips and the steel bearing plate showed no signs of deterioration or damage. However, the HDPE crosstie experienced material yielding, which was not initially detected by visual inspection.
- The deformations and strains experienced in the system during the fatigue testing were very low with the maximum occurring at the railhead horizontal movement and the minimum in the HDPE crosstie.
- The railhead experienced the most significant permanent horizontal deformation. Minor indentation and material yielding was experienced by the HDPE crossties.
- The system survived the fatigue test with normal wear and without any critical or major issues.
- After being subjected to 3 million cycles of fatigue loading, the HDPE crossties experienced a reduction in the stiffness and strength. Even though this reduction was small, it was significant enough to be taken into consideration when predicting service lives.
- The results of this experimental study illustrate that HDPE crossties have great performance and durability to be considered as a viable solution in real application after further field-testing.

SECTION 6 REFERENCES

1. Thierfelder T and Sandstrom E. The creosote content of used railway crossties as compared with European stipulations for hazardous waste. Sci Total Environ 2008; 402:106–112.
2. Zagier AS. Creosote: 'Witch's Brew'. http://www.mindfully.org/Pesticide/2004/Creosote-Illness-Death24may04.htm (accessed 24 May 2014).
3. Morris T. Poisonous railway sleepers pose health risk. October 2008. http://lists.greens.org.au/mailman/public/media/2008-October/010679.html (accessed 28 May2014).
4. Pruszinski A. Review of the landfill disposal risks and the potential for recovery and recycling of preservative treated timber. Environmental Protection Agency Report, 1999. South Australia: Sinclair Knight Merz.
5. Coffin B. Coalition sues EPA to ban toxic wood preservatives. Risk Mngmnt 2003; 50: 2.
6. Schunt JH. They've been working on the railroad. April 2004. Plastic Technology [Online magazine], www.ptonline.com (accessed 26 May 2014).
7. Goldgaber A. Plastic railroad ties: growing market for alternative materials, www.SmallcapInsights.com (2009, accessed 5 May 2014).
8. Weart W. With a weak economy at the forefront and railroad spending cuts on the horizon, crosstie demand will be restrained for the rest of '09, then drop in '10. Progressive Railroading [Online magazine], http://www.progressiverailroading.com/ (accessed 10 June 2014).
9. Jackson LM and Nosker TJ. Technology, applicability, and the future of thermoplastic lumber. In: The DoD corrosion conference, 2009.
10. Manalo A, Aravinthan T, Karunasena Wand Ticoal A. A review of alternative materials for replacing existing timber sleepers. Compos Struct 2010; 92: 603–611.
11. Jimenez R. Vertical track modulus in plastic composite ties test zones at FAST. Report no. DOT/FRA/ORD-03/13, 2003. Pueblo, CO: Transportation Technology Center, Inc.
12. Lampo RG, Nosker TJ and Sullivan HW. Development, testing, and applications of recycled plastic composite cross ties. In: World Congress on Railway Research, Edinburgh, Scotland, UK, 28 September – 1 October 2003.
13. Roybal S. Composite crosstie test cyclic load. Report no. P-09-003, 2009. Pueblo, CO: Transportation Technology Center, Inc.
14. Reiff R, Trevizo C. Cracking and impact performance characteristics of plastic composite ties. Report no. DOT/FRA/ORD-12/03, 2012. Pueblo, CO: Transportation Technology Center, Inc.
15. America Railway Engineering and Maintenance of-Way Association. Evaluative tests for tie systems. In: AREMA specifications, 2011.

16. Lotfy I, Farhat M, Issa M, and Al-Obaidi M. Flexural behavior of high-density polyethylene railroad crossties. Journal of Rail and Rapid Transit; In press, accepted for publication on 17 November 2014. DOI: 10.1177/0954409714565655.
17. Lotfy I, Farhat M, and Issa M. Temperature Effect on the performance of Glass Fiber Reinforced High Density Polyethylene Composite Railroad Crossties. Journal of Rail and Rapid Transit; In review.
18. Lotfy I, Farhat M, and Issa M. Effect of Pre-drilling, Loading Rate and Temperature Variation on the Behavior of Railroad Spikes used for High Density Polyethylene Crossties. Journal of Rail and Rapid Transit; In review.

Contacts

Principal Investigator
Mohsen A. Issa
Professor of Civil and Material Engineering
University of Illinois at Chicago
312-996-2426
missa@uic.edu

NURail Center
217-244-4444
nurail@illinois.edu
http://www.nurailcenter.org/

National University Rail Center - NURail
US DOT OST-R Tier 1 University Transportation Center

NURail Project ID: NURail2012-UIC-R02-E

Accelerated Bridge Construction for Railroad Elevated Structures

By

Mohsen A. Issa
Professor of Civil and Material Engineering
University of Illinois at Chicago
missa@uic.edu

Ibrahim Lotfy
PhD Student of Civil and Material Engineering
University of Illinois at Chicago
ilotfy2@uic.edu

and

Maen Farhat
PhD Student of Civil and Material Engineering
University of Illinois at Chicago
mfarha3@uic.edu

DISCLAIMER

Funding for this research was provided by the NURail Center, University of Illinois at Urbana - Champaign under Grant No. DTRT12-G-UTC18 of the U.S. Department of Transportation, Office of the Assistant Secretary for Research & Technology (OST-R), University Transportation Centers Program. The contents of this report reflect the views of the authors, who are responsible for the facts and the accuracy of the information presented herein. This document is disseminated under the sponsorship of the U.S. Department of Transportation's University Transportation Centers Program, in the interest of information exchange. The U.S. Government assumes no liability for the contents or use thereof.

National University Rail Center - NURail
US DOT OST-R Tier 1 University Transportation Center

TECHNICAL SUMMARY

Title

Accelerated Bridge Construction for Railroad Elevated Structures

Introduction

In this report, a proof-of-concept for construction or replacement operations for urban railroad bridges was performed using full-scale modeling. Two prefabricated simple span bridges were considered for both freight and passenger rail. The bridges were considered supporting railroad tracks using HDPE crossties. The full-scale models featured all the material models and the interactions and recommendations achieved in previous studies.

Approach and Methodology

The full-scale model was considered for urban environment, specifically a metropolitan city layout as the large traffic density further encourages ABC. The location of the bridge was chosen in the city of Chicago, IL; it is a bridge supporting a transfer station located on the "Red Line" of the CTA; Wilson Station.

The first system selected was pretensioned U-Girders with full-depth precast panel deck system. The U-Girders have been used for highway bridges in the state of Florida. The system has an efficient cross section that can accommodate presstressing as well as ABC construction methods.

Another system, which was also selected for investigation in this study; was the post-tensioned Box girder system. This system was adopted by the California High-Speed Train Project (CHSTP) as a typical section for aerial structures. This system can achieve the required structural performance and economy with adequate safety and pleasing aesthetic. It is recommended for implementation with a simple span and a span-to-depth ratio of 10.

Both models were assumed doubly symmetric about the mid-span and the middle of the bridge cross section, with symmetry boundary conditions applied accordingly. Since both rail tracks were simultaneously loaded as per AREMA recommendations, symmetry about the middle of the bridge cross section was true and valid. Boundary conditions were applied by restraining the vertical movement of the support bearing line in addition to the symmetric boundary conditions.

Findings

Both system behaved as expected showing appropriate deflection due to dead load, camber due to prestressed and normal service and ultimate deflections. The noticeable difference between the two systems is the deflection at service load. The main reason for this discrepancy is the prestressing profiles. Since the U-Girder featured straight strands, higher tensile stresses at the top of the section are introduced near the supports, which were manifested in the deflected shape. However, for the Box girder system, the profile of the PT tendons were designed to pass through the centroid of the cross section at the supports, which eliminates these additional tensile stresses, and thus yielding a normal deflected shape.

The crossties were subjected to bending stresses due to the applied wheel loads. However, contrary to ballast, the bending stresses induced compressive stresses at the top fibers of the cross-section. This is due to the fact that the crossties experienced the same deformations as the supporting slabs.

The maximum shear stresses occurred under the axle loads as expected. Moreover, the distribution of the shear stresses along the length of the crossties was close to that of the uniformly distributed case but with concentration under the steel bearing plates. As noticed, all the shear stresses were within the allowable range. The maximum interfacial shear stresses occurred underneath the steel bearing plates while elsewhere it was almost non-existent, which agrees with the results obtained previously.

Conclusion

- ABC plays a major role in new or replacement construction operations for railroad bridges due to the limited construction window.
- The material models implemented in the full-scale mode provided accurate representation of the behavior of the full system in actual railroad bridges.
- Both ABC system studied showed favorable performance, which provided a proof-of-concept for future upgrade to HSR in urban setting.
- The pretensioned U-Girder with full-depth precast panels system illustrated great performance showing higher carrying capacity and less deflection than the post-tensioned Box girder system. However, the Box girder system showed a much higher ductility before failure.
- Cracking initiated in the Box girder system significantly before the U-Girder system, at about 70% less load due to the efficiency and multiple girder setup of the cross-section design of the U-Girder system. Thus, it is proposed for future applications.
- The U-Girder system performed better that expected outperforming the Box girder system. Thus it is recommended for future investigations and implementation.

Publications

None

Contact

Principal Investigator

Mohsen A. Issa
Professor of Civil and Material Engineering
University of Illinois at Chicago
312-996-2426
missa@uic.edu

NURail Center

217-244-4444
nurail@illinois.edu
http://www.nurailcenter.org/

TABLE OF CONTENTS

LIST OF FIGURES

SECTION 1 INTRODUCTION

The major difference between highway and railroad bridges in the US is that the railroad industry is privately owned as oppose to most countries where it is publically funded (1). Another major difference between highway and railroad bridges is that the traffic of highway bridges can be diverted using nearby routes whereas railroad traffic cannot. Moreover, since most of the railroad bridges are privately owned, stringent limitations are placed on traffic delays and closures times, therefore, the main focus of railroad bridge projects is economics and safety while constructing under traffic or during short time windows (1). For this reason, prefabricated simple spans bridges are favored over continuous spans as they can be replaced, one-to-one, between consecutive trains with little interruption to traffic flow.

In this report, a proof-of-concept for construction or replacement operations for urban railroad bridges was performed using full-scale modeling. Two prefabricated simple span bridges were considered for both freight and passenger rail. The bridges were considered supporting railroad tracks using HDPE crossties. The full-scale models featured all the material models and the interactions and recommendations achieved in previous studies (2 to 5).

SECTION 2 ACCELERATED BRIDGE CONSTRUCTION

2.1 Location and ABC system

The full-scale model was considered for urban environment, specifically a metropolitan city layout as the large traffic density further encourages ABC. The location of the bridge was chosen in the city of Chicago, IL; it is a bridge supporting a transfer station located on the "Red Line" of the CTA; Wilson Station. The station was built in 1923 and serves about 6,300 passenger a week. This station had four rail tracks and the bridge was composed of three branches separated by the two platforms where the passengers can board the trains. The middle branch was the largest as it supported the two main rail tracks while the side branches support the sidetracks. The main branch was considered in this study supporting two the two main rail tracks with two passenger platforms on each side.

The original design of the existing bridge used steel girders with shot spans. Currently the bridge is scheduled for reconstruction using concrete girders with longer spans; 42 to 58 ft (12.8 to 17.7 m). This study explores the possible future reconstruction and upgrade to higher speeds trains using maximum spans of 60 ft (18.3 m) to accommodate the city roads layout and precast prestressed concrete technology allowing for fast construction (**Figure 1** presents the bridge layout). Therefore, the most suitable precast prestressed concrete systems were identified in terms of allowing fast construction time while having efficient design to maintaining excellent performance. Two precast system were identified and used in the full-scale modeling; pretensioned U-Girders with full-depth precast panels and post-tensioned box girders.

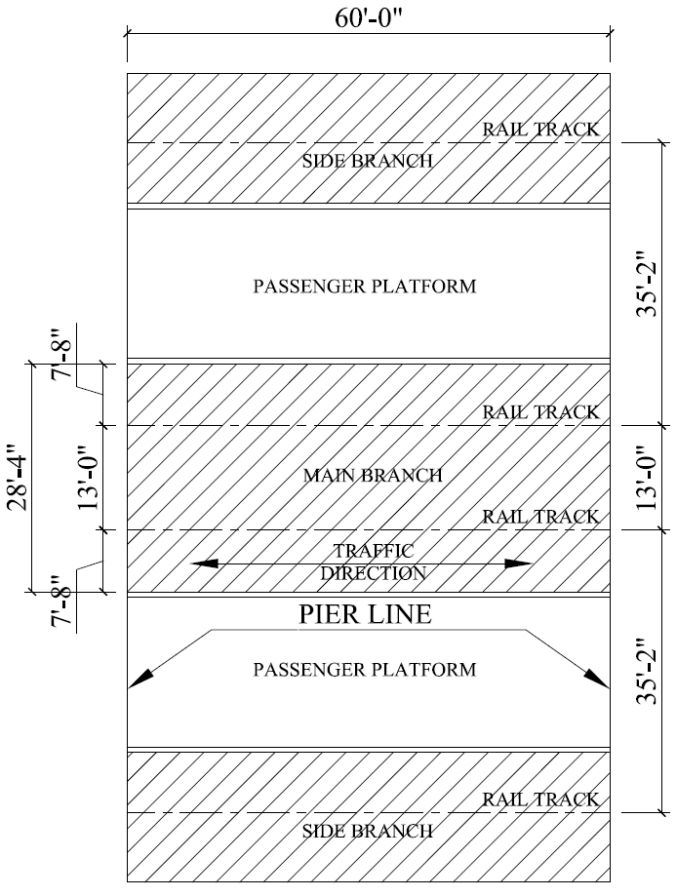

Figure 1. Bridge layout.

2.2 Pretensioned U-Girder with full-depth precast deck panels system

The first system selected was pretensioned U-Girders with full-depth precast panel deck system. The U-Girders have been used for highway bridges in the state of Florida. The system has an efficient cross section that can accommodate presstressing as well as ABC construction methods. The full depth precast panel system dates back to the sixties and has been used in highway applications in more than 20 states in the US (6). This system has significantly shorter construction time and traffic disruption while maintaining excellent performance. However, it was typically used with conventional steel of precast concrete girders. In this study, the full depth precast deck panel system will be adopted with the presetressed U-Girders to offer and efficient system with low construction time suitable for new and replacement operation for railroad bridges. **Figure 2** presents the different components of the system adopted.

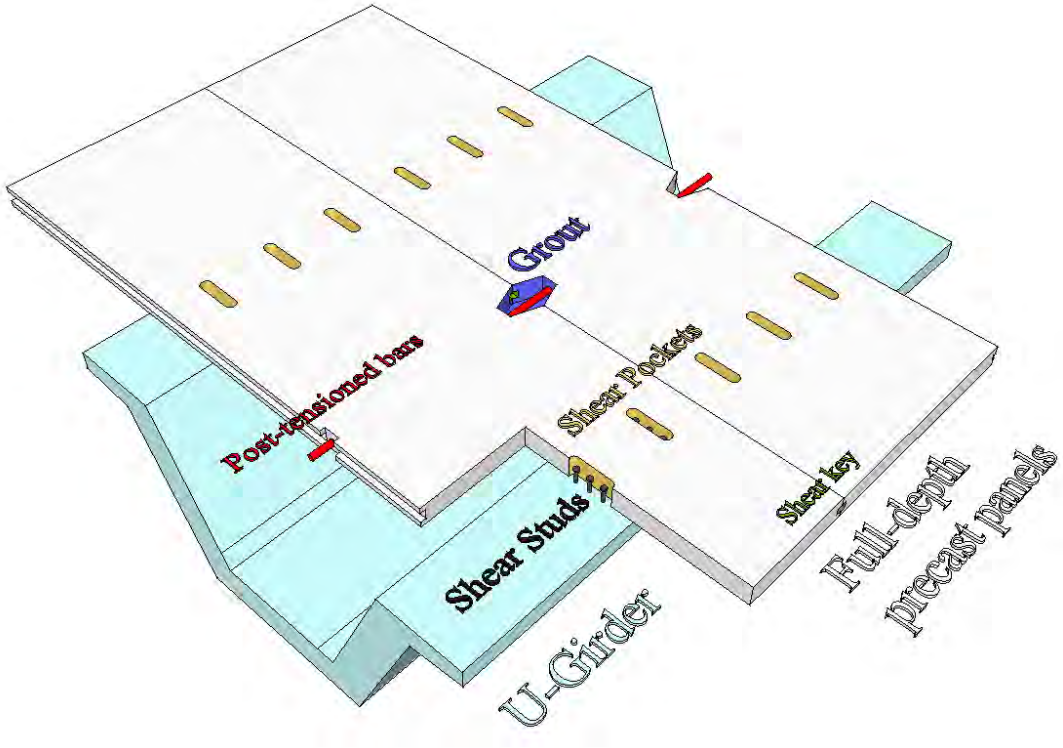

Figure 2. Prestressed U-Girders with full-depth precast deck panel system.

The system is composed of fully precast panels with the required depth and width (typically bridge width). The length of the panels (along the bridge longitudinal axis) is typically from 8 to 12 ft (2.45 to 3.65 m). In this study, panels of 8 in. (20.32 cm) thickness with 28.33 ft (8.63 m) width and 8 ft (2.45 m) length were used.

The connections of this system are vital to its performance, thus extra care must be exerted when designing and constructing them. The precast panels are manufactured with shear pocket to accommodate the shear connectors prefabricated in the U-Girders. After the panels are placed in their location, these shear pockets are fully grouted to enable full composite action. Several researchers have investigated the behavior of shear pockets in the past to determine the optimal distribution, spacing, shape, orientation, and shear studs density including (7 to 11). In this study, 12 in. × 20 in. (30.48 cm × 50.8 cm) shear pockets were used every 28 in. (71.12 cm) spacing yielding two shear pockets per length of the panels. The distribution, spacing, and shear studs number are not included in the design specifications yet, therefore, in this study, the recommendation of the PCI state-of-the-art report on full-depth precast panels were followed (6). It outlines a design methodology derived from the AASHTO specifications (12) for horizontal shear and adopted it for full-depth precast panels (6).

The connections between two consecutive panels are achieved by transverse shear key connections. In higher loading applications, these connections are often post-tensioned using

high strength threaded bars to ensure that the connections remain in compression. In this study, post-tensioning the transverse connection was not required as the grouted shear keys were sufficient to transmit the load without cracking.

The bridge system was comprised of two U-Girders with a depth of 6 ft (1.83 m). Each U-Girder was location directly underneath a rail track to ensure simple load transition and avoid excessive bending stresses on the full-depth precast panels. The center-to-center spacing of the two girder was taken the same as the spacing between the rail track as 13 ft (3.96 m). The total width of the bridge was 28.33 ft (8.63 m). At the support locations, 32 in. (81.28 cm) diaphragms were used to transmit the load to the piers. A preliminary design was performed for this bridge prior to the full-scale modeling to determine the necessary dimensions, reinforcements and the required level of prestressing. The design was performed using hand calculations as well as grillage modeling using SAP2000 (highlighted later in this report). **Figure 3** presents the final dimensions, reinforcements and prestressing for this system at the mid-span as well as the support locations.

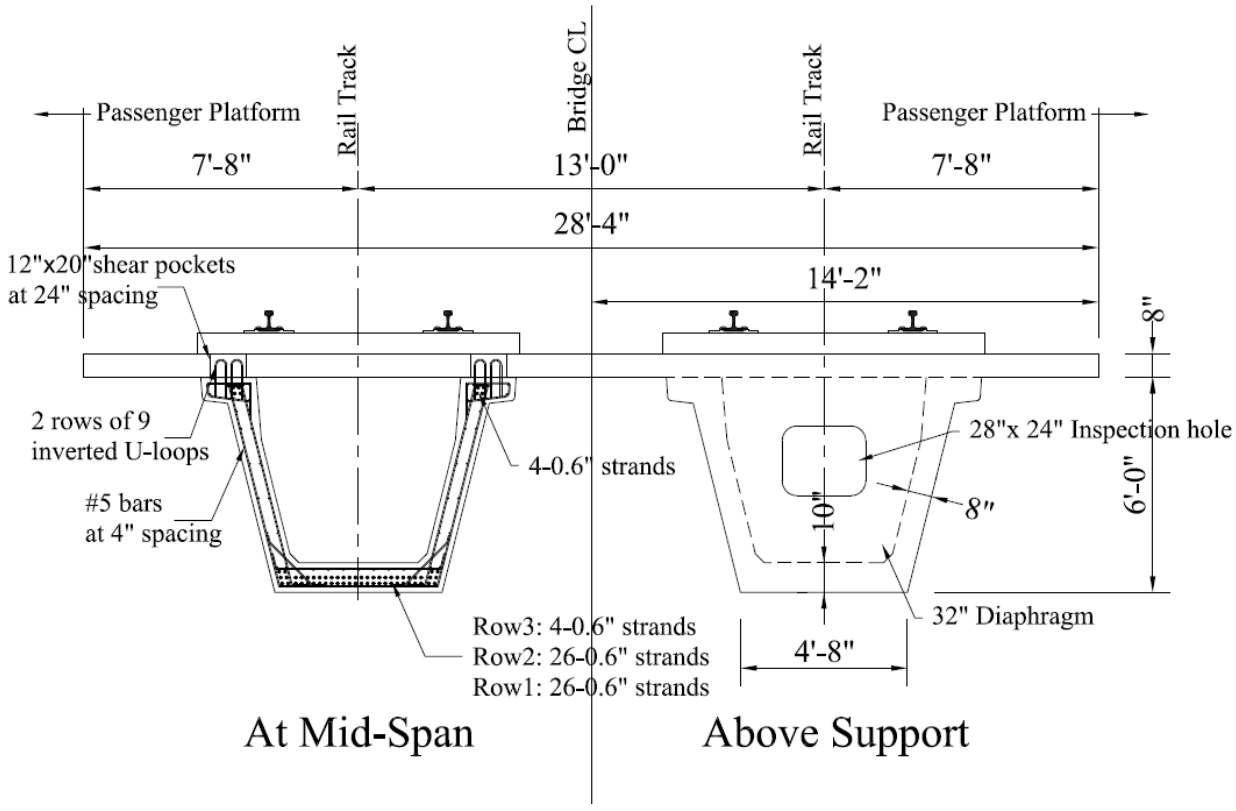

Figure 3. Prestressed U-Girders with full-depth precast deck panel system (1" = 2.54 cm).

2.3 Post-tensioned Box Girder system

Another system, which was also selected for investigation in this study; was the post-tensioned Box girder system. This system has been used overseas in several countries around the world. It

is an efficient section that can accommodate presstressing and ABC construction methods. This system was adopted by the California High-Speed Train Project (CHSTP) as a typical section for aerial structures. This system can achieve the required structural performance and economy with adequate safety and pleasing aesthetic (13). It is recommended for implementation with a simple span and a span-to-depth ratio of 10. The main appeal of this system is dominant in its excellent structural performance, especially torsion resistance, as well as its simple installation procedures, as the number of required connections is limited. In bridge applications where the required span exceeds 170 ft (52 m), this system can be adopted using segmental post-tensioned construction technique, which has been implemented in the US for highway bridges.

In this study, the bridge system was comprised of a box girder with a depth of 6 ft (1.83 m). Each web of the box girder was kept as close as possible to the centerline rail tracks to ensure simple load transition and avoid excessive bending stresses on the top slab. The center-to-center spacing of the two rail tracks and the total width of the bridge were the same as before; 13 ft (3.96 m) and 28.33 ft (8.63 m), respectively. At the support locations, 52 in. (132.08 cm) diaphragms were used to transmit the load to the piers as well as stiffen the ends of the box girder to withstand the bursting stresses of the anchorage zone of the post-tensioned tendons. A preliminary design was performed for this bridge prior to the full-scale modeling to determine the necessary dimensions, reinforcements and the required level of prestressing. The design was performed using hand calculations as well as grillage modeling using SAP2000 (highlighted later in this report). **Figure 4** present the final dimensions, reinforcements and prestressing for this system at the mid-span as well as the support locations.

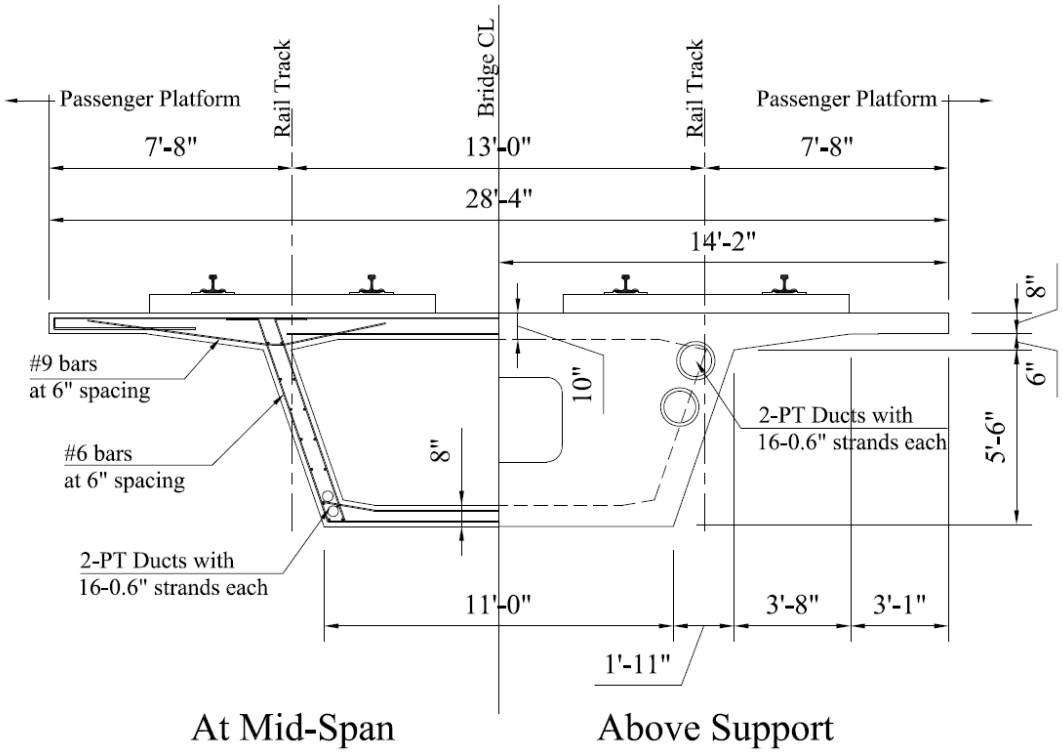

Figure 4. Post-tensioned box girder system (1" = 2.54 cm).

2.4 Construction Procedures

As evident from the multiple implementations by Caltrans, prestressed concrete technology has proven to be the most cost effective solution for the elevated structures in California, especially with the emphasis being directed towards seismic performance (13). Prestressed concrete offers the best and most consistent quality of concrete with the most efficient method of reinforcement as well as allowing for fast construction speed, which results in cost savings.

The multiple operations required for cast-in-place concrete, such as shoring, false-work, concrete poring and curing, consume a lot of time and labor compared to precast concrete (13). In addition, prefabricated ABC technology allows for limited disruption or closure of traffic, which is vital for railroad bridges as traffic divergence is not feasible (1). Railroad owners have expressed that long closure times are economically unacceptable (1). A very effective solution used for erection of prefabricated railroad bridges in the allowed construction time window is replacing each the bridge span-by-span while allowing traffic to flow in between spans.

For the full-depth precast deck panel system, caution is recommended while construction the connections of the system. The following details have to be considered according to (6):

Shear Connectors: For precast concrete girders, the most common type of shear connector is extending the shear reinforcement from the girder to the shear pockets in the full-depth precast

panels using either loops, hairpin or L-shaped bars. In this study, 2 rows of 9 loops were extended in each shear pockets as illustrated in **Figure 3**.

Panel Installation: Typically, welding screws, steel angles, and shims are used to control the elevation, position and leveling of the panels and the haunches. Moreover, it allows for the pouring of the grouted connection and shear pockets.

Transverse Panel Connections: Female-to-female shear keys are the most common type of joints used for panel-to-panel connections. However, the use of match-cast, male-to-female, shear joints is also allowed. Epoxy resin is used to ensure proper bond and mitigate joint leakage.

Post-tensioning: If necessary, panel-to-panel connections are post-tensioned using grade 150 ksi (1034 MPa) steel bars or, if required, grade 270 ksi (1861 MPa) steel strands to negate any tensile stresses in the connection and mitigate any cracking, and in turn, joint leakage.

2.5 Loading and Design

In this full-scale model, both freight and high-speed passenger train loading were considered. The AREMA manual (15) was followed for the freight loading and the guideline of the CHSTP were followed for the HSR loading (14). Presented below is a summary of the load considered for the full-scale model according to both publications.

Dead Loads:

- Concrete unit weight was considered as 150 pcf (2400 kg/m^3)
- Track rails, guardrails, and fastenings were taken as 200 lb per linear foot of track. (3 kN/m)
- The unit weight of HDPE crossties was considered as 56.8 pcf (910 kg/m^3).

Live Loads:

- The Cooper E-80 was considered for freight loading; refer to **Figure 5**.
- The modified Cooper E-50, AMTRAK Acela express and the Bombardier-Zerfiro 380 were considered for HSR loading.
- The full live load was considered on both adjacent rail tracks simultaneously.
- Impact magnification was considered as: $225/\sqrt{\text{span(ft)}}$

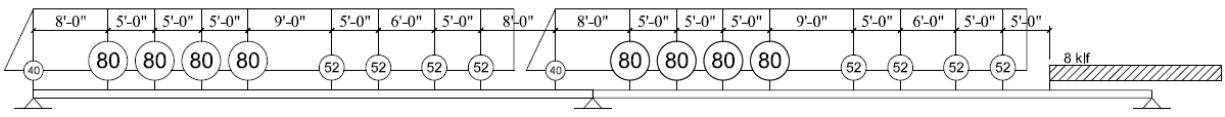

Figure 5. Cooper E-80 loading schematic (15).

Wind Loads:

- The wind load on the vertical projection of the bridge was considered as 45 psf (2.16 MPa).

- The wind load on the train was considered as 300 lbs per linear foot (4.4 kN/m)

Longitudinal Loads

- The longitudinal load was considered as 45 + 1.2(span(ft)) (in kips) for braking
- The longitudinal load was considered as $25/\sqrt{\text{span(ft)}}$ (in kips) for traction.

Load Combinations:

Two sets of load combinations were used; Allowable Stress Design (ASD) load combinations were used for the freight loading as per the AREMA manual (15), and Load and Resistance Factored Design (LRFD) load combinations were used for HSR loading as per the guidelines of the CHSTP (14).

Design

Prior to the full-scale modeling preliminary design was performed to determine the required structural dimensions, reinforcements, and level of prestressing necessary. This design was carried out though hand calculations in conjuncture with grillage analysis using SAP2000. Presented below are the assumptions which the design was based upon.

Span Data:

- Design Span = 60 ft
- Girder is simply supported
- Straight Right Angle Bridge

Bridge Cross-Section Data:

- Number Tracks = 2
- Number Girders = 2 for U-Girder system and 1 for Box girder system.
- Girder Spacing = 13 ft for U-Girder system and N/A for Box girder system.
- Track Spacing = 13 ft
- Overall Width = 28.3 ft

Deck Thickness:

- Bridge Deck Thickness = 8.00 in for U-Girder system and N/A for box girder system.

Girder Type:

- U-Girder or Box girder

Girder Concrete:

- f'c = 8.0 ksi @ 28 days

- f`ci = 6.5 ksi @ Release
- wc = 0.150 kcf

Deck Concrete:

- f`c = 6.0 ksi for U-Girder system and N/A for box girder system.
- wc = 0.150 kcf for U-Girder system and N/A for box girder system.

Prestressing Steel:

- Type: 0.6-in Diameter 270 ksi Low Relaxation Seven-Wire Strands
- Eps = 28,500 ksi
- Pull: 80% (0.75fpu)
- Time to Release= 24 hrs
- Profile: Straight for U-Girder system and parabolic for Box girder system.

Reinforcing Steel (Non-Prestressed)

- fy = 60 ksi
- Es = 29,000 ksi

The final designs were already presented earlier in **Figure 3 and 4**. It should be noted that the profile of the prestressed steel was straight in the pretentioned U-Girder system however, it was parabolic in the post-tensioned Box girder system. A total of 56 0.6"-7 wire strands were used in each U-girder and a total of four post-tensioning (PT) tendons, housing 16 0.6"-7 wire strands each, were used in the box girder. The profile of the PT ducts in the post-tensioned Box girder is illustrated in **Figure 6**.

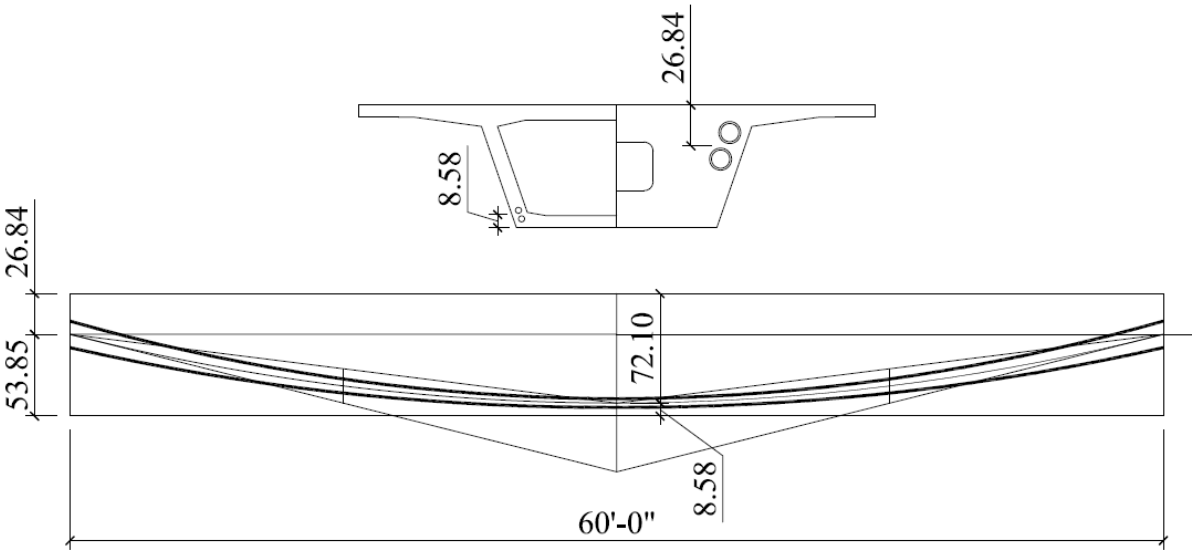

Figure 6. PT tendons' profile in the post-tensioned Box girder.

The SAP2000 finite element analysis software along with the CSI Bridge Module were used as a structural analysis tool to validate the loads obtained through hand calculations in order to increase the level of confidence in the design. **Figure 7** presents the grillage model for the U-Girder system in SAP2000, while **Figure 8** presents the Box girder model in CSI Bridge Module.

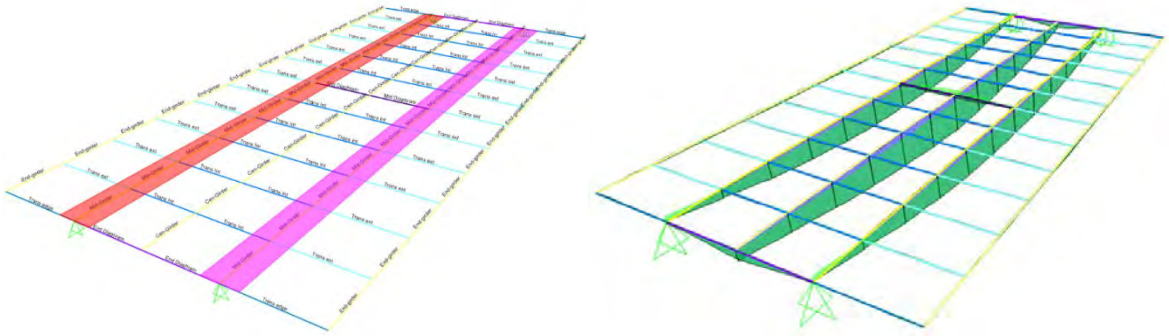

Figure 7. Grillage modeling in SAP2000 for the U-Girder system.

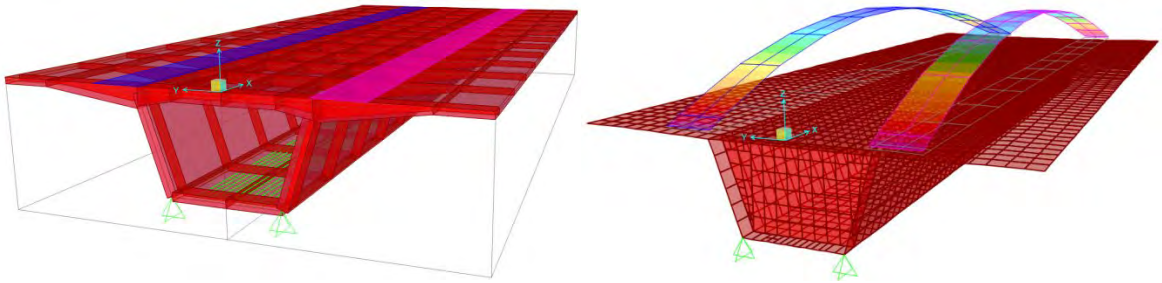

Figure 8. CSI Bridge module modeling for the box girder system.

SECTION 3 FULL-SCALE MODELING

3.1 Material Models for Individual Components

In order to accurately portray the behavior of full-scale model, each individual component should be represented with a calibrated or a trusted material model. Therefore, all the calibrated models presented earlier in this study were implemented in this full-scale model. Trusted material models, which existed for a long time and were validated in the literature, were used for the components that were not tested in the study. However, due to the scale of the model, the material models for the components were simplified as much as possible without sacrificing their accuracy. Since the material models developed earlier in this study were very detailed, the reduction in accuracy due to these simplifications was minimized determined.

Starting with the rail; the typically known steel material model was used for the rail; a bilinear, elastic-plastic, with yield stress of 75,000 psi, initial modulus of 29,000,000 psi and tangent modulus of 5000 psi. The fastening system uplift was simulated using the model developed for the spike pullout as well as the results of the e-clip uplift with ratios of 7% and 93% (3). These results were then simplified into a bilinear, elastic-plastic model that was used in the full-scale model. The lateral resistance of the fastening system uplift was simulated using the material model developed for the spike lateral restraint (simplified into a bilinear, elastic-plastic) (3). Similarly, the longitudinal resistance of the fastening system uplift was simulated using the results obtained for the system longitudinal restraint (pure friction model with static and kinetic friction coefficients) (2). The HDPE crossties were simulated using the proposed simplified material model developed in previous studies (5).

For the reinforced concrete, the material model used was the unconfined concrete model developed by Hognestad (16), which has been proven and trusted for a while, with compressive strengths of 8,000 psi for the girders and 4,000 for the deck. The same steel model was used for the reinforcement bars in the concrete (with yield stress of 60,000 psi, initial modulus of 29,000,000 psi and tangent modulus of 3000 psi.) as well as the seven-wire prestressing strands (with yield stress of 245,000 psi, initial modulus of 28,500,000 psi and tangent modulus of 8,000 psi.).

3.2 Full-Scale Model Framework

Similar to the modeling applications presented previously, ANSYS finite element software was used. The full-scale models dimensions and configuration were described as designated in

Figures 1, 3, and 4. Loading was applied as mentioned earlier. The train loads were applied as static wheel loads in the location yielding maximum straining actions on the superstructure.

The rail was represented using beam element having 3 translation and 3 rotational degrees of freedoms at each node; BEAM188 while the steel reinforcement was represented using link element having 3 translation degrees of freedom at each node; LINK180. The HDPE crossties, steel bearing plates and bridge bearings were represented using solid elements in the ANSYS model; specifically SOLID185 which is defined by 8 nodes in each corner having 3 degrees of freedom each; x-axis, y-axis and z-axis translations, for a total of 24 degrees of freedom per element. The girder and deck concrete as well as the grout were represented using SOLID65, which is a specialized element for concrete. It has the same degrees of freedom as SOLID185 with the addition of the ability to defined smeared steel reinforcement in the concrete element as well as simulating concrete damage; cracking and crushing. The concrete damage model has proven to be an appropriate approximation of the flexural cracking and failure of concrete systems (17).

Both models were assumed to be doubly symmetric about the mid-span and the middle of the bridge cross section, with symmetry boundary conditions applied accordingly. Since both rail tracks were simultaneously loaded as per AREMA recommendations, symmetry about the middle of the bridge cross section was true and valid. However, symmetry about the mid-span is an assumption (as train wheels loads are not perfectly symmetric) which will produce slightly more conservative straining actions as illustrated in **Figure 9**, which was acceptable.

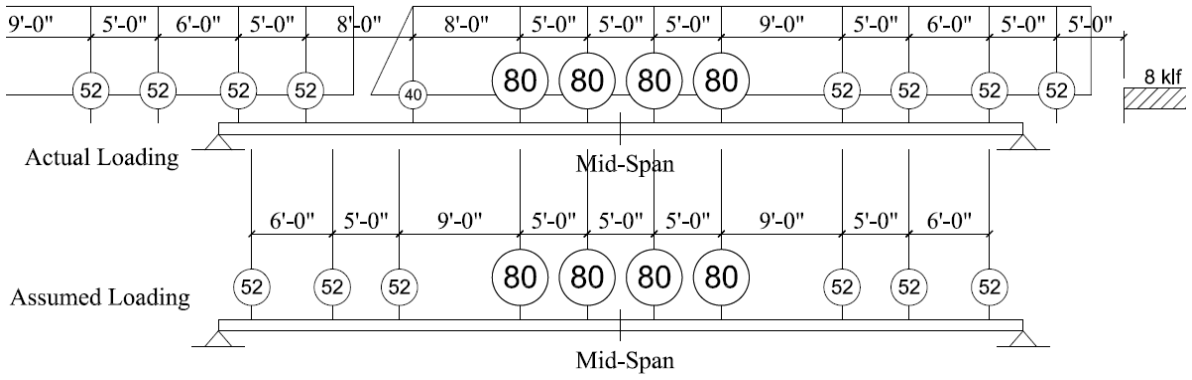

Figure 9. Wheel loading assumed to produce symmetry about mid-span.

Boundary conditions were applied by restraining the vertical movement of the support bearing line in addition to the symmetric boundary conditions. Moreover, the torsional rotation of the rail section was restraint at both ends to simulate the continuity of the rail section. **Figures 10 to 15** show the components of the, quarter symmetry, full-scale model for the U-Girder with full-depth precast panel system and **Figure 16** illustrates its boundary conditions. Likewise, **Figures 17 to**

21 show the components of the quarter symmetry, full-scale model for the Box girder system and **Figure 22** illustrates its boundary conditions.

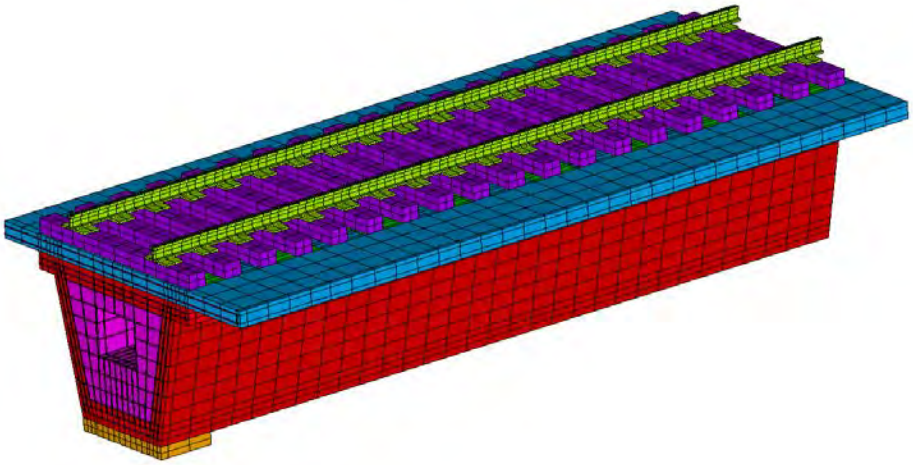

Figure 10. U-Girder with full-depth precast panel model.

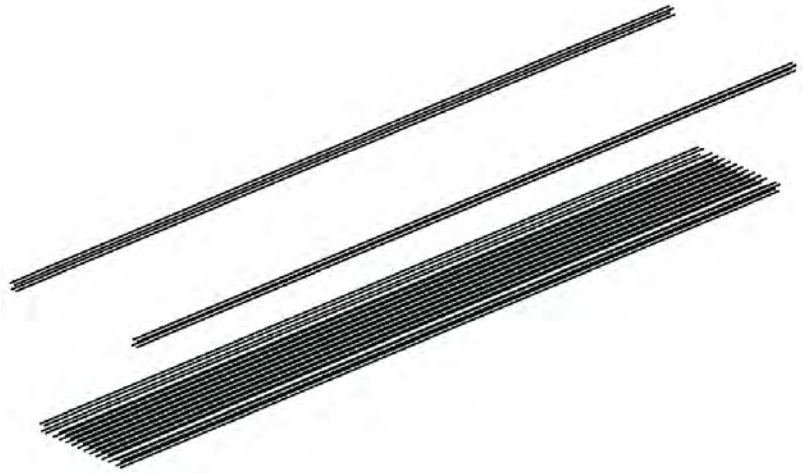

Figure 11. Prestressed strands for in the U-Girder.

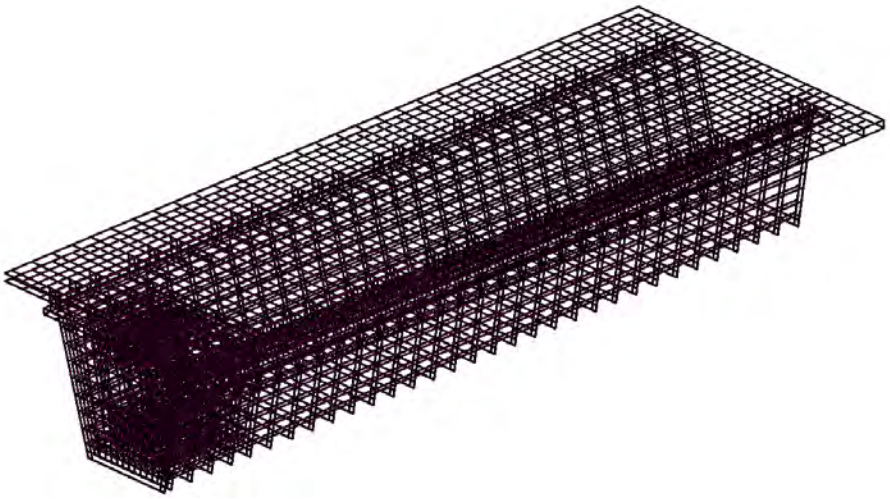

Figure 12. Steel reinforcement in the U-Girder and panels.

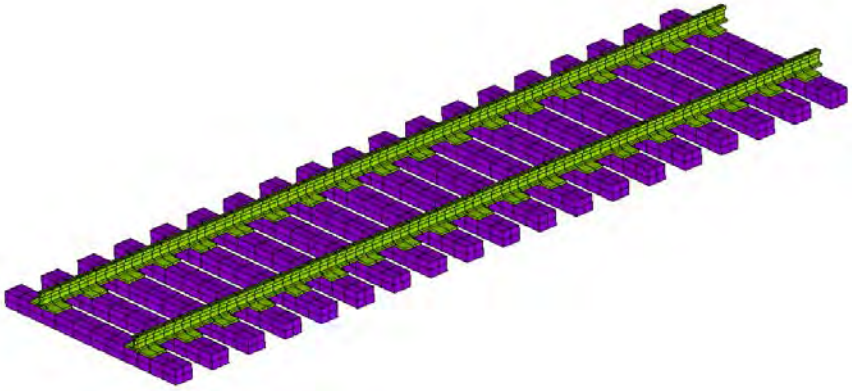

Figure 13. Rail track with HDPE crossties on top of the U-Girder.

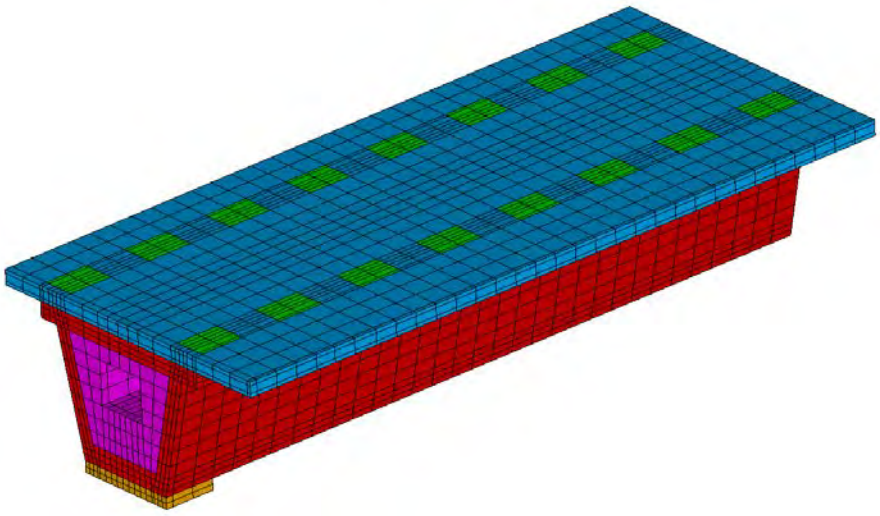

Figure 14. Shear pockets and diaphragm details for the U-Girder.

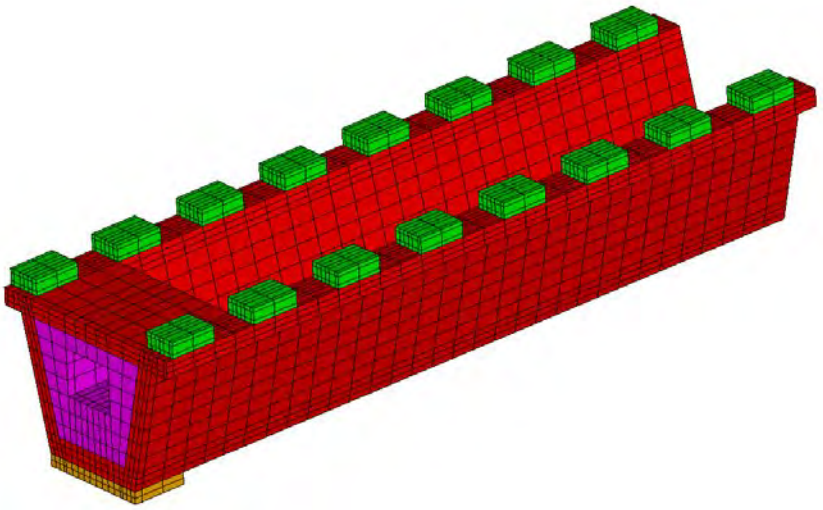

Figure 15. Shear pockets connections with U-Girder.

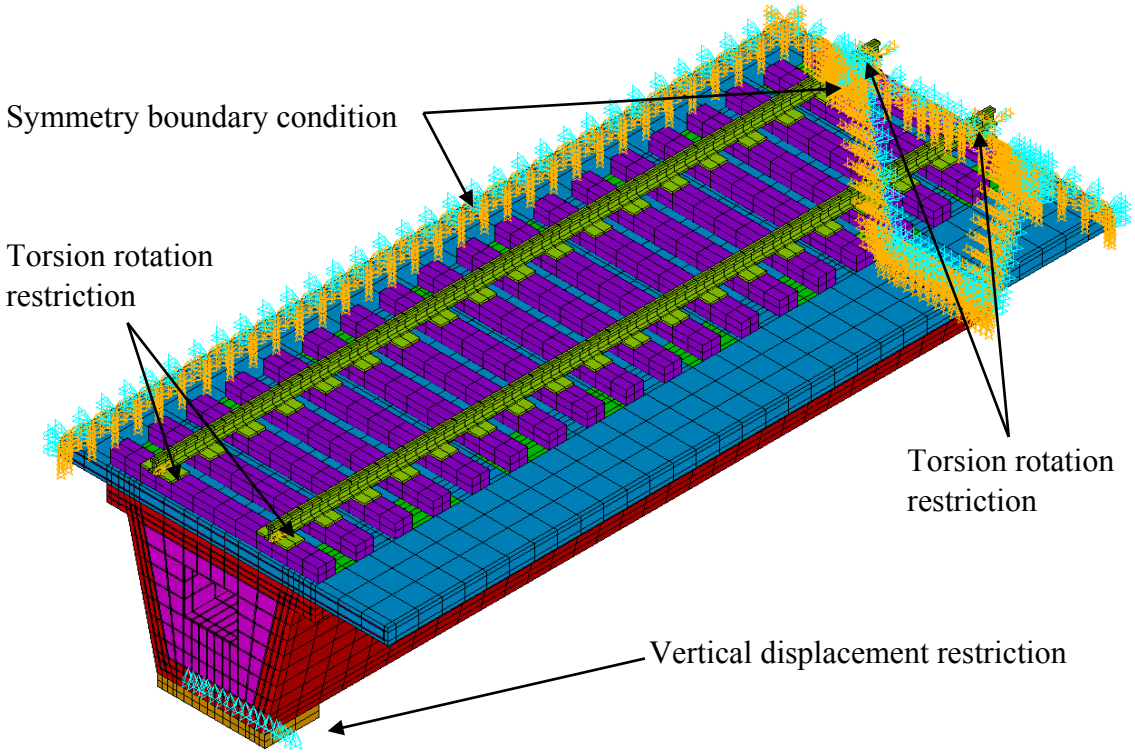

Figure 16. Boundary conditions for the U-Girder model.

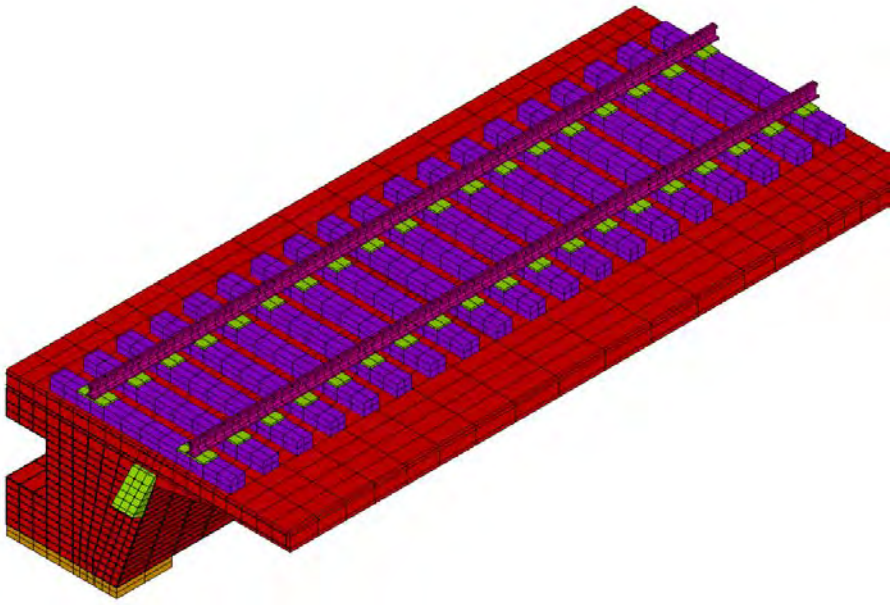

Figure 17. Box girder model.

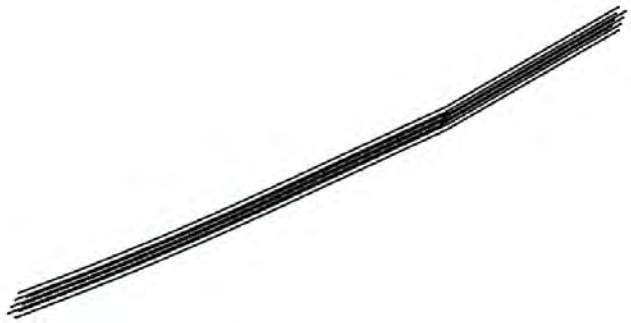

Figure 18. Post-tensioning used in the Box girder.

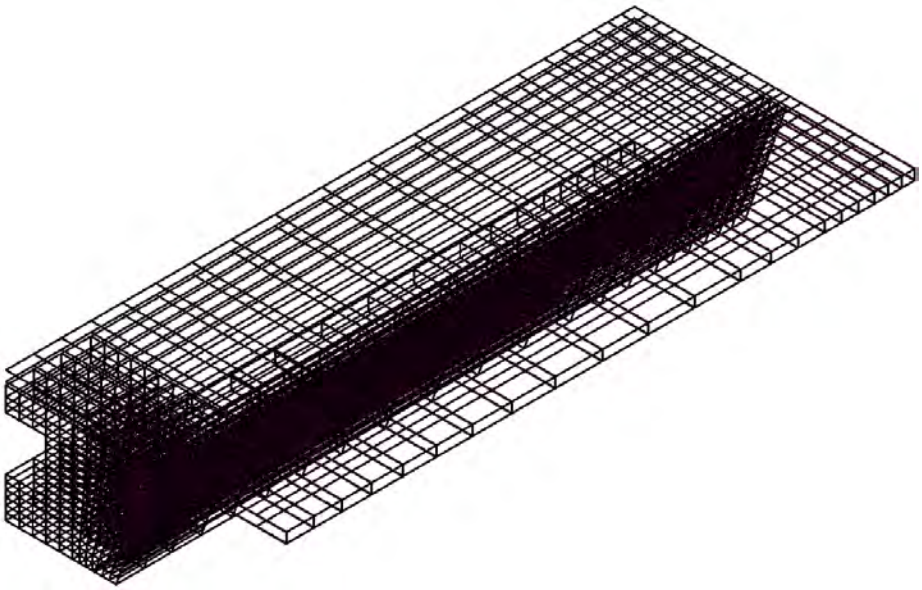

Figure 19 Steel reinforcement in the Box girder.

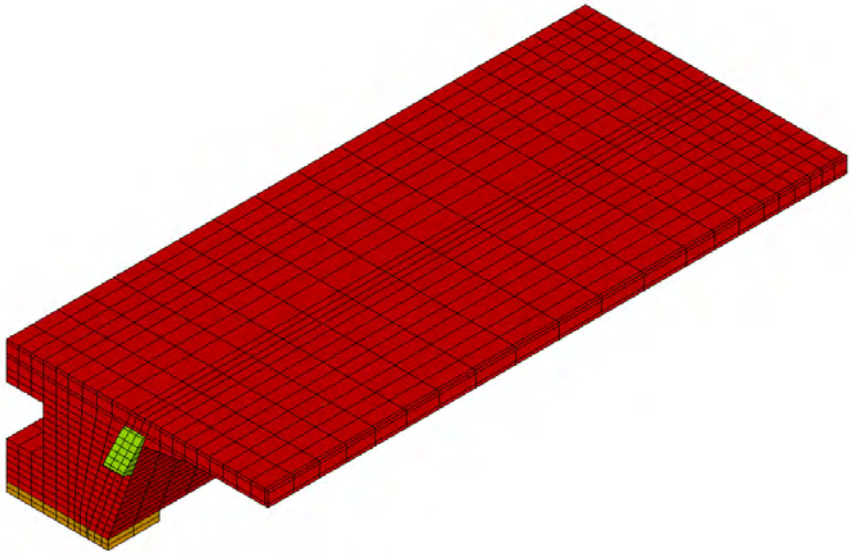

Figure 20. Anchorage plate and diaphragm details for the Box girder.

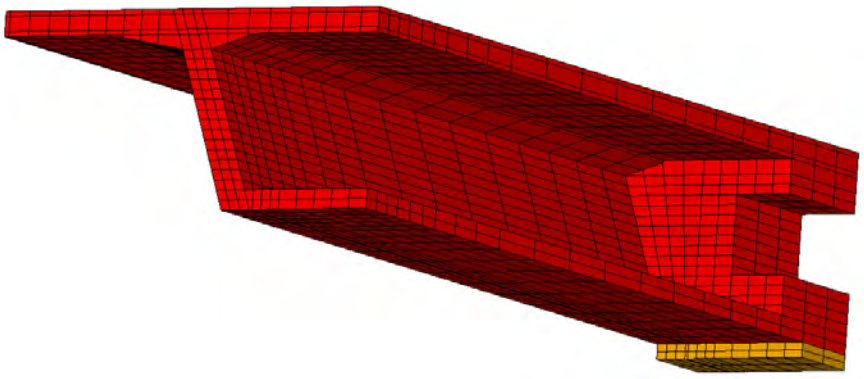

Figure 21. Haunches and bearing support for the Box girder.

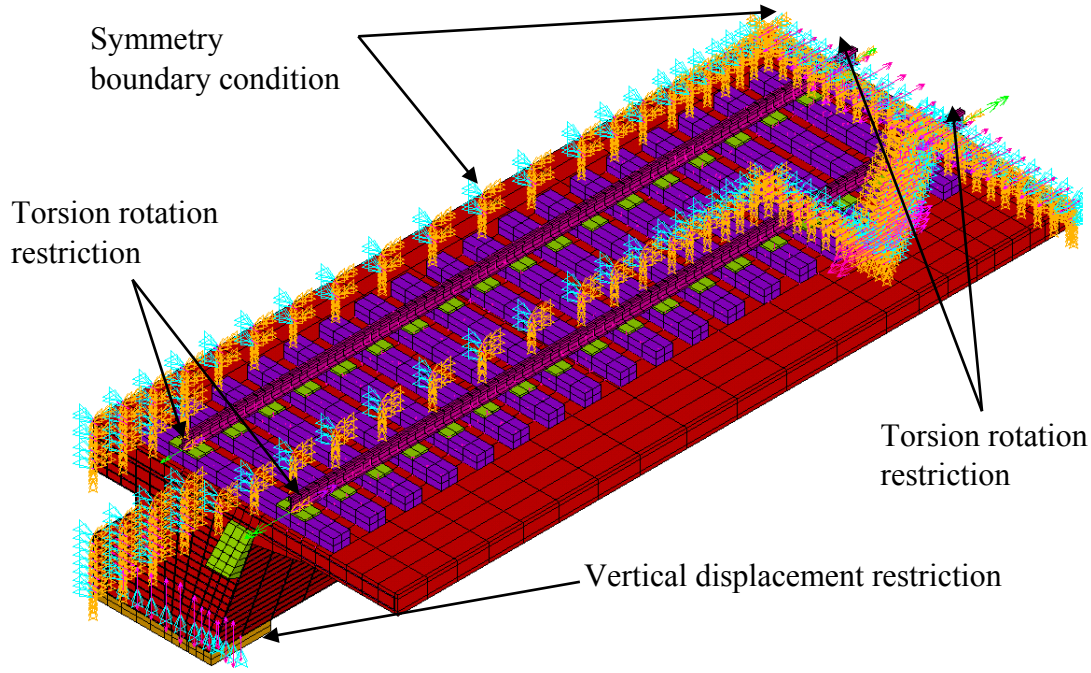

Figure 22. Boundary condition for the Box girder model.

To simulate the interactions between the rail, crossties, and the fastening system components, springs were used with the appropriate material model. The crossties were assumed to be bonded to the concrete deck/slab (direct fixation), which was achieved using, surface-to-surface contact; Multiple Point Constraint algorithm. All the reinforcement and the prestressing were assumed as bonded with the concrete, which was achieved by merging the common nodes between the elements. In the case of the U-Girder system, the full-depth precast panels were connected to the U-Girder using the shear pockets only, refer to **Figure 15**.

In the cross-section, meshing was performed at the location of the reinforcements to allow for node merging between the solid and the link elements. In the longitudinal direction, since the number of stirrups was very high; meshing the model at each stirrup location was not feasible.

Moreover, in order to accommodate the parabolic profile of the post-tensioned tendons, the mesh in the longitudinal direction was created at the intersections between the cross-sectional mesh and the parabolic profile of the PT tendons. Therefore, the stirrups were modeled as a combination of the discrete reinforcement; i.e. link elements were used as allowed by the longitudinal mesh, and smeared reinforcement in the concrete element in between two consecutive discrete stirrups. This method was implemented by Fanning when modeling post-tensioned beams (17). This method produced an efficient mesh without sacrificing accuracy as all the main reinforcements, prestressing and slab reinforcement were represented by discrete link elements and only the stirrups were presented by a combination of both methods. To accommodate the parabolic PT tendons, the mesh in the longitudinal direction was not constant and kept increasing with the slope change of the parabolic profile. However, a finer mesh is required near the mid-span where the maximum stresses and cracking are expected. Additionally, by following the parabolic profile, the mesh at the mid-span becomes highly distorted with larger aspect ratio. Therefore, the mesh was refined near the mid-span and the profile of the PT tendons was slightly modified to be straight near the mid-span. At its worst, the maximum variation between the actual profile and the assumed model was 1.5 in. Since the minimal diameter of the PT ducts was 4 in., this approximation was acceptable. **Figure 23** shows the mesh details for the cross-section for the U-Girder model and **Figure 24** shows the mesh details in the longitudinal direction. **Figure 25** shows the mesh details for the cross-section for the Box girder model and **Figure 26** shows the mesh details in the longitudinal direction with the assumed profile of the PT tendons.

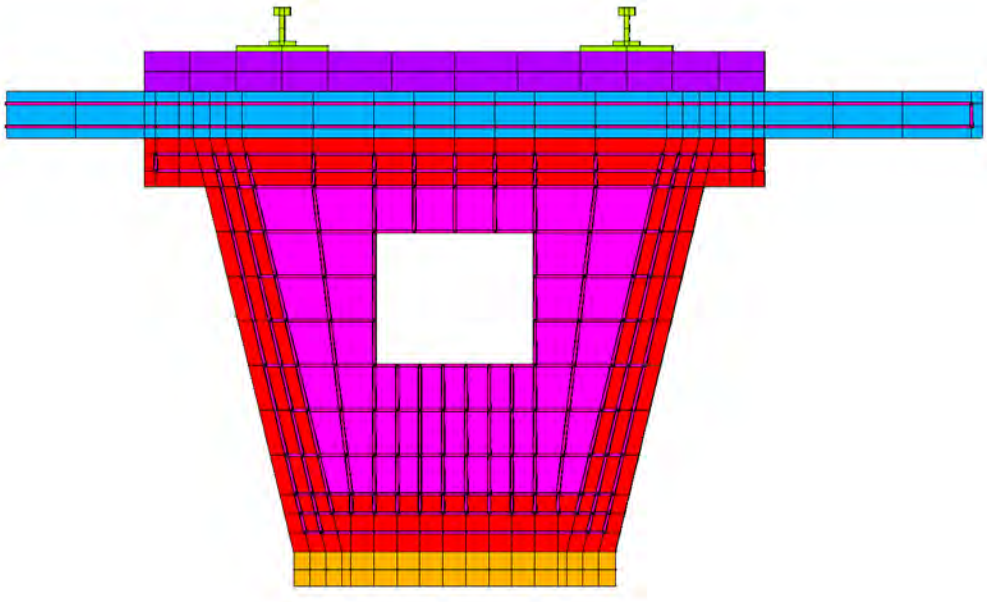

Figure 23. Cross-section mesh details for the U-Girder model.

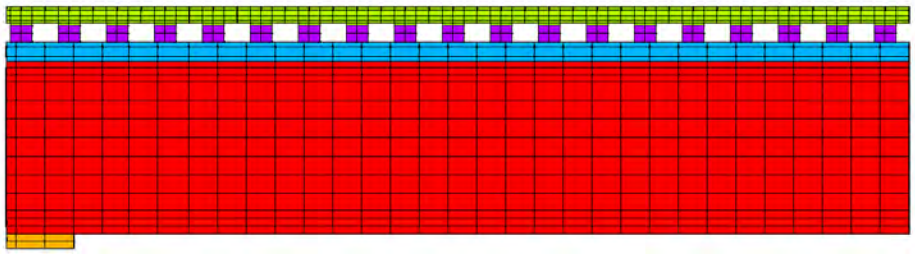

Figure 24. Longitudinal mesh details for the U-Girder model.

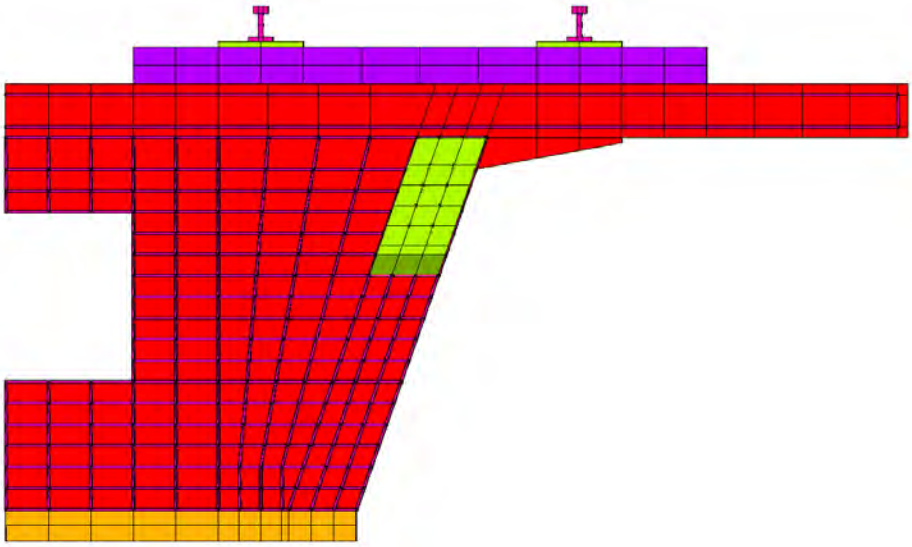

Figure 25. Cross-section mesh details for the Box girder model.

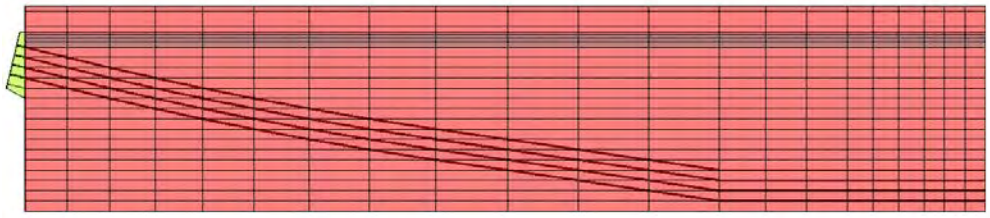

Figure 26. Longitudinal mesh and assumed PT profile details for the Box girder model.

To properly analyze the models, load steps were applied to determine the effect of the different loading stages. The first load step set was the dead load applied on the bridge. In this step, the prestressing was not applied yet. This is more indicative of the actual sequence of loading. The second loading step applied was the prestressing forces, which was applied using a dummy temperature variation. The reasoning for not using the initial strain function in ANSYS to apply the prestress to the link elements was due to the fact that the program considers the initial strain before any other load including the dead load. This was not an accurate representation of the actual loading sequence. Therefore, a dummy coefficient of linear thermal expansion of 0.00568 strain/degree was assigned to the prestressing element. Thus, by applying one degree of temperature variation, a stress of 162 (ksi) was applied to the link elements as prestressing, which is the effective prestressing stress after all the losses calculated in the design. The third load step was the application of the service loads. The fourth load step was the application of the cracking load. After this load step, the model became very computational intensive as the damage model for the concrete was activated. Therefore, the ultimate load was divide onto two smaller load steps to accommodate the convergence of the non-linear solution. The full ultimate load was achieve after the sixth load step. The seventh and final load step was loading until failure occurred. **Tables 1 and** 2 illustrate a sample of the load steps followed for the freight loading for both systems.

Table 1. Load steps followed for the freight loading of the U-Girder.

Load Step	Load Type	Maximum axle load	% of Service Load	% of Ultimate Load
1	Dead Load	---	---	---
2	Prestress Load	---	---	---
3	Service Load	103.2	100	43
4	Cracking Load	187.98	183	78
5	---	190	184	79
6	Ultimate Load	240.6	233	100
7	---	280	271	116
7.56	Failure Load	347.24	336	144

Table 2. Load steps followed for the freight loading of the Box Girder.

Load Step	Load Type	Maximum axle load, kips	% of Service Load	% of Ultimate Load
1	Dead Load	---	---	---
2	Prestress Load	---	---	---
3	Service Load	103.2	100	43
4	Cracking Load	130.83	126	54
5	---	185	179	77
6	Ultimate Load	240.6	233	100
7	---	280	271	116

7.25	Failure Load	289.95	281	121

As noticed from **Tables 1 and** 2, the U-Girder system exhibited higher cracking load as well as failure load than the Box girder system. It can also be observed that both system are efficiently designed as they failed shortly after the ultimate design load; not at the ultimate load nor a lot higher than the ultimate load.

3.3 Results

The results of the models are presented in this section. **Figures 27 to 32** present the deformed shape of the U-Girder system throughout the different loading stages. Using the symmetric expansion functionality in ANSYS, the quarter symmetry model can be expanded to give the results of the full bridge as illustrated in **Figure 33** for the U-Girder. Similarly, **Figures 34 to 40** present the deformed shape of the Box girder system.

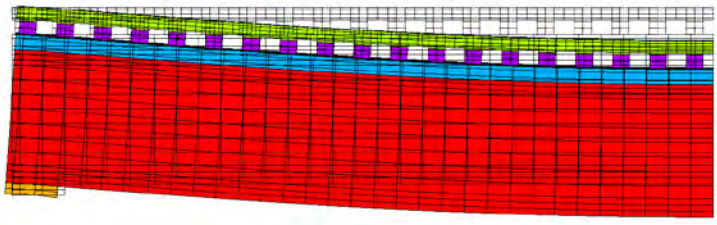

Figure 27. Deformed shape of the U-Girder system due to dead load.

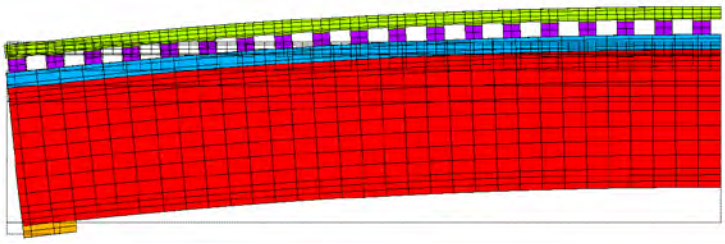

Figure 28. Deformed shape of the U-Girder system after the prestress load.

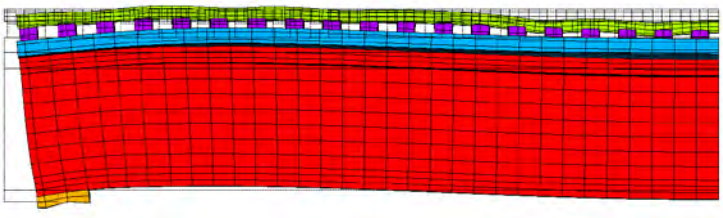

Figure 29. Deformed shape of the U-Girder system at service load.

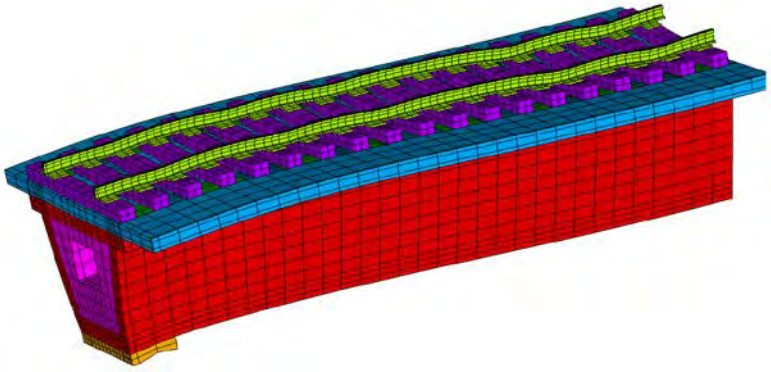

Figure 30. Rail deformation due to train wheels for the U-Girder system at service load.

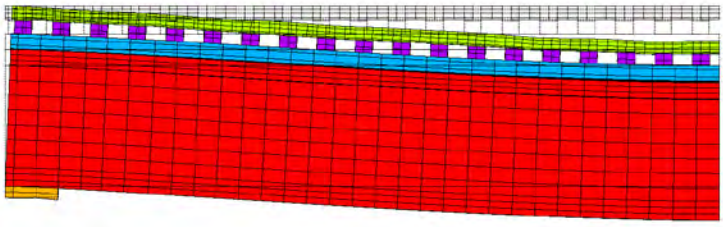

Figure 31. Deformed shape of the U-Girder system at ultimate load.

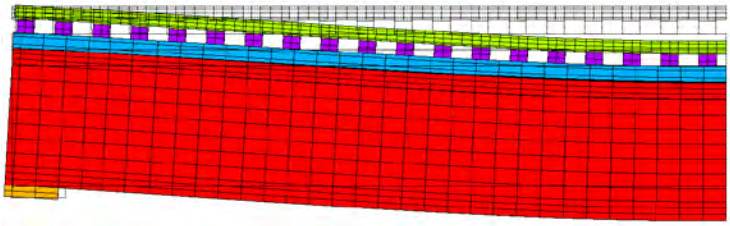

Figure 32. Deformed shape of the U-Girder system at failure.

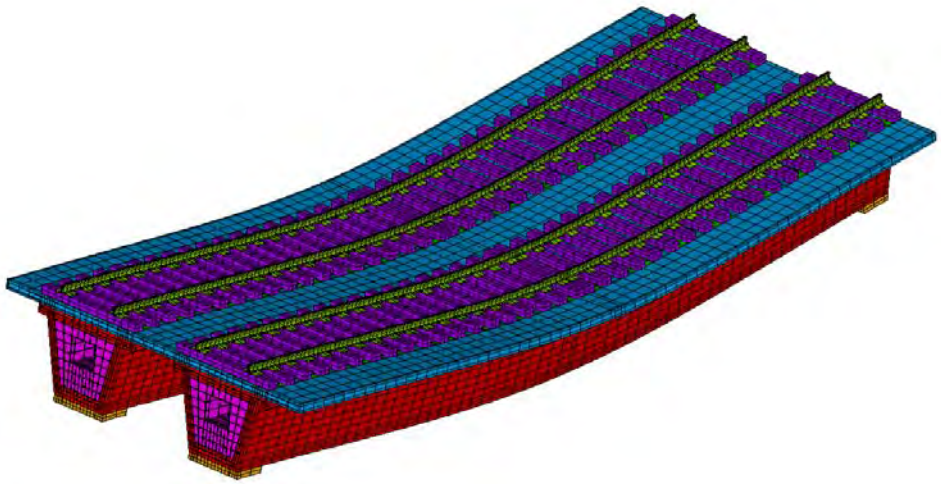

Figure 33. Symmetric expansion of the deformed shape of the U-Girder system at failure.

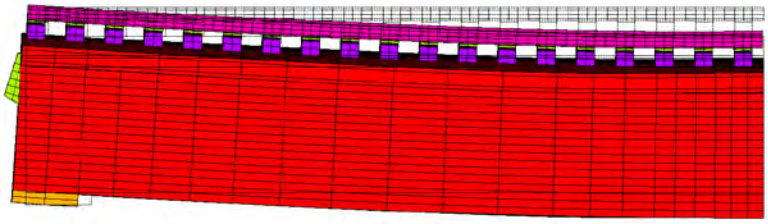

Figure 34. Deformed shape of the Box girder system due to dead load.

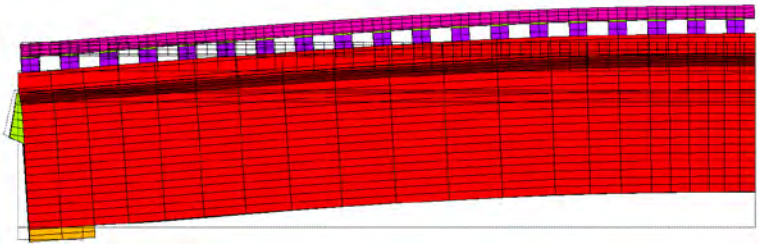

Figure 35. Deformed shape of the Box girder system after the prestress load.

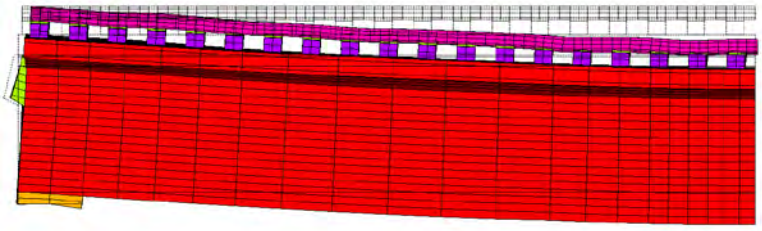

Figure 36. Deformed shape of the Box girder system at service load.

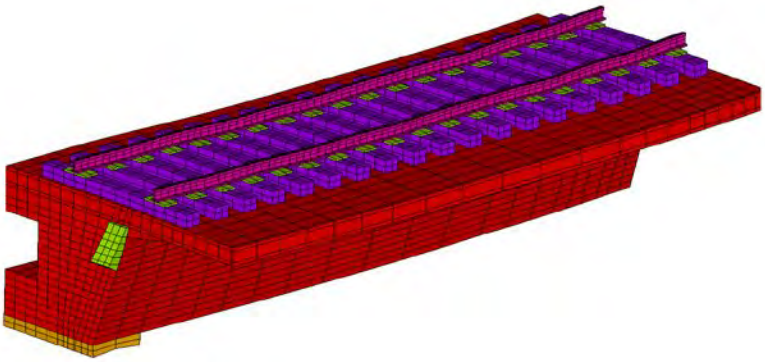

Figure 37. Rail deformation due to train wheels for the Box girder system at service load.

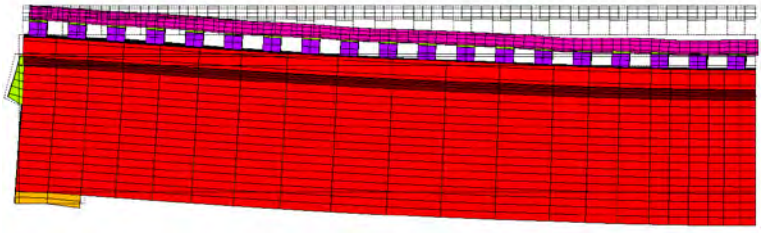

Figure 38. Deformed shape of the Box girder system at ultimate load.

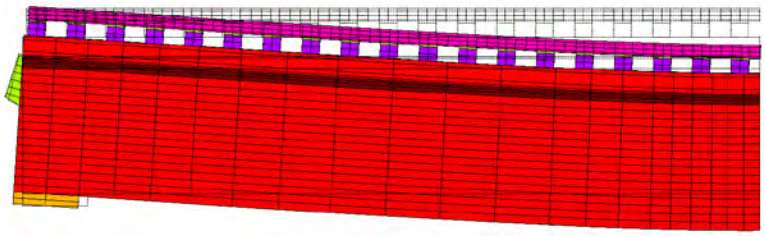

Figure 39. Deformed shape of the Box girder system at failure.

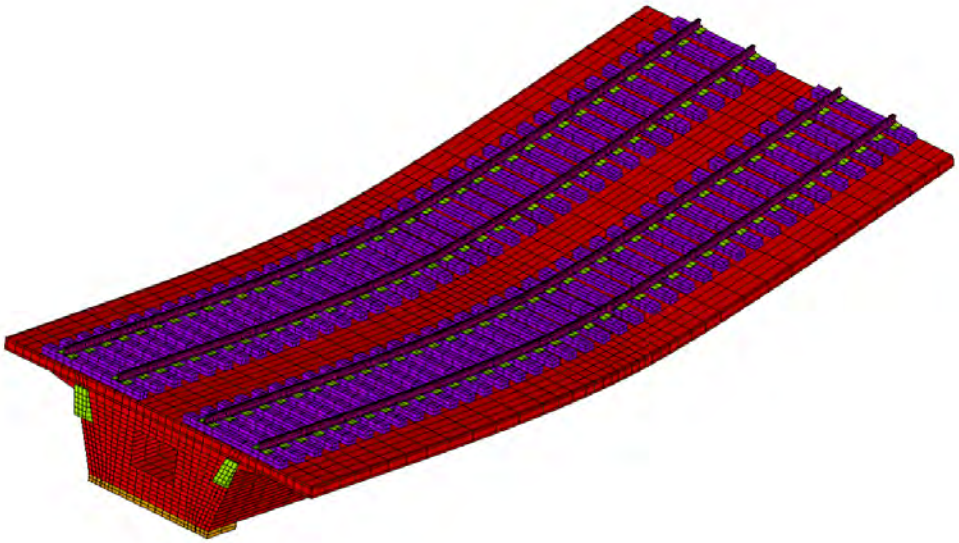

Figure 40. Symmetric expansion of the deformed shape of the Box girder system at failure.

As noticed from the deformed shapes presented above, both system behaved as expected showing appropriate deflection due to dead load, camber due to prestressed and normal service and ultimate deflections. The noticeable difference between the two systems is the deflection at service load; refer to **Figures 29, 30, 36, and 37**. The main reason for this discrepancy is the prestressing profiles. Since the U-Girder featured straight strands, higher tensile stresses at the top of the section are introduced near the supports, which were manifested in the deflected shape shown in **Figures 29 and 30**. However, for the Box girder system, the profile of the PT tendons were designed to pass through the centroid of the cross section at the supports, which eliminates

these additional tensile stresses, and thus yielding a normal deflected shape as illustrated in **Figures 36 and 37**.

3.3.1 HDPE crossties, Rail, and fastening Assembly:

From the model, the applied stresses and strains on the crossties can be obtained throughout the loading stages. The effect of the loads is expected to be high close to the train axles. **Figures 41 and 42** illustrate the bending stresses applied on the crossties at service and failure load respectively. As indicated, the maximum straining actions are applied on the crossties located underneath the axles of the trains.

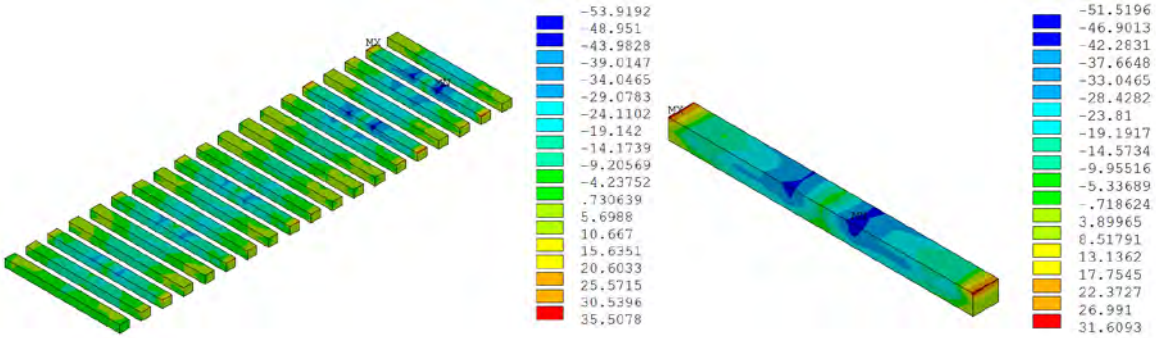

Figure 41. Bending stress at service load (1 psi = 6.9 kPa).

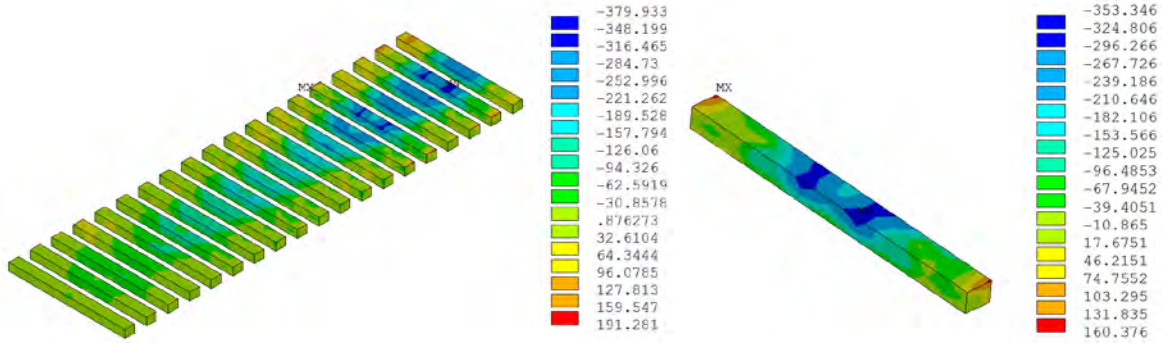

Figure 42. Bending stress at failure load (1 psi = 6.9 kPa).

Inspection of **Figures 41 and 42** reveals that the crossties were subjected to bending stresses due to the applied wheel loads. However, contrary to ballast, the bending stresses induced compressive stresses at the top fibers of the cross-section. When the crossties are supported on a uniformly distributed surface; like a ballast layer, bending action induces tensile stresses at the top fibers of the cross-section. However, in this case, the crossties are supported on the precast panels, which in turn, experienced deflections due to the applied loads; therefore, the crossties experienced the same deformations as the supporting slabs and experienced compressive stresses at the top fibers of the cross-section. Due to this behavior, the crossties experienced insignificant

tensile stresses during all loading stages and up to failure as illustrated in **Figures 41 and 42**. Moreover, **Figure 43** further validates this by showing the ultimate strains in the HDPE crossties at failure.

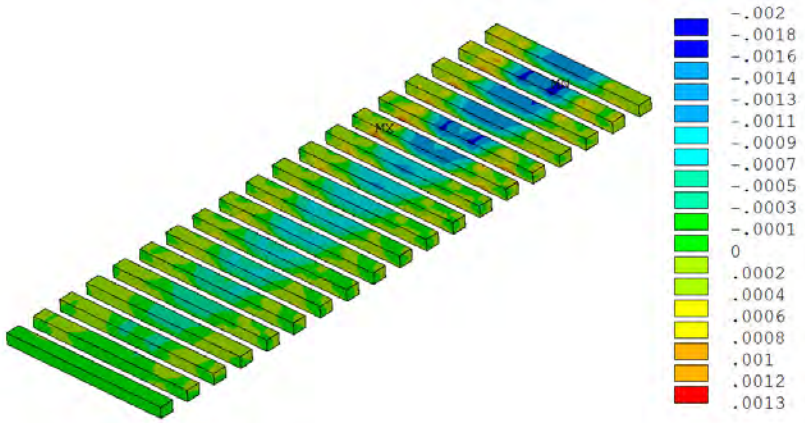

Figure 43. Bending stress at failure load (1 psi = 6.9 kPa).

The shear stresses applied on the HDPE crossties as a result of the axle loads is shown in **Figure 44 and 45**. As illustrated, the maximum shear stresses occurred under the axle loads as expected. Moreover, the distribution of the shear stresses along the length of the crossties was close to that of the uniformly distributed case but with concentration under the steel bearing plates as shown in **Figure 45**. As noticed, all the shear stresses were within the allowable range.

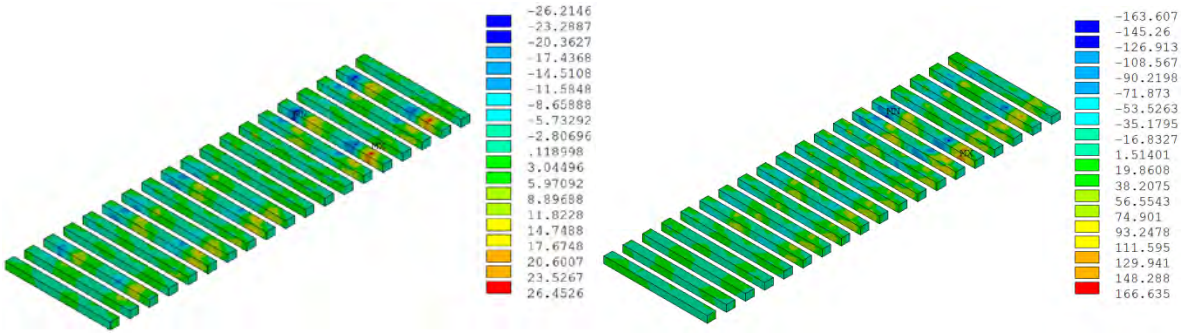

Figure 44. Shear stresses on the crossties at service (left) and failure load (right).

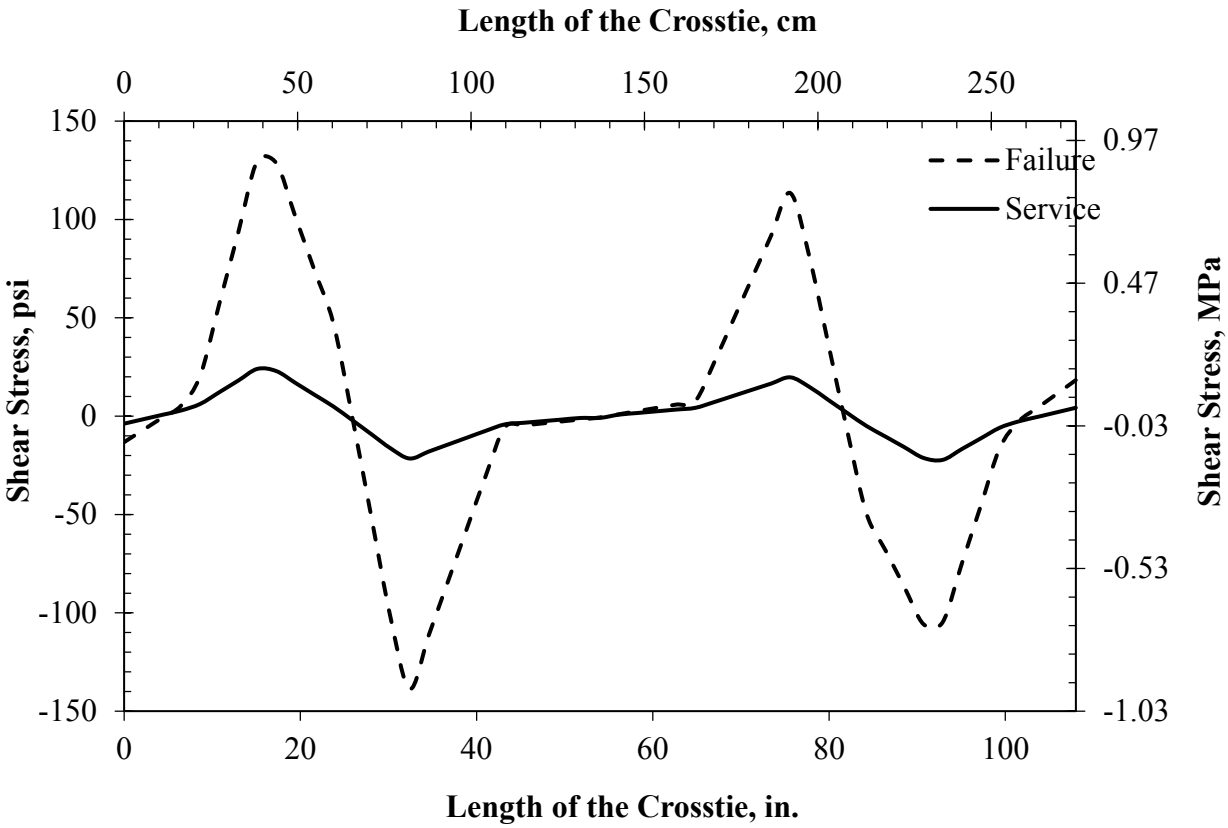

Figure 45. Shear stresses on the crossties at service (left) and failure load (right).

In addition to the bending and shear actions, the rail-seat compressive actions had to be checked. **Figures 46, 47, and 48** illustrate the distribution of the compressive stresses applied at the on the crossties at the rail-seat during service, ultimate and failure load respectively.

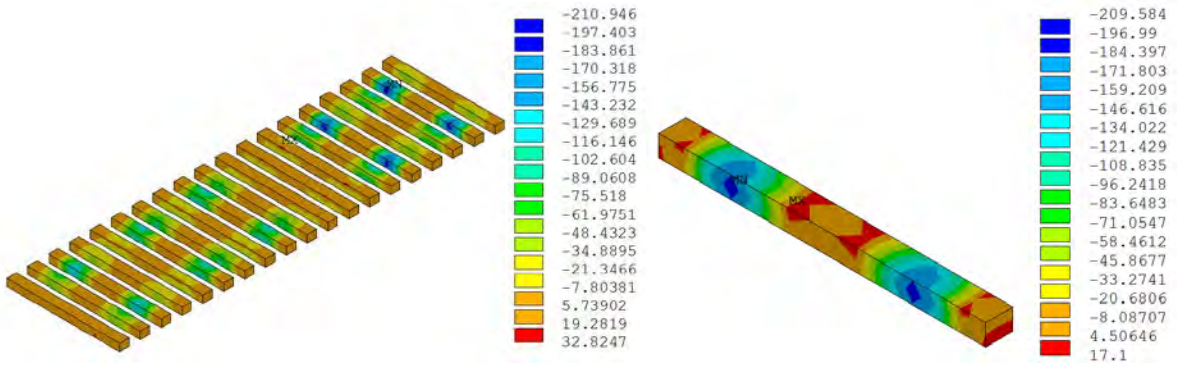

Figure 46. Rail-seat compressive stresses on the crossties at service load.

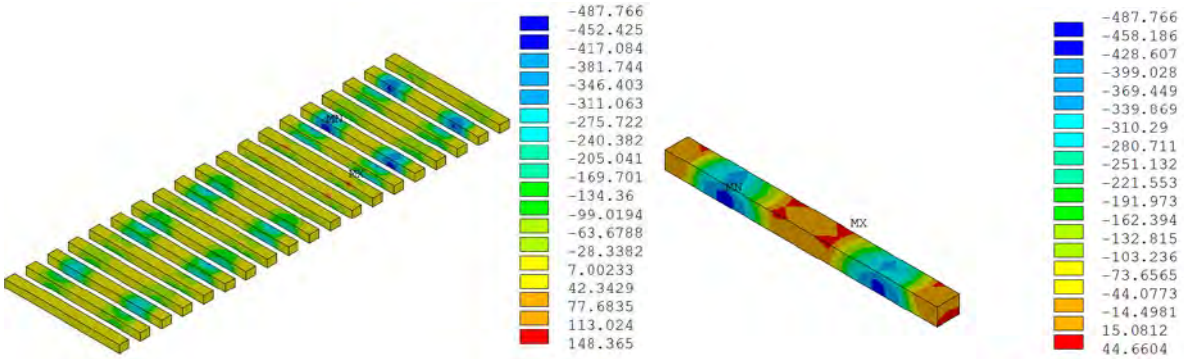

Figure 47. Rail-seat compressive stresses on the crossties at ultimate load.

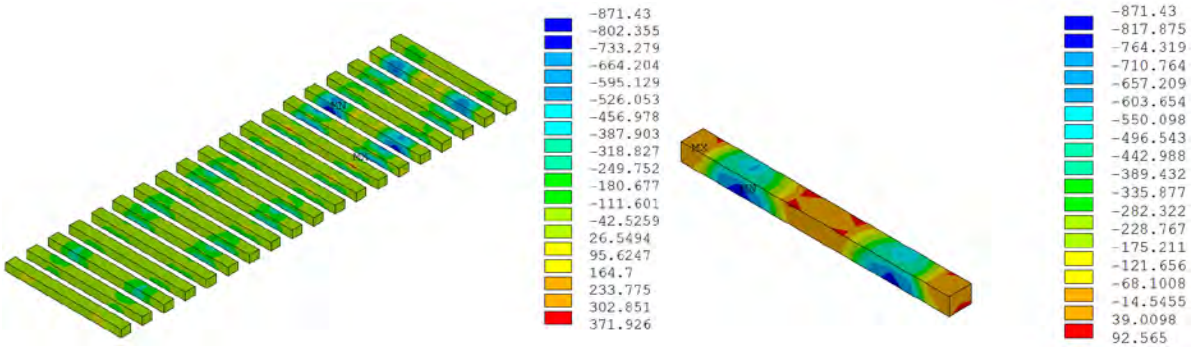

Figure 48. Rail-seat compressive stresses on the crossties at failure load.

Inspection of **Figures 46, 47, and 48** validates that the maximum rail-seat compression experienced by the crosstie was located directly under the axle loads of the trains. Furthermore, the distribution of the stresses in the long-direction of the crossties (short direction of the bridge) would dissipate shortly after the steel bearing pads. It is also observed that all the stresses experienced were within the elastic range of the crossties, which indicate that no excessive stresses or anomalies occurred during the loading stages.

The crossties were assumed as directly fixed in the bridge deck, which can be achieved using embedment slots in the concrete and grouting the connections. The shear stresses at the interface between the crossties and the concrete was checked and is shown in **Figures 49 and 50**.

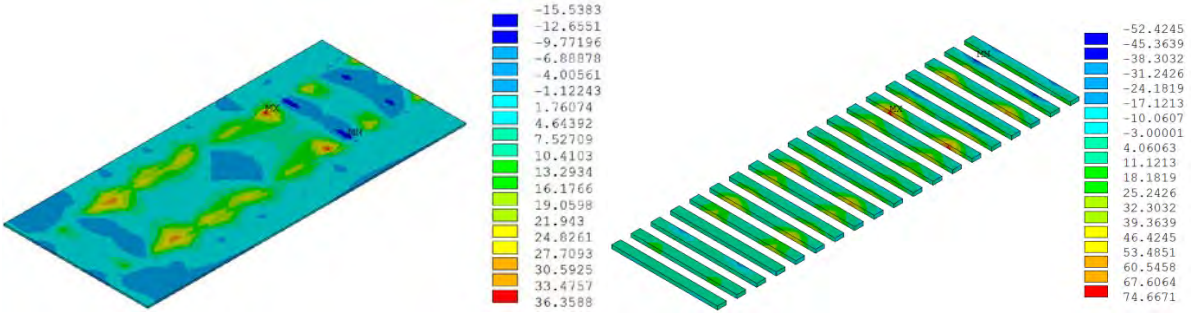

Figure 49. Interface shear stresses between the crossties and the concrete at service load.

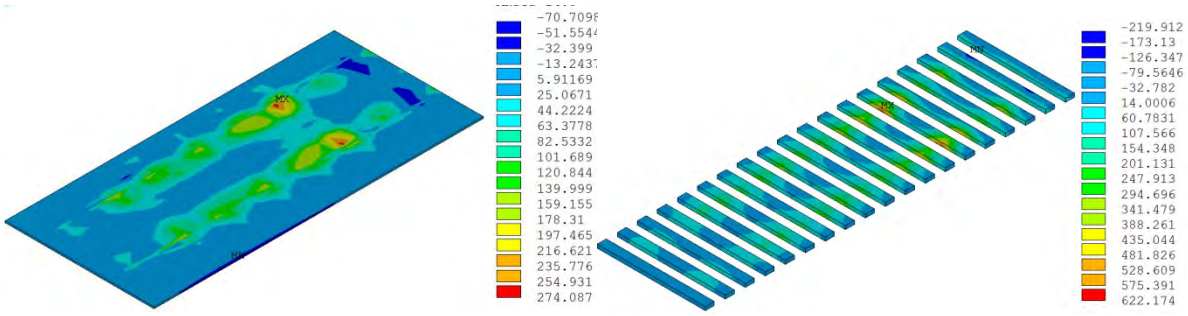

Figure 50. Interface shear stresses between the crossties and the concrete at failure load.

Inspection of **Figures 49 and 50** yields a clear indication on the load path thought the connection between the crossties and the concrete. These interfacial shear stresses were carried by the concrete (the sides of the embedment depth) and the grout in the connection. As noticed, all the horizontal shear stresses were concentrated around the connection and were almost zero otherwise. Proper installation and construction of these connections are vital to avoid any failures in the system connectivity. **Figures 51 and 52** present the shear stresses between the crossties and the steel bearing plate connecting them to the rail.

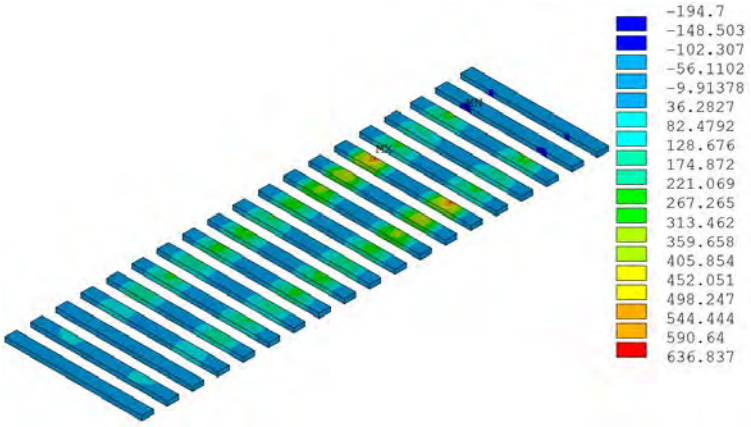

Figure 51. Interface shear stresses between the crossties and the bearing plates at failure.

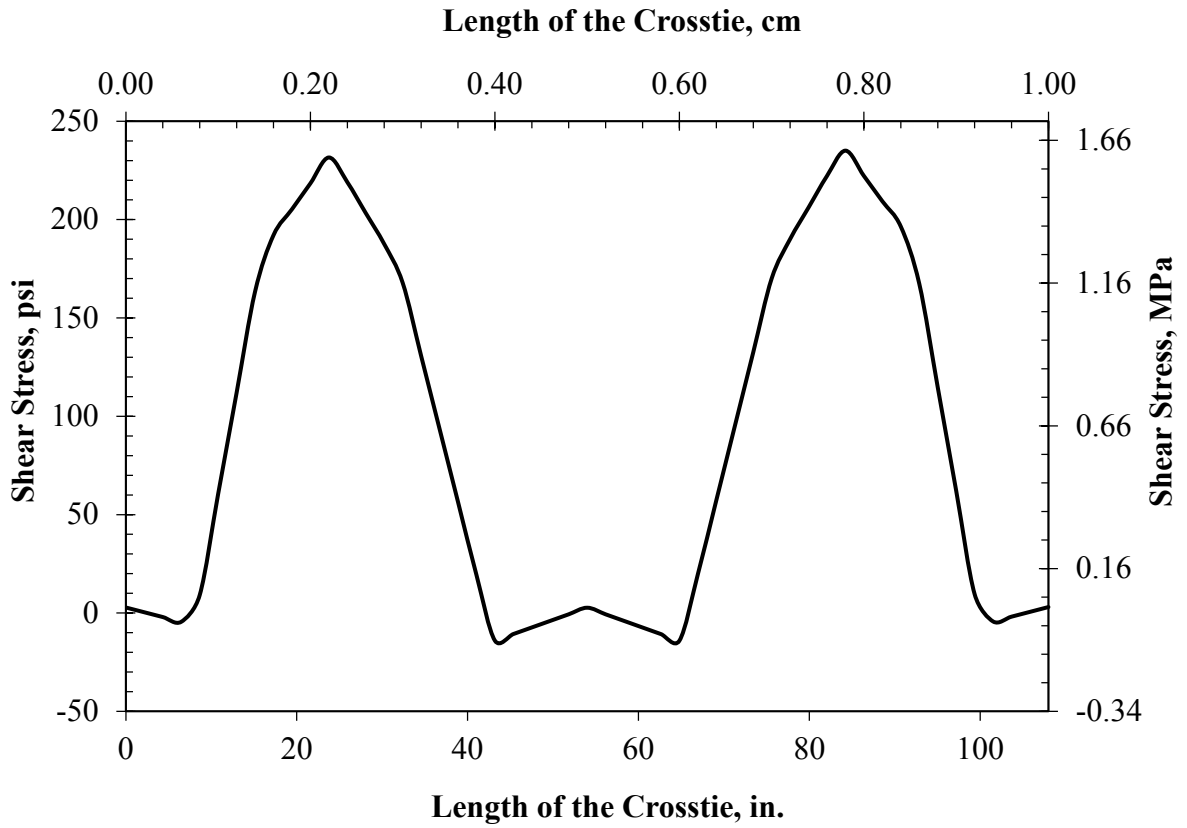

Figure 52. Interface shear stresses between the crossties and the bearing plates at failure.

Inspection of **Figures 51 and 52** indicates that the maximum interfacial shear stresses occurred underneath the steel bearing plates while elsewhere it was almost non-existent, which agrees with the results obtained previously. These stresses are resisted mainly by the spike lateral resistance, which exceeded the applied stresses by a significant margin. Even when ignoring friction between the steel bearing plates and the HDPE crossties, the lateral resistance of the spikes was sufficient to resist all the straining action without yielding.

3.3.2 U-Girder with full depth precast panel system connections:

The connections of this system are vital to its performance, thus extra care must be exerted when designing and constructing them. The precast panels are manufactured with shear pockets to accommodate the shear connectors extending from the top of the U-Girders. After the panels are placed in their location, these shear pockets are fully grouted to enable full composite action. Additionally, anchors bolts can be drilled and epoxied in the precast U-Girders in case additional shear connectors are required. Several researchers have investigated the behavior of shear pockets in the past to determine the optimal distribution, spacing, shape, orientation, and shear studs density including (7 to 11). In this study, 12 in. × 20 in. (30.48 cm × 50.8 cm) shear pockets were used every 28 in. (71.12 cm) spacing yielding two shear pockets per length of the

panels. Two rows of 9 U-loops were extended from #5 shear reinforcement in the U-Girders to act as shear connectors and enable full-composite action. The recommendations of the PCI state-of-the-art report on full-depth precast panels were adopted in this study (6).

The transverse connections, panel-to-panel connections, were achieved using female-to-female grouted shear keys. However, the use of match-cast, male-to-female, shear joints is also allowed. Epoxy resin was used to ensure proper bond and mitigate joint leakage.

To ensure that the system achieved full composite action, the deformation of the system at ultimate load was cross-examined with the location of the shear pockets. **Figure 53** illustrates the deformation of the system at ultimate load with the location of the shear pockets and free nodes indicated by solid and dashed lines respectively.

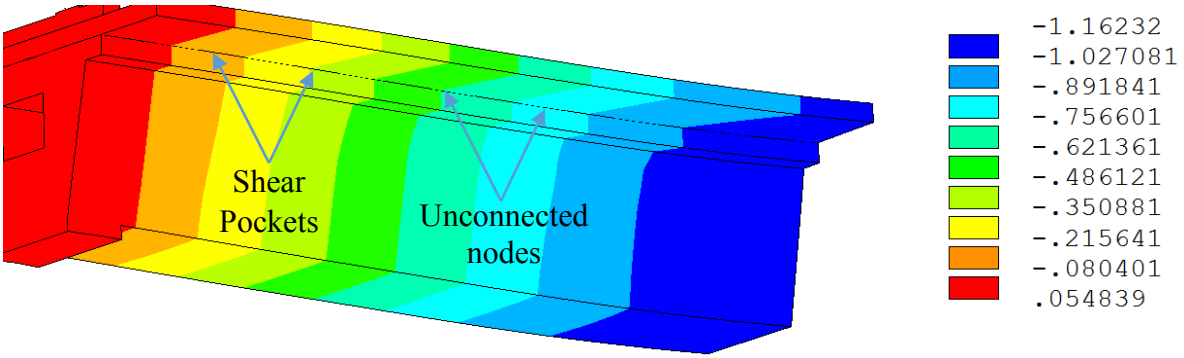

Figure 53. Deformation of the system at ultimate, in. (1 in. = 2.54 cm).

As noticed from continuity of the deformed shape illustrated in **Figure 53**, the system experienced full composite action between the precast panels and the U-Girder. To further investigate the connections, the interface shear stresses between the U-Girders and the precast panels were explored at ultimate and failure loads, see **Figures 54 and 55**.

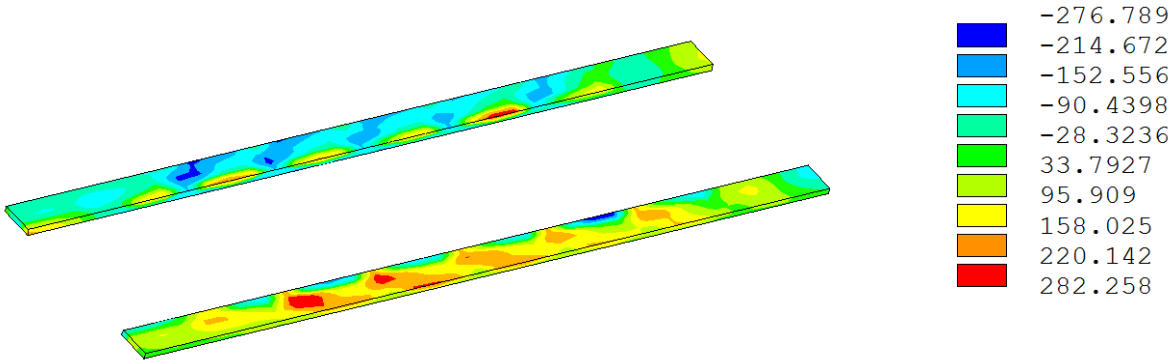

Figure 54. Interface shear at ultimate, psi (1 psi = 6.9 kPa).

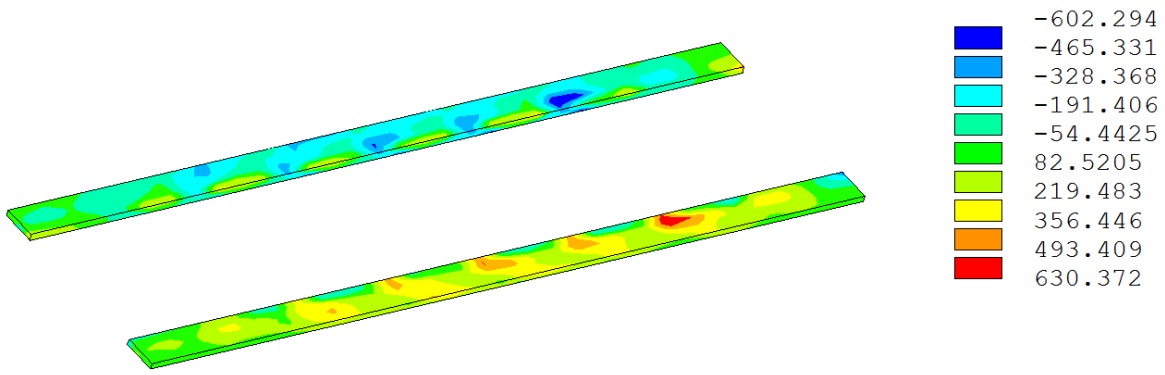

Figure 55. Interface shear at failure, psi (1 psi = 6.9 kPa).

As noticed from **Figures 54 and 55**, the interface shear in transmitted from the U-Girder to the precast panels through the shear pockets, as illustrated by the shear stress concentrations at the shear pockets locations. The maximum magnitude of the shear stresses at failure was 630 psi, which indicated that the system experienced full-composite action between the U-Girders and the precast panels, as the capacity of the shear pockets, calculated in the interface shear design in Appendix D, was 1,660 psi. Additionally, **Figure 56** presents the interface shear at ultimate and failure loads along with the position of the shear pockets.

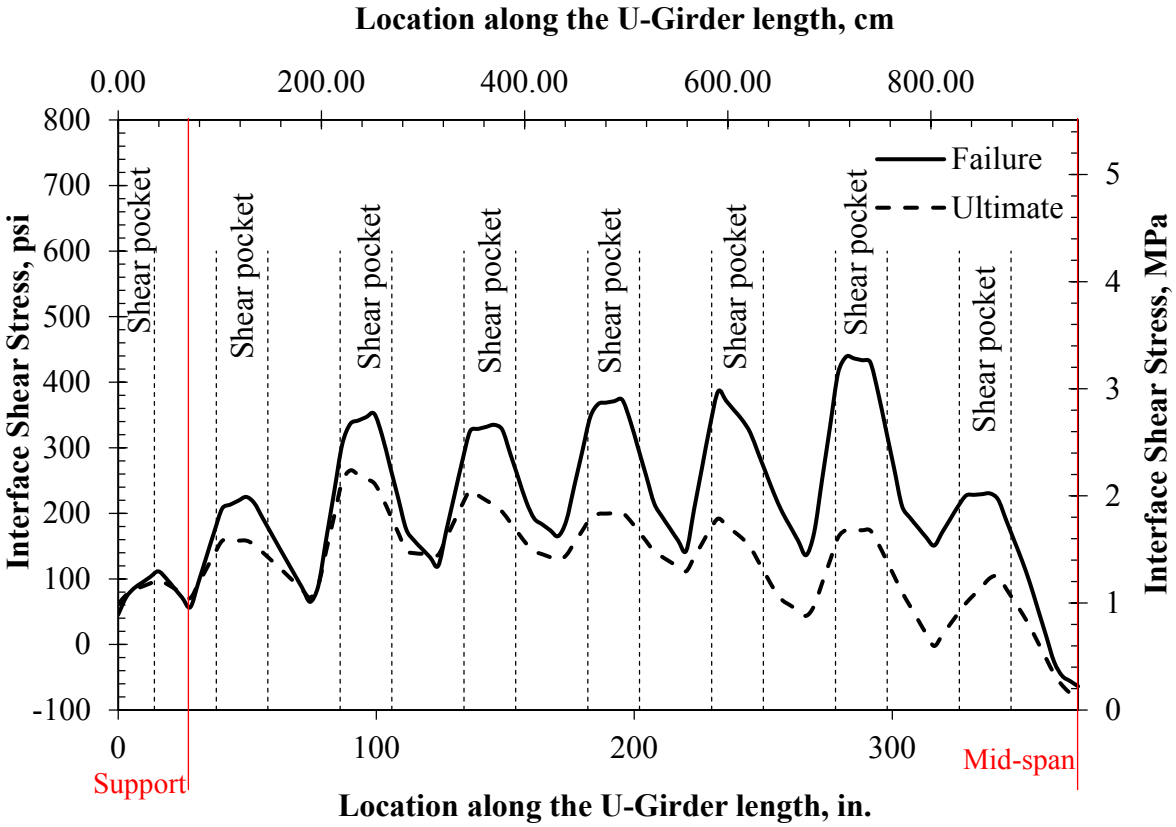

Figure 56. Interface shear and shear pocket locations at ultimate and failure.

Inspection of **Figure 56** reveals that the interface shear was transmitted through the shear pockets while little shear forces existed in the unconnected zones between consecutive shear pockets. This further validates that the shear pockets distribution and number of shear connectors used achieved full composite action between the U-Girder and the full-depth precast panels.

Figures 57 to 68 present the bending stresses; i.e. stresses in the direction of the longitudinal axis of the bridge, for both systems throughout the different loading stages. **Figures 69 to 92** present the cracking progression for both systems throughout the different loading stages.

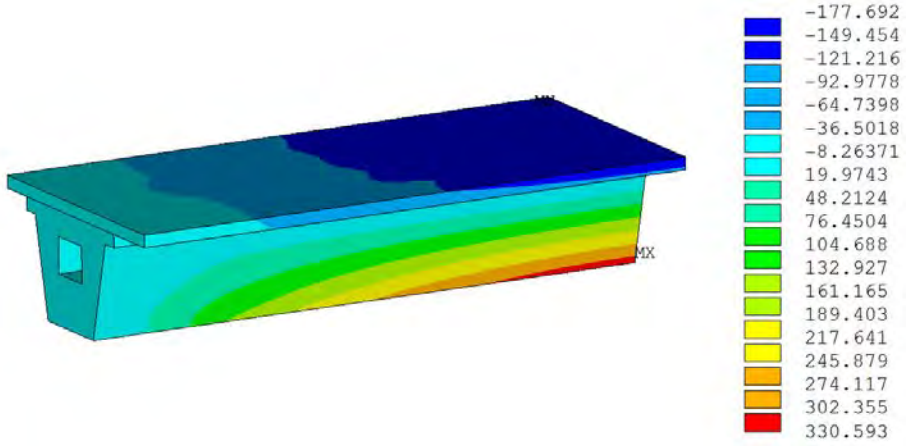

Figure 57. Bending stresses of the U-Girder system due to dead load, psi (1psi = 6.9kPa).

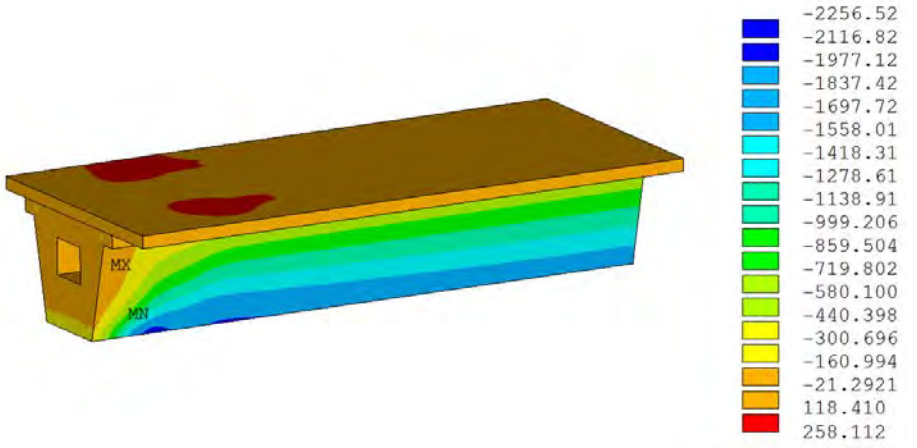

Figure 58. Bending stresses of the U-Girder system after prestress, psi (1psi = 6.9kPa).

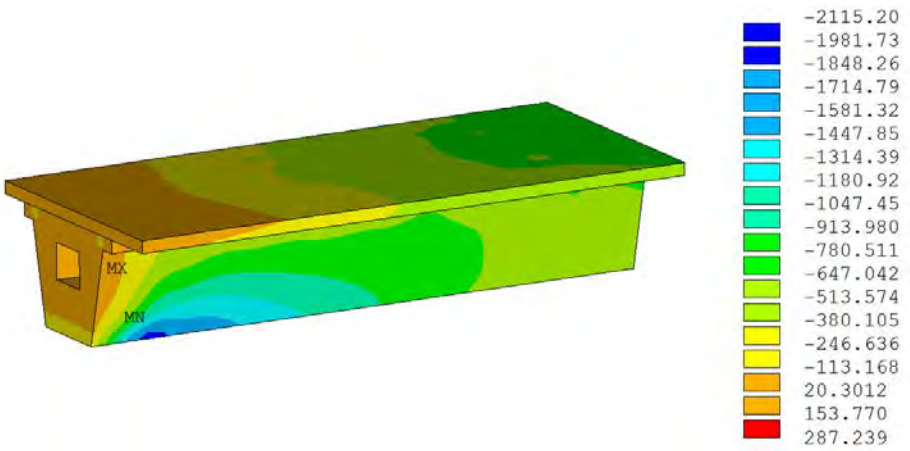

Figure 59. Bending stresses of the U-Girder system at service load, psi (1psi = 6.9kPa).

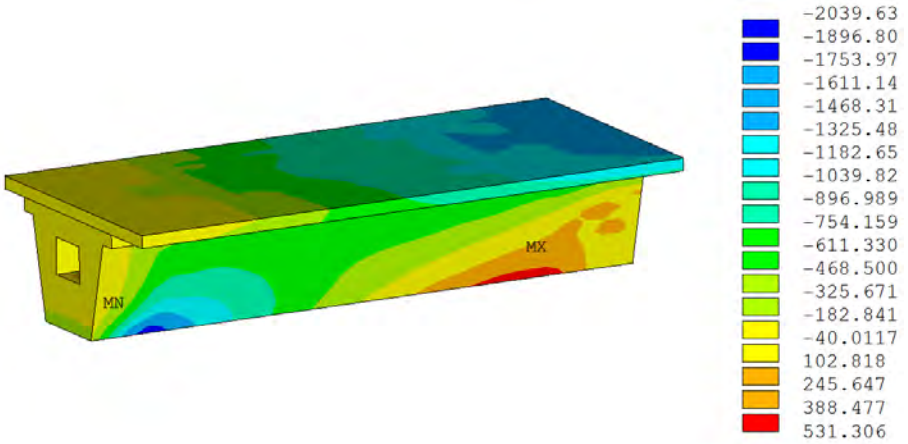

Figure 60. Bending stresses of the U-Girder system at cracking load, psi (1psi = 6.9kPa).

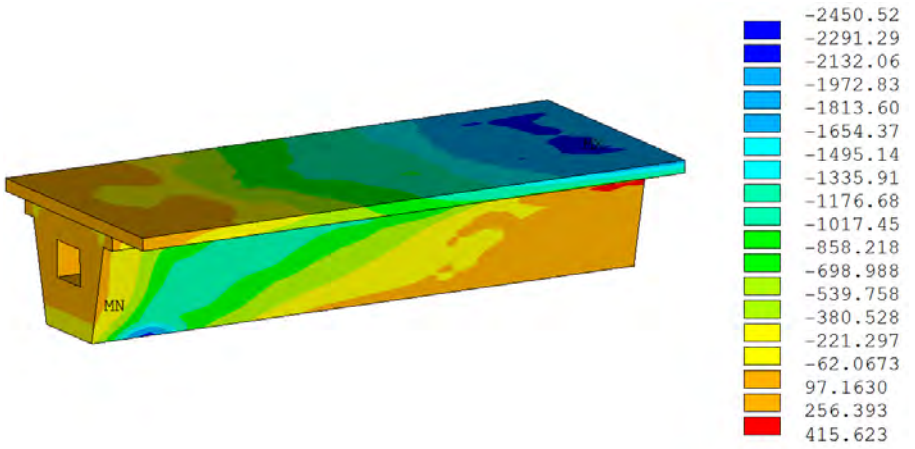

Figure 61. Bending stresses of the U-Girder system at ultimate load, psi (1psi = 6.9kPa).

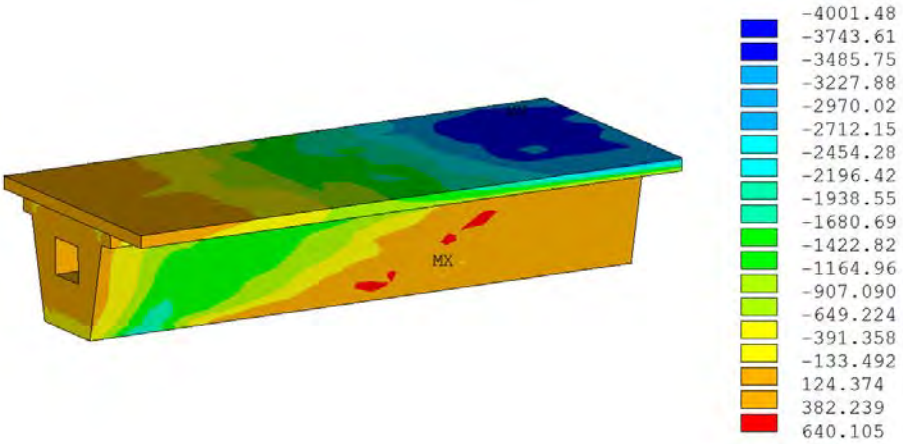

Figure 62. Bending stresses of the U-Girder system at failure, psi (1psi = 6.9kPa).

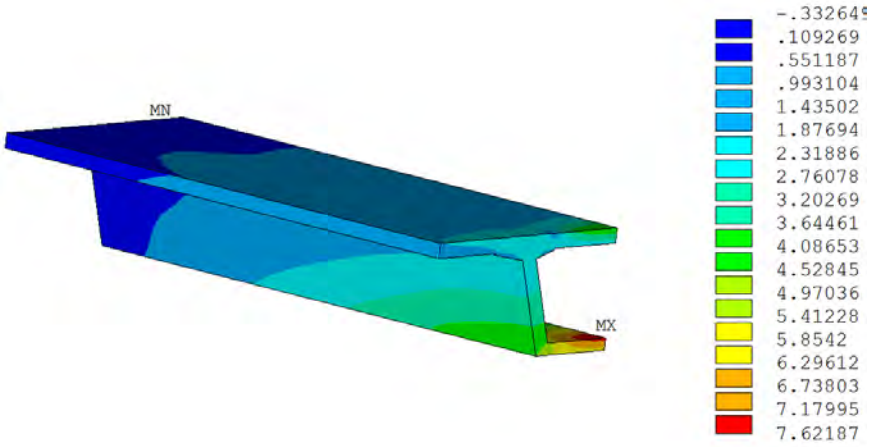

Figure 63. Bending stresses of the Box girder system due to dead load, psi (1psi = 6.9kPa).

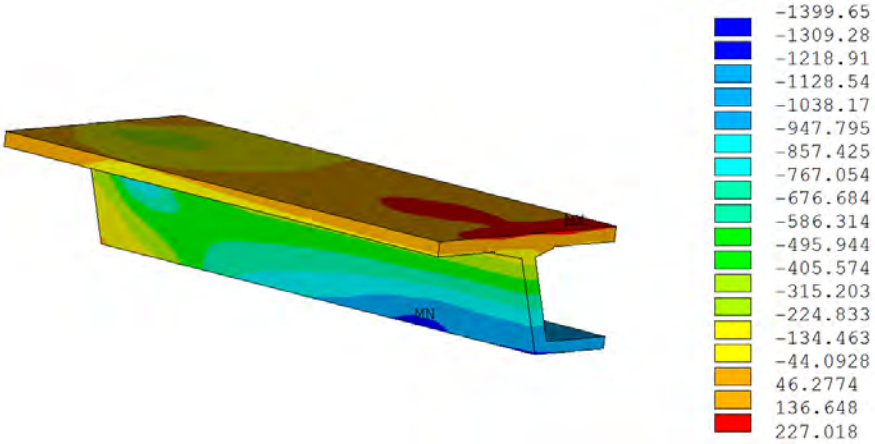

Figure 64. Bending stresses of the Box girder system after prestress, psi (1psi = 6.9kPa).

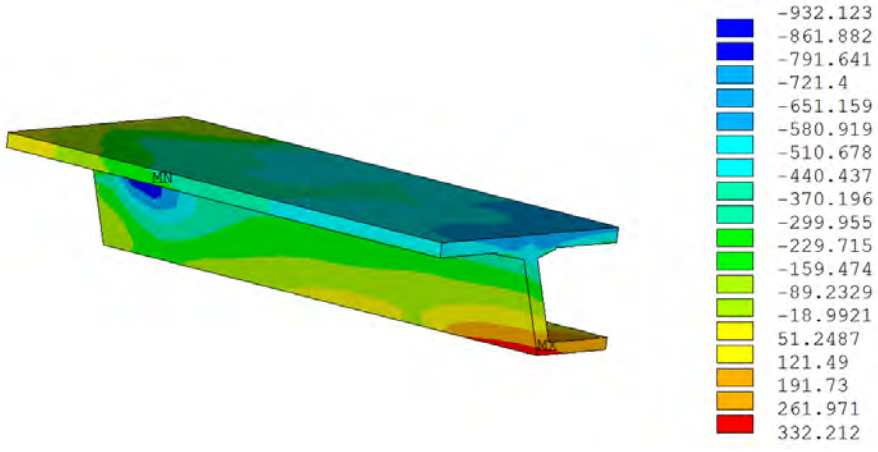

Figure 65. Bending stresses of the Box girder system at service load, psi (1psi = 6.9kPa).

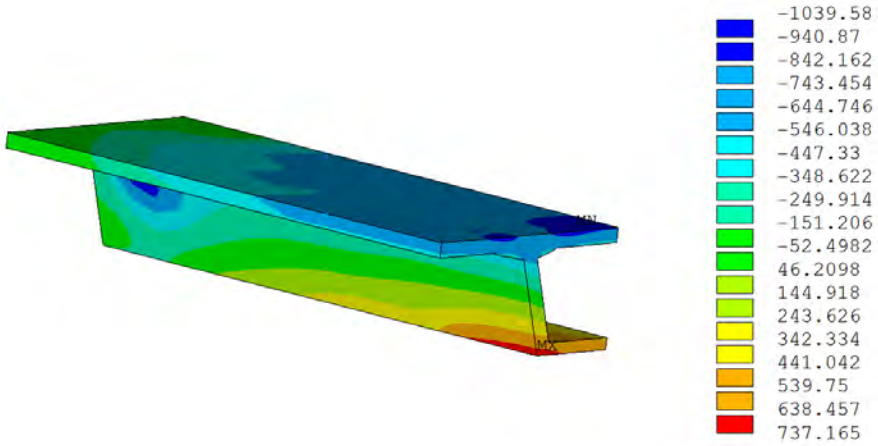

Figure 66. Bending stresses of the Box girder system at cracking load, psi (1psi = 6.9kPa).

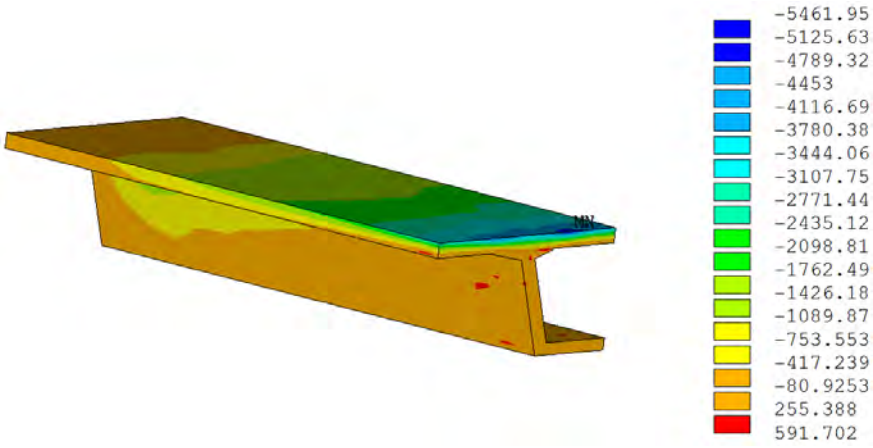

Figure 67. Bending stresses of the Box girder system at ultimate load, psi (1psi = 6.9kPa).

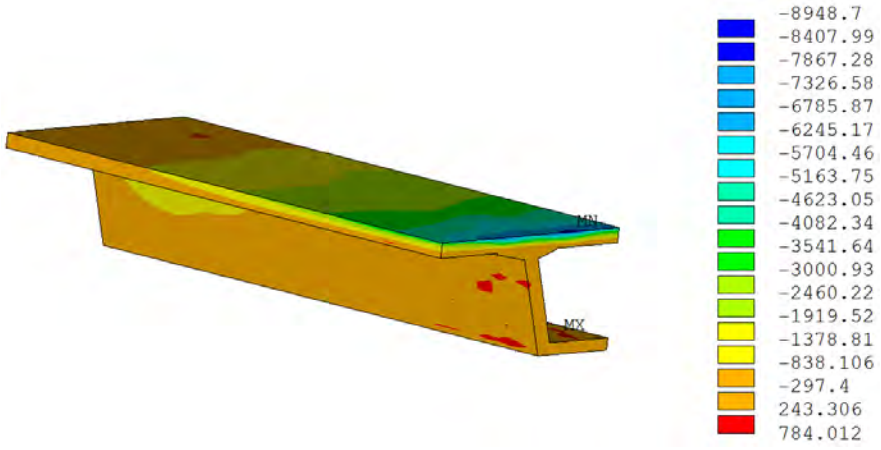

Figure 68. Bending stresses of the Box girder system at failure, psi (1psi = 6.9kPa).

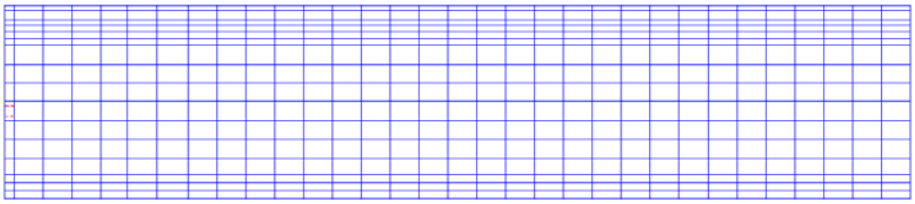

Figure 69. Cracking pattern for the U-Girder system at service load.

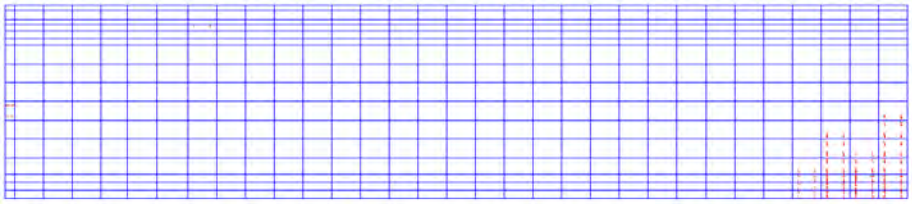

Figure 70. Cracking pattern for the U-Girder system at cracking load.

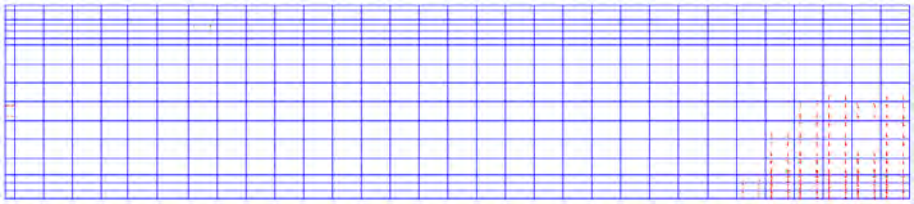

Figure 71. Cracking pattern for the U-Girder system at 1.84 service load

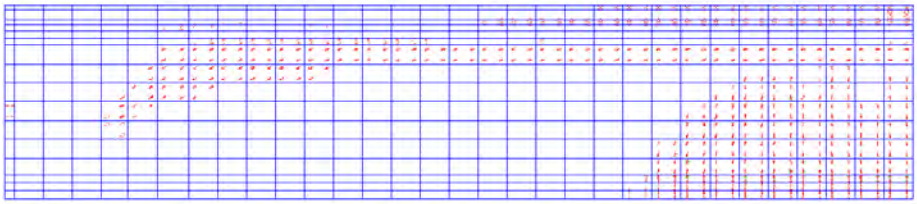

Figure 72. Cracking pattern for the U-Girder system at 2.09 service load.

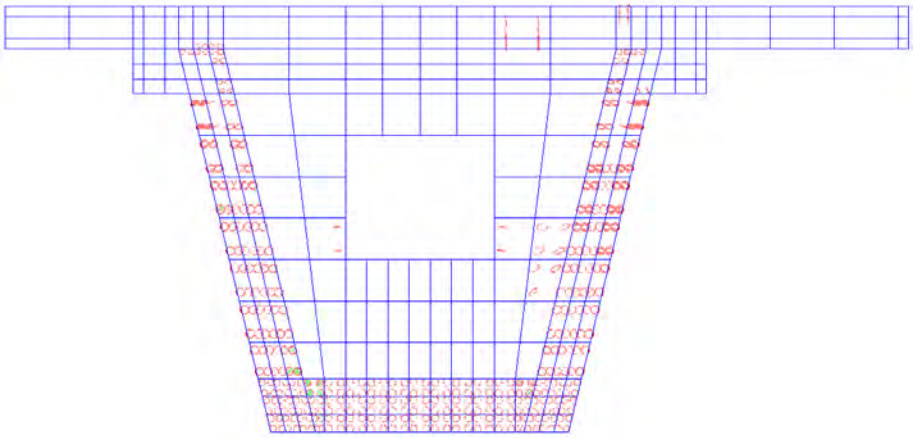

Figure 73. Cross section cracking for the U-Girder system at 2.09 service load.

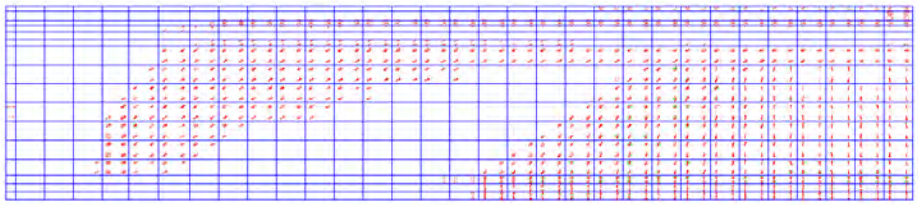

Figure 74. Cracking pattern for the U-Girder system at ultimate load (2.33 service load).

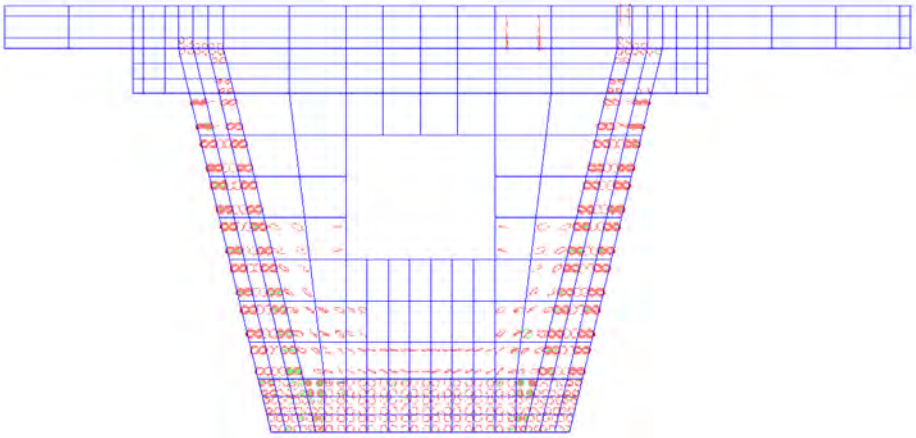

Figure 75. Cross section cracking for the U-Girder at ultimate load (2.33 service load).

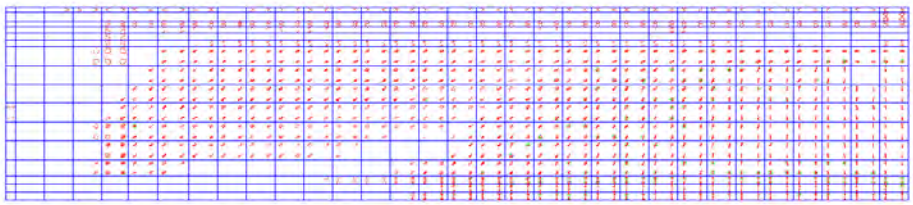

Figure 76. Cracking pattern for the U-Girder system at (2.52 service load).

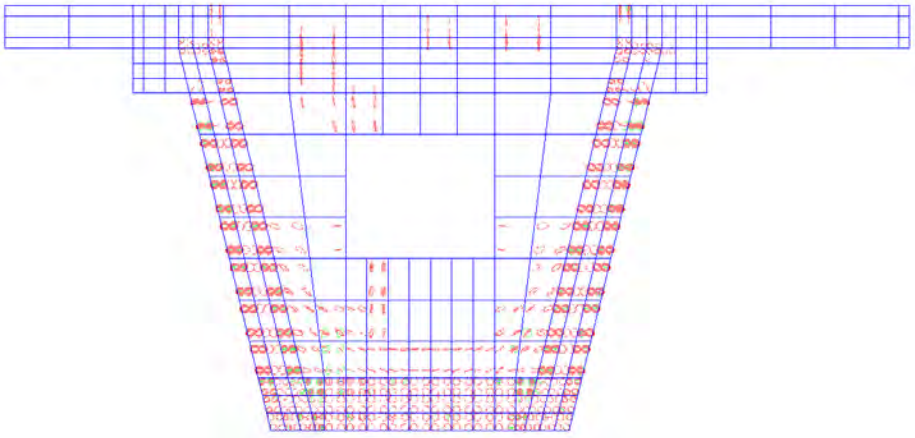

Figure 77. Cross section cracking for the U-Girder system at 1.08 ultimate load.

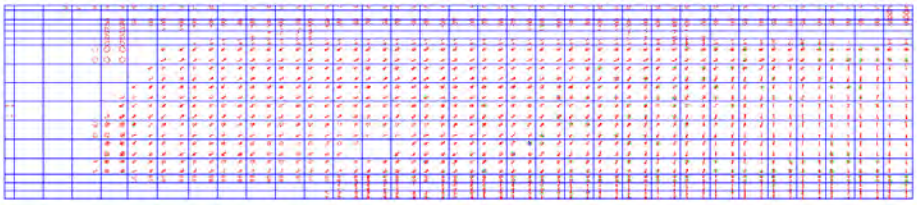

Figure 78. Cracking pattern for the U-Girder system at 1.16 ultimate load.

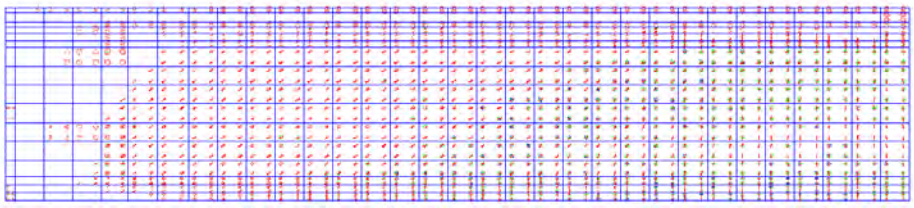

Figure 79. Cracking pattern for the U-Girder system at failure.

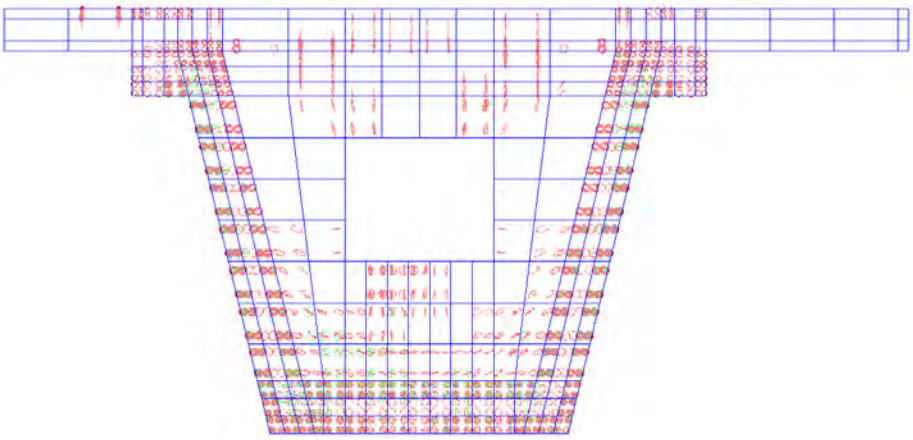

Figure 80. Cross section cracking for the U-Girder system at failure.

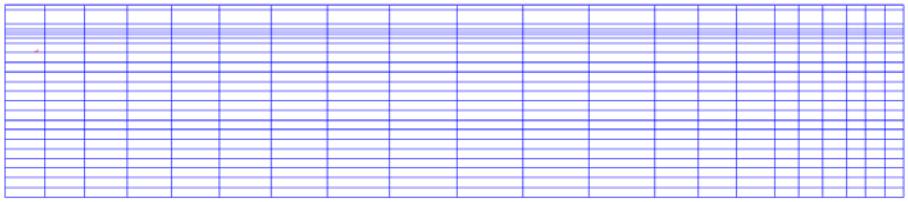

Figure 81. Cracking pattern for the Box girder system at service load.

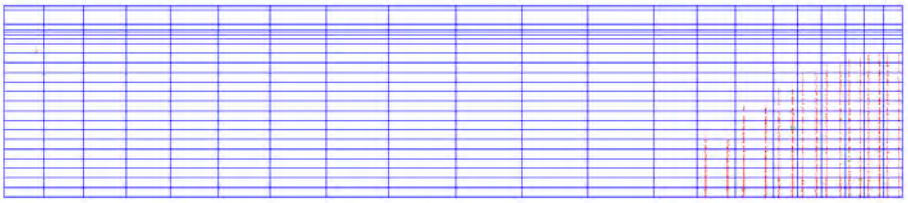

Figure 82. Cracking pattern for the Box girder system at cracking load.

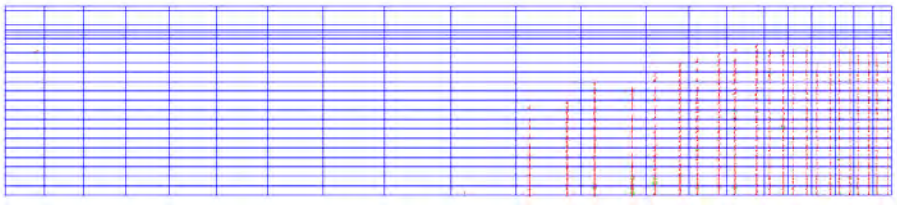

Figure 83. Cracking pattern for the Box girder system at 1.53 service load.

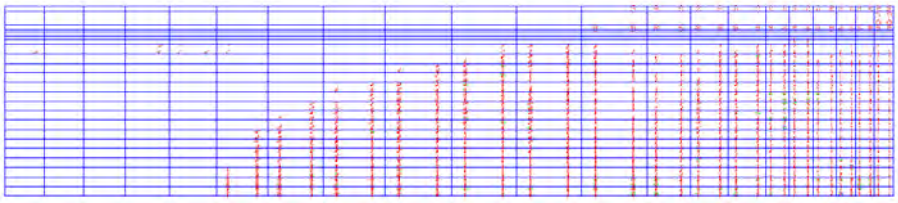

Figure 84. Cracking pattern for the Box girder system at 1.79 service load.

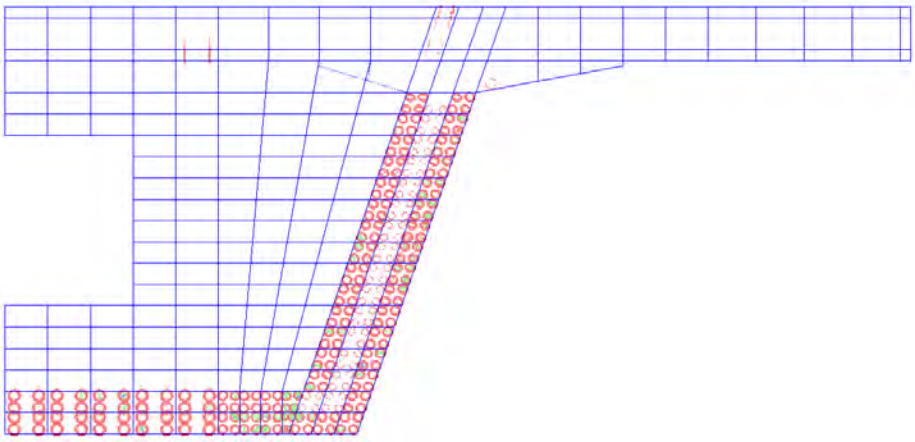

Figure 85. Cross section cracking for the Box girder system at 1.79 service load.

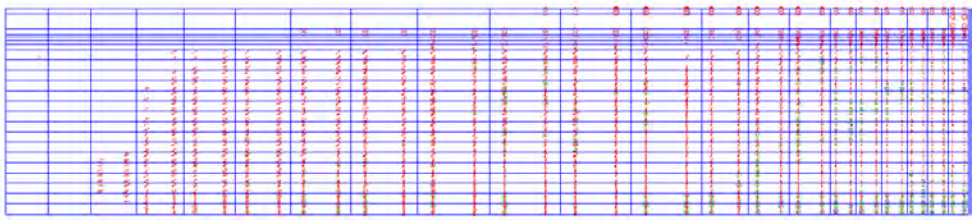

Figure 86. Cracking pattern for the Box girder system at ultimate load.

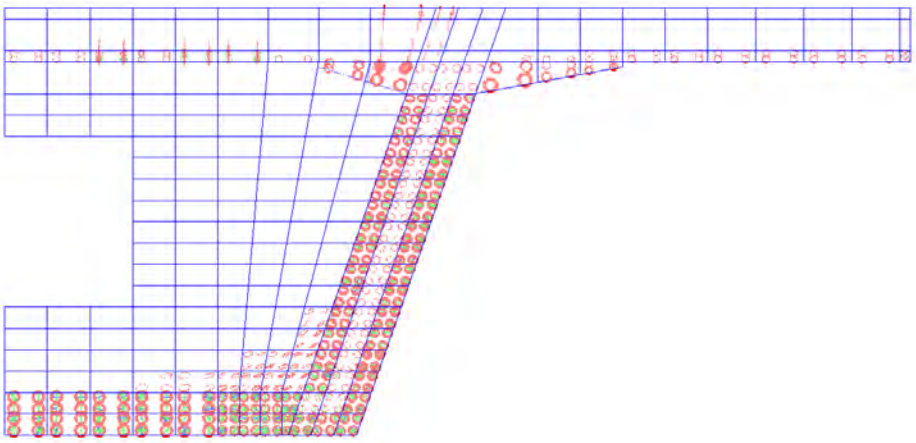

Figure 87. Cross section cracking for the Box girder system at ultimate load.

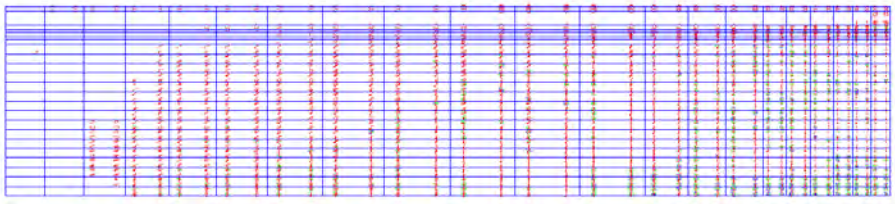

Figure 88. Cracking pattern for the Box girder system at 1.08 ultimate load.

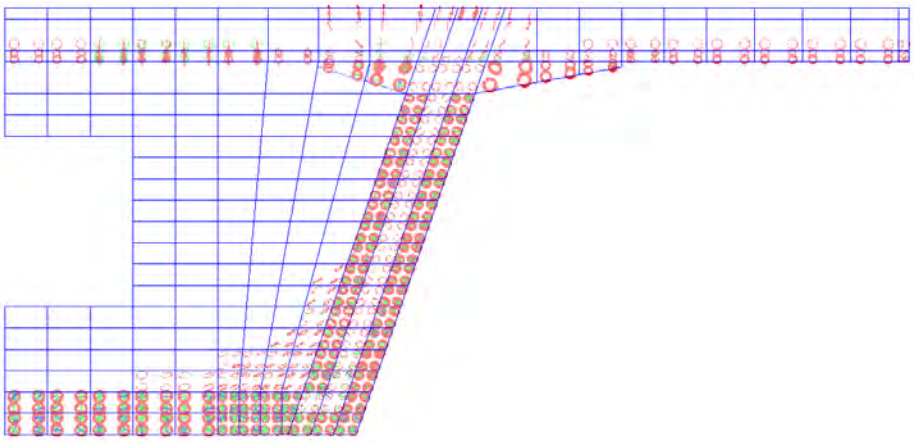

Figure 89. Cross section cracking for the Box girder system at 1.08 ultimate load.

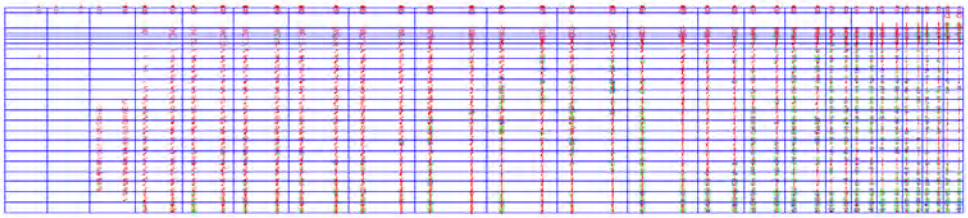

Figure 90. Cracking pattern for the Box girder system at 1.16 ultimate load.

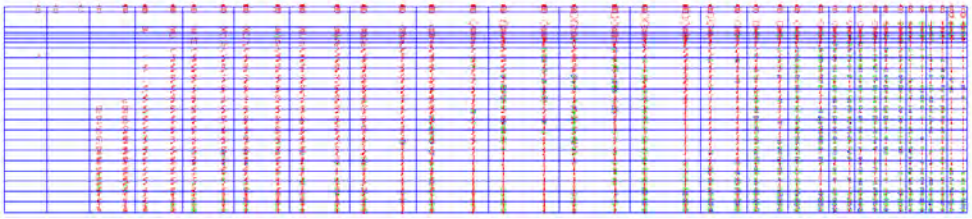

Figure 91. Cracking pattern for the Box girder system at failure.

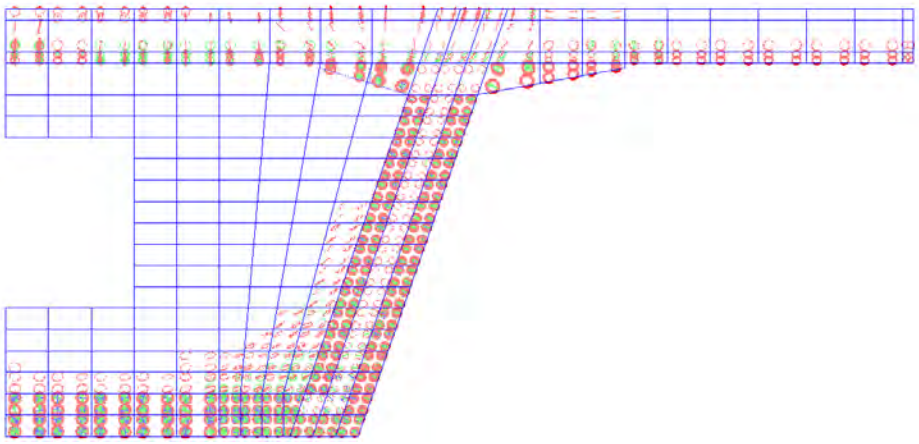

Figure 92. Cross section cracking for the Box girder system at failure.

As noticed from the results presented above, both system showed no cracks before service load and crack initiation and failure were both caused by the flexural stresses at mid-span. Moreover, it is evident from the stress and crack distributions that each system behaved in a different manner due to the same applied loads. The Box girder system exhibited normal flexural behavior with crack initiation starting at mid-span, due to the tensile stresses generated from the bending moment. After cracking, the formation of cracks propagated towards the supports and their orientation was shifted to mimic the inclination of the compressive struts resisting shear forces. No pure shear cracks were noticed, which was due to the prestressed tendons profile as the large inclined prestress force near the support eliminated all the diagonal tension stresses and, in turn, shear cracks. After the maximum compressive stress was reached, the concrete failed in compression directly above the webs of the Box girder.

On the other hand, the behavior of the U-Girder was different. Cracking initiated normally at mid-span, due to the tensile stresses generated from the bending moment. After cracking, the formation of cracks propagated towards the supports. However, due to the geometry of the cross-section, illustrated in **Figure 3**, the shear forces were directly transferred from the rails to the webs of the U-Girder, and due to the absence of the inclined prestessing forces, shear crack formation occurred. After yielding of the main steel reinforcement at mid-span, the flexural cracks at mid-span propagated towards the supports and their orientation was shifted to mimic the inclination of the compressive struts resisting shear forces. Then after the maximum compressive stress was reached, the concrete failed in compression.

The deflection obtained for both systems were within the acceptable ranges. AREMA recommends limiting service deflections to $Span/640$, which means that service deflection limit is 1.125 in. The Box girder experienced more deflections as it underwent significant yielding before failure. **Figure 93** presents the load vs the mid-span deflection for both systems and **Table 3** presents a comparison between both systems.

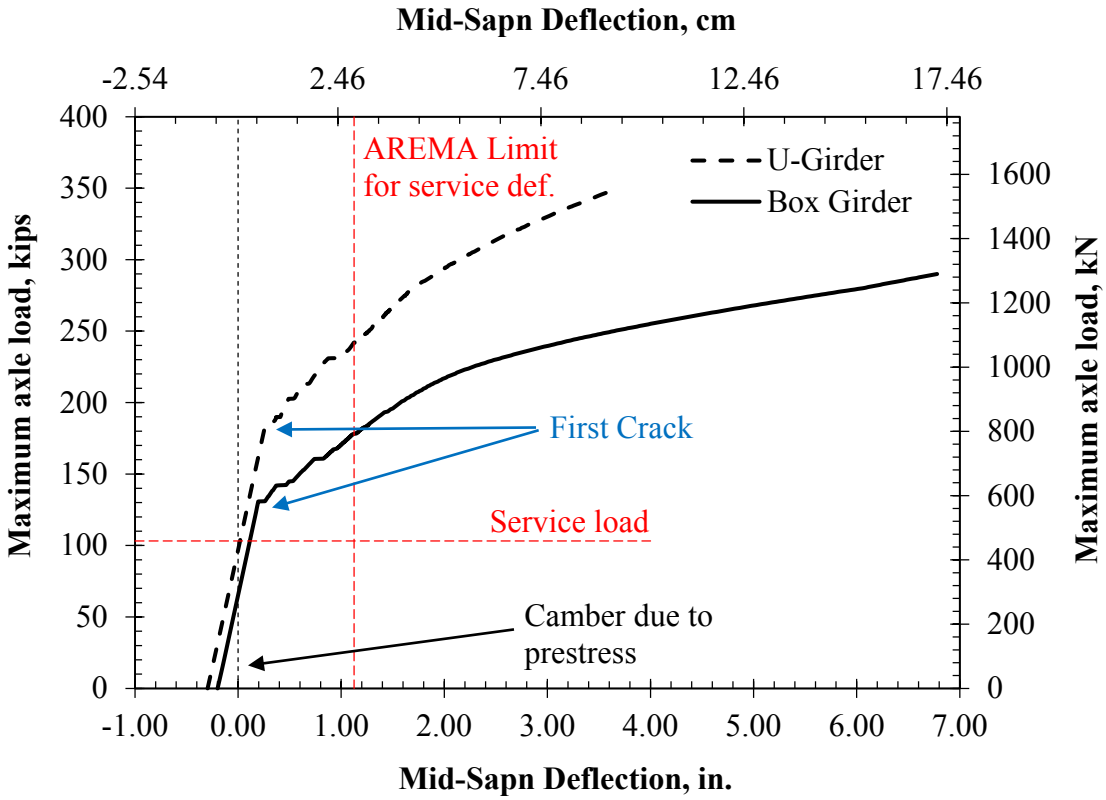

Figure 93. Load-deflection curve for both systems.

Table 3. Comparison between the U-Girder and Box girder systems.

Criterion	U-Girder system	Box girder system
Weight, kip/ft	1.886 for girders and 1.42 for the precast panels [Total 5.2]	6.1
Prestress profile	Straight	Parabolic
Prestressed elements	56-0.6" strands at the bottom 8-0.6" strands at the top [for each girder]	4 PT tendons with 16-0.6" strands
Span to depth ratio	9	9
Service mid-span deflection, in.	0.02	0.19
Ultimate mid-span deflection, in.	1.16	3.06
Failure mid-span deflection, in.	3.59	6.78
Axle load at cracking, kips	187.98	130.83
Axle load at failure load, kips	347.24	289.95
Cracking pattern	Compression-shear pattern	Pure flexural pattern
Mode of failure	Mid-span concrete crushing in compression	Mid-span concrete crushing in compression

Inspection of **Figure 93 and Table 3** reveals that the U-Girder system showed higher carrying capacity and less deflection than the Box girder system. However, the Box girder system showed a much higher ductility before failure. Cracking initiated in the Box girder system significantly before the U-Girder system, at about 70% less axle load. This can be attributed to the efficiency of the cross-section design of the U-Girder system, illustrated in **Figure 3**. The rail loading were directly transferred to the webs of the U-Girder without inducing bending stresses in the precast panels, while the Box girder system load path induced higher bending stresses in the top slab. Moreover, the presence of two U-Girders helped the distribution of loads better than the one Box girder.

SECTION 4 SUMMARY AND CONCLUSION

- ABC plays a major role in new or replacement construction operations for railroad bridges due to the limited construction window.
- The material models implemented in the full-scale mode provided accurate representation of the behavior of the full system in actual railroad bridges.
- Both ABC system studied showed favorable performance, which provided a proof-of-concept for future upgrade to HSR in urban setting.
- The pretensioned U-Girder with full-depth precast panels system illustrated great performance showing higher carrying capacity and less deflection than the post-tensioned Box girder system. However, the Box girder system showed a much higher ductility before failure.
- Cracking initiated in the Box girder system significantly before the U-Girder system, at about 70% less load due to the efficiency and multiple girder setup of the cross-section design of the U-Girder system. Thus, it is proposed for future applications.
- The U-Girder system performed better that expected outperforming the Box girder system. Thus it is recommended for future investigations and implementation.

References

1. Moreu F and LaFave J. Current Research Topics: Railroad Bridges and Structural Engineering. Report no. NSEL-0.32, Urbana-Champaign, IL: Newmark Structural Engineering Laboratory, October 2012.
2. Lotfy I and Issa M. Evaluation of the longitudinal restraint, uplift resistance, and long-term performance of High Density Polyethylene crosstie rail support system using static and cyclic loading. Journal of Rail and Rapid Transit; In review.
3. Lotfy I, Farhat M, and Issa M. Effect of Pre-drilling, Loading Rate and Temperature Variation on the Behavior of Railroad Spikes used for High Density Polyethylene Crossties. Journal of Rail and Rapid Transit; In review.
4. Lotfy I, Farhat M, and Issa M. Temperature Effect on the performance of Glass Fiber Reinforced High Density Polyethylene Composite Railroad Crossties. Journal of Rail and Rapid Transit; In press, accepted for publication on 17 March 2015. DOI: 10.1177/0954409715583384.
5. Lotfy I, Farhat M, Issa M, and Al-Obaidi M. Flexural behavior of high-density polyethylene railroad crossties. Journal of Rail and Rapid Transit; In press, accepted for publication on 17 November 2014. DOI: 10.1177/0954409714565655.

6. PCI Committee on Bridges. State-of-the-Art Report on Full-Depth Precast Concrete Bridge Decl Panels. Precast/Prestressed Concrete Institute, Chicago, IL, 2011.
7. Issa, M.A., Idriss, A., Kaspar, I.I., and Khayyat, S.Y., "Full depth precast and precast, prestressed concrete bridge deck panels," PCI Journal, V. 40, No. 1, pp. 59-80, Jan.- Feb 1995c.
8. Issa, M.A., Yousif, A.A., and Issa, M.A., "Experimental behavior of full-depth precast concrete panels for bridge rehabilitation," ACI Structural Journal, V. 97, No. 3, pp. 397-407, May-June 2000.
9. Issa, M.A., Yousif, A.A., Issa, M.A., "Construction procedures for rapid replacement of bridge decks," Concrete International, V. 17, No. 2, pp. 49- 52, Feb. 1995a.
10. Issa, M.A., Yousif, A.A., Issa, M.A., Kaspar, I.I., and Khayyat, S.Y., "Field performance of full depth precast concrete panels in bridge deck reconstruction," PCI Journal, V. 40, No. 3, pp. 82-108, May-June 1995b.
11. Issa, M.A., Yousif, A.A., Issa, M.A., Kaspar, I.I., and Khayyat, S.Y., "Analysis of full depth concrete bridge deck panels," PCI Journal, V. 43, No. 1, pp. 74-85, Jan.-Feb 1998.
12. American Association of State Highway and Transportation Officials. AASHTO LRFD bridge design specifications: customary U.S. unit. 2012.
13. Califorcnia High-Speed Train Project. Design Guidelines for High-Speed Aerial Structures. Technical Memorandum. TM 2.3.3, 2009.
14. Califorcnia High-Speed Train Project. Structure Design Loads. Technical Memorandum. TM 2.3.2, 2011.
15. America Railway Engineering and Maintenance-of-Way Association, Chapter 30, Part 2, Evaluative Tests for Tie Systems. In AREMA Specifications.; 2011.
16. Hognestad, E. A study on combined bending and axial load in reinforced concrete members. Univ. of Illinois Engineering Experiment Station, Univ. of Illinois at Urbana-Champaign, IL, 43-46, 1951.
17. Fanning, P, "Nonlinear Models of Reinforced and Post-tensioned Concrete Beams", Electronic Journal of Structural Engineering, 2001.

NURail Project ID: NURail2012-UIC-R02-F

Structural Adhesive Behavior – Experimental and Computational Study

By

Mohsen A. Issa
Professor of Civil and Material Engineering
University of Illinois at Chicago
missa@uic.edu

Aiman Shibli
PhD Student of Civil and Material Engineering
University of Illinois at Chicago
ashibli2@uic.edu

TECHNICAL SUMMARY

Title

Structural Adhesive Behavior – Experimental and Computational Study

Introduction

Adhesive joints are being increasingly used in structural applications due to their unique characteristics and advantages. Recently, many structural industries have considered utilizing adhesive for i) rehabilitation and for ii) joining load-bearing components. Structural adhesive is an excellent candidate for replacing the traditional joining methods such bolting and riveting, especially for scenarios involving joining brittle materials such Recycled Plastics composites (RPL). The attractiveness of adhesives stems from their unique combinations of properties which include: high strength, light weight, dimensional stability, and high resistance to environmental degradation and ease of use.

The traditional bolted joint methods have gone a long way in creating appropriate technologies and gained years of design experience, which cannot be easily replaced. Accordingly switching from traditional joining methods to adhesives bonding in civil infrastructure applications requires a large investment to establish a level of understanding comparable to that associated with traditional joining methods. In particular, it is crucial to characterize and fully understand bonded joint behavior, strength and failure properties, and to be able to predict them for a given geometries and loads.

The objectives of this research are:

i) Investigate the behavior of structural adhesive by characterizing their mechanical properties
ii) Establish a representative material model that can mimic their behavior and can be used in numerical models for computational studies.
iii) Utilize virtual testing using simulation to investigate different design options to utilize structural adhesive to rehabilitate and connect RPL beams

Approach and Methodology

- Structural adhesive was tested under tensile and shear load modes according to ASTM-D638 and ASTM-3983. These tests were conducted in order to extract the tensile and shear bulk property of the structural adhesive.
- Different material models were proposed and created based on the test data. Those material models were used in simulation in order to mimic the actual behavior of the structural adhesive.
- Sandwich structures were constructed where the adhesive was sandwiched between two substrates (Al and PC). Two configurations were considered, equal length plate sandwich structure and unequal length plate sandwich. These Sandwich structures were tested under quasi-static and dynamic loadings.
- Sandwich structures were tested under four point bend testing (quasi-static loading) and ball drop testing (dynamic loading). Force-displacement and force-strain curves were extracted at low rate and high rate testing.
- Sandwich structures were simulated under four point bend testing (quasi-static loading) and ball drop testing (dynamic loading). Force-displacement and force-strain curves were extracted from simulation.
- Comparitive study has been performed betweein exprimental and simulation resuls.

Findings

- Quasi-Static bend simulations of the equal-length-plate sandwich structure show good correlation between experimental and simulation results, for all adhesive material models used in the simulations. Results show that force-displacement response is not affected by the adhesive stiffness which is expected as the adhesive layer will not affect the overall sandwich structure since it is much thinner and less stiff than the adherend substrates. However, for force-strain response, the results are more interesting because they are not affected by the adhesive material modeling approach. This is attributed to the fact that the bottom rollers forcing the PC plate to have the same curvature as the Al plate. The equal-length-plate configuration does not seem to serve as a good validation tool.
- Quasi-Static bend simulations of the unequal-length-plate sandwich structure show that the overall behavior of the structure is sensitive to the adhesive material modeling approach. Force-displacement results and force-strain results show that the linear-elastic material model will over predict the stiffness of the sandwich structure where the elastic-plastic material model mimics the experimental results much better. As the elastic material model does not account for plasticity, the adhesive does not soften up in simulations; and therefore, the PC plate will follow the Al plate curvature. The force-displacement results and the force-strain results show that simulation correlates well with experiments when elastic-plastic material model is used.
- Dynamic bend simulations with unequal-length-plate sandwich structure show that the overall behavior of the structure is sensitive to the adhesive material modeling approach. Strain-time simulation results at the center of top Al plate do not exhibit any dependence on the adhesive modeling approach; this is expected as the force is applied directly on the Al plate. However, strain-time simulation results at the bottom PC plate are sensitive to the

adhesive material modeling approach. The elastic-plastic material modeling approach predicts the testing results very well, unlike the elastic and elastic-viscoelastic material modeling approaches which correlate poorly with experimental results because they do not account for plasticity.

Conclusions

Through the results which are specific to the sandwich structure materials used in this study, the following conclusions and recommendations can be drawn:

- The sandwich structure with unequal-length plates is able to capture the sensitivity to the adhesive material modeling approaches. However, the sandwich structure with equal-length plates is insensitive to the adhesive layer and failed as a configuration for capturing or investigating adhesive behavior and properties.
- Comparison between numerical and experimental results from both the quasi-static and dynamic simulation results show that the elastic-plastic material model mimics the adhesive material behavior better than the elastic and elastic-viscoelastic material models, due to the ability of the elastic-plastic model to account for adhesive plasticity.
- Although both of the elastic and plastic phases of this specific adhesive are loading rate dependent, plastic behavior of the adhesive has bigger impact than its elastic behavior on the overall sandwich structure behavior. This is due to the fact that the adhesive will start deforming while the adhered substrates are still in their elastic regions.

Contacts

Principal Investigator
Mohsen A. Issa
Professor of Civil and Material Engineering
University of Illinois at Chicago
312-996-2426
missa@uic.edu

NURail Center
217-244-4444
nurail@illinois.edu
http://www.nurailcenter.org/

TABLE OF CONTENTS

LIST OF FIGURES

.

SECTION 1 INTRODUCTION

Civil infrastructure applications have been increasingly using Fiber-reinforced polymer (FRP) composites due to their advantageous material properties such as their high strength, high stiffness, light weight, high resistance to environmental degradation and rapid installation. However, structural FRP components are difficult to connect using bolted joints due to the brittleness of this material. The current traditional joining methods such as bolting and riveting create stress concentrations which lead to premature failure. Many structural industries have considered utilizing adhesives for joining load-bearing components as an excellent candidate for replacing the traditional bolted joint methods, especially when dealing with fibrous materials such composites. They have been attracted to use adhesives due to several reasons: high strength, dimensional stability, and ease of use. Furthermore, using adhesive joints will lead to uniform loading without stress concentrations as compared to the bolted joints. Holes in the bolted joints are areas for stress concentrations and moisture ingress, which can impact the overall structure durability.

The traditional bolted joint methods have gone a long way in creating appropriate technologies and gained years of design experience, which cannot be easily replaced. Switching from traditional joining methods to adhesives bonding in the civil infrastructure applications requires a large investment. Currently adhesive joints for civil infrastructure applications are in its infancy due to the lack of design guidelines and consistent specifications. Although adhesive bonding have been studied and used widely in the fields of aerospace and automotive, these studies cannot be directly transferred to the civil infrastructure domain. Adhesive bonding for civil structural application have essential differences with respect to type of materials, loadings, geometries and environmental conditions.

There are several studies on structurally adhesive joints; most of these studies follow the same two assumptions. The first of which is that structural adhesives behave elastically linear. The second of which is that structural adhesives always fail cohesively. Buyukozturk et al. pointed out that more realistic assumption are needed to provide better approximations of joint strength and behavior. Reza studied the adhesive joints which are used to bond CFRP laminates to steel substrate using experimental and numerical approaches. He concluded that non-linear deformation of adhesive can contribute to redistribution of strain and joint capacity.

One of the important steps towards greater use of structural adhesives in civil structural applications is to characterize their behavior. The present study was undertaken to investigate the structural adhesive behavior and its impact on a sandwich structure behavior.

SECTION 2 QUASI-STATIC AND DYNAMIC BEND TESTING

Sandwich structures were constructed where the adhesive was sandwiched between two substrates (Al and PC); two configurations were considered as shown in figure-1. These Sandwich structures were tested under quasi-static and dynamic loadings.

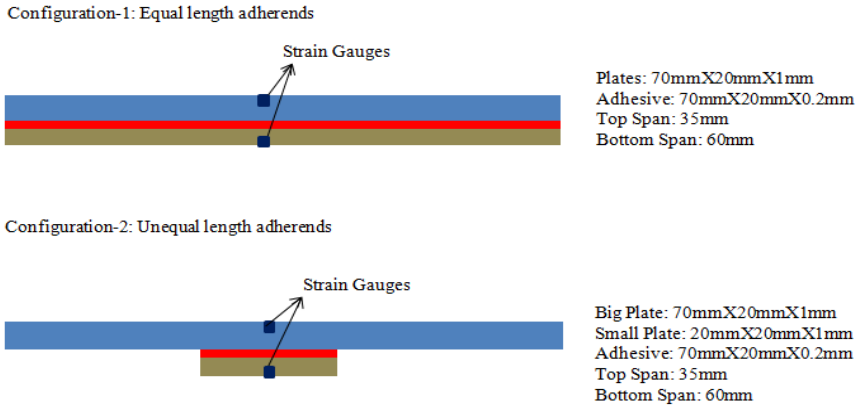

Figure 1: Two different sandwich structure configurations, equal-length plate and unequal-length plate

2.1. QUASI-STATIC BEND TEST

The planar bend test (four-point bend) has been extensively used to determine the strength of brittle materials. Similar technique was used in this study to bend the sandwiched plates in order to induce stress and strain state to the structure. The rollers from the top and bottom spans of the 4-point bend fixture were positioned 35mm and 60mm apart respectively. Two strain gauges were mounted on the sandwiched plates, one at the center of the top plate and one at the center of the bottom plate. The following are the Force-Displacement and Force-Strain test results for the two configurations:

2.1.1. Equal-length-plate sandwich structure

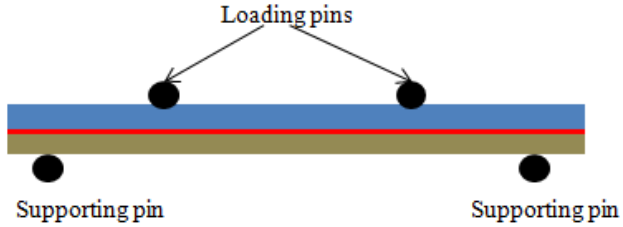

Figure 2: Equal-length-plate sandwich structure under quasi-static loading

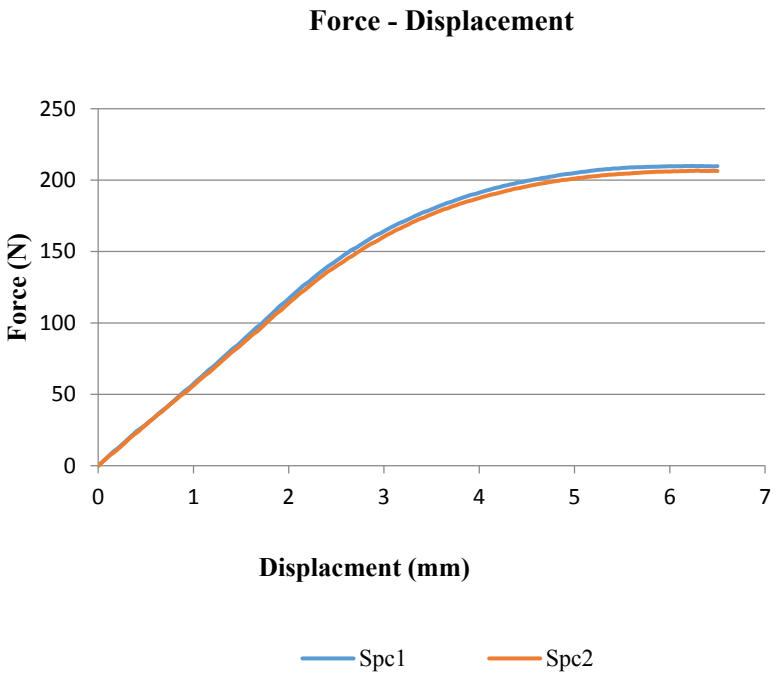

Figure 3a: Force-displacement results for the equal-length-plate sandwich structure.

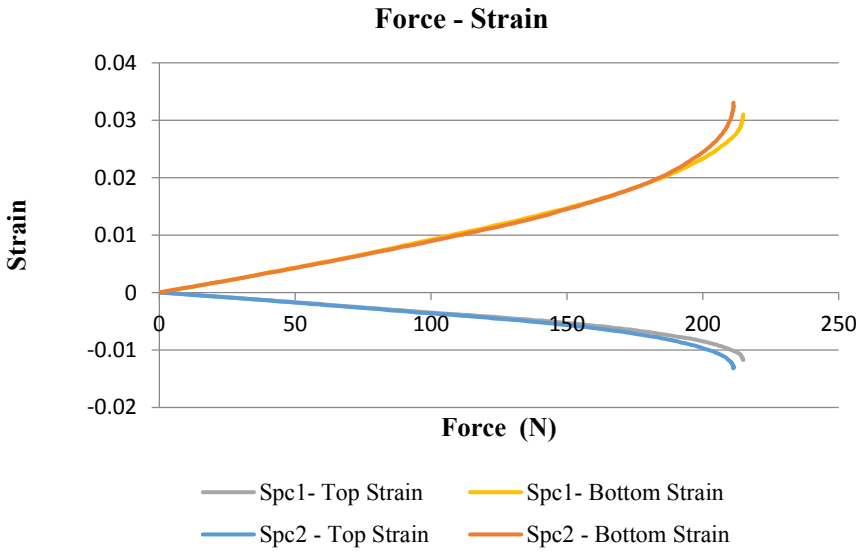

Figure 3b Force-strain results for the equal-length-plate sandwich structure.

2.1.2. Unequal-length-plate sandwich structure

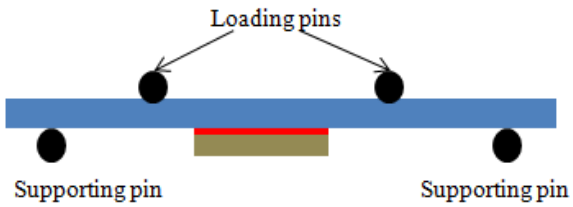

Figure 4: Unequal-length-plate sandwich structure under quasi-static loading

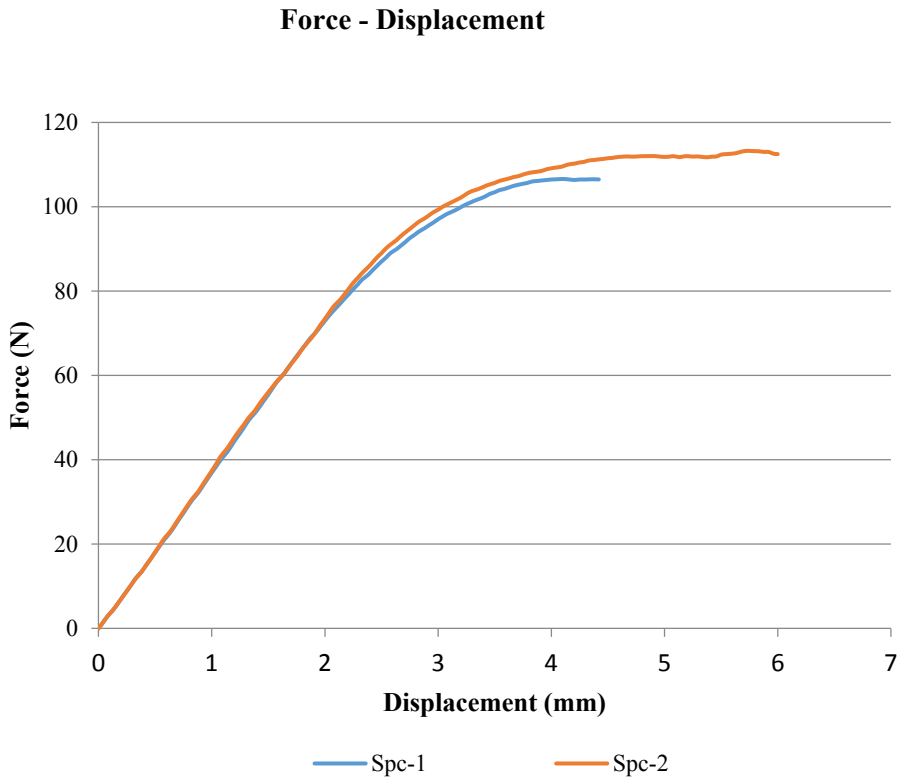

Figure 5a: Force-displacement results for the unequal-length-plate sandwich structure.

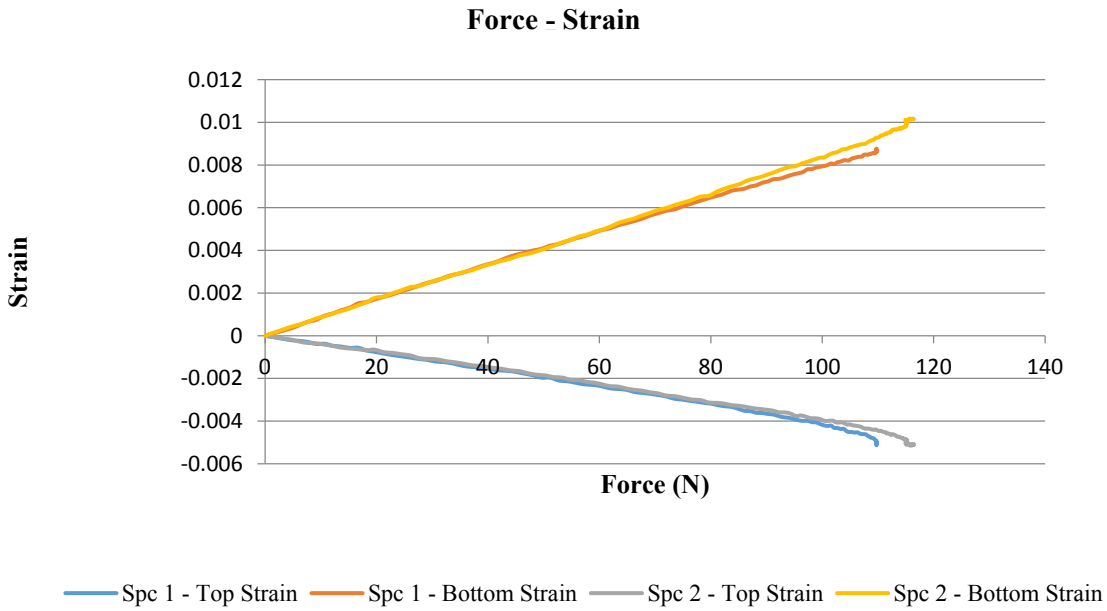

Figure 5b: Force-strain results for the unequal-length-plate sandwich structure.

2.2. DYNAMIC BEND TEST

The test fixture used to generate dynamic planar loading of the sandwich structure was similar to that described by Reiff et al. The test vehicle was centered in the 4-point bend fixture, such that during testing the bending direction was oriented along the longitudinal axis of the sandwich structure. A steel ball was dropped on the top span in order to generate the dynamic loadings. Acceleration was monitored and used as boundary conditions in the dynamic bend simulations.

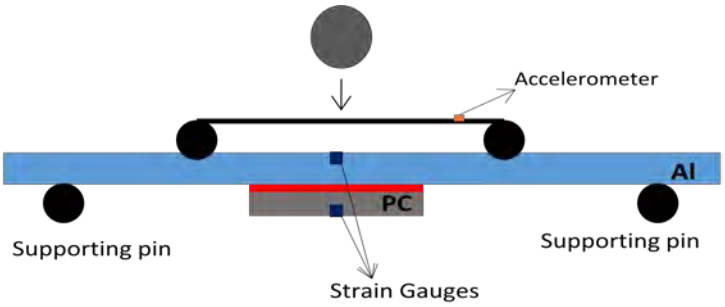

Figure 6: Unequal-length-plate sandwich structure under dynamic loading test

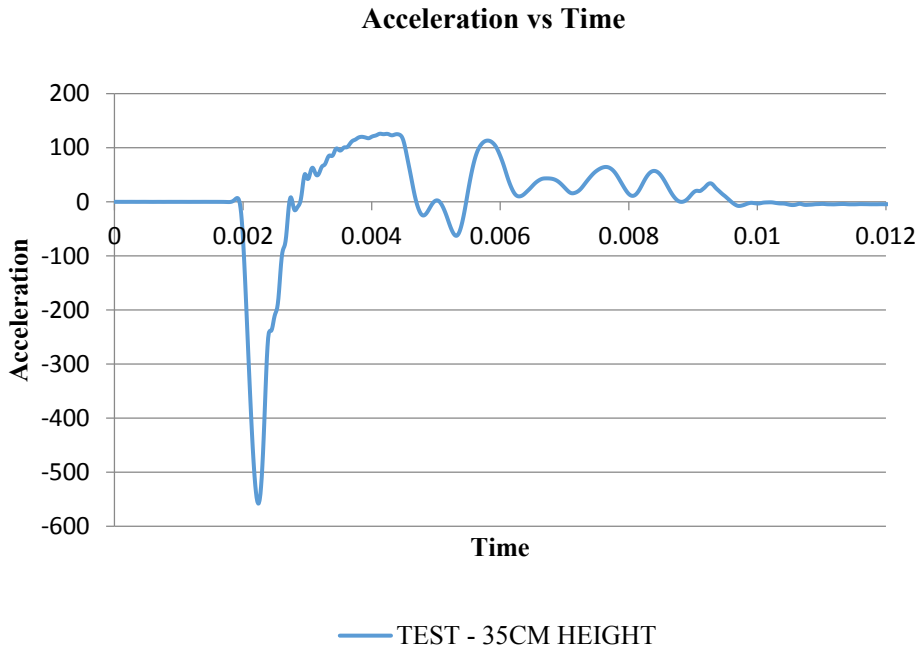

Figure 7: Acceleration test measurement of top roller during the 35cm ball drop test

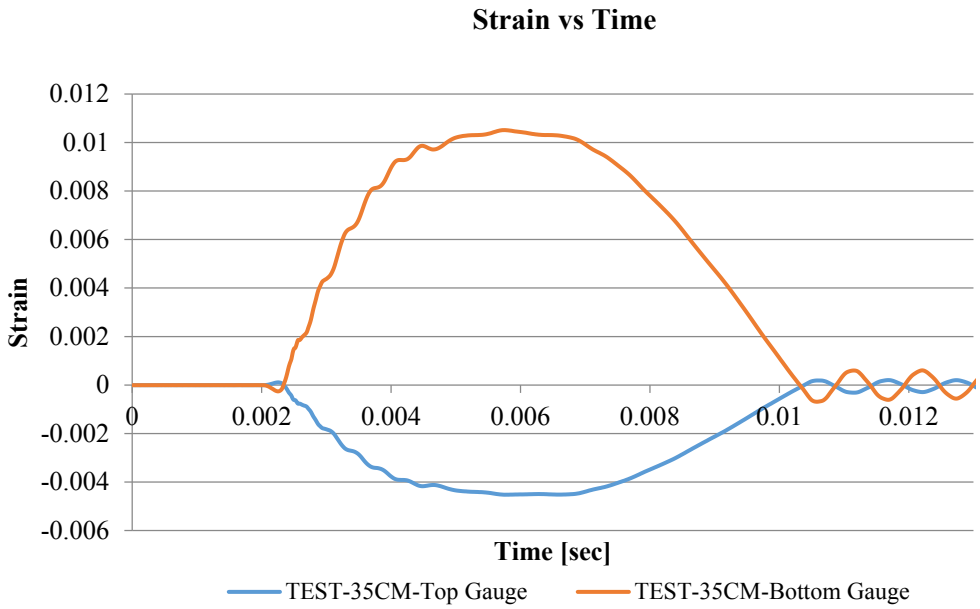

Figure 8: Strain test measurement of the top and bottom strain gauges during the dynamic test

SECTION 3 FINITE ELEMENT ANALYSIS

A full three-dimensional finite element model of the sandwiched structure (Al plate, Adhesive and PC plate), and the supports of the four-point bend fixture were built using the modeling software ABAQUS. The Plates and the adhesive were modeled with reduced-integration brick elements. The two strain gauges were modeled as two membrane elements [0.8x0.8mm]. Supports of the four-point bend fixture were modeled using analytical rigid surfaces. Appropriate contact definitions were defined between the rollers and plates surfaces. The bottom support was constrained in all directions in order to prevent rigid body motion. The top support was also constrained in every direction except the vertical direction.

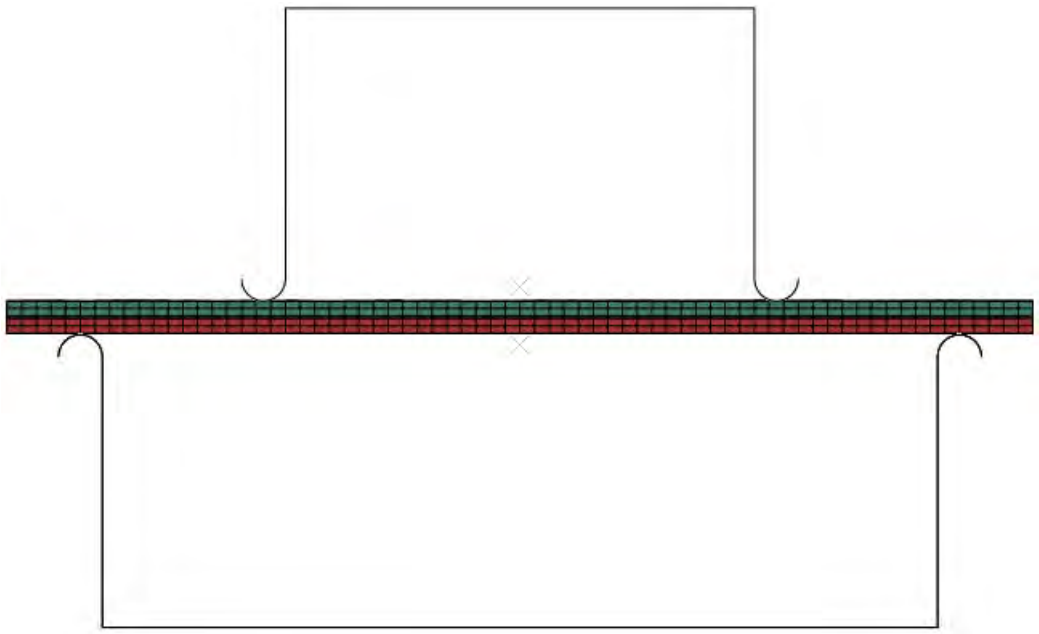

Figure 9: Plot of the simulation mesh model

3.1. QUASI-STATIC BEND SIMULATION

Two sandwich structure configurations were investigated in the quasi-static simulation as we showed earlier in figure-1 .Elastic-plastic material models were used for the substrates (Al and PC), where two different material models (elastic and elastic-plastic) were explored for the adhesive. Displacement loading was applied at a reference node of the top roller fixture. Force, displacement and strain (at the top plate center and at the bottom plate center) results were reported and correlated with experimental results to verify the best material modeling approach. The following are the results:

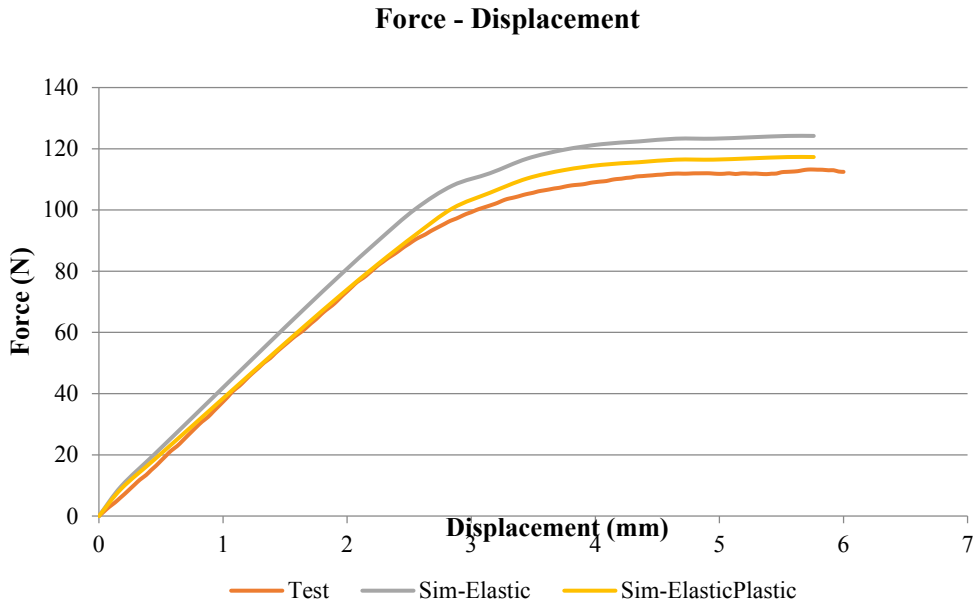

Figure 10: Force-displacement testing and simulation results of the unequal-length-plate sandwich structure

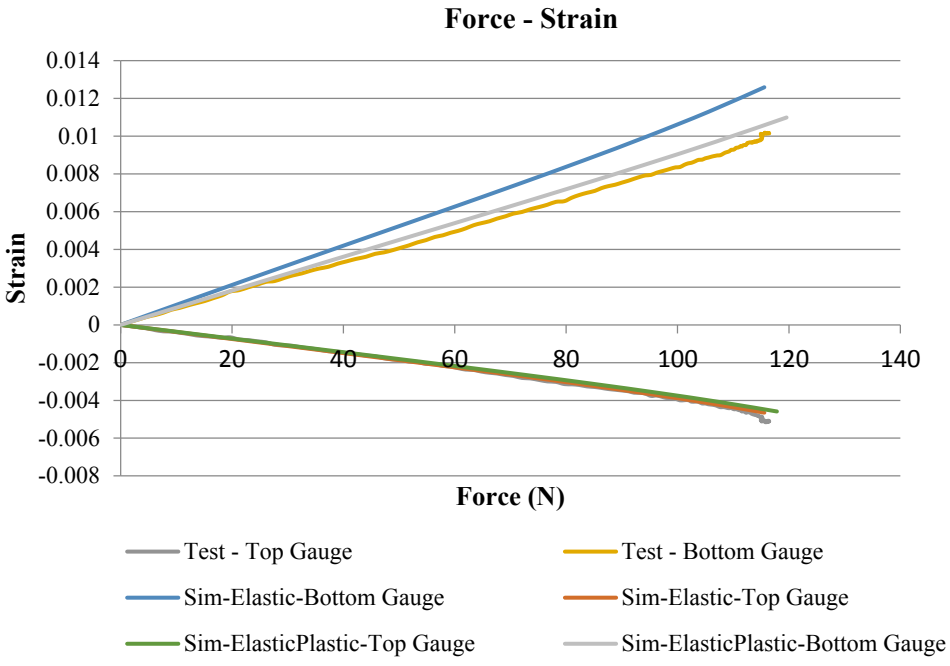

Figure 11: Force-strain testing and simulation results of the unequal-length-plate sandwich structure

4.2. DYNAMIC BEND SIMULATION

The unequal-length-plate sandwich structure was investigated in the dynamic simulation. Elastic-plastic material models were used for the substrates (Al and PC), where three different material models (elastic, elastic-plastic and elastic-viscoelastic) were explored for the adhesive.

Reference node of the top roller fixture was controlled by acceleration data monitored and captured during testing. The methodology employed here is similar to that presented by Tee et al [8]. Acceleration was applied at a reference node of the top roller fixture. This modeling approach renders a very effective way to model the flexural behavior of the sandwiched structure during impact accurately and simultaneously avoids the complexity of numerical modeling of the interface material between the ball and top roller fixture. Top and bottom strain results were reported and correlated with experimental results to verify the best material model that can mimic the adhesive behavior under dynamic loading. The following are the results:

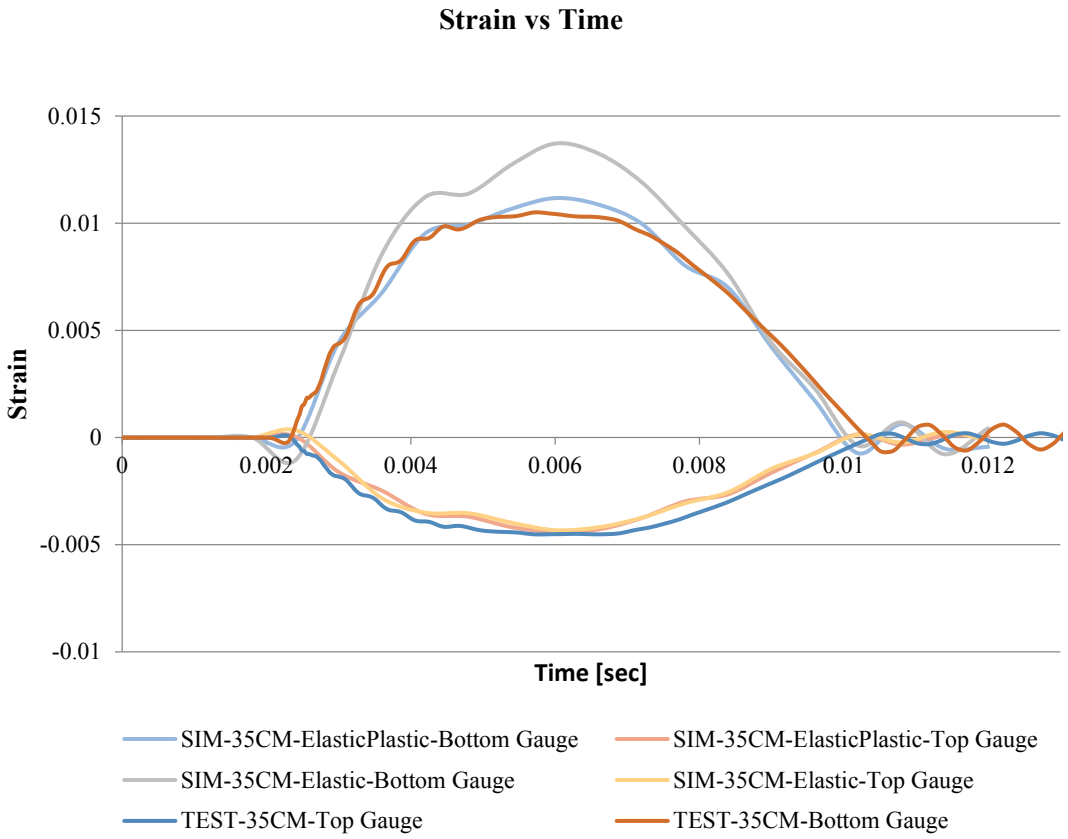

Figure 12: Strain results of the top and bottom strain gauges during dynamic testing and simulation

SECTION 4 DISCUSSION

- Quasi-Static bend simulations of the equal-length-plate sandwich structure show good correlation between experimental and simulation results, for all adhesive material models used in the simulations. Results show that force-displacement response is not affected by the adhesive stiffness which is expected as the adhesive layer will not affect the overall sandwich structure since it is much thinner and less stiff than the adherend substrates. However, for force-strain response, the results are more interesting because they are not affected by the adhesive material modeling approach. This is attributed to the fact that the bottom rollers forcing the PC plate to have the same curvature as the Al plate. The equal-length-plate configuration does not seem to serve as a good validation tool.
- Quasi-Static bend simulations of the unequal-length-plate sandwich structure show that the overall behavior of the structure is sensitive to the adhesive material modeling approach. Force-displacement results and force-strain results show that the linear-elastic material model will over predict the stiffness of the sandwich structure where the elastic-plastic material model mimics the experimental results much better. As the elastic material model does not account for plasticity, the adhesive does not soften up in simulations; and therefore, the PC plate will follow the Al plate curvature. The force-displacement results and the force-strain results show that simulation correlates well with experiments when elastic-plastic material model is used.
- Dynamic bend simulations with unequal-length-plate sandwich structure show that the overall behavior of the structure is sensitive to the adhesive material modeling approach. Strain-time simulation results at the center of top Al plate do not exhibit any dependence on the adhesive modeling approach; this is expected as the force is applied directly on the Al plate. However, strain-time simulation results at the bottom PC plate are sensitive to the adhesive material modeling approach. The elastic-plastic material modeling approach predicts the testing results very well, unlike the elastic and elastic-viscoelastic material modeling approaches which correlate poorly with experimental results because they do not account for plasticity.

SECTION 5 CONCLUSION

A numerical and experimental study that investigates the behavior of a structural adhesive under quasi-static and dynamic loading is presented. Through the presented results which are specific to the sandwich structure materials used in this study, the following conclusions can be drawn:

- The sandwich structure with unequal-length plates is able to capture the sensitivity to the adhesive material modeling approaches. However, the sandwich structure with equal-length plates is insensitive to the adhesive layer and failed as a configuration for capturing or investigating adhesive behavior and properties.
- Comparison between numerical and experimental results from both the quasi-static and dynamic simulation results show that the elastic-plastic material model mimics the adhesive material behavior better than the elastic and elastic-viscoelastic material models, due to the ability of the elastic-plastic model to account for adhesive plasticity.
- Although both of the elastic and plastic phases of this specific adhesive are loading rate dependent, plastic behavior of the adhesive has bigger impact than its elastic behavior on the overall sandwich structure behavior. This is due to the fact that the adhesive will start deforming while the adhered substrates are still in their elastic regions.

SECTION 6 REFERENCES

1. Keller T. Recent all-composite and hybrid fiber reinforced polymer bridges and buildings. Progress Struct Eng Mater 2001;3/2:132–40.
2. Keller T, Tirelli T. Fatigue behavior of adhesively connected pultruded GFRP profiles. Compos Struct 2004;65/1:55–64.
3. Keller T, de Castro J, Schollmayer M. Load-carrying behavior of adhesively bonded GFRP-sandwich girders. J Compos Construct 2004;8/5:461–70.
4. Buyukozturk O, Gunes O, Karaca E. Progress on understanding debonding problems in reinforced concrete and steel members strengthened using FRP composites. Constr Build Mater 2004;18:9–19.
5. Haghani R (2010). Analysis of adhesive joints used to bond FRP laminates to steel members a numerical and experimental study, Construction and Building Materials, vol 24(11), 2243-2251.
6. Scholten, H.; Dortmans, L.; With G.; Smet B.; Bach P., "Weakest-link Failure Prediction for Ceramics II: Design and Analysis of Uniaxial and Biaxial Bend Test," Journal of the European Ceramic Society, 10 (1992), p.33-40.
7. Simulia, ABAQUS Documentation, version 6.12
8. Tee, T.Y.; Luan, J.-en; Pek, E.; Lim, C.T.; Zhong, Z., "Advanced Experimental and Simulation Techniques for Analysis of Dynamic Responses during Drop Impact," Proc. 54th Electronic Components and Technology Conference, Las Vegas, NV, USA, June 2004, pp. 1088-1094.

Contacts

Principal Investigator
Mohsen A. Issa
Professor of Civil and Material Engineering
University of Illinois at Chicago
312-996-2426
missa@uic.edu

NURail Center
217-244-4444
nurail@illinois.edu
http://www.nurailcenter.org/